Synthesis of Functionalised Polysaccharides for Hydraulic Fracturing Applications

ANDREW JOHN LONGSTAFF

Synthesis of Functionalised Polysaccharides for Hydraulic Fracturing Applications

A thesis submitted for the degree of

Doctor of Philosophy

by

Andrew John Longstaff

Department of Chemistry

Durham University

England

2017

I dedicate this thesis to my Grandad.

Words cannot describe how much you are missed.

Abstract

This thesis involves the chemical modifications of the highly reactive primary hydroxyl groups of 2-hydroxyethyl cellulose (HEC) to give rise to possible reaction sites with group(IV) metal-based crosslinkers, leading to the formation of viscous gel materials and possible applications in hydraulic fracturing. This is to offer an alternative to guar, a popular crosslinkable polysaccharide that is obtained from natural products and used routinely in fracturing applications, as its availability is often cast in doubt from year to year due to fluctuating crop harvests.

In Chapter 1, a general introduction to hydraulic fracturing is provided, including details on the types of polysaccharides, crosslinking agents and chemical additives utilised in fracturing fluids, along with possible mechanisms of crosslinking. This chapter also introduces Click chemistry and ring opening polymerisation (ROP) techniques used in this work.

Chapter 2 describes the use of trehalose, a disaccharide molecule, as a model compound for HEC as it has acomparable core skeleton structure, reactivity and solubility properties. The primary hydroxyl groups were converted to thiol groups *via* a three-step process. Each step was fully characterised by 1D and 2D NMR spectroscopy, and FT-IR spectroscopy. The thiolated trehalose was then utilised in a UV mediated thiol-ene Click reaction with a catechol-containing norbornene compound.

In Chapter 3, HEC is modified with small carbonyl-containing molecules *via* acid catalysed condensation reactions to impart diol or catecholic end group functionalities. The surface esterification of HEC *via* the ring opening of succinic anhydride using DMAP as a catalyst is also performed, leading to acid end group functionality. These materials were characterised using inverse-gated ^{13}C NMR spectroscopy and FT-IR spectroscopy.

Chapter 4 describes the synthetic methods used to impart thiol functionality to HEC. This was initially based on the knowledge gained from Chapter 2, but ultimately was found to be unsuccessful when applied to HEC. However, an alternate one-pot synthetic route utilising triphenyl phosphine, carbon tetrabromide and a sulfur nucleophile of either sodium thiobenzoate or potassium thioacetate was successfully used. Thiolated HEC, with approximately 15% of the primary hydroxyl groups converted to SH, was then reacted with the aforementioned norbornene compound in a UV mediated thiol-ene Click reaction. Inverse-

gated ^{13}C NMR, DEPT ^{13}C NMR and FT-IR spectroscopy were useful characterisation methods.

Chapter 5 investigates the utilisation of HEC as a macroinitiator in the anionic ring opening polymerisation (ROP) of the latent AB_2 monomer glycidol. This will impart numerous hydroxyl groups within close proximity to each other, increasing the likelihood of participating in crosslinking reactions with group(IV) metal ions. The graft copolymers were purified by dialysis, then characterised by inverse-gated ^{13}C NMR and DEPT ^{13}C NMR spectroscopy, FT-IR spectroscopy, TGA and SEC. HEC-*g*-polyglycerol was then also utilised as a macroinitiator in the tin(II) ethylhexanoate-catalysed ROP of ε-caprolactone, to afford the novel graft copolymers HEC-*g*-polyglycerol-*g*-PCL_n, where n = 10, 50, 100 or 250. Upon grafting, the hydroxyl end groups of the flexible PCL chains will be further away from the HEC backbone, thus reducing steric hindrance and increasing the likelihood of interacting with group(IV) metal ions of crosslinking agents. The two graft copolymers with the smallest PCL chains retained their water solubility, whilst the longer PCL chain graft copolymers were found to be hydrophobic. All of the PCL containing graft copolymers were fully characterised using 1D and 2D NMR spectroscopy, SEC, TGA, DSC and FT-IR spectroscopy. AFM analysis also determined the structural architectures of these graft copolymers, with a capillary-like network afforded when n = 10, and larger globules afforded when n = 250. It was calculated that each globule actually represents one individual macromolecule.

Chapter 6 describes crosslinking reactions carried out with guar and functionalised HEC materials. Triethanolamine-based zirconium crosslinkers containing different molar equivalents of water added during synthesis were shown to afford different delay times in the gelation of aqueous guar solutions. Crosslinking efficacy was shown to be dependent on the age of the crosslinker, with crosslinkers aged seven months affording much longer delay times. The six-coordinate alkanolamine ligand analogues *N,N,N',N'*-tetrakis(2-hydroxyethyl)ethylenediamine (THEED) and *N,N,N',N'*-tetrakis(2-hydroxypropyl)ethylenediamine (THPED) were used to synthesise the complexes $[Ti(THEED)]_2$, $[Zr(THEED)]_2$ and $[Zr(THPED)]_2$. These complexes afforded no crosslinking ability with guar. The THEED-containing complexes were successfully recrystallised and single crystal X-ray diffraction crystallography was used to determine the structures of the complexes. These were found to be seven-coordinate dimers, with a binucleating oxygen atom from each ligand acting as a bridge to form a central M_2O_2 ring. ESI-MS data also helped confirm this. The $[Ti(THEED)]_2$ complex was found to be a chiral species showing signs of

disorder, whilst the $[Zr(THEED)]_2$ complex was found to be centrosymmetric with a planar M_2O_2 ring. The structure of the $[Zr(THPED)]_2$ complex could not be identified by X-ray crystallographic methods as single crystals could not be isolated, however, ESI-MS evidence supports it also being a seven-coordinate dimer. Aqueous solutions of the graft copolymers HEC-*g*-polyglycerol, HEC-*g*-polyglycerol-*g*-PCL_{10}, HEC-*g*-polyglycerol-*g*-PCL_{50} and the functionalised polymer succinylated HEC were evaluated for their crosslinking abilities with a triethanolamine zirconate crosslinker and a α-hydroxycarboxylic acid zirconate crosslinker. All of the graft copolymers showed no signs of gelation with either crosslinking agent. Succinylated HEC showed no signs of gelation with the triethanolamine zirconate crosslinker. However, gelation of succinylated HEC was induced by the addition of α-hydroxycarboxylic acid zirconate crosslinker. Unfortunately, this was with a 3.0 wt.% polymer concentration, which is greater than the limits utilised in industrial fracturing applications.

In Chapter 7, general conclusions and future perspectives for the work are discussed.

Acknowledgments

Firstly, I would like to thank Dr Ezat Khosravi for giving me the opportunity to study at Durham University, travel to Thailand and Slovenia, and for his supervision over the past four years, enabling me to become a better chemist. I would like to thank Catalytic Technologies Ltd. for funding this project, particularly Dr Alan Cooper and Dr Richard Ward.

I would also like to thank the Durham University NMR and MS services, Dr Dmitry Yufit for his help with X-ray crystallography, Dr Richard Thompson and Dr Stephen Boothroyd for help with AFM imaging and Dr Serena Agostini of Malvern Instruments for performing SEC experiments and analysis. Thank you to Douglas Carswell for performing thermal analysis, the entertaining conversation and being a friendly face in the department.

A massive thank you to the members of the Khosravi group for making the lab such an enjoyable place to work: Dr David Cole, Dr Peter King, Dr Russell Balster, Dr Catherine Blackwell, Dr Shenghui Hou, Kieran Atter and Rose Simnett. Also thank you to all other members of CG156/162 who I have had the pleasure of knowing.

I would also like to say a special thank you to those I met during my undergraduate studies at Newcastle University who I am glad I still keep in touch with. You all know who you are. Thank you for your friendship, encouragement and providing much needed escapes from my studies when things got tough.

Finally, sincere thanks to my Mam and Dad- Ellen and John, sister- Stephanie and Gran- Maureen. Thank you for all of your continual love, support, and encouragement, not just throughout my PhD but in everything I strive to achieve in life. Without you, I would not be the person I am today. I am grateful and I love you all.

Memorandum

The work reported in this thesis was carried out in the Department of Chemistry, Durham University, between October 2012 and June 2016. This work has not been submitted for any other degree in Durham or elsewhere and is the original work of the author except where acknowledged by means of appropriate reference.

Signed: _____ Date: _____

Statement of Copyright

Financial Support

I gratefully acknowledge Catalytic Technologies Ltd. for their funding of this research.

Table of Contents

Chapter 2- Modification of Trehalose as a Model Compound

Chapter 3- Modifications of HEC

Chapter 4- Thiolation and Click of HEC

Chapter 7- Conclusions and Future Perspectives

List of Abbreviations

Ac	Acetyl
AFM	Atomic force microscopy
AGU	Anhydroglucopyranose unit
Bz	Benzoyl
$CDCl_3$	Deuterated chloroform
CMC	Carboxymethyl cellulose
Đ	Dispersity (M_w/M_n)
D_2O	Deuterium oxide
DCC	*N,N′*-Dicyclohexylcarbodiimide
DEPT	Distortionless enhancement by polarisation transfer
DMAP	4-(Dimethylamino)pyridine
DMF	*N,N′*-Dimethylformamide
DMPU	*N,N′*-Dimethylpropylene urea
DMSO	Dimethylsulfoxide
$\overline{DP}$	Degree of polymerisation
DS	Degree of substitution
DSC	Differential scanning calorimetry
ε-CL	Caprolactone
ESI-MS	Electrospray ionisation mass spectroscopy
FT-IR	Fourier transform infrared spectroscopy
ΔH_c	Enthalpy of crystallisation
ΔH_m	Enthalpy of melting
ΔH_m^o	Standard enthalpy of melting
HEC	2-Hydroxyethyl cellulose
HSQC	Heteronuclear single-quantum coherence spectroscopy
MeCat	4-Methyl catechol
M_n	Number average molecular weight
MS	Molar substitution
M_w	Weight average molecular weight
NMR	Nuclear magnetic resonance
NPZ	Zirconium(IV) n-propoxide
PCL	Poly(ε-caprolactone)

ROP	Ring-opening polymerisation
SEC	Size exclusion chromatography
T_c	Crystallisation temperature
T_m	Melting Temperature
TEA	Triethanolamine
TGA	Thermogravimetric analysis
THEED	*N*,*N*,*N'*,*N'*-tetrakis(2-hydroxyethyl)ethylenediamine
THPED	*N*,*N*,*N'*,*N'*-tetrakis(2-hydroxypropyl)ethylenediamine
TIPT	Titanium(IV) tetraisopropoxide
Ts	Tosyl
TsCl	*p*-Toluenesulfonyl chloride
X_c	% Crystallinity

Chapter 1

General Introduction

1.1 Hydraulic Fracturing

Hydraulic fracturing (also known as 'fracking') is a well stimulation technique involving the propagation of small fractures within rock layers deep underground, with the main industrial aim of increasing production by improving the flow of hydrocarbons from oil and gas wells.[1] Fractures can occur naturally or can be man-made as a result of drilling a wellbore into reservoir rock formations deep below the Earth's surface, which can range anywhere from 1,500 to 4,000 metres deep.[2] Often the well will contain horizontal or directional sections which extend for hundreds of metres through the soft rock layers and may also connect to pre-existing fractures, pockets and flow pathways.[3] The aim of this is to connect a larger volume of the reservoir to the well in order to maximise the amount of oil and gas flow recovered at the surface. Figure 1.1 illustrates the positioning of the well within the rock formation, leading to fracturing at the horizontal section in the shale layer in order to stimulate flow in nearby gas pockets. The initial section of the well near the surface is reinforced with a steel casing and cement to isolate it from any nearby water tables and aquifers, in order to prevent contamination to local water systems.[4]

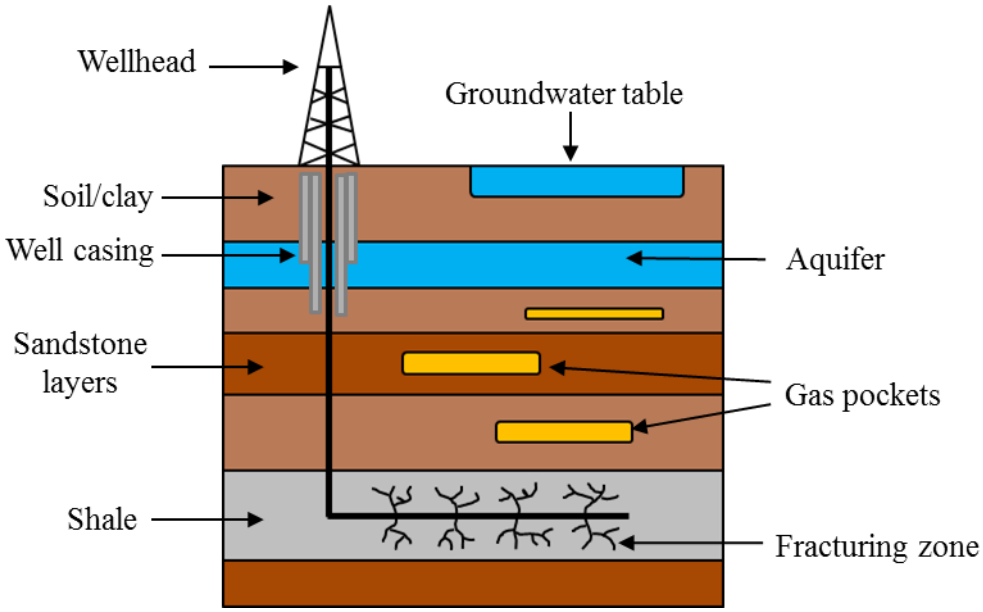

Figure 1.1: Diagram of wellbore drilled through rock layers, with a horizontal extension in the shale layer where fracturing will occur

At such depth the rock layers may show extremely low natural permeability (such as in shales),[5] which is insufficient to allow oil and gas to flow into the wellbore at an economic rate. Therefore, conductive fractures are created by applying high pressures at the top of the wellbore and pumping in a fracturing fluid. The highly pressurised viscous fluid exceeds the strength of the rock and causes the fractures to open, which are then filled by a solid proppant that is also transported in the fluid. This prevents the fractures from closing once the pressure is removed.

Once the hydrocarbons have been recovered, the fracturing process is completed by removing the fluid in a clean-up step in order to prevent damage to the rock formation, as this could potentially decrease further hydrocarbon recovery from the well. This is typically achieved by either chemically or thermally degrading the fluid so that it can easily be flushed from the fractures with water back to the surface, known as 'flowing back the well'.[6]

1.2 Fracturing Fluid Composition

The mixture injected into the wellbore is known as fracturing fluid and since their introduction have been continuously improved from simple oils to sophisticated water-based polymer-containing gels.[7] Initially, the main focus of fracturing fluids was to direct and successfully place as much proppant as possible, but then focus was altered to minimise environmental impact by improving post-fracturing production and clean up. Currently, there is interest in the development of fluids that have enhanced rheological properties, achieve better fracture permeability and cause minimal damage when fluid residues are left behind.[8] The general composition of a fracturing fluid is outlined in Figure 1.2. It is largely comprised of water (~96%) and proppant (~3.5%), with less than 0.5% of the total fluid volume accounting for chemical additives.[9]

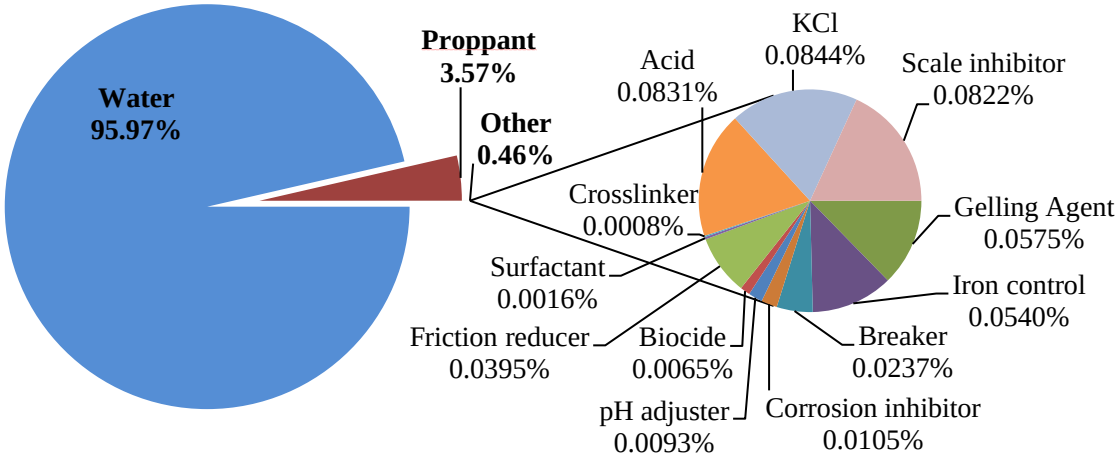

Figure 1.2: Typical components of a fracturing fluid

A single fracturing process may use 2-4 million US gallons of fluid per well, with additional fluid required for each refracturing. This can occur multiple times over a period of 5 to 20 years, depending on the productivity of the well.[10]

It is important to note that the overall fluid composition and ratio of chemical additives varies depending on the specific conditions of the well, such as the type of rock formation, depth of

well and maximum down well temperature encountered. Therefore, there is no standard ‘one size fits all’ solution, and fluids must be tailored to meet individual needs.

1.2.1 Proppant

A proppant is a solid material that is transported by the fluid into the fractures once hydraulic pressure has been induced in the well. It acts as a permeable pack to hold fractures open once the pressure is withdrawn, providing long term conductivity of the fracture, therefore it should be mechanically strong to withstand closure stresses. Untreated silica (sand) is the most common proppant, but tends to degrade into finer particles quickly, so epoxy resin coated silica can be used for improved strength.[11] Ceramic materials and sintered bauxite-based proppants are deemed to be more effective alternatives as they are more uniform in size and shape, afford a higher crush resistance and are more thermally and chemical stable.[12] Figure 1.3 illustrates how a proppant (in this case sand) works to flood the fractures within shale and serves to keep the fracture open upon the removal of hydraulic pressure, allowing the natural gas to flow into the well for extraction.[13]

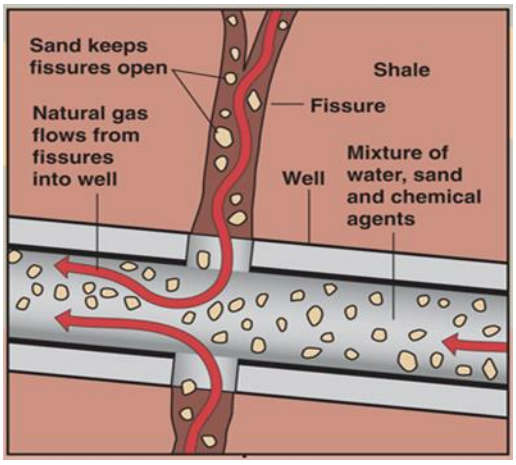

Figure 1.3: Illustration of how a proppant pack works during hydraulic fracturing

The viscosity of the fluid must be sufficient to suspend the proppant particles in order to carry them through the well and prevent settling or sinking due to gravity. Because of this, the move towards ultra-lightweight proppant is becoming more popular. These materials afford a much lower specific gravity and can penetrate deeper into the rock formation. This means lower pumping rates can be employed, leading to lower energy costs, as a proppant with a lower density is more easily transported *via* the viscosity and elasticity of the fluid, rather than the velocity at which it is pumped.[14] Initial ultra-lightweight proppants included natural products such as walnut shells and fruit pits, or hollow glass spheres.[15] But these showed limited strength

and were found to deform and shatter easily; the natural products were reinforced by being impregnated with a styrene-divinylbenzene copolymer resin.[16] The addition of this thermoset polymer matrix allows slight deformation to occur without shattering of the natural product due to its high elastic modulus, whilst still retaining its ultra-light weight.

1.2.2 Chemical Additives

Of particular interest with regards to this project is the gelling agent component, or more specifically the choice of polymer and the crosslinker agent, both of which will be discussed in later sections. The chemical additives generally serve three main purposes: 1) to enhance fracture propagation, 2) to enhance proppant carrying capability and 3) to minimise formation damage.[17]

Exact combinations of additives are generally unknown, due to many oil and gas companies not publicly disclosing their recipes in order to protect their intellectual property from rival corporations. Unfortunately, this compounds the concern that fracturing fluids contain additives that may harm human health and the environment, or leads to claims that companies are injecting fluids containing chemicals that they cannot identify.

Although there are hundreds of chemicals that could possibly be used as additives, there are a limited number which are routinely used in the process.[18] These include additives with the role of assisting fracture creation such as the aforementioned gelling agents, chloride salts as clay stabilisers and polyelectrolytes (such as poly(acrylic acid)) as fluid-loss control materials. Additives which reduce damage to the rock formation include: quaternary ammonium salt biocides in order to eliminate bacteria present in the water which may lead to corrosive by-products, low M_w alcohols which act as surfactants and corrosion inhibitors, and peroxide or persulfate gel breakers which allow easier well clean-up. pH regulators and adjustors such as bases (hydroxide or carbonate solutions) and weak acids (acetic or citric acid) are used to help maintain the effectiveness of the other additives (shown in Figure 1.2) and prevent degradation of the fractured rock.[19]

1.2.3 Polymers Utilised

Preferably, the polymer used in the fracturing fluid composition is a polysaccharide, chosen from cellulose derivatives, guar gums and gum derivatives. These are soluble in water, non-toxic and can produce a large viscosity build when present in low concentrations in solution.

1.2.3.1 Cellulose and its Derivatives

Cellulose is a naturally occurring polymer which is an important structural component in the cell wall of green plants. As such, it is the most abundant organic polymer on Earth. The majority of the cellulose used in industrial applications is obtained from wood pulp and cotton.[20]

The chemical structure of cellulose (Figure 1.4) is comprised of a linear chain of six-membered D-anhydro glucopyranose units (AGU) linked via β-(1,4) glycosidic covalent bonds. Polymer chains can contain between several hundred to over ten thousand units, forming a macromolecular structure.[21] These covalent bonds are acetal linkages formed by the reaction of an alcohol group at C_4 of one glucose unit with a hemiacetal at C_1 of another, resulting in the elimination of a water molecule.[22] The cellulose molecule contains three different kinds of AGU: the non-reducing end group with a free hydroxyl at C_4, the reducing end group with a free hemiacetal (or aldehyde) group at C_1 and the aforementioned internal units linked at C_1 and C_4. Due to long polymer chain lengths, it is the chemistry of the hydroxyl groups on the internal units that dominates.

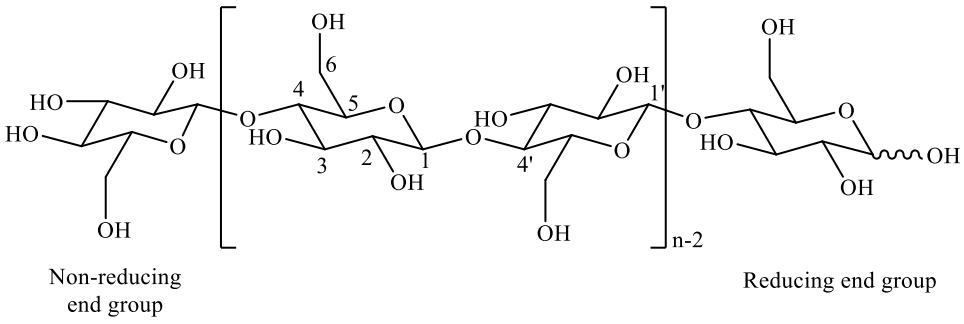

Figure 1.4: Chemical structure of cellulose

The stereochemistry of the acetal linkages is important. In a linear glucose molecule, the stereochemistry at C_2, C_3, C_4 and C_5 is fixed, but when the glucose molecule forms a pyranose ring, the C_5 hydroxyl can attack the C_1 carbonyl from either above or below, resulting in opposite stereochemistry at the C_1 carbon. When the glucopyranose molecule is drawn in the Haworth projection, if the anomeric C_1 hydroxyl and the C_5 $–CH_2OH$ groups are on opposite sides of the rings plane, this is a *trans* arrangement and designated "*α*-". However in cellulose, both the C_1 and C_6 groups are on the same side of the plane in a *cis* arrangement, this is designated a *β*-configuration. When drawn in a chair conformation, all other functional groups are in the equatorial position within the ring, this causes the cellulose chain to effectively grow in a linear fashion, with AGU units rotated by 180° with respect to each other due to the

constraints of the *β*-linkage. This combination of properties results in cellulose being an effective fibre-forming polymer.[22]

The high degree of linearity means that the individual chains can easily approach within a close proximity to each other. Due to the large number of readily available equatorial hydroxyl groups, extensive hydrogen bonding can occur not only inter-molecularly between nearby chains (Figure 1.5.A), but also intra-molecularly within a single chain (Figure 1.5.B).[21]

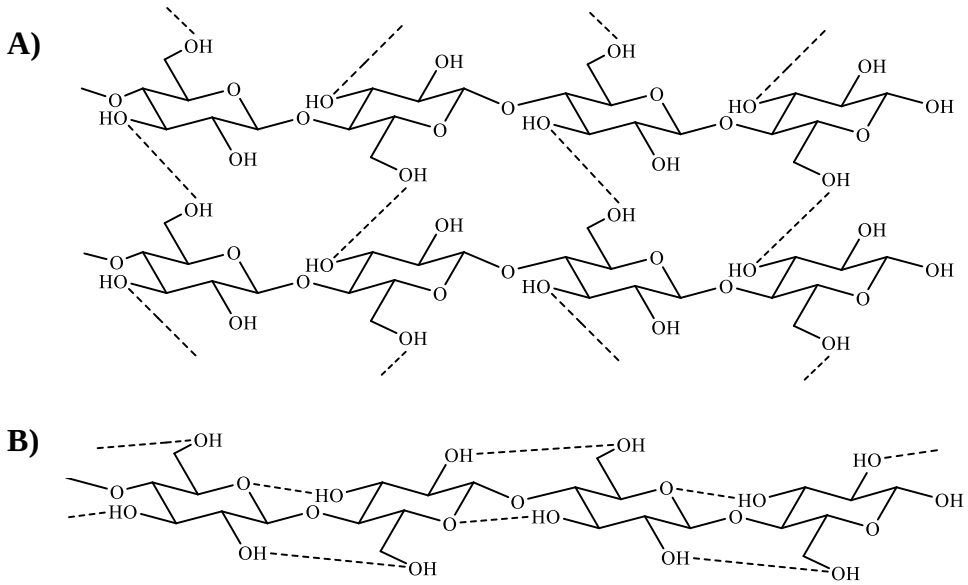

Figure 1.5: A) Inter-chain hydrogen bonding between adjacent cellulose chains and B) Intra-chain hydrogen bonding within a single cellulose chain

This results in highly ordered strong fibres and affords non-thermoplastic characteristics, such as preventing cellulose from melting. This fibrous structure also means cellulose is insoluble in a number of solvents, including water, *N,N'*-dimethylformamide (DMF) and dimethyl sulfoxide (DMSO). In less ordered regions, the chains are further apart and can therefore hydrogen bond with other molecules, such as water. As a result of this, cellulose can absorb large quantities of water. Thus, cellulose will swell in water but does not dissolve.[22]

In order to overcome the problem of insolubility, the hydrogen bonded network must be broken. This is achieved by chemical modification of the hydroxyl groups. The structure of a general modified cellulose derivative is shown in Figure 1.6. Table 1.1 gives a brief overview of some of the most commonly produced cellulose derivatives and their applications.

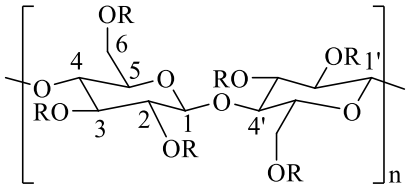

Figure 1.6: Structure of a modified cellulose derivative, where R = H or R from Table 1

Table 1.1: Commercially important modified cellulose materials and their applications

Cellulose Derivative	Functional Group (R)	DS[23]	Solubility	Applications[23, 24]
Hydroxyethyl cellulose (HEC)	$-CH_2CH_2OH$	0.1-1.0	Water, brine, DMF, DMSO	Hydraulic fracturing, personal products, paints, coatings
Carboxymethyl cellulose (CMC) (often used in its Na^+ salt form)	$-CH_2COONa$	0.5-1.2	Water, brine	Hydraulic fracturing, paints, adhesives, pharmaceuticals
Cellulose acetate	$-C(O)CH_3$	1.0-3.0	Acetone, chloroform	Coatings, textile treatment
Cellulose nitrate	$-NO_2$	1.5-3.0	Methanol, ethers	Films, fibres, explosives
Cellulose xanthate	-C(S)SNa	0.5-0.8	Water, brine	Cellophane, textiles

Each AGU has three hydroxyl groups available for substitution, at the C_2, C_3 and C_6 positions, which are mainly responsible for the reactions of cellulose. The hydroxyl groups at C_2 and C_3 are secondary alcohols, while the hydroxyl at C_6 is a primary alcohol. The reactivity of these groups is affected not only by their inherent chemical nature but by steric effects of the reacting/modifying agents, as well as the steric effects resulting from the supramolecular fibre structure of cellulose.[25] Based on esterification studies,[26] the C_2 hydroxyl group has been observed to react twice as fast as the C_3 hydroxyl group. In comparison, the primary C_6 hydroxyl group has an axis of free rotation about the C_5 to C_6 bond; rotational isomers have been observed by infrared spectroscopy, and the good reactivity of primary hydroxyl groups of polysaccharides is related to this isomerisation.[26] In general, the relative reactivity of the hydroxyl groups of cellulose can be expressed as C_6-OH >> C_2-OH > C_3-OH.

The degree of substitution (DS) value describes the number of chemically modified hydroxyl groups per AGU. This can range from DS = 0 (natural cellulose) to DS = 3 (completely substituted cellulose).[25] The molar substitution (MS) value of a polysaccharide describes the number of substituents introduced onto the AGU. If the grafted substituent contains functional groups capable of further reactions, e.g. hydroxyl groups, then multiple molar substitutions can

occur. Therefore, the MS can assume values greater than three. As different parts of the constituent cellulose fibrils display very different accessibilities to the same reagent, cellulose derivatives may be considered to be very random block copolymers.[27] AGUs with different extents of functionalisation will be present throughout the polymer chain, including the possibility that some AGUs may carry no substituent groups or be fully substituted, leading to a range of DS and MS values being observed.

Etherification and esterification reactions are most commonly used to modify cellulose. Etherification generally uses a base to deprotonate the cellulose hydroxyl groups, then an alkyl halide is used as the reagent (such as chloroacetic acid in the synthesis of carboxymethyl cellulose (CMC), Scheme 1.1).[28] An alcohol, such as isopropanol, is utilised as a solvent, as it acts as a swelling agent and diluent, facilitating good penetration of NaOH into the cellulose structure. In the case of hydroxyethyl cellulose (HEC), the strained three-membered ring ethylene oxide is used as the etherifying agent. Further information on HEC is provided in Section 1.4.2.

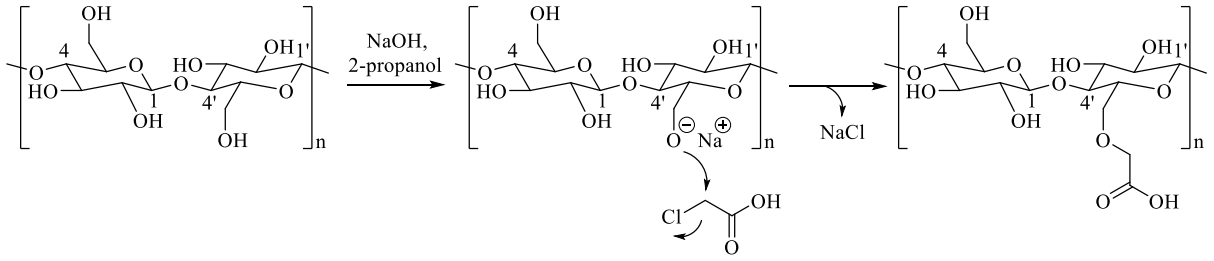

Scheme 1.1: Synthesis of carboxymethyl cellulose (CMC)

Esterification of cellulose generally utilises acids to bring about swelling of the fibres, allowing penetration of reagents throughout the cellulose structure. A combination of acetic acid, acetic anhydride and sulfuric acid is used to produce cellulose acetate, whilst reaction of an aqueous slurry of cellulose in the presence of nitric acid and sulfuric acid was found to lead to the formation of explosive cellulose trinitrate in the 19th century, Scheme 1.2.[29] Cellulose nitrates are still produced using this method, but tuning the DS to lower values affords safer materials that can be used for other purposes, such as filmstock and protective coatings.[28]

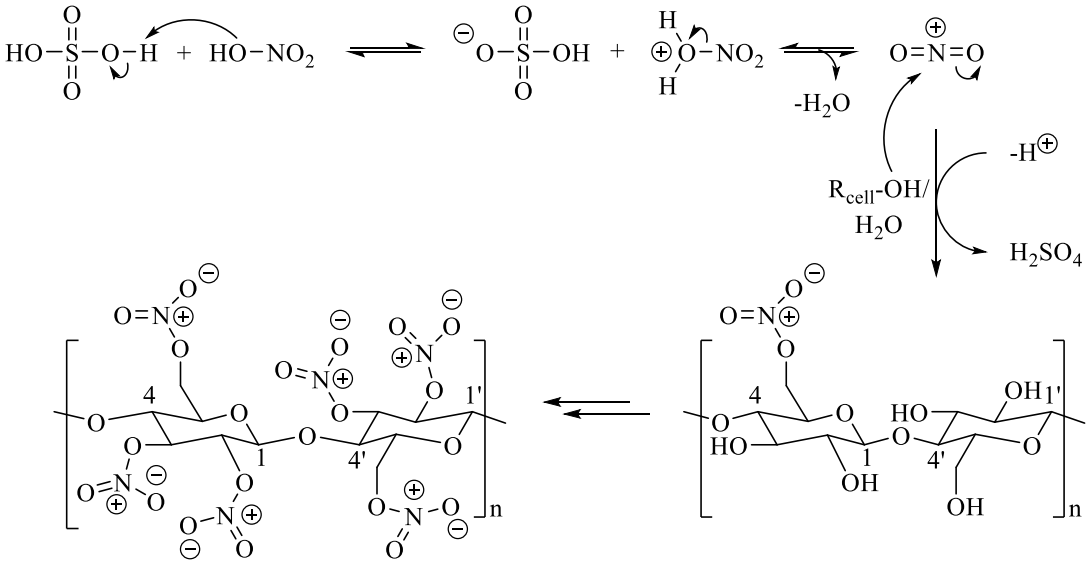

Scheme 1.2: Synthesis of cellulose trinitrate

CMC and HEC are used in hydraulic fracturing as they show good water solubility, affording very little insoluble residue, are non-toxic and commercially available at reasonable cost. CMC can participate in crosslinking reactions via chelation through the carboxylate groups. HEC only acts as a linear viscosifer within fracturing fluids.

1.2.3.2 Guar and its Derivatives

Guar gum is a naturally occurring polysaccharide obtained from the ground endosperm of guar beans. India is the largest producer, growing approximately 80% of the world's crops.[30] Guar and guar derivatives are the most common polymers used in fracturing fluids as they can quickly hydrate, afford better solubility (and are therefore highly dispersible in brines, cold and hot water), and show an enhanced thermal stability in comparison to their cellulose based counterparts.[31] They form solutions of a much greater viscosity, even when present in low concentrations and can also undergo crosslinking reactions with boron and group(IV) metal ions. The chemical structure of guar, shown in Figure 1.7, consists of a linear backbone chain of β-(1,4) linked D-mannopyranose units, with D-galactopyranose branches bonded by α-(1,6) linkages.

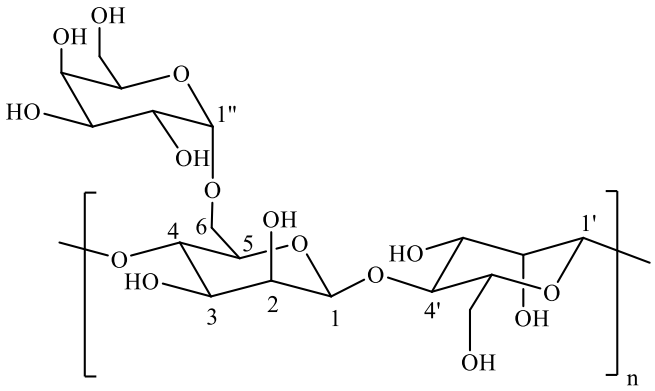

Figure 1.7: Chemical structure of guar

On average the galactose branches occur on every other mannose unit.[32] Mannose and galactose are, respectively, the C_2 and C_4 epimers of glucose, which means that they only differ in the configuration of one stereogenic centre about the specified carbon.[33]

The increased viscosity in solution is due to the extra pyranose ring grafted to the polymer backbone, which affords extra hydrogen bonding sites. Furthermore, as the hydroxyl groups on the C_2 and C_3 carbon atoms of the mannose ring, and the C_3 and C_4 carbon atoms of the galactose ring are in the *cis* configuration relative to each other, guar is also susceptible to crosslinking with group(IV) metal or borate ions at these sites. These ions link two guar chains together, which helps to build up a larger 3D network.[34, 35] Guar contains the same amount of substitutable OH groups per backbone ring as cellulose, therefore the maximum DS value is also three. Guar can undergo the same reactions and modifications as cellulose; however, the MS value is often greater in comparison due to the availability of the extra OH groups on the galactose unit.

In recent years, the production and availability of guar in order to meet demand has been cast in doubt. In 2012, for example, the cost of guar increased by approximately 1000%.[36] This was due to inventory stockpiling by companies such as Haliburton, Schlumberger and Baker Hughes, amidst the fear of shortage as a result of ongoing droughts throughout India. The fluctuation and uncertainty of the size of each crop harvest year to year can be problematic for the hydraulic fracturing industry as a whole, with larger corporations monopolising the product. To counteract this, efforts have been made to introduce guar bean crops into new areas, such as semiarid areas of the United States, Australia and Africa.[37]

1.2.4 Crosslinking Agents

Fracturing fluids of high viscosity can be obtained by increasing the polysaccharide concentration or by inducing crosslinking of the polymer chains. Increasing the polymer concentration is generally not cost effective, may lead to operational or handling problems and decrease fracture conductivity later in the formation's life.[38, 39] Addition of millimolar amounts of crosslinking agent such as borate or group(IV) metal ions significantly increase the viscosity of a guar solution by several orders of magnitude.[6]

1.2.4.1 Boron

In recent years, boron has seen greater use as the crosslinking method of choice. It is usually added to the fracturing fluid as boric acid ($B(OH)_3$), which upon contact with hydroxide anions (from water or other additives) dissociates to form tetrahydroxyborate anions (Scheme 1.3.A). These are then capable of inducing crosslinking between two guar polymer chains (Scheme 1.3.B).[39]

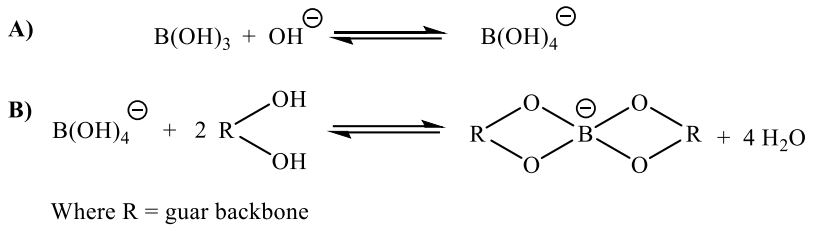

Scheme 1.3: A) Dissociation of boric acid to borate anion. B) Borate anion linking two guar polymer chains together

The increase in popularity of borate crosslinking agents is due to the unique feature that the viscosity of the guar/borate gel is reversible to mechanical shear. This is generally taken as evidence that the guar/borate complexation reaction is chemically reversible.[6] As the pH of the fluid increases, more borate ions are available for crosslinking due to the established equilibrium in Scheme 1.3.A. At a pH above 8.5, crosslinking occurs almost instantaneously.[40] As the dissociation of boric acid to borate anions is an exothermic reaction, as the temperature of the well increases the dissociation equilibrium shifts backwards in order to counter this. This causes the pH value to fall, causing the fluid to thin due to less borate ions being available in solution.[39] Viscosity then recovers as the temperature decreases and pH rises.

However, the limitation of borate crosslinking agents is that they are only effective over a small pH range, typically 8.0-11.0. At pH values greater than 11.0, different borate complexes of

varying stabilities are formed which cannot participate in crosslinking reactions, whilst also reducing the concentration of available borate ions that can.[41]

1.2.4.2 Group(IV) Metals

Group(IV) metal alkoxide complexes, primarily those that are titanium or zirconium based, have been utilised as crosslinking agents in fracturing fluids since the 1970's and 1980's, respectively.[42] Titanium-containing agents were initially popular due to the abundance of titanium-containing materials and low cost, but aqueous-based zirconium crosslinkers showed an increase in popularity and are now widely used.[43] Hafnium-containing complexes have been synthesised and evaluated for hydraulic fracturing applications, but have yet to establish themselves as being commercially viable.[44]

In contrast to boron crosslinking agents, group(IV) metal crosslinkers show a greater stability and operate over wider ranges of pH and temperature (up to 200 $^{\circ}$C) values.[43] Preferably, the ligands attached to the metal centre should be Lewis basic, such as OH, alkoxide, α-hydroxycarboxylic acids or alkanolamine (alkane backbone containing both hydroxyl and amino functionality) groups.[45] The complexed ligands can be tuned to meet the requirements of wells with specific conditions when required.[35]

Another beneficial feature of group(IV) metal crosslinkers is that upon mixing with the fluid, the crosslinking reaction can be controlled in such a way that it is delayed. This is often desired in order to minimise friction in turbulent-flow conditions as a less viscous fluid initially travels through the well, which in turn also leads to reduced pumping costs. Shear effects are also reduced which helps prolong the lifetime of the crosslinked fluid. In contrast to borate crosslinked fluids, fluids crosslinked by titanium and zirconium are shear sensitive and do not recover their viscosity upon shear reduction in the well formation.[46] Controlled, delayed gelation occurring at a predetermined position also improves the efficacy of proppant transport and delivery.[47]

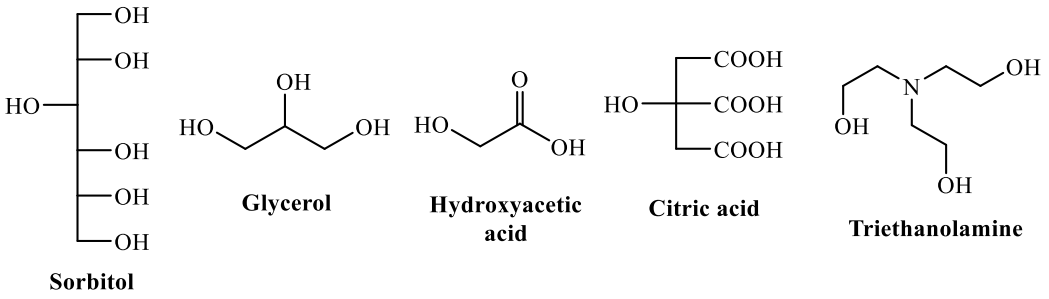

Figure 1.8: Commonly used ligands utilised in group(IV) metal crosslinkers to control delayed gelation

Polyfunctional organic chelating ligands have been employed as delay agents, such as those presented in Figure 1.8.[47] The formation of multiple strong bonds to the metal centre confers good stability to the initial complex, therefore it will take longer for the ligands to be displaced by saccharide functional groups, slowing the rate of crosslinking.

1.2.4.3 Methods of Crosslinking

Due to a number factors contributing to hydraulic fracturing, the exact mode of crosslinking between metal ions present in a crosslinking agent and polysaccharide chains has not been determined. However, Moorhouse *et al.* stated that group(IV) metal crosslinking is likely to occur through the hydroxyl groups present on guar or its derivatives, or through the carboxyl-functionality on carboxyalkyl derivatives of guar.[43] Hypothesised mechanisms of the crosslinking of guar-containing non-ionic functionality *via* covalent bonding, and guar-containing ionic functionality *via* chelation, are shown in Figure 1.9.A and Figure 1.9.B, respectively.

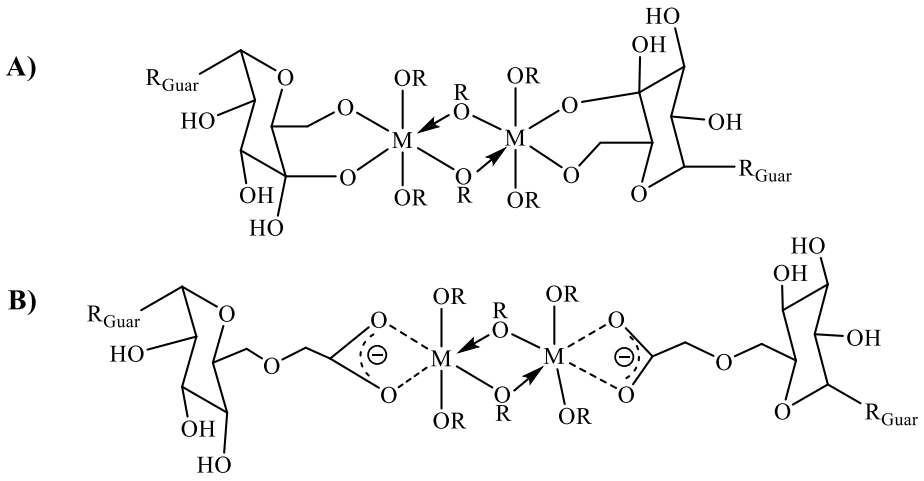

Figure 1.9: Hypothesised mechanisms of crosslinking between a group(IV) metal crosslinking agent and A) non-ionic guar and B) ionic guar

1.2.4.4 Limitations of Crosslinking

For a reliable rate of crosslinking to occur, a sufficient number of saccharide polymer chains must be present in the fluid with enough active sites that can participate in crosslinking reactions. A sufficient number of borate or metal ions must also be present in order to build up the network structure. Therefore, a careful balance of the ratio of these components, as well as management of the fluid pH, temperature and other additives that could interfere with the crosslinking agents must be considered in order to produce and maintain a stable system.

There is also the possibility that crosslinking may occur through intramolecular means between two active sites on the same polymer chain, which is undesirable as this does not afford any increase to the overall molecular weight of the polymer network. The literature does not explain steps taken to prevent or counteract intramolecular crosslinking, but it is thought that borate crosslinking of guar provides a better level of intermolecular crosslinking in comparison to group(IV) crosslinking agents, due to the reversible nature of the guar/borate chemical bonds.[48]

1.3 Hydrolysis and Structures of Group(IV) Metal Alkoxides

Group(IV) metal alkoxide complexes in solution are generally dynamic species, undergoing a constant exchange of labile ligands. The metal ions will prefer to achieve favoured co-ordination geometries by forming alkoxide bridges via dative bonds from the oxygen atom substituent; therefore leading to the formation of dimers, trimers and even longer chain oligomeric and polymeric structures.[49]

1.3.1 Hydrolysis

Generally, metal alkoxide complexes are very reactive due to the presence of highly electronegative OR groups (acting as hard π-donors), which stabilise the metal centre in its highest oxidation state, but also render the metal susceptible to nucleophilic attack.[50] Upon contact with water, these compounds react vigorously *via* hydrolysis reactions, forming reactive metal hydroxides and hydrated oxides. This general reaction of the formation of a metal hydroxide is proposed to be *via* the three-step associative substitution mechanism as described in Scheme 1.4.

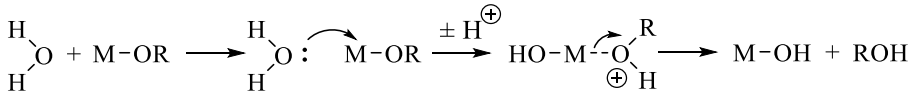

Scheme 1.4: General mechanism of metal alkoxide with water

The first step in Scheme 1.4 is the nucleophilic addition of a water molecule to the positively charged metal atom. This leads to an intermediate where the coordination number of the metal has increased by one. The second step involves a proton transfer from the entering water molecule to an adjacent OR group, forming a second intermediate. The protonated OR is now the better leaving group, which departs. The nucleophilic character of the entering molecule, the stability of the leaving group and the ability to transfer a proton all determine the kinetics of the reaction.[51]

The reaction times for the hydrolysis of titanium and zirconium alkoxide complexes have been shown to occur on timescales of milliseconds and microseconds, respectively.[52] This is due to their high Lewis basicity and ability to easily form stable cationic complexes. In comparison to the associative substitution mechanism proposed in Scheme 1.4, these features were experimentally shown to facilitate ligand exchange *via* a proton-assisted S_N2 mechanism in titanium and zirconium alkoxides, as shown in Scheme 1.5.[53]

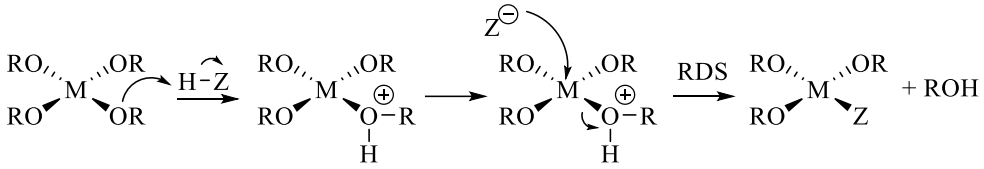

Scheme 1.5: Proton-assisted S_N2 ligand exchange where M = Ti or Zr. Hydrolysis reaction when Z = OH

The first step in Scheme 1.5 involves the protonation of an alkoxide oxygen atom. The dissociation of the proton from HZ in this step exists in a rapid pre-equilibrium. The newly formed donor ligand (Z^-) then coordinates to the positively charged cationic species, and a molecule of alcohol is released. In this reaction, the kinetics are determined by the nucleophilicity of the Z^- group.[53, 54]

After the initial reaction, the alkoxide complexes can undergo subsequent hydrolysis reactions, or they can form M-O-M oxo bridges *via* condensation reactions with the elimination of a molecule of water or alcohol. Condensation is a complex process and depending upon the experimental conditions, three competitive mechanisms can be considered- oxolation, alcoxolation and olation.[51, 55]

The mechanism of oxolation is shown in Scheme 1.6, where the bridging oxo group is formed by the elimination of a water molecule. The mechanism of alcoxolation, Scheme 1.7, follows the same mechanism as oxolation, but it is an OR group that is protonated and a molecule of

alcohol is eliminated. This reaction is analogous to the hydrolysis presented in Scheme 1.4, but with a metal replacing a proton in the entering group. Both oxolation and alcoxolation reactions are governed by the strength of the entering nucleophile, electrophilicity of the metal and the stability of the leaving group.

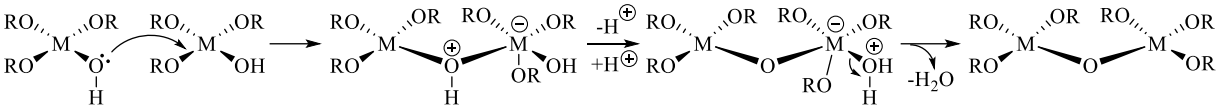

Scheme 1.6: Mechanism of oxolation, with the elimination of a molecule of water

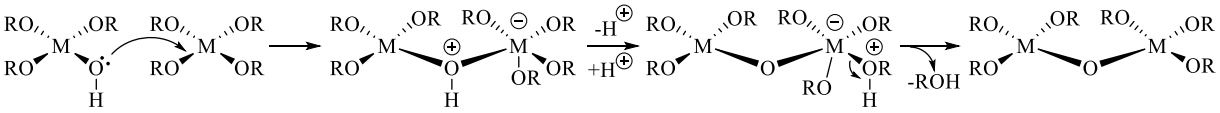

Scheme 1.7: Mechanism of alcoxolation, with the elimination of a molecule of alcohol

The third competitive mechanism of olation is presented in Scheme 1.8. Olation occurs when the full coordination of a metal atom is not achieved (as is the usual case for zirconium, titanium and hafnium) and the metal is solvated by one or more solvent molecules. The oxo bridge is formed by the elimination of a solvent molecule, which can either be water (Scheme 1.8.A) or alcohol (Scheme 1.8.B), depending upon the water concentration of the medium.

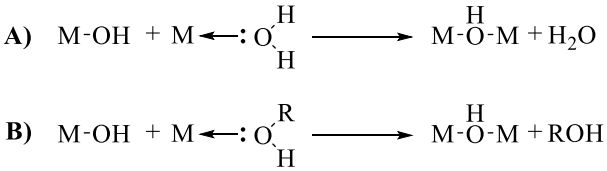

Scheme 1.8: Mechanism of olation with the elimination of a solvent molecule of A) water and B) alcohol

The kinetics of olation reactions are governed by the charge distribution, and are strongly favoured when the nucleophilicity of the entering group and electrophilic strength of the solvent coordinated metal are high. These reactions also occur quickly due to the lack of proton transfer in the intermediate compared to oxolation and alcoxolation.

1.3.2 Structure Determination

The exact structures of metal alkoxides can be difficult to characterise by NMR spectroscopy in solution, depending upon the size and complexity of the structure, due to the near constant

exchange of ligands and solvent molecules amongst the metal centres. Single crystal X-ray diffraction is considered to be a good technique utilised in structure determination.

For complexes that do not undergo crystallisation, therefore meaning that single crystal X-ray diffraction cannot be performed, ^{17}O NMR spectroscopy has been utilised to afford structural architecture information. Detailed hydrolysis studies have been carried out using ^{17}O-enriched water.[56, 57] Ligand exchange can be performed as outlined in Scheme 1.5, then condensation pathways cause the enriched ^{17}O atoms to end up in oxo bridging positions- the terminal alkoxides are not enriched.

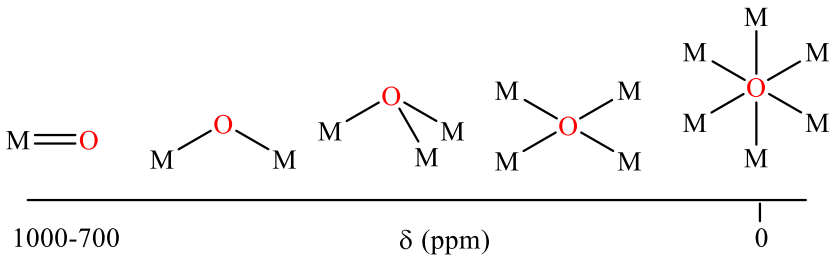

Figure 1.10: ^{17}O NMR spectroscopy chemical shift trend relative to metal atom coordination

The number of metal atoms coordinated to the ^{17}O containing molecule can be determined by ^{17}O NMR spectroscopic methods, as outlined in Figure 1.10, as the different coordination modes of ^{17}O show resonances at different chemical shifts. The greater the number of metal atoms coordinated to a ^{17}O atom, the lower the value of chemical shift observed. The ^{17}O NMR shift is very sensitive and therefore a good indication of the types of bridging oxo groups present in the complex, providing help with structure elucidation.

1.4 Saccharides of Interest in this Work

1.4.1 α,α-D-Trehalose

α,α-D-Trehalose is a naturally occurring symmetrical disaccharide composed of two molecules of D-glucose connected by an α,α-1,1-linkage, Figure 1.11. It is found in many organisms such as plants, mushrooms, yeasts and insects.[58] Trehalose has been shown to be extremely stable over a wide pH range (3.5-10) and at high temperatures (up to 120 °C for 90 min), and is non-reducing.[59] It also shows strong resistance to hydrolysis, attributed to the very low energy content of its glycosidic bond (1 kcal mol^{-1}).[60]

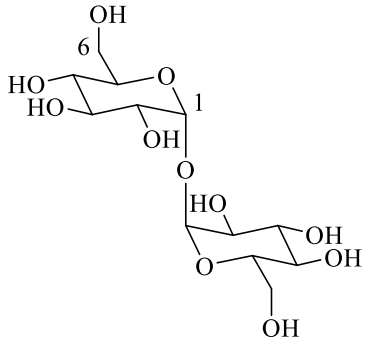

Figure 1.11: Chemical structure of α,α-D-trehalose

Trehalose was considered too expensive to extract from natural products or synthesise industrially in any meaningful quantities. It has only been synthesised industrially since 1994, and in 2000 the process was refined to utilise and break down of longer starch chains.[61, 62]

This viable method of synthesis, combined with the desirable physical properties led to an increase of trehalose in commercial applications. These include in cosmetics as an active surface ingredient, storage stabiliser and odour masker; within food as a flavour enhancer and preservative; and in pharmaceuticals as a dietary sugar and tablet binder.[63]

Furthermore, trehalose is utilised in a host of biomedical applications. It has been shown to be an effective stabiliser of proteins, enzymes and viruses within vaccines, extending their shelf lives.[63-65] It is also being developed for use in cryopreservation of organs awaiting transplant, reducing damage to soft tissues during long term storage as evidenced with human lungs and pancreas.[66, 67]

The fact that trehalose affords the same core skeleton structure, reactivity and solubility properties as HEC, whilst being significantly more tractable in solution in comparison, make it a suitable model compound in the work reported here to initially evaluate chemical reactions before they are applied to the larger molecular weight molecule of HEC.

1.4.2 2-Hydroxyethyl Cellulose

2-Hydroxyethyl cellulose is a derivative of cellulose, where some or all of the hydroxyl groups on each AGU have been replaced by hydroxyethyl ether groups. This modification imparts water solubility to the molecule, in comparison to unmodified cellulose which is water insoluble. In the synthesis of HEC (Scheme 1.9), cellulose is reacted with sodium hydroxide in order to produce swollen alkali cellulose slurry. This alkali-treated cellulose is much more chemically reactive than cellulose. Ethylene oxide is then added, upon which the strained three-

membered ring undergoes ring-opening with the cellulose to form ether linkages. Once a hydroxyethyl unit is attached, it can further react with additional molecules of ethylene oxide. This reaction can theoretically continue as long as there is ethylene oxide monomer present in the reaction mixture.[68]

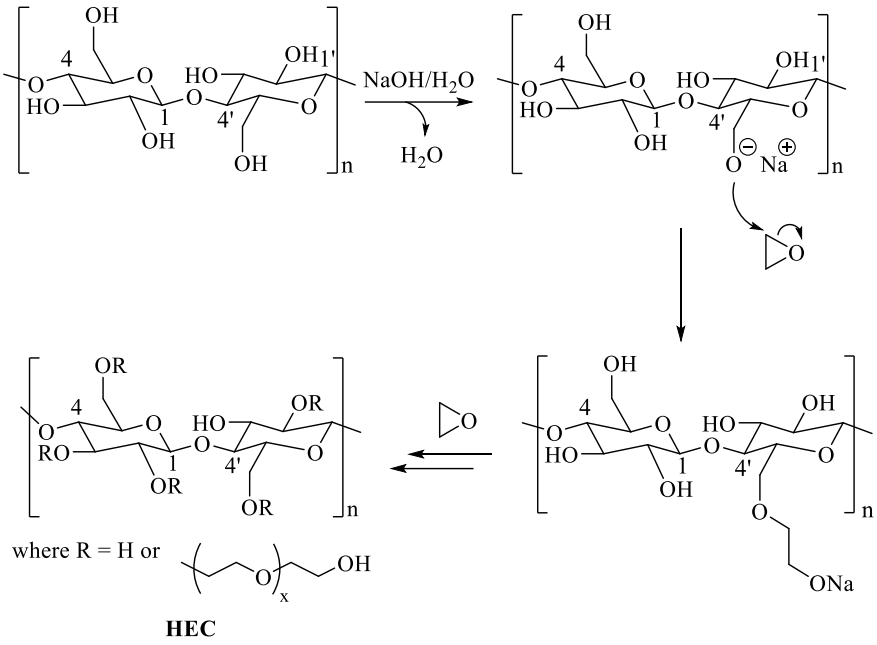

Scheme 1.9: Synthesis of hydroxyethyl cellulose (HEC)

HEC is an FDA approved, non-ionic polymer that is utilised in a range of applications, as it can thicken, bind, emulsify, stabilise, retain water and is film forming.[69, 70] It is used in cosmetics and personal care products such as shampoos and lotions as a thickener and emulsifier, providing the feeling of wetness whilst allowing easy dispersion when applied to the body. In food applications, it is not only utilised as a thickener and binder, but also as a stabiliser in ice creams and frozen desserts, preventing the formation of large ice crystals due to its ability to readily bind water.

When combined with certain surfactants, HEC shows an increase in its thixotropic behaviour,[71] meaning that although the fluid is viscous when stationary, it will flow more easily when agitated or exposed to shear stresses. HEC has also been shown to undergo silylation reactions to afford hydrophobic trimethylsilyl capped side chains, Scheme 1.10, resulting in silylation conversion yields of approximately 80%. This was done in an attempt to impart solubility in common organic solvents such as toluene.[72]

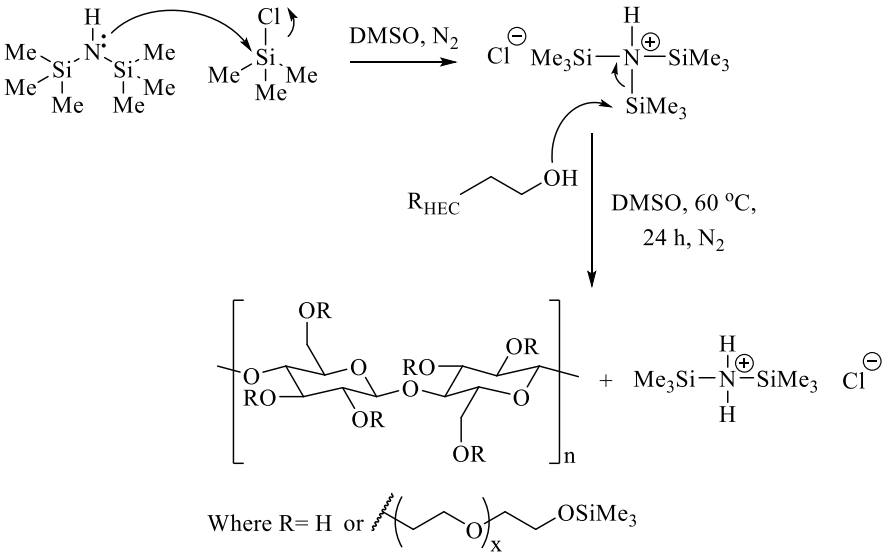

Scheme 1.10: Synthesis of trimethylsilyl capped HEC

HEC is also a popular saccharide utilised in hydraulic fracturing fluid applications, due to its solubility in water and fluid thickening ability. However, due to the hydroxyl groups on HEC being in the *trans* configuration relative to each other, it cannot undergo crosslinking and therefore is used only as a linear gel viscosifier.[35] As a result of this, higher concentrations of HEC are required in order to obtain a more viscous fluid, which is not cost effective. Further chemical modification of HEC is therefore required to impart functionality that will allow HEC to participate in crosslinking reactions.

1.5 Click Chemistry

The term "Click" chemistry was introduced by Sharpless *et al.* in 2001 to describe a class of chemical reactions with a modular approach to synthesis.[73] It describes a way of generating complex products by linking together smaller molecules *via* heteroatoms. The overall methodology is inspired by nature, which also generates substances by joining together small modular units.

Desirable criteria in order for a reaction to be useful in the context of Click chemistry as defined by Sharpless *et al.* are that: it is modular, with simple reaction conditions; high chemical product yields are afforded; it is insensitive to oxygen and moisture from the atmosphere; it is stereospecific; it can be performed in bulk, or if a solvent is used it should be benign or easily removed; it affords products that are easily isolated by non-chromatographic methods (such as recrystallisation or distillation); and only inoffensive by-products are formed.

In essence, the term “Click” is synonymous with simplicity and efficiency, where “spring-loaded” reactants give particular products through reactions with a large thermodynamic driving force (>20 kcal mol^{-1}) and high reaction rates.

The last few years have seen the development of a Click toolbox, which includes, for example, Diels-Alder cycloadditions, oxime formation, copper(I)-catalysed Huisgen azide-alkyne cycloadditions (CuAAC) and thiol-ene additions.[74, 75] The work in this thesis utilises thiol-ene Click chemistry. However, CuAAC has become most popular Click reaction to date, being defined by Sharpless as “the premier example of a Click reaction.”[76] Hence, the term “Click” chemistry is almost exclusively used to denote this reaction.

1.5.1 Azide-Alkyne Cycloaddition Click Chemistry

The formation of triazole systems was first reported by Michael in the 1890’s. It was not until the 1960’s the full scope and mechanism of these 1,3-dipolar cycloadditions were realised by Huisgen, after studies of their reaction conditions and kinetics were carried out.[77, 78] The standard, non-catalysed reaction is slow, not regioselective and requires high temperatures in order to reach satisfactory yields.[77] The reaction affords a mixture of 1,4- and 1,5- triazole adducts, Scheme 1.11.

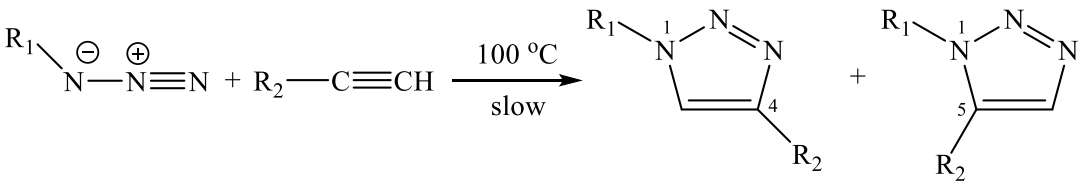

Scheme 1.11: 1,2,3-Triazole formation *via* Huisgen 1,3-dipolar azide-alkyne cycloaddition

The improved copper(I) catalysed Huisgen 1,3-dipolar cycloaddition was discovered in 2002 concurrently by Sharpless *et al.* and Meldal *et al.*[79, 80] The copper(I) catalysed version of this reaction exclusively affords the 1,4- adduct and can be carried out at lower temperatures, Scheme 1.12.

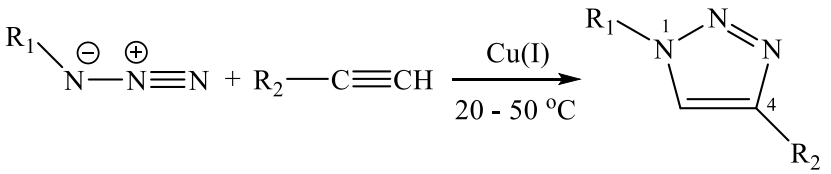

Scheme 1.12: Copper(I) catalysed Huisgen 1,3-dipolar azide-alkyne cycloaddition (CuAAC)

Mechanistic investigations into reactions involving copper are particularly difficult, due to the low reduction potential of copper, it's susceptibility for Cu^{+} species to disproportionate in solution and the tendency of copper complexes to aggregate.[81, 82] Because of this, the mechanism of CuAAC reactions has yet to be fully elucidated, although it has been postulated by kinetic studies and density functional theory calculations that the mechanism is stepwise. The proposed mechanism involves the *in-situ* formation of a σ-bound copper(I) acetylide and formation of an intriguing six-membered metallocycle intermediate.[83, 84] Recent studies have hypothesised the possible involvement of polynuclear copper(I) intermediates.[85, 86] After the initial formation of the σ-bound copper(I) acetylide, the mechanism then utilises a second copper atom that weakly π-bonds to the alkyne in order to form the catalytically active complex, before continuing in the aforementioned stepwise method, Scheme 1.13.

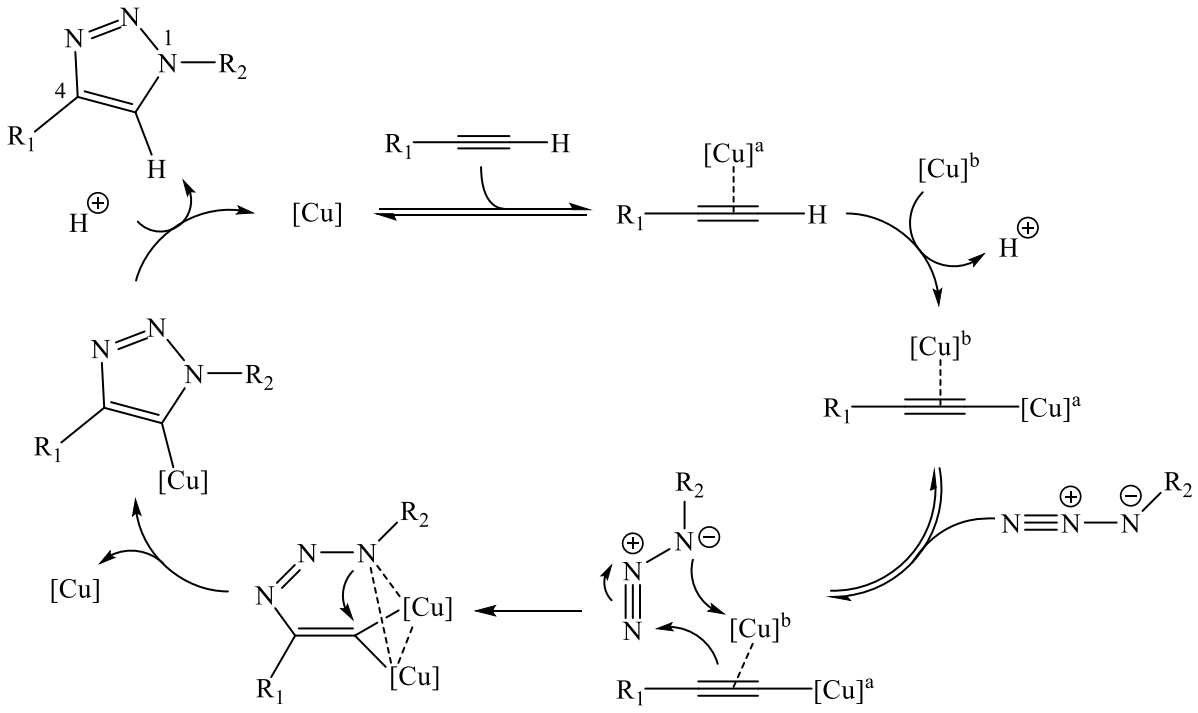

Scheme 1.13: Postulated mechanism for CuAAC with two copper atoms

Worrell *et al.* carried out kinetic experiments in which a mononuclear σ-bound copper(I) acetylide was treated with a stoichiometric amount of azide in the presence or absence of a second copper(I) catalyst ($Cu(PPh_3)_2NO_3$).[86] The reaction progress was tracked by real-time heat flow reaction calorimetry. It was determined that the catalysed cycloaddition rapidly reached completion within 20 min, whereas the non-catalysed reaction showed little conversion within the same timeframe. It was also determined that lowering the concentration of the catalyst also resulted in a decrease in the maximum rate, showing a positive-order dependence

on the added copper species. Furthermore, metal isotope crossover experiments using enriched ^{65}Cu found that the two copper atoms can undergo exchange, leading to the equivalence of the two copper atoms during the cycloaddition steps.

There are a range of methods to generate the active copper catalyst for CuAAC. The most common is the reduction of copper(II) salts to copper(I) salts, such as using copper(II) sulfate pentahydrate with sodium ascorbate.[87] The advantages of this method are that copper(II) salts are inexpensive, the reaction can be performed in water and it does not require a deoxygenated atmosphere.[79]

Another method to generate the catalyst is by the direct addition of Cu(I) salts, such as CuBr, CuI and $[Cu(NCCH_3)_4][PF_6]$, without the need for a reducing agent. However, the disadvantages of this method are that it must be carried out in a deoxygenated atmosphere in order to afford a purer product. This method is conducted in an organic solvent (or co-solvent system), meaning a nitrogen base such as trimethylamine or pyridine is required. [79]

Moves to replace copper with other transition metal catalysts led to $NiCl_2$, $PdCl_2$, and $PtCl_2$ being used in the Click polymer grafting reaction of propargyl ether with azide terminated polystyrene. Although all afforded polymer products, none of them displayed catalytic activity as fast or as great in comparison to CuBr.[88]

In 2005, pentamethylcyclopentadiene ruthenium(II) complexes (Cp*Ru) such as $Cp^*Ru(PPh_3)_2$, were discovered to be good catalysts for azide-alkyne cycloaddition.[89] When $Ru(OAc)_2(PPh_3)_2$ is used, the RuAAC reaction exclusively affords the 1,5-triazole adduct with terminal alkynes, nicely complementing CuAAC. Furthermore, the RuAAC reaction was found to also tolerate internal alkynes, giving rise to the synthesis of 1,4,5-triazole adducts.[90]

1.5.2 Thiol-ene Click Chemistry

Based on the established premise of Click chemistry, the relatively weak sulfur-hydrogen bond of the thiol functional group can undergo chemical reactions with carbon-carbon double bonds (alkenes), resulting in almost quantitative yields under mild conditions. Moreover, these reactions are transition metal free, which make them suitable for *in-vivo* applications, as copper ions are potentially toxic to living organisms.

The concept of the efficient reactions of thiols with alkenes has been well known since the early 1900's,[91] and recently the reaction of thiol-ene free-radical addition, Scheme 1.14, became of particular note.

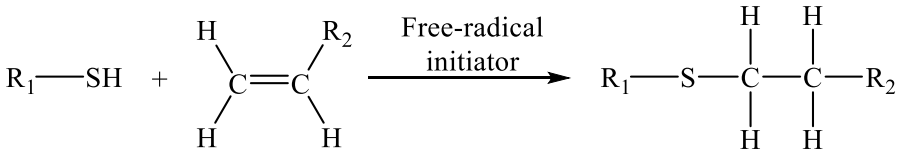

Scheme 1.14: General thiol-ene coupling by free-radical addition reaction

Any sterically unhindered terminal alkene is capable of participating in a radical-mediated thiol-ene reaction, with electron-rich (vinyl ether) and strained (norbornene) alkenes reacting more rapidly than electron-deficient alkenes. The free-radical addition of thiol-ene Click reactions has been known to proceed *via* a step-growth chain process for several decades,[92, 93] the mechanism of which is shown in Scheme 1.15.A. The ideal thiol-ene reaction would consist of only pure step-growth reactions- no homopolymerisation (chain growth), in which the carbon-centred radical propagates through another alkene moiety. Therefore, the overall reaction would simply be the combination of the thiol and alkene functional groups.[94] This has been observed to be the case with norbornenes and vinyl ethers, implying that the overall rates of propagation and chain transfer are essentially identical.[95]

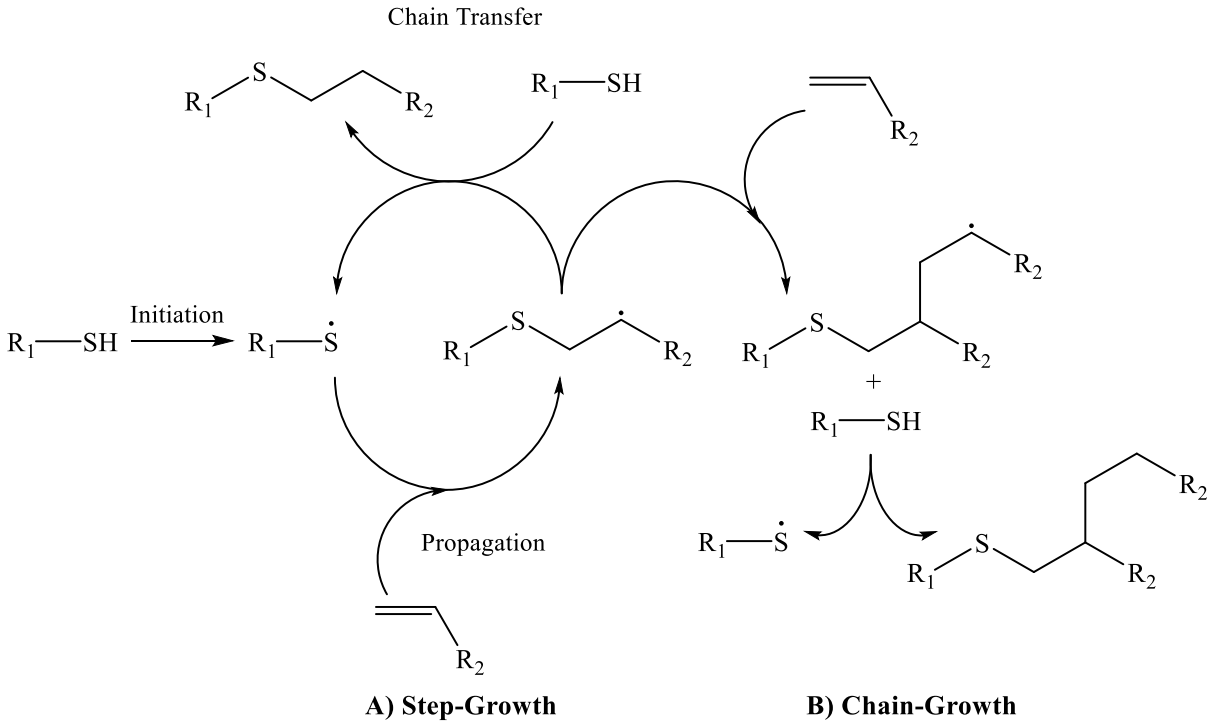

Scheme 1.15: Schematic showing A) an ideal thiol-ene reaction (step-growth) and B) possible homopolymerisation side reactions (chain-growth)

However, investigations into the mechanistic and kinetic properties of thiol-ene reactions revealed that some chain-growth homopolymerisation side reactions (Scheme 1.15.B) can occur, and is more prominent when an electron-deficient alkene is used.[96-98] This class of alkenes includes acrylates, methacrylates, styrene and conjugated dienes.

The chemical properties and concentrations of both the thiol and alkene components, and also the relative rates of the steps labelled in Scheme 1.15 ultimately determine the final polymer network structure.

Thiol-ene reactions require a method of initiation in order to produce a free-radical on the sulfur atom of the thiol group. This radical formation can be photoinduced–irradiation by a UV light source or exposure to natural sunlight are effective methods to initiate the thiol-ene free-radical functionalization process. Light mediated thiol-ene processes can be activated at specific times and locations, giving rise to a powerful method of chemical synthesis and tailorable materials fabrication. In the absence of photoinduction, thermal initiation in combination with the use of a common radical initiator such as azobisisobutyronitrile (AIBN) will also suffice.

1.5.3 Applications of Click Reactions in Polymer Synthesis

CuAAC Click chemistry has been utilised for the synthesis of polymeric materials for biomedical applications, as these reactions can occur under conditions similar to those of biological environments (e.g. aqueous medium, body temperature). Due to concerns over the cytotoxicity of copper, different copper containing species are being developed. Complexes with either water soluble ligands in order to enhance cell penetration, or chelating ligands in order to increase the effective concentration of Cu(I) lead to a reduction of the dosage that is required.[99] The highly polar 1,2,3-triazole rings have very good water solubility, making *in-vivo* administration much easier.[87] As such, CuAAC lends itself well to the synthesis of dendrimers for drug delivery applications, site-specific bioconjugation of peptides and proteins, and labelling of alkyne functionalised virus particles.[77, 100, 101]

Thiol-ene chemistry is being applied in the manufacture of novel self-healing materials, such as protective coatings, paints and hydrogels. These materials are based on the self-healing mechanisms found in biological systems, which have the ability to repair damage using resources inherently available to the system after suffering an injury.[102] In the case of coatings and paints, the thiol and alkene monomers are often encapsulated separately. Upon damage to the coating, the capsules rupture and the contents mix together- the presence of natural light or contact with a catalyst embedded in the matrix triggers the healing reaction, repairing the microcrack, Figure 1.12.[103, 104]

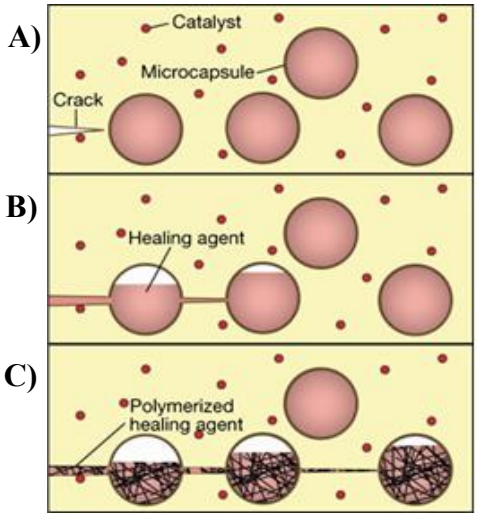

Figure 1.12: The capsule-catalyst self-healing process. Where: A) a crack occurs, B) the capsules rupture as the crack propagates, C) the monomers and embedded catalyst mix together, forming a polymer that heals the crack

Thiol-ene photoinduced polymerisation is also utilised in the development of novel dental fillers, restoratives and adhesives, in a move to replace current dimethacrylate systems. The rapid curing time of the monomers pentaerythritol tetra(3-mercaptopropionate) (PETMP) and triallyl-1,3,5-triazine-2,4,6-trione (TATATO), Scheme 1.16, by UV light makes this system advantageous for both dentist and patient.[105] This polymeric material also affords the desirable properties of lower volumetric shrinkage and good fracture strength compared to the dimethacrylate system.

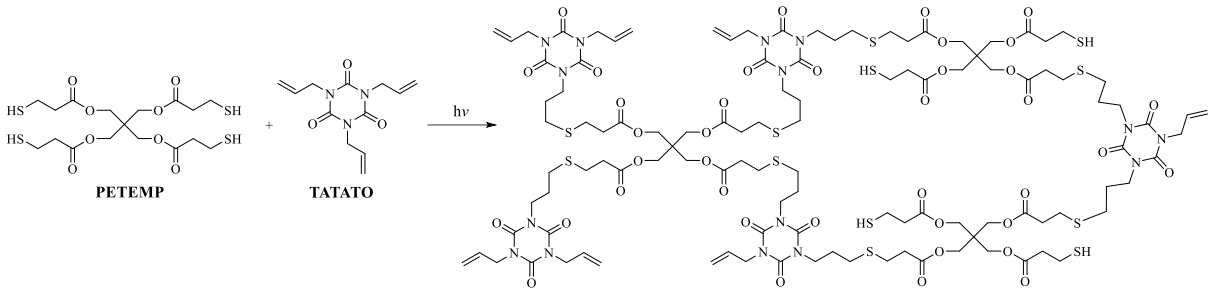

Scheme 1.16: UV mediated thiol-ene Click polymerisation of PETMP and TATATO, resulting in the formation of a polymeric network

1.6 Polymerisation of Glycidol

Glycidol is a small organic molecule that contains both epoxy and hydroxyl functionalities. The strained epoxide ring is highly reactive and will readily undergo ring opening. Glycidol is a latent cyclic AB_2 monomer, where A and B are two different functional groups, and upon ring opening gives two propagating sites.[106] The ring opening polymerisation (ROP) of glycidol leads to the formation of the polyol polyglycerol. The propagation of both the primary and newly formed secondary hydroxyl sites leads to the formation of hyperbranched polyglycerol (Scheme 1.17.A). The term "hyperbranched" was introduced in the late 1980's by Kim and Webster to define dendritic molecules with random branch-on-branch topology prepared using AB_m-type monomers.[107] However, a linear polyglycerol can be synthesised by first protecting the hydroxyl group of glycidol before polymerisation, then performing the subsequent deprotection of the primary hydroxyl groups once the polymer is formed (Scheme 1.17.B).[108]

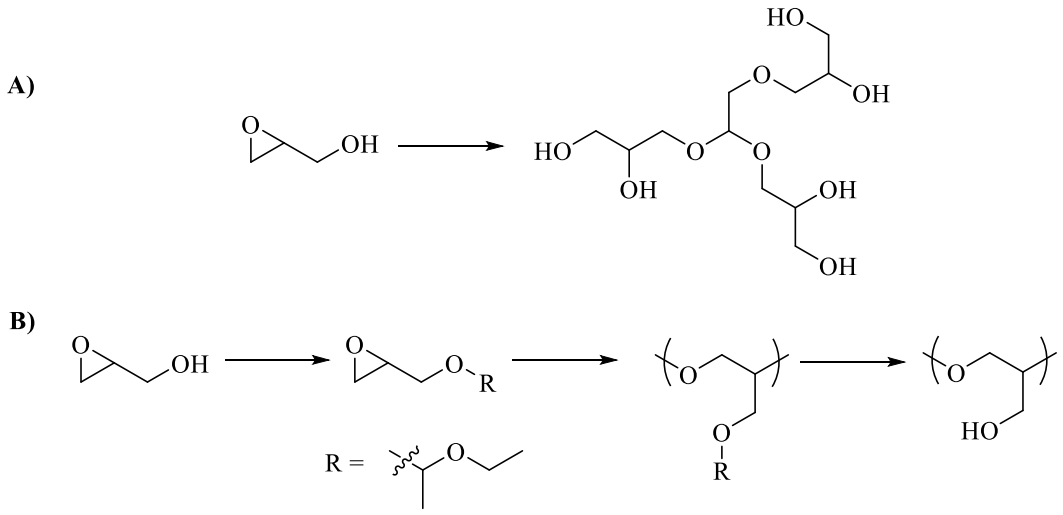

Scheme 1.17: Synthesis of A) hyperbranched and B) linear polyglycerol

Hyperbranched polymers offer an alternative to dendrimers for multifunctional polymeric materials that display high functional group content. An advantage of hyperbranched polymers is that their synthesis is often carried out in a simple single step, therefore avoiding the laborious protection-deprotection stepwise reactions in dendrimer synthesis.[109] However, they do not display the structural perfection of dendrimers, as the functional groups are randomly distributed throughout the polymer, often leading to less uniform molecular weights and high dispersity (Đ) values.[106] The 3D structure of hyperbranched polyglycerol lends itself well to the formation of hydrogels. Polyglycerol is also FDA approved and biocompatible, leading to potential biomedical applications as scaffolds and drug delivery agents.[110] The two most utilised

techniques in the synthesis of hyperbranched polyglycerol materials are by either cationic ROP or anionic ROP.

The incorporation of polyglycerol hyperbranches onto HEC will impart numerous hydroxyl groups within close proximity to each other on a flexible aliphatic polyether backbone. This is anticipated to increase the likelihood of participation of HEC in the non-ionic mechanism of crosslinking with group(IV) metal crosslinkers as shown in Figure 1.9.A. The abundance of hydrophilic hydroxyl groups also affords extremely good solubility of the polyglycerol material in water, as required for application in hydraulic fracturing.[106]

1.6.1 Cationic Method

The mechanism of cationic ROP of glycidol (Scheme 1.18) requires activation of the epoxide ring by an electrophile from either a Lewis acid (BF_3OEt_2, $SnCl_4$) or a monoprotic acid (CF_3COOH, CF_3SO_3H).[111] The epoxide ring can open at two possible positions, as shown by *a* and *b*. The hydroxyl groups then react with further glycidol monomer, propagating the chain.

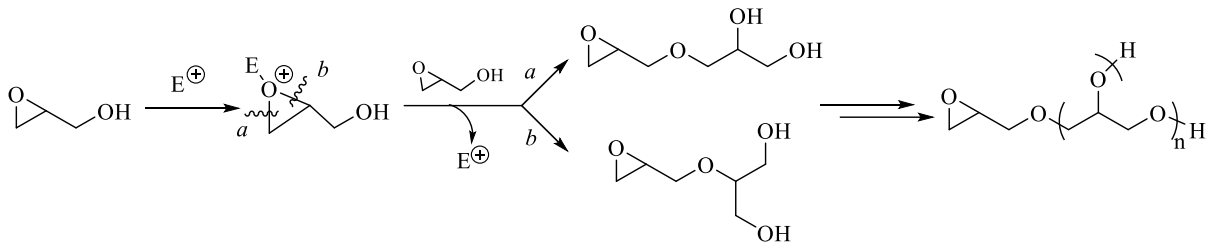

Scheme 1.18: Synthesis of polyglycerol *via* cationic ROP

The polymerisation reaction occurs quickly, however, it is difficult to control. This leads to hyperbranches of low molecular weights (< 6,000 g mol^{-1}), and high Đ values (often > 5).[112] Therefore, this method is rarely used.

1.6.2 Anionic Method

The synthesis of hyperbranched polyglycerol with controlled molecular weight and Đ was first achieved by Sunder *et al.* through anionic ROP.[113] The general mechanism of anionic ROP of glycidol (Scheme 1.19) uses a partially deprotonated initiator, and it is crucial that slow monomer addition conditions are employed in order to obtain a polyether structure in a controlled manner.

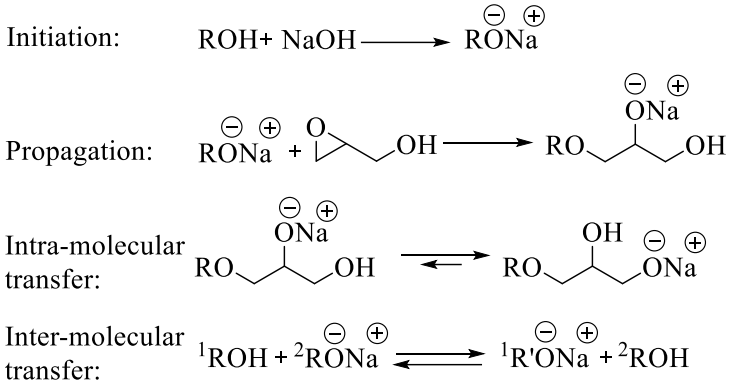

Scheme 1.19: General mechanism of the anionic ROP of glycidol

The mechanism, as described by Vandenberg *et al.*,[114] was found to rapidly undergo both inter- and intra-molecular exchange equilibria in protonation and deprotonation processes to form primary and secondary alkoxide anions. It is the primary alkoxide active sites which can then readily further propagate, resulting in branched glycerol structures. These conditions led to the complete incorporation of the alkoxide initiator into the hyperbranched macromolecules, affording polyglycerols with values of Đ below 1.5.

One problem encountered during the polymerisation of AB_2 monomers is the decrease in concentration of active propagating sites as the reaction proceeds, which limits the reaction. To counteract this, polyfunctional macroinitiator cores comprised of multiple potential initiation sites are often used, such as polyol oligomers (triols) or hyperbranched polyglycerols, allowing higher molecular weights to be achieved.[115] The use of these types of core also has the benefit of bestowing chain-growth-like kinetics,[116] greater control of the molecular weight *via* the monomer/core ratio and also greatly reduces Đ.[106] Another problem encountered in anionic ROP is the formation of cyclic products by the intramolecular ring opening of a glycidol molecule acting as an initiator. This only occurs if no initiator is used, or if the concentration of the monomer is considerably higher than that of the initiator.[113]

1.7 Polymerisation of ε-Caprolactone

Polyesters can be prepared either through the polycondensation of compounds containing both hydroxyl and carboxylic acid groups, or by the ring opening polymerisation (ROP) of cyclic esters. The synthesis of polycaprolactone (PCL) can occur through the polycondensation of 6-hydroxyhexanoic acid, or the ROP of ε-caprolactone, Scheme 1.20.

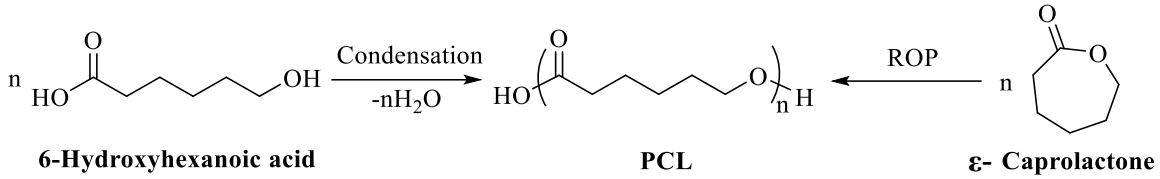

Scheme 1.20: Synthesis of PCL *via* the polycondensation of 6-hydroxyhexanoic acid, or *via* the ROP of ε-caprolactone

PCL is a semi-crystalline aliphatic polyester, and can have a crystallinity of up to 69%.[117] Its physical, mechanical and thermal properties are determined by the number of repeat units and degree of crystallinity. It is approved by the FDA, is biodegradable and biocompatible, due to the presence of hydrolysable ester linkages under physiological conditions.[118] PCL is utilised in a wide range of applications, including thermoplastic packaging, feedstock in 3D printing, controlled drug delivery systems and medical implants and sutures.[119]

Upon the grafting of PCL to HEC, the hydroxyl end groups will be further away from the backbone on flexible chains, reducing steric hindrance, thus increasing the likelihood of interacting with group(IV) metal ions of crosslinking agents.

1.7.1 Polycondensation

The synthesis of PCL *via* polycondensation was achieved in the 1990's by Braud *et al.*[120] The reaction was performed without the addition of catalyst, and required high temperatures of 150 $^{\circ}$C and vacuum distillation to drive the equilibrium to the formation of polymer. However, this method only resulted in the formation of oligomers and small chain polymers with average molecular weights of below 1000 g mol^{-1}.

1.7.2 Ring Opening Polymerisation of ε-CL

The general mechanism for ROP of ε-CL involves either initiation by anionic, cationic or coordination-insertion mechanisms. The thermodynamic driving force in relieving ring strain helps with the ring-opening of the ε-caprolactone monomer. The aforementioned ROP

mechanisms allow the synthesis of higher molecular weight polymers to be achieved and it is preferred over the polycondensation technique.

1.7.2.1 Anionic Method

The mechanism of anionic ROP (Scheme 1.21) requires the formation of an anionic species (usually from an organometallic compound) which attacks the carbonyl carbon atom of ε-caprolactone. Ring opening occurs at the ester linkage, leading to an alkoxide propagating species, with the attached metal atom stabilising the anionic charge of the oxygen.

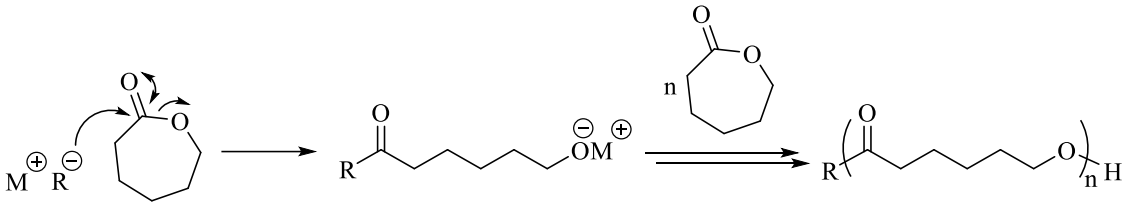

Scheme 1.21: Synthesis of PCL *via* anionic ROP

This method is rarely used as the propagating species is susceptible to transesterification reactions, or "back-biting", in later stages of the reaction.[118] This leads to the formation of cyclic polymers, or low molecular weight polymers if the reaction is quenched before back-biting can occur. It was found that the most common undesired side-products had molecular weights of 342 g mol^{-1} and 456 g mol^{-1}, corresponding to cyclic trimers and tetramers, respectively.[121]

1.7.2.2 Cationic Method

The mechanism of cationic ROP (Scheme 1.22) involves the coordination of a cationic species to the oxygen atom of the ester linkage. The carbon atom of the carbonyl group is attacked by another molecule of ε-caprolactone in an S_N2 reaction.[122]

Initiators used in the formation of the cationic species include trifluoromethanesulfonic acid and trifluoromethanesulfonate alkyls, however, this method affords poor control of the polymerisation and reaction times are often long even at higher temperatures.[123, 124] Therefore, this method is rarely used.

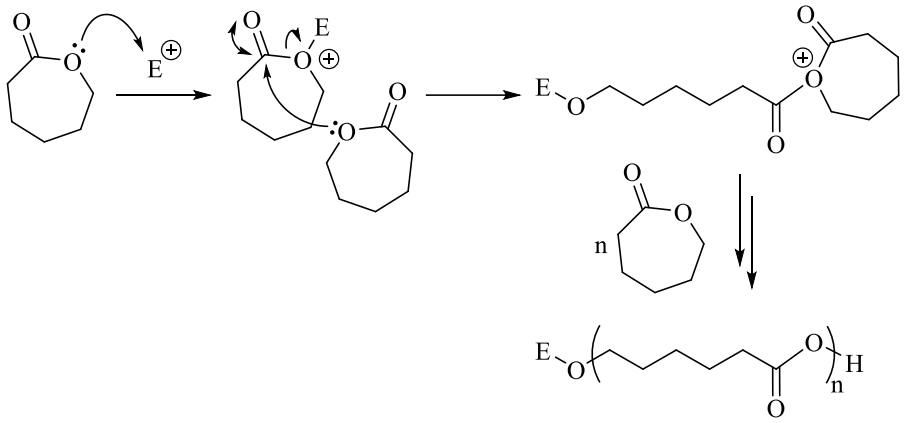

Scheme 1.22: Synthesis of PCL *via* cationic ROP

1.7.2.3 Coordination-Insertion Method

Coordination-insertion ROP is the most popular approach, as it is facile and produces high molecular weight polymers. A metal alkoxide initiator is required, such as $R_nAl(OR')_{2-n}$, $R_nSn(OR')_{3-n}$, $Fe(OR)_3$ or $Ti(OR)_4$.[125] The most widely used catalyst is tin(II) 2-ethylhexanoate ($Sn(Oct)_2$), Figure 1.13, due to its wide commercial availability, FDA approval, ease of use and solubility in common organic solvents.

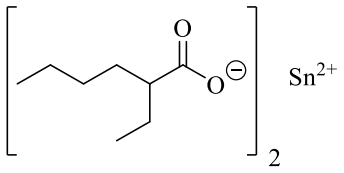

Figure 1.13: Structure of $Sn(Oct)_2$

The mechanism of coordination-insertion ROP (Scheme 1.23) is believed to proceed by the combination of $Sn(Oct)_2$ with a molecule containing a nucleophilic hydroxyl group in order to form the initiating tin complex.[118, 126]

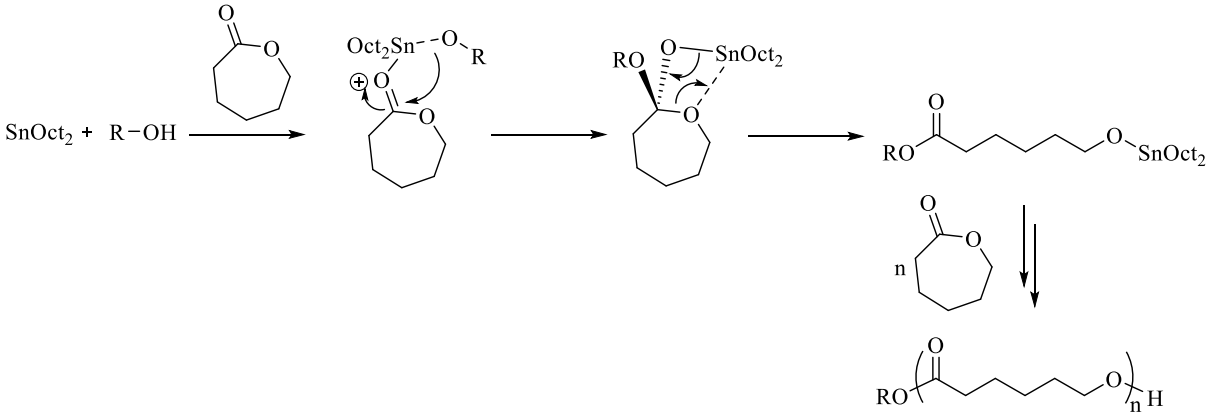

Scheme 1.23: Synthesis of PCL *via* coordination-insertion ROP

The initiating tin complex coordinates to the carbonyl group of ε-caprolactone, followed by monomer insertion into the metal chain end and cleavage of the acyl-oxygen bond. Propagation proceeds by insertion of a new ε-caprolactone monomer, throughout which the growing chain is attached to the metal *via* an alkoxide bond.

Polymers over a range of molecular weights (from 7,200 g mol^{-1} to 58,100 g mol^{-1}) have been prepared using $Sn(Oct)_2$ as catalyst, affording narrow dispersity (Đ) values of 1.1-1.6.[127] One disadvantage of initiation by $Sn(Oct)_2$ is that high temperatures are required in order for the ROP reaction to proceed. This increases the probability of transesterification and back-biting reactions occurring, which could lead to broad Đ values.[128]

1.8 Aims

2-Hydroxyethyl cellulose (HEC) is a form of modified cellulose utilised in fracturing fluid applications as a linear viscosifier. It is FDA approved, water soluble and commercially available at low cost. However, it cannot participate in crosslinking reactions with group(IV) metal-based crosslinkers due to the C_2 and C_3 hydroxyl groups on the backbone being in the *trans* configuration relative to each other.

This project involves further chemical modifications of the highly reactive primary hydroxyl groups of HEC to give rise to possible reaction sites with group(IV) metal-based crosslinkers, leading to the formation of viscous gel materials and possible applications in hydraulic fracturing. This is to offer an alternative to guar, a popular crosslinkable polysaccharide that is obtained from natural products and used routinely in fracturing applications. The motivation here is that the availability of guar is often cast in doubt from year to year due to fluctuating crop harvests, leading to inflated costs.

The disaccharide trehalose is to be utilised as a model compound, as it affords the core skeleton structure, reactivity and solubility properties as HEC. Selective tosylation of the primary hydroxyl groups shall provide good leaving groups for substitution reactions to occur with thiol containing molecules. Acetylation of the secondary hydroxyl groups is predicted to afford easier isolation of the hydrophobic products. The thiolated saccharides will be able to undergo thiol-ene Click reactions with alkenes containing a catecholic moiety. The catechol functional group is anticipated to chelate to metal ion centres, allowing crosslinking with titanium and zirconium based crosslinking agents to occur.

The attachment of the small molecule IBPA by condensation reaction should impart diol "hook" functionality, and the ring-opening of succinic anhydride should impart carboxylic acid functionality to HEC. It is expected that the attachment of these groups will allow crosslinking with metal ions *via* covalent linkages or chelation, respectively.

The use of HEC as a macroinitiator in the anionic ring-opening polymerisation of glycidol should lead to grafting of polyglycerol hyperbranches containing an abundance of primary and secondary hydroxyl functionalities in close proximity to each other, promoting crosslinking reaction with group(IV) metal ions. Furthermore, these HEC-*g*-polyglycerol materials can be used as macroinitiators in the $Sn(Oct)_2$ catalysed ROP of ε-caprolactone, to afford novel graft copolymer materials containing varying PCL arm lengths. The long PCL chains mean that the hydroxyl end groups are further away from the HEC backbone. Therefore, the end groups should be readily accessible as they are less sterically hindered, increasing the likelihood of participation in crosslinking reactions with group(IV) metal ions.

Ideally, crosslinking of the functionalised HEC polymers should occur when present within the range of 0.35-2.0 wt.% in aqueous solution.[129] The functionalised polymers should crosslink at pH 5.3 when an α-hydroxycarboxylic acid-based zirconate crosslinker is used, or pH 10.25 when a triethanolamine-based zirconate is used. These pH values were determined by Catalytic Technologies Ltd. to provide the optimum efficacy for the respective crosslinkers.

1.9 References

1. M. J. Economides, K. G. Nolte, *Reservoir Stimulation*, 3rd ed., John Wiley and Sons, Sussex, **2000**.
2. "Injection Wells: An Introduction to Their Use, Operation, and Regulation", Groundwater Protection Council, Oklahoma City, OK, **2006.**
3. L. D. Underwood, M. L. Payne, *Petroleum Well Construction*, John Wiley and Sons, USA, **1997**, 37-40.
4. S. McSurdy, "State Oil and Natural Gas Regulations Designed to Protect Water Resources", US Department of Energy, USA, **2009.**
5. D. Jarvie, "Evaluation of Hydrocarbon Generation in the Barnett Shale", Humble Geochemical Services, USA, **2004.**
6. R. Jasinski, D. Redwine, G. Rose, *J. Polym. Sci. Part B Polym. Phys.*, **1996**, *34*, 1477.
7. N. Goel, S. N. Shah, W. L. Yuan, E. A. O'Rear, *J. Appl. Polym. Sci.*, **2001**, *82*, 2978.
8. J. Weaver, E. Schonelzl, M. Jamieson, G. Schiffner, in *SPE Gas Technology Symposium*, Calgary, Alberta, Canada, **2002**.
9. J. D. Arthur, "Evaluating the Environmental Implications of Hydraulic Fracturing in Shale Gas Reservoirs", ALL Consulting, Tulsa, OK, **2008.**
10. "Modern Shale Gas Development in the United States: A Primer", Ground Water Protection Council, USA, **2009.**
11. J. Penny, "ISO 13503-2", International Organization for Standardization, Switzerland, **2006.**
12. J. R. Hellman, B. E. Scheetz, W. G. Luscher, D. G. Hartwich, R. P. Koseski, *Am. Ceram. Soc. Bull.*, **2014**, 28.
13. What is Hydraulic Fracturing?, https://www.earthworksaction.org/issues/detail/hydraulic_fracturing_101#.WDLgVrniu1U, (Accessed 17/11/2016).
14. F. Liang, M. Sayed, G. A. Al-Muntasheri, F. F. Chang, L. Li, *Petroleum,* **2016**, *2*, 26.
15. A. R. Rickards, H. D. Brannon, W. D. Wood, C. J. Stephenson, Annual Technical Conference and Exhibition Denver, Colorado, **2003**, *Paper SPE-115258*.
16. J. Bicerano, US 20070161515 A1, **2007.**
17. P. C. Harris, *J. Petrol. Tech.*, **1988**, *40*, 1277.
18. "Chemicals Used in Hydraulic Fracturing", FracFocus Chemical Disclosure Registry, Oklahoma, USA, **2012.**

19. "Analysis of Hydraulic Fracturing Fluid Data", US Environmental Protection Agency, Washington, DC, **2015.**
20. D. Klemm, B. Heublein, H.-P. Fink, A. Bohn, *Angew. Chem. Int. Ed.*, **2005**, *44*, 3358.
21. D. Roy, M. Semsarilar, J. T. Guthrie, S. Perrier, *Chem. Soc. Rev.*, **2009**, *38*, 2046.
22. S. Kalia, A. Dufresne, B. M. Cherian, B. S. Kaith, L. Averous, J. Njuguna, E. Nassiopoulos, *Int. J. Polym. Sci.*, **2011**, *2011*, 1.
23. V. K. Varshney, S. Naithani, in *Cellulose Fibers: Bio- and Nano-Polymer Composites*, Springer, Berlin, **2011**, 43.
24. R. Swatloski, J. Holbrey, S. Spear, R. Rogers, *Electrochem. Soc. Proc.*, **2002**, *19*, 155.
25. P. J. Wakelyn, *Handbook of Fiber Chemistry*, Marcel Dekker, New York, **1998**, 642–654.
26. G. Tegge, *Starch - Stärke*, **1981**, *33*, 432.
27. T. P. Nevell, S. H. Zeronian, *Cellulose Chemistry and Its Applications*, Ellis Horwood Limited, Chichester, **1985**.
28. S. Kamel, N. Ali, K. Jahangir, S. M. Shah, A. A. El-Gendy, *Exp. Polym. Lett.*, **2008**, *2*, 758.
29. L. C.Wadworth, D. Daponte, in *Cellulose Chemistry and its Applications* (Eds.: T. P. Nevell, S. H. Zeronian), Ellis Horwood, Chichester, **1985**, 349–362.
30. D. Mudgil, S. Barak, B. S. Khatkar, *J. Food. Sci. Technol.*, **2014**, *51*, 409.
31. X. Wu, Y. Ye, Y. Chen, B. Ding, J. Cui, B. Jiang, *Carbohyd. Polym.*, **2010**, *80*, 1178.
32. K. Behari, R. Kumar, M. Tripathi, K. P. Pandey, *Macromol. Chem. Phys.*, **2001**, *202*, 1873.
33. M. B. Smith, J. March, *March's Advanced Organic Chemistry: Reactions, Mechanisms and Structure*, 6th ed., Momo Peon & Sons, Inc., Hoboken, NJ, **2007**.
34. C. Lei, P. E. Clark, *J. Soc. Petrol. Eng.*, **2007**, 316.
35. C. Montgomery, in *Effective and Sustainable Hydraulic Fracturing* (Eds.: A. P. Bunger, J. McLennan, R. Jeffrey), InTech, **2013**, 25.
36. Guar Pricing and History, http://sriguargum.com/products/guar-pricing-history/, (Accessed 19/11/2016).
37. C. Trostle, PhD Thesis, Texas A&M University, **2013**.
38. P. C. Harris, *J. Petrol. Tech.*, **1988**, *SPE 17112*, 1277.
39. K. Armstrong, R. Card, R. Navarrete, E. Nelson, K. Nimerick, M. Samuelson, "Advanced Fracturing Fluids Improve Well Economics ", Schlumberger, Oklahoma, USA, **1995.**

40. D. N. Harry, F. Malekahmadi, C. Gallagher, US 20150094239 A1, **2013.**
41. A. Bahamdan, PhD Thesis, Louisiana State University, **2005**.
42. D. N. Harry, D. E. Putzig, R. Moorhouse, T. DelPesco, P. Jernakoff, in *SPE International Symposium on Oilfield Chemistry, Vol. SPE 50731*, Houston, Texas, **1999**.
43. R. Moorhouse, D. N. Harry, U. Merchant, SPE India Oil and Gas Conference and Exhibition, New Delhi, India, **1998**, *SPE 39531*.
44. D. E. Vaughn, R. H. Duncan, D. N. Harry, D. A. Williams, US2009/0288828 A1, **2009.**
45. L. R. Norman, J. R. Carlise, J. J. C. Corbea, J. William S. Rees, M. Weck, US 7595391 B2, **2009.**
46. G. A. Al-Muntasheri, *SPE Prod. Oper.*, **2014**, *November 2014*, 243.
47. D. E. Putzig, J. D. St.Clair, in *Hydraulic Fracturing Technology Conference, Vol. SPE 105066*, Houston, Texas, USA, **2007**.
48. N. Goel, PhD Thesis, University of Oklahoma, **2001**.
49. D. Peter, T. S. Ertel, H. Bertagnolli, *J. Sol-Gel Sci. Technol.*, **1994**, *3*, 91.
50. C. J. Brinker, G. W. Scherer, *Sol-gel Science: The Physics and Chemistry of Sol-gel Processing*, Academic Press, London, **1990**.
51. G. I. Spijksma, *Modification of Zirconium and Hafnium Alkoxides*, Enschede, The Netherlands, **2006**, 18-21.
52. M. T. Harris, A. Singhal, J. L. Look, J. R. Smith-Kristensen, J. S. Lin, L. M. Toth, *J. Sol-Gel Sci. Technol.*, **1997**, *8*, 41.
53. V. G. Kessler, G. I. Spijksma, G. A. Seisenbaeva, S. Hakansson, D. H. A. Blank, H. J. M. Bouwmeester, *J. Sol-Gel Sci. Technol.*, **2006**, *40*, 163.
54. K. C. Fortner, J. P. Bigi, S. N. Brown, *Inorganic Chemistry*, **2005**, *44*, 2803.
55. N. Y. Turova, E. P. Turevskaya, V. G. Kessler, M. I. Yanovskaya, *The Chemistry of Metal Alkoxides*, Kluwer Academic Publishers, Norwell, MA, USA, **2002**.
56. V. W. Day, T. A. Eberspacher, W. G. Klemperer, C. W. Park, F. S. Rosenberg, *J. Am. Chem. Soc.*, **1991**, *113*, 8190.
57. G. Zhang, C. Liu, D.-L. Long, L. Cronin, C.-H. Tung, Y. Wang, *J. Am. Chem. Soc.*, **2016**, *138*, 11097.
58. A. B. Richards, S. Krakowka, L. B. Dexter, H. Schmid, A. P. M. Wolterbeek, D. H. Waalkens-Berendsen, A. Shigoyuki, M. Kurimoto, *Food Chem. Toxicol.*, **2002**, *40*, 871.
59. M. Walmagh, R. Zhao, T. Desmet, *Int. J. Mol. Sci.*, **2015**, *16*, 13729.
60. B. Roser, *Biopharm. Technol. Bus. Biopharm.*, **1991**, *4*, 47.

61. M. J. Paul, L. F. Primavesi, D. Jhurreea, Y. Zhang, *Annu. Rev. Plant Biol.*, **2008**, *59*, 417.
62. T. Higashiyama, A. B. Richards, in *Sweeteners and Sugar Alternatives in Food Technology*, Wiley-Blackwell, **2012**, 417-431.
63. S. Ohtake, Y. J. Wang, *J. Pharm. Sci.*, **2010**, *100*, 2020.
64. S. Ohtake, C. Schebor, S. P. Palecek, J. J. d. Pablo, *Cryobiology*, **2004**, *48*, 81.
65. E. A. Corbanie, J. P. Remon, K. V. Reeth, W. J. Landman, J. H. v. Eck, C. Vervaet, *Vaccine*, **2007**, *25*, 8306.
66. T. Bando, J. M. Albes, T. Nusse, H. Wada, S. Hitomi, T. Wahlers, H. Schafers, *Euro. Surg. Res.*, **1998**, *30*, 297.
67. G. M. Beattie, J. H. Crowe, A. D. Lopez, V. Cirulli, C. Ricordi, A. Hayek, *Diabetes*, **1997**, *46*, 519.
68. T. Heinze, K. Petzold, in *Monomers, Polymers and Composites from Renewable Resources* (Eds.: M. N. Belgacem, A. Gandini), Elsevier, New York, **2008**, 343-368.
69. W. Sun, D. Sun, Y. Wei, S. Liu, S. Zhang, *J. Colloid Interface Sci.*, **2007**, *311*, 228.
70. S. Erkselius, O. J. Karlsson, *Carbohydr. Polym.*, **2005**, *62*, 344.
71. U. Kastner, H. Hoffmann, R. Donges, R. Ehrler, *Colloids Surfaces A. Physicoehem. Eng. Aspects* **1996**, *112*, 209.
72. C. Jiang, X. Wang, P. Sun, C. Yang, *Int. J. Bio. Macromol.*, **2011**, *48*, 210.
73. H. C. Kolb, M. G. Finn, K. B. Sharpless, *Angew. Chem. Int. Ed.*, **2001**, *40*, 2004.
74. J. E. Moses, A. D. Moorhouse, *Chem. Soc. Rev.*, **2007**, *36*, 1249.
75. J.-F. Lutz, H. Schlaad, *Polymer*, **2008**, *49*, 817.
76. H. C. Kolb, K. B. Sharpless, *Drug Discov. Today*, **2003**, *8*, 1128.
77. L. Liang, D. Astruc, *Coord. Chem. Rev.*, **2011**, *255*, 2933.
78. R. Huisgen, *Proceedings of the Chemical Society of London*, **1961**, 357.
79. V. V. Rostovtsev, L. G. Green, V. V. Fokin, K. B. Sharpless, *Angew. Chem. Int. Ed.*, **2002**, *41*, 2596.
80. C. W. Tornøe, C. Christensen, M. Meldal, *J. Org. Chem.*, **2002**, *67*, 3057.
81. W. M. Haynes, *CRC Handbook of Chemistry and Physics* 93 ed., CRC Press, Boca Raton, USA, **2012**.
82. A. Moen, D. G. Nicholson, *J. Chem. Soc., Faraday Trans.*, **1995**, *91*, 3529.
83. F. Himo, T. Lovell, R. Hilgraf, V. V. Rostovtsev, L. Noodleman, K. B. Sharpless, V. V. Fokin, *J. Am. Chem. Soc.*, **2005**, *127*, 210.
84. V. O. Rodionov, V. V. Fokin, M. G. Finn, *Angew. Chem. Int. Ed.*, **2005**, *44*, 2210.

85. G.-C. Kuang, P. M. Guha, W. S. Brotherton, J. T. Simmons, L. A. Stankee, B. T. Nguyen, R. J. Clark, L. Zhu, *J. Am. Chem. Soc.*, **2011**, *133*, 13984.
86. B. T. Worrell, J. A. Malik, V. V. Fokin, *Science*, **2013**, *340*, 457.
87. V. D. Bock, H. Hiemstra, J. H. v. Maarseveen, *Euro. J. Org. Chem.*, **2006**, *1*, 51.
88. P. L. Golas, N. V. Tsarevsky, B. S. Sumerlin, K. Matyjaszewski, *Macromolecules*, **2006**, *39*, 6451.
89. L. Zhang, X. Chen, P. Xue, H. H. Y. Sun, I. D. Williams, K. B. Sharpless, V. V. Fokin, G. Jia, *J. Am. Chem. Soc.*, **2005**, *127*, 15998.
90. J. R. Johansson, T. Beke-Somfai, A. Said Stålsmeden, N. Kann, *Chem. Rev.*, **2016**, *116*, 14726.
91. T. Posner, *Ber. Dtsch. Chem. Ges.*, **1905**, *38*, 646.
92. C. R. Morgan, F. Magnotta, A. D. Ketley, *J. Polym. Sci.: Polym. Chem. Ed.*, **1977**, *15*, 627.
93. N. B. Cramer, C. N. Bowman, *J. Polym. Sci. Part A: Polym. Chem.*, **2001**, *39*, 3311.
94. C. N. Bowman, C. E. Hoyle, *Angew. Chem. Int. Ed.*, **2010**, *49*, 1540.
95. N. B. Cramer, S. K. Reddy, A. K. O'Brien, C. N. Bowman, *Macromolecules*, **2003**, *36*, 7964.
96. H. Y. Wei, A. F. Senyurt, S. Jonsson, C. E. Hoyle, *J. Polym. Sci. Part A: Polym. Chem.*, **2007**, *45*, 822.
97. T. Y. Lee, J. Carioscia, Z. Smith, C. N. Bowman, *Macromolecules*, **2007**, *40*, 1473.
98. D. Crich, F. Brebion, V. Krishnamurthy, *Org. Lett.*, **2006**, *8*, 3593.
99. C. Uttamapinant, A. Tangpeerachaikul, S. Grecian, S. Clarke, U. Singh, P. Slade, K. R. Gee, A. Y. Ting, *Angew. Chem. Int. Ed.*, **2012**, *51*, 5852.
100. M. L. Hovlid, J. L. Lau, K. Breitenkamp, C. J. Higginson, B. Laufer, M. Manchester, M. G. Finn, *ACS Nano*, **2014**, *8*, 8003.
101. Craig S. McKay, M. G. Finn, *Cell Chem. Bio.*, **2014**, *21*, 1075.
102. B. J. Blaiszik, S. L. B. Kramer, S. C. Olugebefola, J. S. Moore, N. R. Sottos, S. R. White, *Annu. Rev. Mater.Res.*, **2010**, *40*, 179.
103. E. T. A. van den Dungen, B. Klumperman, *J. Polym. Sci. Part A: Polym. Chem.*, **2010**, *48*, 5215.
104. D. Döhler, P. Michael, W. Binder, in *Self-Healing Polymers: From Principles to Applications* (Ed.: W. Binder), Wiley VHC, **2013**, 7-58.
105. H. Lu, J. A. Carioscia, J. W. Stansbury, C. N. Bowman, *Dent. Mater.*, **2005**, *21*, 1129.
106. D. Wilms, S.-E. Stiriba, H. Frey, *Acc. Chem. Res.*, **2009**, *43*, 129.

107. Y. H. Kim, O. W. Webster, *Polym. Prepr. (Am. Chem. Soc., Div. Polym. Chem.)*, **1988**, *29*, 310.
108. S.-E. Stiriba, H. Kautz, H. Frey, *J. Am. Chem. Soc.*, **2002**, *124*, 9698.
109. C. Gao, D. Yan, *Prog. Polym. Sci.*, **2004**, *29*, 183.
110. M. Calderon, M. A. Quadir, S. K. Sharma, R. Haag, *Adv. Mater.*, **2010**, *22*, 190.
111. R. Tokar, P. Kubisa, S. Penczek, A. Dworak, *Macromolecules*, **1994**, *27*, 320.
112. A. Dworak, W. Walach, B. Trzebicka, *Macromol. Chem. Phys.*, **1995**, *196*, 1963.
113. A. Sunder, R. Hanselmann, H. Frey, R. Mülhaupt, *Macromolecules*, **1999**, *32*, 4240.
114. E. J. Vandenberg, *J. Polym. Sci., Polym. Chem. Ed.*, **1985**, *23*, 915.
115. D. Wilms, F. Wurm, J. Nieberle, P. Böhm, U. Kemmer-Jonas, H. Frey, *Macromolecules*, **2009**, *42*, 3230.
116. R. Hanselmann, D. Hölter, H. Frey, *Macromolecules*, **1998**, *31*, 3790.
117. J. O. Iroh, *Polymer Data Handbook*, Oxford University Press, New York, **1999**, 361-362.
118. M. Labet, W. Thielemans, *Chem. Soc. Rev.*, **2009**, *38*, 3484.
119. R. M. Mohamed, K. Yusoh, *Adv. Mater. Res.*, **2016**, *1134*, 249.
120. C. Braud, R. Devarieux, A. Atlan, C. Ducos, V. Michel, *J. Chrom. B: Biomed. Sci. Appl.*, **1998**, *706*, 73.
121. K. Ito, Y. Hashizuka, Y. Yamashita, *Macromolecules*, **1977**, *10*, 821.
122. H. R. Kricheldorf, J. M. Jonte, R. Dunsing, *Makromol. Chem.*, **1986**, *187*, 771.
123. H. R. Kricheldorf, R. Dunsing, *Makromol. Chem.*, **1986**, *187*, 1611.
124. O. Nuyken, S. D. Pask, *Polymers*, **2013**, *5*, 361.
125. S. Penczek, M. Cypryk, A. Duda, P. Kubisa, S. Słomkowski, *Prog. Polym. Sci.*, **2007**, *32*, 247.
126. Y.-J. Chen, H.-J. Fang, S. C. N. Hsu, N.-Y. Jheng, H.-C. Chang, S.-W. Ou, W.-T. Peng, Y.-C. Lai, J.-Y. Chen, P.-L. Chen, C.-H. Kao, Z.-X. Zeng, J.-L. Chen, H.-Y. Chen, *Polym. Bull.*, **2013**, *70*, 993.
127. M. Sobczak, *Polym. Bull.*, **2012**, *68*, 2219.
128. M. Möller, R. Kånge, J. L. Hedrick, *J. Polym. Sci. A Polym. Chem.*, **2000**, *38*, 2067.
129. G. L. Brode, J. P. Stanley, E. M. Partain, US 0 176 940 B1, **1991**.

Chapter 2

Modification of Trehalose as a Model Compound

2.1 Introduction

Trehalose is a naturally occurring symmetrical disaccharide, composed of two glucose units bound by an α,α-1, 1-linkage. It is stable over a wide pH range, shows high thermal stability and lacks any reducing power.[1] These useful properties have been recognised and trehalose began to be produced on an industrial scale since 1994.[2] In 2000, development of an inexpensive technology refined the process to utilise longer chain starch.[3] As such, the cost of trehalose production was sufficiently reduced to permit widespread application in food, beverages, cosmetics and personal care products, revolutionising the way trehalose was obtained, distributed and consumed.

Trehalose is found in many living organisms, including mushrooms, shrimp and yeasts, protecting against various environmental stresses. It allows certain organisms to survive when 99% of their water content has been removed and then resume their vital functions as soon as contact with water is made.[4] When experiencing the effects of dehydration, it is hypothesised that this survival is achieved by the replacement of water with trehalose in the organism through hydrogen bonding interactions with polar groups on membrane lipids and proteins.[5]

Trehalose is the main component of blood sugar in arthropods, fuelling the rapid energy consumption required for flight in insects. This is due to the efficient release of two molecules of glucose when the linkage is cleaved by the enzyme trehalase in the insect, as opposed to only one glucose molecule when the linkage is cleaved in starch.[6]

The interest in trehalose stemmed from not only its unique properties, but also from its use as a saccharide model compound. It affords the core skeleton structure and functionalities of polysaccharides, in particular 2-hydroxyethyl cellulose (HEC), which will be discussed in detail in chapters 3, 4 and 5. Trehalose also shares similar solubility properties with HEC. This chapter will investigate the thiolation of trehalose and its participation in thiol-ene Click reactions. The characterisation of the products will provide a valuable insight for evaluating thiol-ene Click reactions on HEC.

This chapter will also investigate the formation of titanium complexes with a model catechol moiety and a norbornene-catechol moiety. The aim of this is to show that multiple catechols can chelate to one titanium centre, allowing crosslinking reactions to take place.

2.2 Experimental

2.2.1 Materials

α,α-D-Trehalose dihydrate, *p*-toluenesulfonyl chloride (TsCl), acetic anhydride, pyridine, potassium thioacetate (KSAc), dopamine hydrochloride, 5-norbornene-2-carboxylic acid (98% *endo*), *N,N'*-dicyclohexylcarbodiimide (DCC), 4-(dimethylamino)pyridine (DMAP), potassium methoxide (KOMe), titanium(IV) tetraisopropoxide (TIPT) and 4-methyl catechol (MeCat) were all purchased from Sigma-Aldrich and used without further purification. All dry solvents were obtained from Durham Chemistry Department Solvent Purification System (SPS). All other solvents were analytical grade purchased from Fisher Scientific and used without any purification. The NMR solvents deuterated chloroform ($CDCl_3$), deuterated dimethylsulfoxide (DMSO-d_6) and deuterium oxide (D_2O) were purchased from Apollo Scientific and used as supplied.

2.2.2 Instrumentation and Measurements

^{1}H Nuclear magnetic resonance (NMR) spectra were recorded using Avance-400 or VNMRS 600 spectrometers that operate at 400 MHz and 600 MHz, respectively. ^{13}C NMR spectra were recorded using Avance-400 or VNMRS 600 spectrometers that operate at 100 MHz and 150 MHz, respectively. Measurements of NMR spectra were conducted under ambient temperature; chemical shifts are quoted in ppm, and spectra are referenced to their respective solvent traces: $CDCl_3$ (^{1}H: 7.26 ppm, ^{13}C: 77.0 ppm), DMSO-d_6 (^{1}H: 2.50 ppm, ^{13}C: 39.5 ppm) or D_2O (^{1}H: 4.79 ppm). The following abbreviations are used in describing NMR spectra: s = singlet, d = doublet, t = triplet, q = quartet, m = multiplet, b = broad, dd = doublet of doublets, td = triplet of doublets, o = overlapped. 2D NMR experiments were also used to fully assign the proton and carbon environments in the products. ^{1}H-^{13}C **H**eteronuclear **S**ingle **Q**uantum **C**oherence (HSQC) spectroscopy demonstrated correlation between directly bonded proton and carbons atoms.

Fourier-transform Infrared Spectroscopy (FT-IR) was performed on a PerkinElmer 1600 series FT-IR.

Elemental (CHN) analysis of small molecules were obtained using an Exeter CE-440 elemental analyser *via* the Durham University service.

Electrospray ionisation mass spectra (ESI-MS) were recorded by a TQD mass spectrometer setup for flow injection analysis with an operating mass range of 100-2000 u.

2.2.3 Synthesis of 2,3,4,2',3',4'-Hexa-O-Acetyl-6,6'-Ditosyl-6,6'-Dideoxy-D-Trehalose 2.1

The product **2.1** was prepared based on a known literature procedure.[7] In a dry, two-necked round bottom flask equipped with magnetic stirrer and septum, trehalose dihydrate (3.0 g, 11 mmol) was dissolved in pyridine (50 mL) and kept under N_2 atmosphere. *p*-Toluenesulfonyl chloride (10.0 g, 53 mmol) was dissolved in pyridine (9 mL) and was added slowly, upon which an exotherm occurred and the colour of the reaction mixture changed from lime green to pale yellow. The reaction was stirred for 1 h at ambient temperature, quenched with the addition of acetic anhydride (56 mL, 594 mmol) and stirred for a further 18 h. The resulting dark brown mixture was poured over ice water (600 mL), stirred and the precipitated solid was recovered by filtration. The crude product was recrystallised from methanol twice. The crystals were dried in an oven overnight at 60 ^oC under reduced pressure to give **2.1** as a white solid, mp 170-173 ^oC, yield 15% (1.07 g, 1.2 mmol).

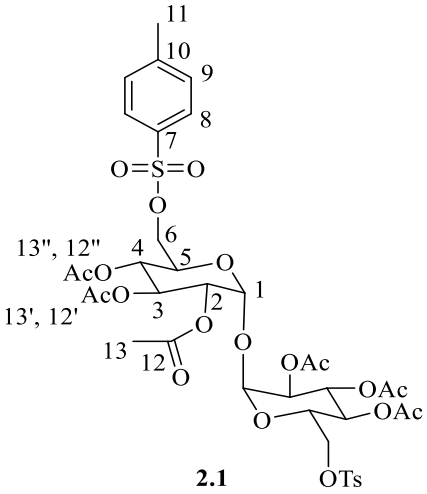

2.1

Figure 2.1: Structure of 2,3,4,2',3',4'-hexa-O-acetyl-6,6'-ditosyl-6,6'-dideoxy-D-trehalose with numerical assignments for NMR

^1H NMR (600 MHz; $CDCl_3$): δ = 7.72 (d, *J* = 12 Hz, 4H, H_8), 7.32 (d, *J* = 12 Hz, 4H, H_9), 5.39 (t, *J* = 9.6 Hz, 2H, H_3), 4.94-4.88 (m, 6H, $H_{1,6}$), 4.11-3.99 (m, 6H, $H_{2,4,5}$), 2.43 (s, 6H, H_{11}), 2.06 (s, 6H); 2.01 (s, 6H); 1.99 (s, 6H) ($H_{13,\ 13',\ 13''}$). ^{13}C NMR (150 MHz; $CDCl_3$): δ = 170.0; 169.7; 169.6 ($C_{12,\ 12',\ 12''}$), 145.4; 132.5; 130.0; 128.2 ($C_{7,\ 8,\ 9,\ 10}$), 92.9 (C_1), 69.9; 69.3; 68.7; 68.3 ($C_{2\text{-}5}$), 67.7 (C_6), 21.8 (C_{11}), 20.7; 20.6; 20.6 ($C_{13,\ 13',\ 13''}$).

FT-IR: ν_{max} = 1740 cm^{-1} (C=O).

CHN: Expected %C = 50.55, %H = 5.14, %N = 0.00; Measured %C = 50.58, %H = 5.14, %N = 0.00.

2.2.4 Synthesis of 2,3,4,2',3',4'-Hexa-O-Acetyl-6,6'-Di-S-Acetyl-6,6'-Dithio-D-Trehalose 2.2

The product **2.2** was prepared based on a known literature procedure.[8] Potassium thioacetate (0.26 g, 2.3 mmol, 2.5 eq.) was added to a solution of protected ditosylated trehalose **2.1** (0.8 g, 0.89 mmol) in dry DMF (50 mL) in a dry two-necked round bottom flask equipped with magnetic stirrer, condenser, and kept under N_2 atmosphere. The mixture was stirred in an oil bath at 70 ^oC for 36 h. The solvent was reduced *in vacuo* to approximately half the volume, and the pale brown mixture poured over ice water (300 mL). The crude precipitated solid was recrystallised from methanol twice. The crystals were dried in an oven overnight at 60 ^oC under reduced pressure to give **2.2** as a light brown solid, mp 151-154 ^oC, yield 74.3% (0.58 g, 0.29 mmol).

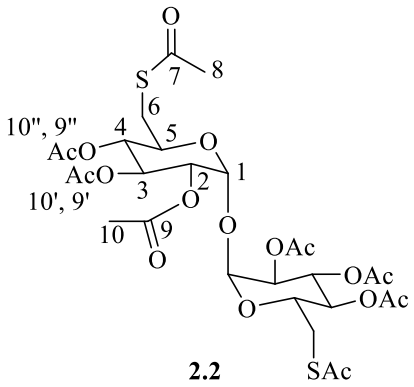

2.2

Figure 2.2: Structure of 2,3,4,2',3',4'-hexa-O-acetyl-6,6'-di-S-acetyl-6,6'-dithio-D-trehalose with numerical assignments for NMR

^1H NMR (600 MHz; $CDCl_3$): δ = 5.42 (apparent t, *J* = 12 Hz, 2H, H_3), 5.24 (d, *J* = 9.1 Hz, 2H, H_1), 4.98 (dd, J_1 = 12 Hz, J_2 = 4.2 Hz, 2H, H_2), 4.91 (apparent t, *J* = 6 Hz, 2H, H_4), 3.75 (t, *J* = 6 Hz, 2H, H_5), 3.18 (dd, *J* = 12 Hz, 2H, H_6), 2.86 (dd, J_1 = 12 Hz, J_2 = 6 Hz, 2H, $H_{6'}$), 2.32 (s, 6H, H_8), 2.07 (s, 6H); 2.03 (s, 6H); 1.99 (s, 6H) ($H_{10,\ 10',\ 10''}$). ^{13}C NMR (150 MHz; $CDCl_3$): δ = 194.82 (C_7), 170.00; 169.9; 169.9 ($C_{9,\ 9',\ 9''}$), 90.6 (C_1), 71.2; 70.0; 69.9; 69.6 ($C_{2\text{-}5}$), 30.5 (C_8), 30.0 (C_6), 20.8; 20.7; 20.6 ($C_{10,\ 10',\ 10''}$).

FT-IR: ν_{max} = 1748 cm^{-1} (O-*CO*-Me), 1690 cm^{-1} (S-*CO*-Me).

2.2.5 Synthesis of 6, 6'-Dithio-D-Trehalose 2.3

The product **2.3** was prepared using a literature procedure, modified to include a further purification step.[8]

In a one-necked round bottom flask, protected thioacetylated trehalose **2.2** (0.2 g, 0.28 mmol) and a solution of KOMe (0.12 g, 1.68 mmol) in MeOH (10 mL) were mixed and stirred at ambient temperature for 18 h. The precipitate that formed was recovered by filtration, washed with cold acetone and dried in an oven overnight at 60 ^{o}C under reduced pressure to give **2.3** as a light brown solid, mp 112-114 ^{o}C, yield 78% (0.1 g, 0.27 mmol).

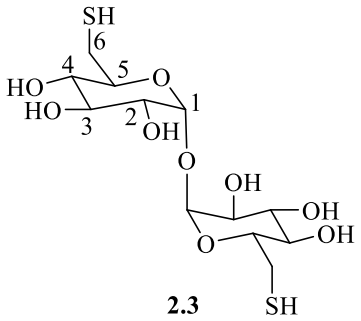

2.3

Figure 2.3: Structure of 6, 6'-dithio-D-trehalose with numerical assignments for NMR

^{1}H NMR (600 MHz; D_2O): δ = 5.10 (d, b, *J* = 3 Hz, 2H, H_1), 3.86-3.78 (m, b, 2H, H_2), 3.70 (td, J_1 = 6 Hz, J_2 = 3.6 Hz, 2H, H_5), 3.55-3.51 (m, 2H, H_4), 3.28-3.24 (m, 2H, H_3), 3.17-3.14 (m, 2H, H_6), 2.86-2.77 (m, 2H, $H_{6'}$). ^{13}C NMR (150 MHz; D_2O): δ = 92.6 (C_1), 72.6 (C_5), 72.3 (C_3), 71.2 (C_4), 71.1 (C_2), 41.3 (C_6).

FT-IR: ν_{max} = 3360 cm^{-1} (OH), 2480 cm^{-1} (SH).

2.2.6 Synthesis of *N*-(3, 4-Dihydroxyphen-ethyl)bicyclo[2.2.1]hept-5-ene-2-Carboxamide 2.4

The product **2.4** was prepared using the literature procedure.[9] DCC (2.27 g, 11 mmol) was added to a solution consisting of dopamine hydrochloride (1.89 g, 10 mmol), 5-norbornene-2-carboxylic acid (1.38 g, 10 mmol) and DMAP (61 mg, 0.5 mmol) in pyridine (50 mL) in a dry two-necked round bottom flask equipped with magnetic stirrer, and kept under N_2 atmosphere. The mixture was stirred at ambient temperature for 24 h, upon which the clear yellow solution turned opaque. The pyridine was removed under reduced pressure to leave an off-white solid. This crude product was then partitioned between water (80 mL) and ethyl acetate (80 mL). The aqueous layer was further washed with ethyl acetate (2 × 80 mL). The combined organic extracts were dried over $MgSO_4$, filtered and the solvent was removed under reduced pressure

to give a brown liquid. This was then purified by silica gel chromatography (hexane:EtOAc) (R_f = 0.26) to give **2.4** as a colourless viscous liquid, yield 51% (1.38 g, 5 mmol), *endo*.

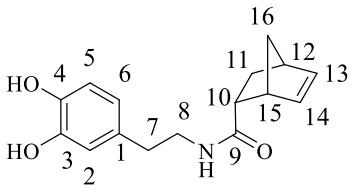

2.4

Figure 2.4: Structure of N-(3, 4-dihydroxyphen-ethyl)bicyclo[2.2.1]hept-5-ene-2-carboxamide with numerical assignments for NMR

^{1}H NMR (600 MHz; $CDCl_3$): δ = 7.88 (s, OH), 7.14 (s, OH), 6.80 (d, *J* = 6.6 Hz, 1H, H_5), 6.72 (d, *J* = 3 Hz, 1H, H_2), 6.52 (dd, J_1 = 12 Hz, J_2 = 1.8 Hz, 1H, H_6), 6.16 (dd, J_1 = 12 Hz, J_2 = 1.8 Hz, 1H, H_{14}), 5.82 (dd, J_1 = 12 Hz, J_2 = 4.8 Hz, 1H, H_{13}), 5.71 (t, *J* = 12 Hz, 1H, NH), 3.40 (q, *J* = 12 Hz, 2H, H_8), 3.05 (s, 1H, H_{15}), 2.86 (s, 1H, H_{12}), 2.85-2.81 (m, 1H, H_{10}), 2.63 (t, *J* = 12 Hz, 1H, H_7), 1.93-1.86 (m, 1H, H_{16}), 1.40 (dd, J_1 = 12 Hz, J_2 = 10.2 Hz, 1H, H_{11}), 1.26-1.21 (m, o, 1H, $H_{11'}$), 1.20-1.16 (m, 1H, $H_{16'}$). ^{13}C NMR (150 MHz; $CDCl_3$): δ = 175.9 (C_9), 144.7 (C_3), 143.3 (C_4), 138.2 (C_{14}), 132.2 (C_{13}), 130.6 (C_1), 120.5 (C_6), 115.8 (C_2), 115.6 (C_5), 50.2 (C_{11}), 46.4 (C_{15}), 45.0 (C_{10}), 42.9 (C_{12}), 41.0 (C_8), 34.8 (C_7), 30.3 (C_{16}).

2.2.7 Thiol-ene Click Reaction between 6, 6'-Dithio-D-Trehalose and *N*-(3, 4-Dihydroxyphen-ethyl)bicyclo[2.2.1]hept-5-ene-2-Carboxamide 2.5

In a vial, 6,6'-dithio-D-trehalose **2.3** (64 mg, 0.17 mmol) and *N*-(3,4-dihydroxyphen-ethyl)bicyclo[2.2.1]hept-5-ene-2-carboxamide **2.4** (96 mg, 0.34 mmol) were dissolved in DMSO-d_6 (1 ml) upon which the reaction mixture turned light brown. The reaction mixture was transferred to an NMR tube and an initial ^{1}H NMR spectrum was obtained. The NMR tube was then irradiated with 36 W UV light (wavelength: 395-405 nm) for six days, with ^{1}H NMR spectra obtained after 48 h, 96 h and six days.

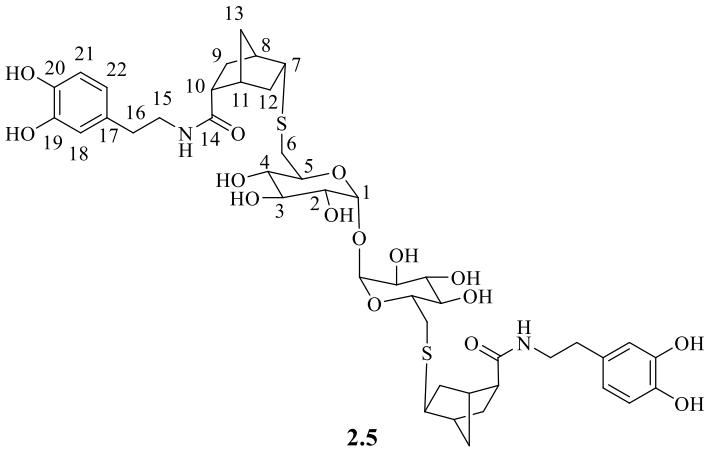

2.5

Figure 2.5: Structure of thiolated trehalose clicked with norbornene catechol moiety with numerical assignments for NMR

^{1}H NMR (600 MHz; DMSO-d_6): δ = 6.60 (d, *J* = 12 Hz, 2H, H_{21}), 6.53 (s, 2H, H_{18}), 6.39 (d, *J* = 12 Hz, 2H, H_{22}), 6.06 (t, b, *J* = 12 Hz, NH), 4.85 (b, 2H, H_1), 4.00-3.86 (m, b, H_8, $H_{12,}$ H_{15}, H_{16}), 3.86 (b, 2H, H_5), 3.53 (b, 2H, H_4), 3.26 (b, H_3), 2.90 (t, *J* = 6 Hz, b, H_7), 2.78-2.73 (m, b, H_6, H_{10}).

2.2.8 Synthesis of Titanium(IV) trismethylcatecholate 2.6

In a vial, 4-methyl catechol (0.66 g, 5.28 mmol, 3 eq.) was dissolved in 2-propanol (10 mL) at ambient temperature to give a clear solution. Upon addition of titanium(IV) tetraisopropoxide (0.5 mL, 1.76 mmol, 1 eq.) a blood red homogenous solution formed. The solvent was removed under reduced pressure to give **2.6** as a dark red solid, which was then dried under reduced pressure at 60 °C for 24 h, yield 97% (0.75 g, 1.82 mmol).

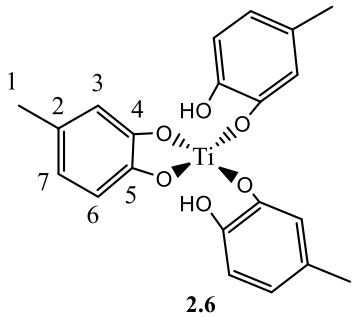

2.6

Figure 2.6: Structure of titanium(IV) trismethylcatecholate with numerical assignment for NMR

^{1}H NMR (600 MHz, $CDCl_3$): δ = 6.71 (d, *J* = 8 Hz, 3H, H_6), 6.64 (s, 3H, H_3), 6.56 (d, *J* = 8 Hz, 3H, H_7), 2.21 (s, 9H, H_1). ^{13}C NMR (150 MHz, $CDCl_3$): δ = 143.3 (C_4), 141.2 (C_5), 131.0 (C_2), 121.5 (C_7), 116.4 (C_3), 115.4 (C_6), 20.8 (C_1).

$C_{21}H_{20}O_6Ti$; MS: *m/z* ES^+, M^+ = 413.7 Da; CHN: Expected %C = 60.58, %H = 4.85, %N = 0.00; measured %C = 60.86, %H = 5.09, %N = 0.00..

2.2.9 Synthesis of Titanium Norbornene-Catecholate Complex 2.7

In a vial, **2.4** (0.10 g, 0.37 mmol, 3 eq.) was dissolved in 2-propanol (5 mL) at ambient temperature to give a pale brown solution. Upon addition of titanium(IV) tetraisopropoxide (0.04 mL, 0.12 mmol, 1 eq.) a blood red homogenous solution formed. The solvent was removed under reduced pressure to give a dark red solid, which was then dried under reduced pressure at 60 °C for 24 h to give **2.7**, yield 63 % (0.16 g, 0.19 mmol).

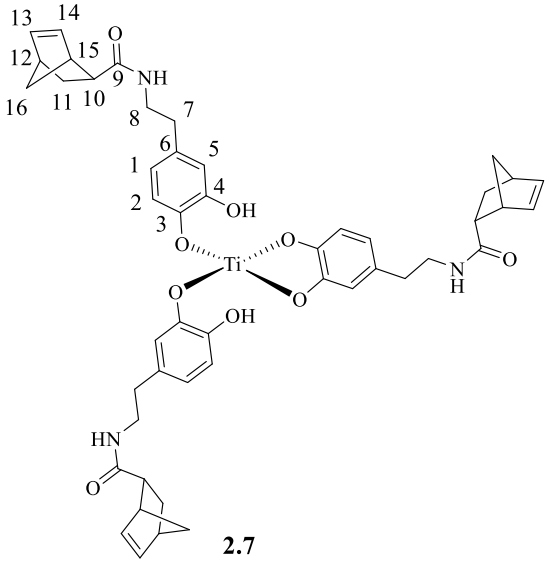

2.7

Figure 2.7: Structure of titanium(IV) triscatechol norbornene

^1H NMR (600 MHz, $CDCl_3$): δ = 7.17-5.26 (m, b, o, 6H, H_2, H_5, H_6, H_{14}, H_{13}, NH), 3.53-3.29 (m, b, o, 6H, H_8, H_{15}, H_{12}, H_{10}, H_7). Key resonances in ^{13}C NMR (150 MHz, $CDCl_3$): δ = 207.2 (C_9), 137.9 (C_{14}), 132.3 (C_{13}), 50.1 (C_{11}), 46.3 (C_{15}), 44.9 (C_{10}), 42.8 (C_{12}), 41.1 (C_8), 33.9 (C_7), 31.0 (C_{16}).

$C_{48}H_{53}N_3O_9Ti$; MS: *m/z* ES^+, $[M+Na]^+$ = 884.7 Da.

2.3 Results and Discussion

2.3.1 Functionalisation of Trehalose with Thiol

The thiol functionalisation of trehalose, as a difunctional saccharide model compound, is based on three steps as outlined in Scheme 2.1.[7, 8] The intermediate **2.1** was prepared *via* the selective tosylation of the two primary hydroxyl groups, followed by the protection of the remaining secondary hydroxyl groups with acetic anhydride. The acetylation of the secondary hydroxyl groups induced hydrophobicity on trehalose and allowed easier isolation of the product. The thioacetation of **2.1** *via* nucleophilic substitution produced protected thioacetate trehalose, **2.2**. This then underwent full deacetylation to give the dithiol functionalised trehalose **2.3**.

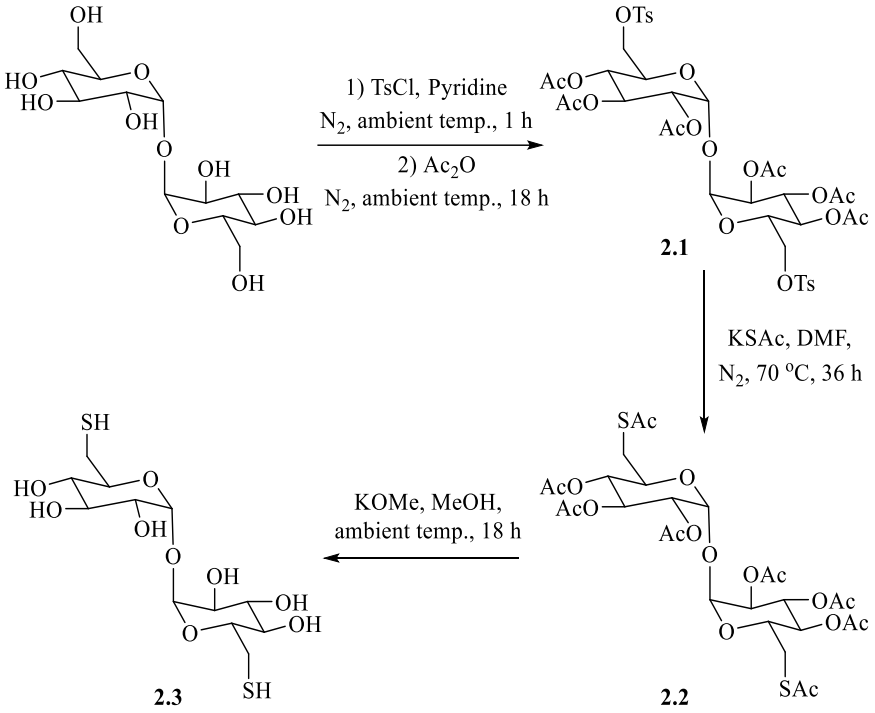

Scheme 2.1: Synthesis of dithiol functionalised trehalose 2.3

The structures of **2.1**, **2.2** and **2.3** were fully characterised by NMR and FT-IR spectroscopies. All characterisation results were in good agreement with their respective literature procedures. Preferential tosylation of both C_6 primary alcohols occurred, whilst all remaining secondary alcohols were acetylated. The ^{1}H NMR spectrum of **2.1** (Figure 2.8.B) in comparison to that of trehalose (Figure 2.8.A) shows the appearance of new resonances corresponding to the tosyl groups, with the aromatic protons ($H_{8,}$ H_9) at 7.72 and 7.32 ppm and methyl protons (H_{11}) at

2.43 ppm. Resonances also appear corresponding to the methyl protons of the acetyl groups ($H_{13, 13', 13''}$) at 2.06, 2.01 and 1.99 ppm. The integration ratios of these resonances compared to the integral of the trehalose proton H_3 are correct for two tosyl groups and six acetyl groups per trehalose unit.

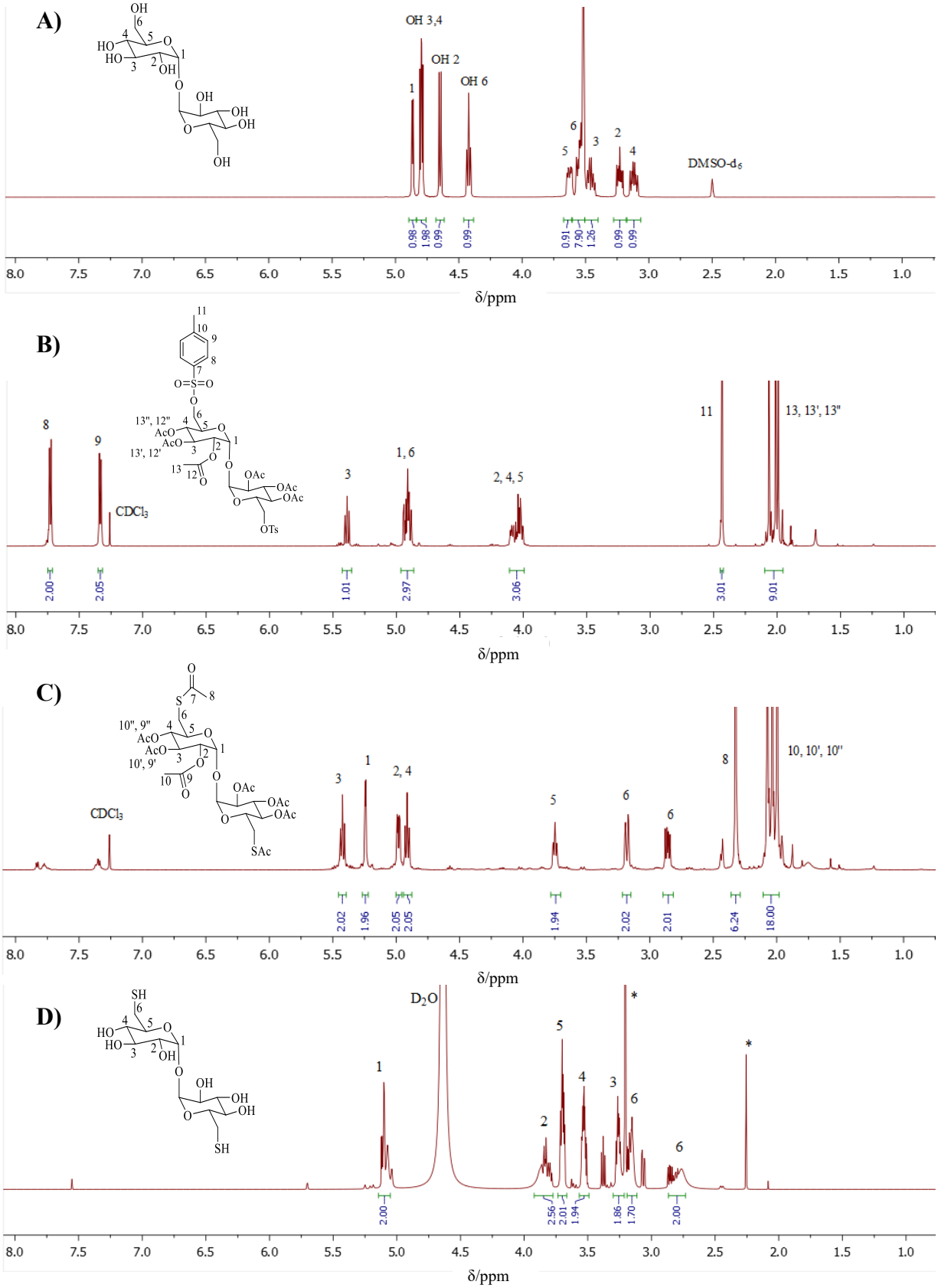

Figure 2.8: ^{1}H NMR spectra of A) trehalose in DMSO-d_6, B) protected ditosylated trehalose 2.1 in $CDCl_3$, C) protected dithioacetylated trehalose 2.2 in $CDCl_3$ and D) dithiotrehalose 2.3 in D_2O

The ^{13}C NMR spectrum of **2.1** (Figure 2.9.B) in comparison to that of trehalose (Figure 2.9.A) also showed the appearance of resonances for carbon atoms associated with the tosyl groups (C_7-C_{11}) at 145.4, 132.5, 130.0, 128.2 and 21.8 ppm, and the acetyl groups ($C_{12,\ 12',\ 12''}$ and $C_{13,\ 13',\ 13''}$) at 170.0, 169.7, 169.6, 20.7 and 20.6 ppm. Also, the resonance attributed to CH_2 (C_6) was observed at a higher δ-value, 67.7 ppm in comparison to that of trehalose at 60.9 ppm. This provides strong evidence for the attachment of the tosyl groups to the methylene bridge and the formation of intermediate **2.1**.

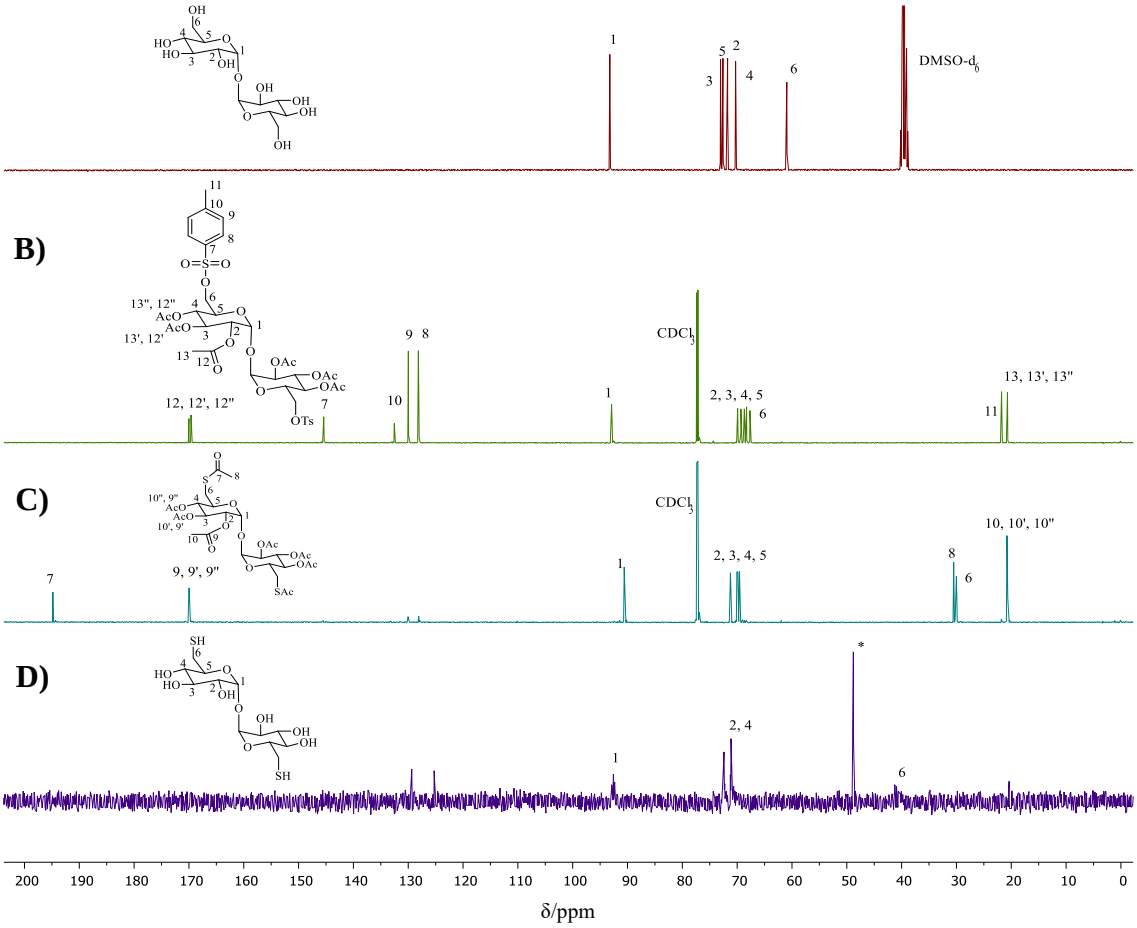

Figure 2.9: ^{13}C NMR spectra of A) trehalose in DMSO-d_6, B) protected ditosylated trehalose 2.1 in $CDCl_3$, C) protected dithioacetylated trehalose 2.2 in $CDCl_3$ and D) dithiotrehalose 2.3 in D_2O

After successful tosylation and acetylation of trehalose, thioacetylation of the C_6 carbon was performed. In the comparison ^1H NMR spectra of **2.1** and **2.2** (Figure 2.8 B and C), the resonances for the aromatic protons ($H_{8,}$ H_9) at 7.72 and 7.32 ppm and methyl protons (H_{11}) at 2.43 ppm of the tosyl group were reduced, whilst those for the acetate groups ($H_{13,\ 13',\ 13''}$) at

2.06, 2.01 and 1.99 ppm remained. These features indicate the near complete detachment of the tosyl group. In Figure 2.8.C there is also the appearance of a methyl resonance (H_8) at 2.32 ppm and a splitting of the H_6 protons into two doublet of doublets at 3.18 and 2.86 ppm. This splitting pattern is due to both protons being in slightly different chemical environments. Both signals have the same *J* values; each H_6 will couple to the other H_6 of the CH_2 and the adjacent H_5 of the trehalose backbone. ^{1}H-^{13}C HSQC spectroscopy (Figure 2.10) was used to confirm that both of these resonances corresponded to H_6, as both H_6 signals correlated to the same C_6 resonance. These new ^{1}H NMR resonances correspond to the attachment of the thioacetate group, of which the integration is correct for two thioacetate groups per trehalose unit. The comparison of the ^{13}C NMR spectra of **2.1** and **2.2** (Figure 2.9 B and C) also shows the near complete loss of the aromatic (C_7, C_8, C_9, C_{10}) and methyl (C_{11}) tosyl resonances at 145.4, 132.5, 130.0, 128.2 and 21.8 ppm, respectively, and the appearance of a new carbonyl resonance (C_7) at 194.8 ppm and methyl group (C_8) at 30.5 ppm. Moreover, the shift to a lower δ-value, 30.0 ppm for the CH_2 resonance (C_6) confirms the attachment of the thioacetate group to give the intermediate **2.2**.

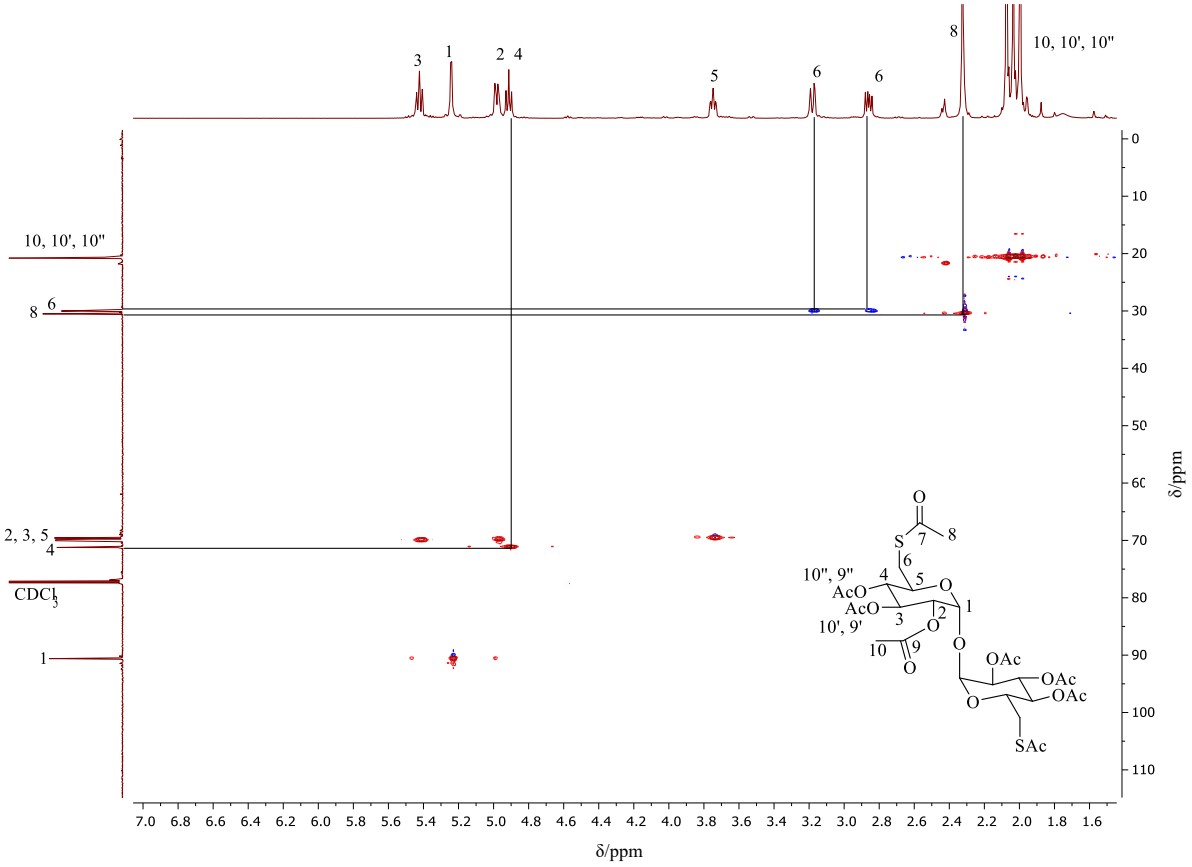

Figure 2.10: ^{1}H-^{13}C HSQC NMR spectrum of 2.2 in $CDCl_3$

Compound **2.2** was then deprotected with KOMe. In the comparison ^{1}H NMR spectra of **2.2** and **2.3** (Figure 2.8 C and D), the resonances of all acetate groups ($C_{8,}$ and $C_{10,\ 10',\ 10''}$) at 2.32, 2.07, 2.03 and 1.99 ppm have disappeared. This indicates full deprotection of the intermediate **2.2**. Compound **2.3** also regains its physical property of being water soluble. Comparison of the ^{13}C NMR spectra of **2.2** and **2.3** shows a disappearance of the acetate resonances corresponding to the carbonyl groups ($C_{7,}$ and $C_{9,\ 9',\ 9''}$) at 194.8, 170.0 and 169.9 ppm and methyl groups (C_8) at 30.5 ppm, however, there is a small residual resonance at 20.8 ppm corresponding to $C_{10,\ 10',\ 10''}$. This contradicts the ^{1}H NMR spectra and indicates that full deprotection has not occurred. Again the methylene (C_6) resonance has shifted downfield to a higher δ-value of 41.3 ppm, providing strong evidence for the deacetylation of the thioacetate group to thiol. ^{1}H-^{13}C HSQC NMR (Figure 2.11) was used to assign the H_6 resonances, both of which couple to the same carbon atom (C_6). In the literature procedure, it is reported that after the initial isolation of the product **2.3** no further purification steps were carried out. No NMR data is presented and the compound is not well characterised.[8] A further precipitation step was performed in an attempt to remove the impurities at 2.25, 3.07, 3.20 and 3.38 ppm; however, no change to these resonance intensities was observed. The impurities at 2.25 and 3.20 ppm can be attributed to AcOMe and residual methanol, respectively, and did not decrease in intensity even after exhaustive drying under reduced pressure, indicating that some solvent molecules are trapped in the compound.

The ^{1}H-^{13}C HSQC NMR spectrum of **2.3** also has a resonance at 3.07 ppm showing a weak correlation to the C_6 atom, implying that it is part of the CH_2 group. The resonance at 3.38 ppm shows a weak correlation to either the C_2 or C_4 carbon. This evidence, and the fact that the resonances observed in the ^{1}H NMR spectrum are broad, could imply that a small amount of acetyl groups remains. This will cause the molecule to be unsymmetrical, leading to the appearance of overlapping signals for each proton on the trehalose backbone, causing their broadness. MeOH can also form strong hydrogen bonds with any remaining acetyl groups, therefore increasing the difficulty of its removal.

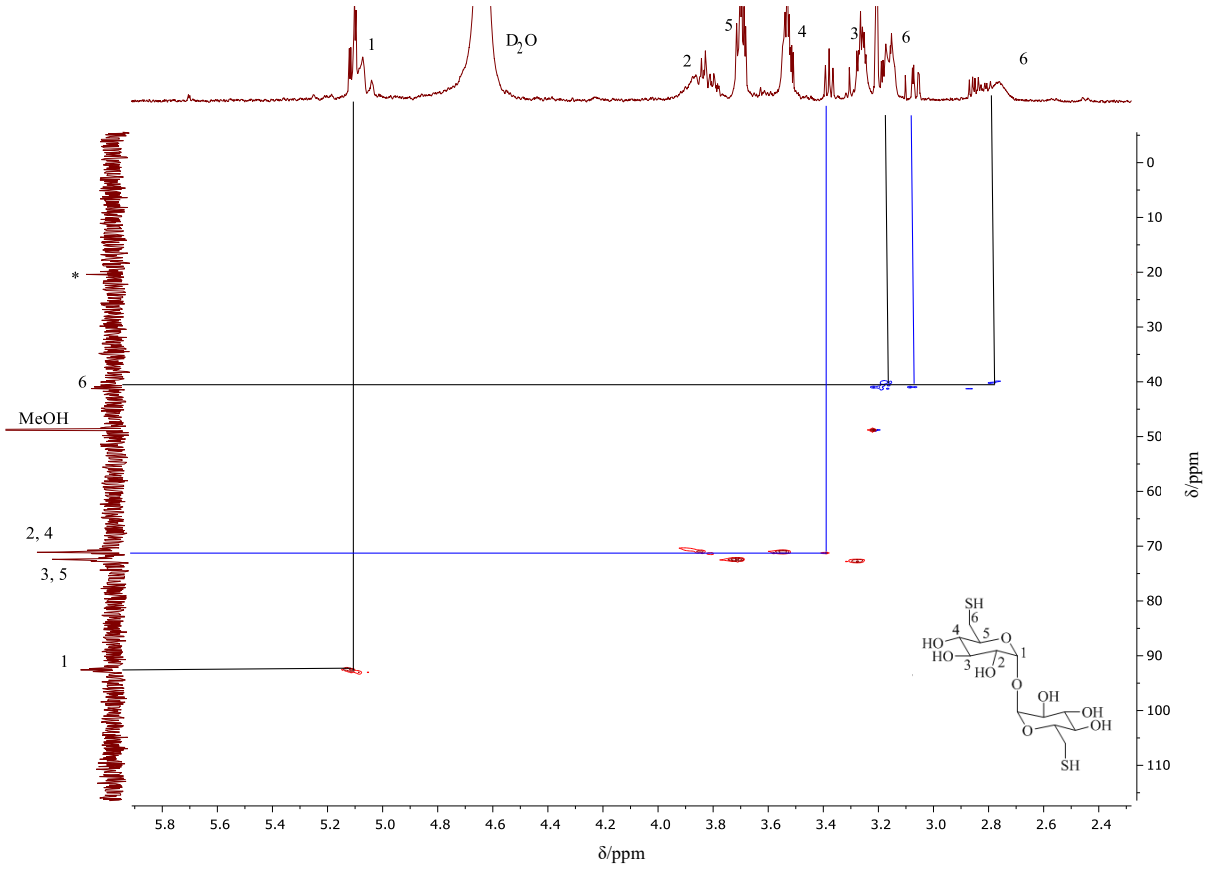

Figure 2.11: ^{1}H-^{13}C HSQC NMR spectrum of 2.3 in D_2O

Distortionless Enhancement by Polarization Transfer-135 (DEPT-135) NMR spectroscopy was found to be an efficient way to follow up the thiol functionalisation of trehalose. The comparison DEPT-135 spectra of trehalose, **2.1**, **2.2** and **2.3** (Figure 2.12) shows the chemical shift of the inverted CH_2 peak (C_6) from 61.2 ppm to 67.7 ppm, then to 30.0 ppm and finally 41.3 ppm depending on the attached group. These obvious shifts illustrate the successful functionalisations occurring at each reaction step.

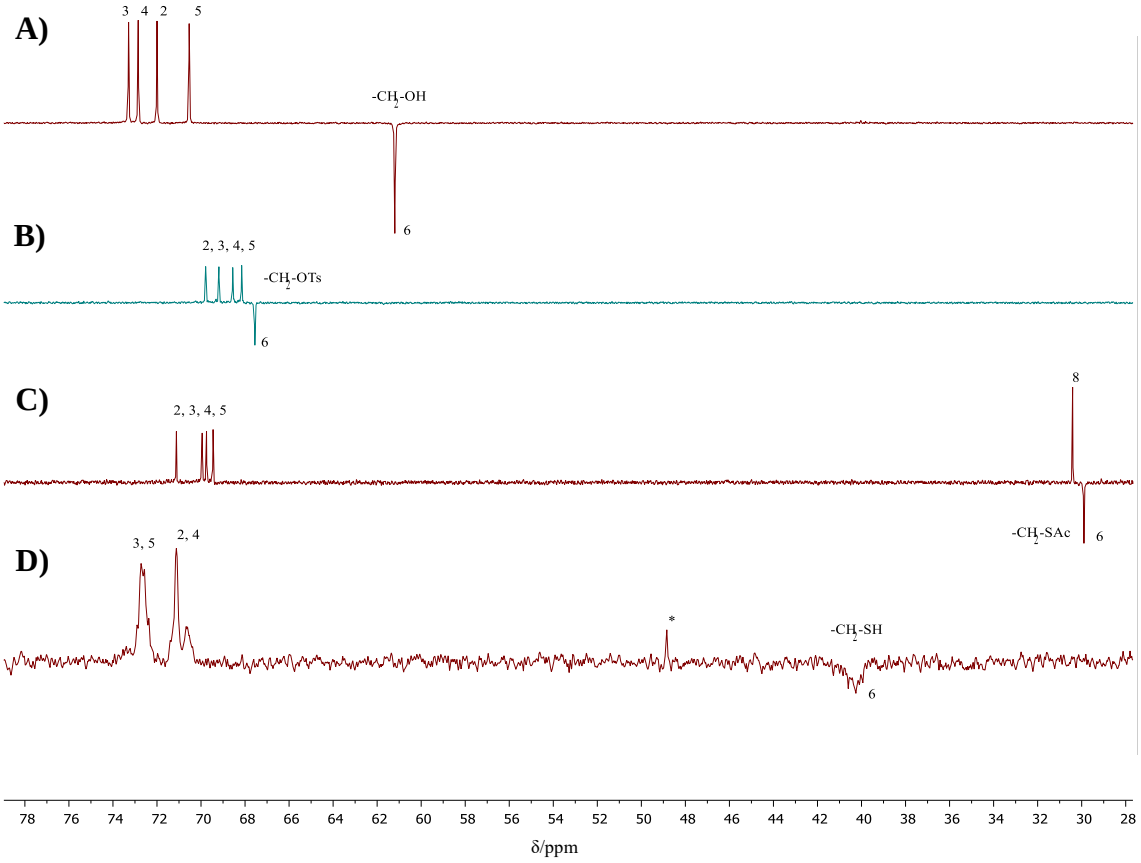

Figure 2.12: DEPT-135 NMR spectra of A) trehalose in DMSO-d_6, B) protected ditosylated trehalose 2.1 in $CDCl_3$, C) protected dithioacetylated trehalose 2.2 in $CDCl_3$ and D) dithiotrehalose 2.3 in D_2O

FT-IR spectroscopy also proved to be another useful method for the characterisation of the reaction products. The FT-IR spectra showed the presence of a strong peak at 1743 cm^{-1} for the carbonyl groups in **2.1** and **2.2** (Figure 2.13 B and C) and the loss of a broad peak at 3307 cm^{-1} attributed to the hydroxyl groups on trehalose (Figure 2.13.A). The IR spectrum for **2.3** showed the reappearance of a broad peak at 3360 cm^{-1} due to hydroxyl groups, indicating successful deprotection and also the appearance of a broad peak at 2480 cm^{-1} attributed to the thiol groups (Figure 2.13.D).

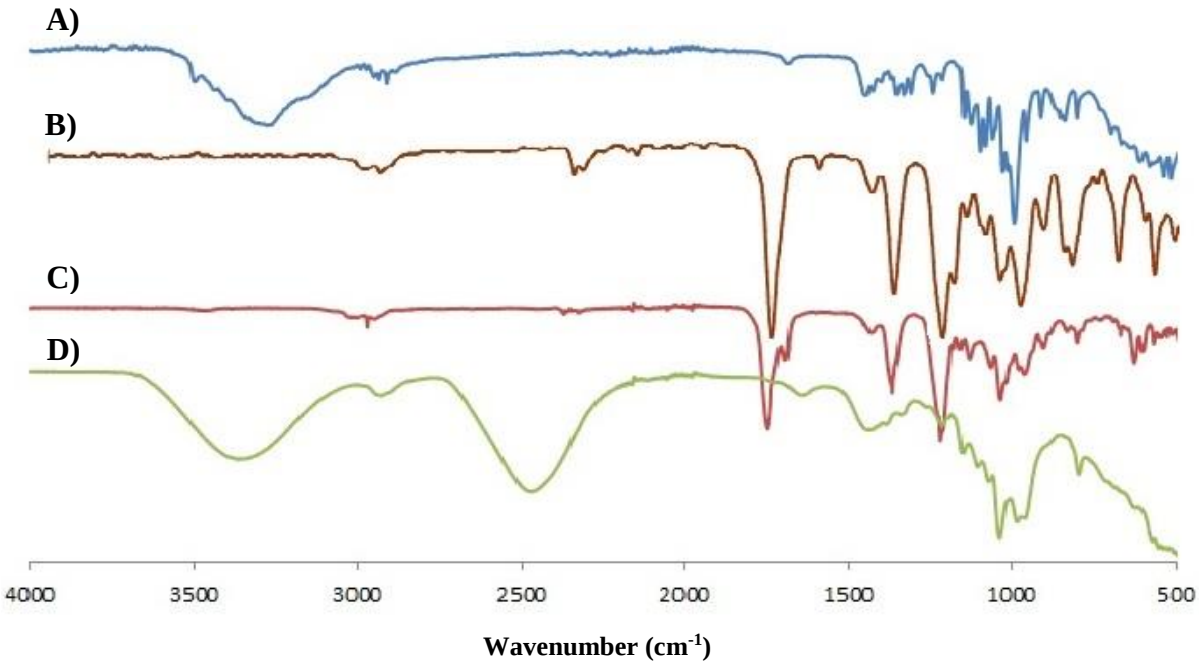

Figure 2.13: FT-IR spectra of A) trehalose, B) protected ditosylated trehalose 2.1, C) protected dithioacetylated trehalose 2.2 and D) dithiotrehalose 2.3

Although the thiolation of trehalose was successful, the overall yield of tosylation followed by acetylation was 15%. However, this low yield is consistent with the literature, which was reported at 14%.[7] This is believed to be due to the multiple recrystallisation steps required for purification. However, the thioacetylation and deprotection steps afforded higher yields, at 74 and 78%, respectively. The yield for the thioacetylation was reported to be 90%, whilst no yield was reported for the dithiolated trehalose.[8] The dithiolated product **2.3** was also poorly characterised in the literature, with no NMR data presented at all. This could be due to the difficulty in the assignment of peaks due to their broadness, or the lack of available 2D-NMR characterisation to the authors.

2.3.2 Functionalisation of Trehalose *via* Thiol-ene Click

The alkene component of the thiol-ene Click reaction was a norbornene-based compound modified with a catecholic moiety. Dopamine hydrochloride was attached to norbornene carboxylic acid *via* an amide linkage in a DCC/DMAP coupling reaction to give the product **2.4** (Scheme 2.2).[9] The product was fully characterised by NMR and FT-IR spectroscopy.

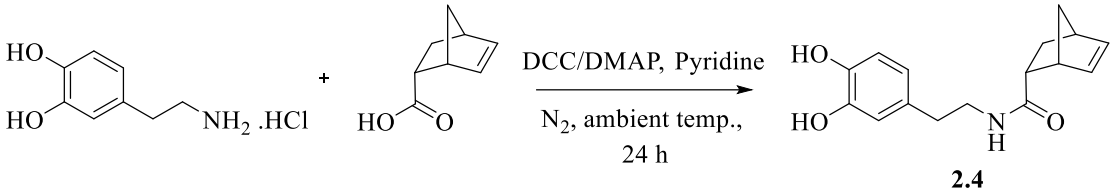

2.4

Scheme 2.2: Synthesis of norbornene-catechol compound 2.4

The ^{1}H NMR data was in good agreement with the literature.[9] The ^{1}H NMR spectrum of **2.4** (Figure 2.14) clearly shows resonances corresponding to both the catecholic and norbornene components of the molecule. The catecholic resonances at 6.80, 6.72 and 6.52 ppm were due to H_5, H_2, and H_6, respectively. The norbornene resonances 6.16, 5.82, 3.05, 2.86, 2.83, 1.90, 1.40, 1.23 and 1.18 were due to H_{14}, H_{13}, H_{15}, H_{12}, H_{10}, H_{16}, H_{11}, $H_{11'}$ and $H_{16'}$, respectively. Resonances at 2.04 and 4.12 ppm are due to residual EtOAc used in the column chromatography purification step. These resonances were still present after exhaustive drying under reduced pressure, potentially due to the solvent forming hydrogen bonds with the catechol moiety.

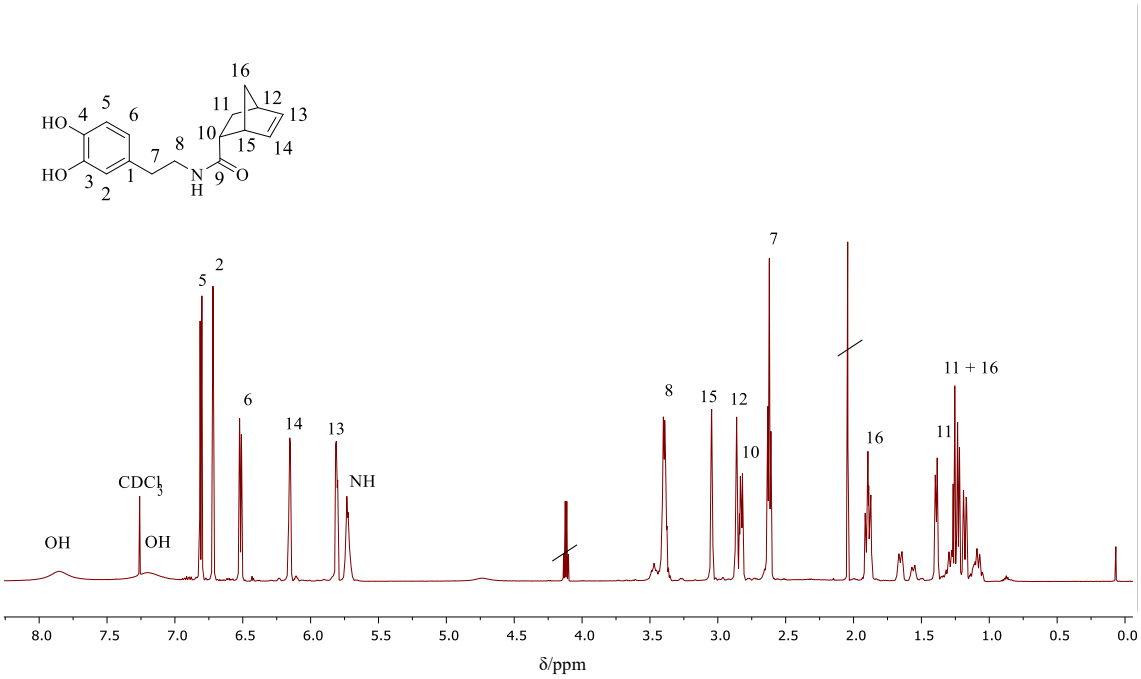

Figure 2.14: ^{1}H NMR spectrum of the norbornene-catechol compound 2.4 in $CDCl_3$

The ^{13}C NMR spectrum of **2.4** is shown in Figure 2.15. The resonance at 175.9 ppm (C_9) clearly illustrates the presence of the amide linkage, and the resonances at 144.7 (C_3), 143.3 (C_4), 130.6 (C_1), 120.5 (C_6), 115.8 (C_2), 115.6 (C_5) ppm are characteristic of the aromatic ring of the catechol.

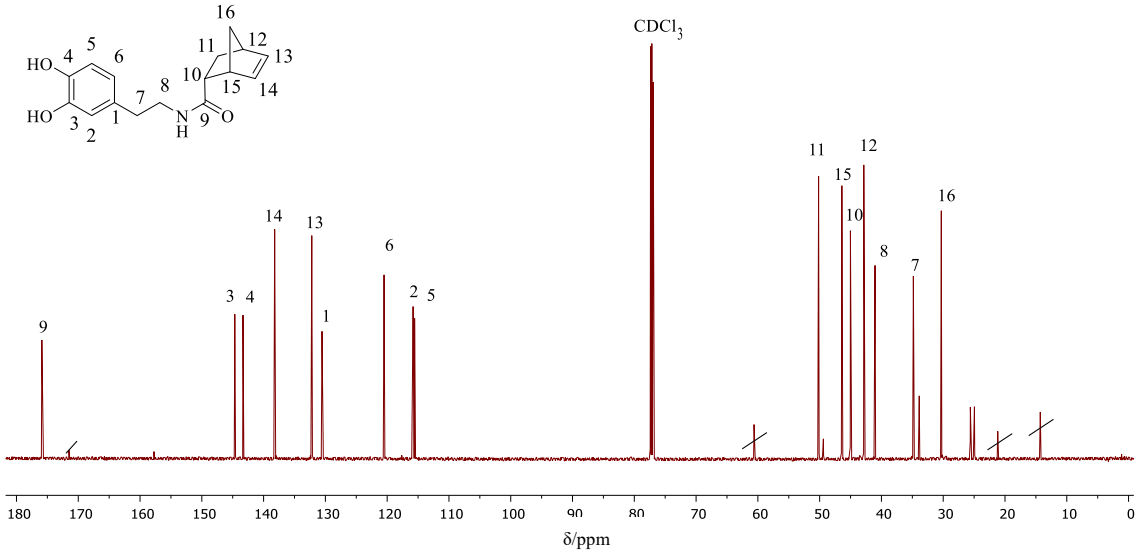

Figure 2.15: ^{13}C NMR spectrum of the norbornene-catechol compound 2.4 in $CDCl_3$

HSQC 2D NMR spectroscopy was utilised to help assign the correct signals. The ^{1}H-^{13}C HSQC spectrum of **2.4** (Figure 2.16) clearly shows the ^{1}H resonances of H_8, H_{12} and H_{10} at 3.40, 2.86 and 2.81 ppm coupling to carbon resonances 41.0 (C_8), 42.9 (C_{12}) and 45.0 (C_{10}) ppm, respectively. The ^{1}H-^{13}C correlation due to the methylene protons H_{11} at 1.86 and 1.23 ppm and H_{16} at 1.40 and 1.20 ppm each couple to one carbon atom, 50.2 ppm (C_{11}) and 30.3 ppm (C_{16}), respectively. This indicates both protons of each methylene group are in slightly different chemical environments. The magnified region of Figure 2.16 shows the resonances assigned to the catecholic protons H_5, H_2 and H_6 at 6.80, 6.72 and 6.52 ppm coupling to the carbon resonances at 115.6 (C_5), 115.8 (C_2) and 120.5 (C_6) ppm, respectively.

Therefore, some of the peak assignments reported in the literature were incorrect, in particular the resonances attributed to the proton bound carbon atoms within the aromatic ring (C_2, C_5, C_6), and some norbornene resonances (C_{10}, C_{11}, C_{12}).[9]

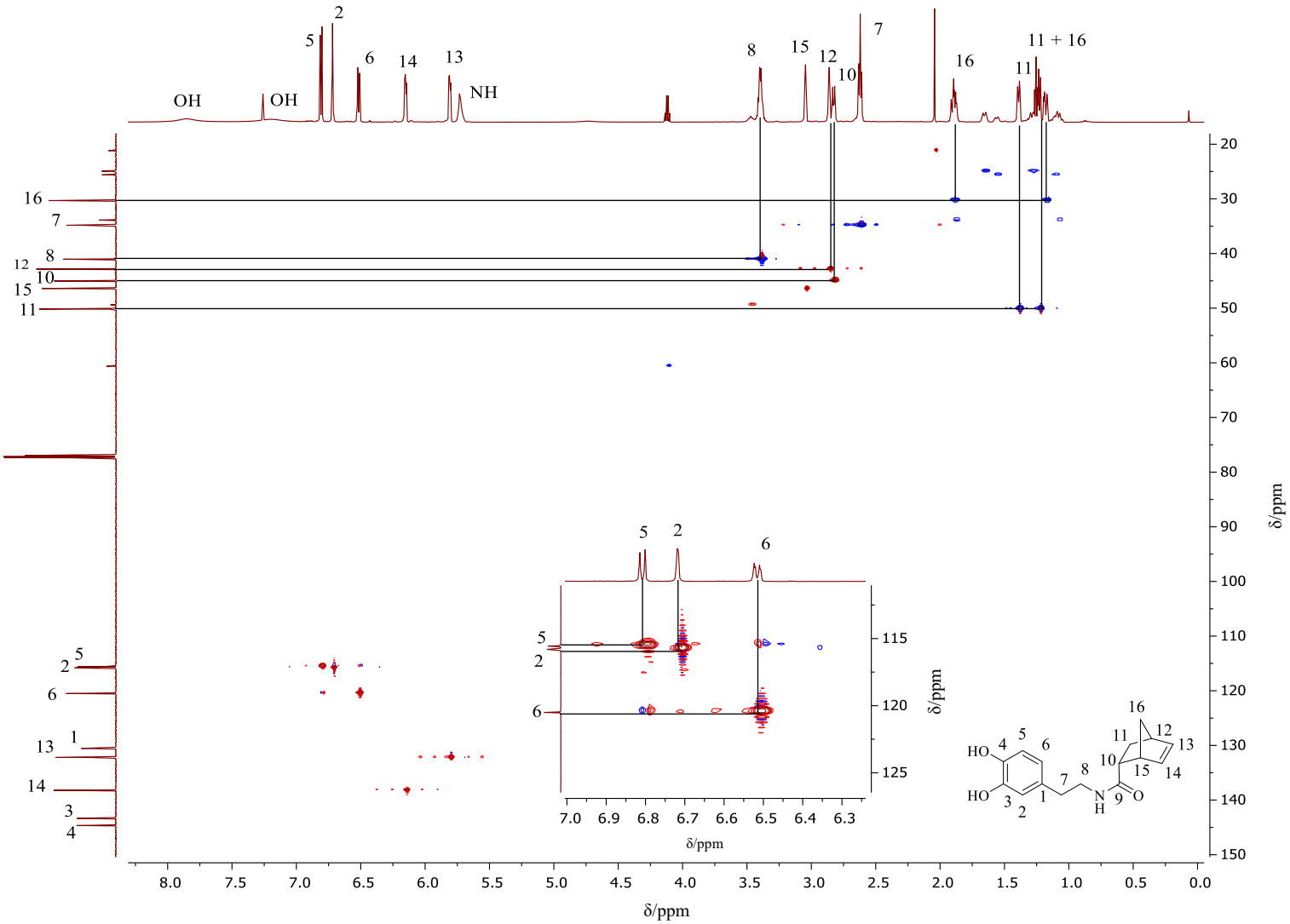

Figure 2.16: ^{1}H-^{13}C HSQC NMR spectrum of 2.4 in $CDCl_3$

Compounds **2.3** and **2.4** were then mixed together and irradiated with UV light in order to induce a thiol-ene Click reaction to give product **2.5**, as outlined in Scheme 2.3.

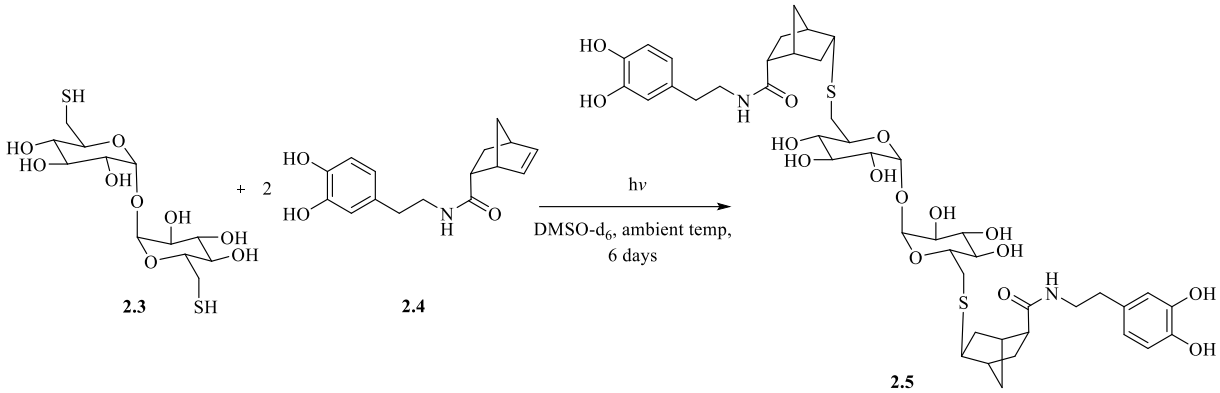

Scheme 2.3: Synthesis of thiol-ene Click product 2.5

The reaction was carried out on an NMR scale in order to follow the progress of the reaction over time. The ^{1}H NMR spectrum of **2.5** after six days of UV irradiation is shown in Figure 2.17. The resonances observed are generally very broad and therefore difficult to accurately integrate. We would expect the intensity of the resonances attributed to the alkene protons of **2.4** at 5.72 ppm and 6.06 ppm (H_{13} and H_{14} in Figure 2.14) to decrease upon irradiation, as the thiol reacts with the strained double bond to form an alkyl sulfide.

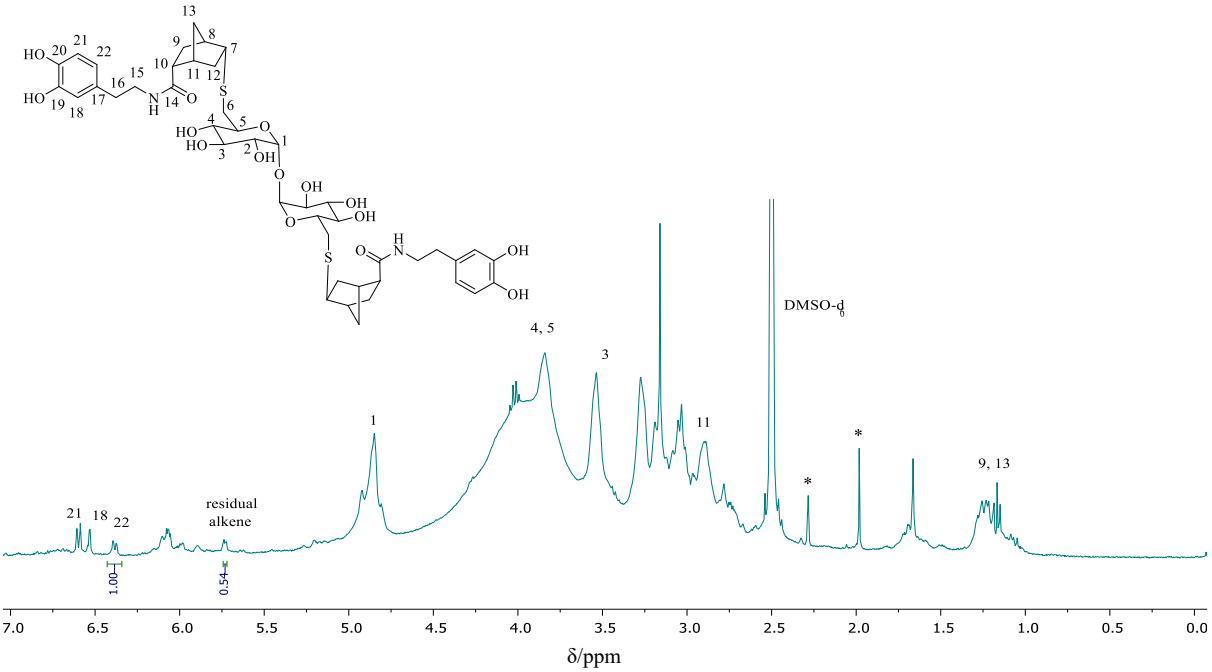

Figure 2.17: ^{1}H NMR spectrum of 2.5 in DMSO-d_6

Taking the cleanest alkene resonance at 5.72 ppm and integrating it against the resonance attributed to the aromatic proton H_{22}; before irradiation the ratio of these signals is 1:1, as expected. After irradiation, the ratio had decreased to 1:0.54, indicative of approximately 46% of the norbornene compound successfully undergoing a thiol-ene reaction with **2.3**. It was expected that the alkene resonances would completely disappear, as two equivalents of norbornene should react completely with one equivalent of dithiotrehalose. This may well be due to the participation of only one of the thiol groups of **2.3** in the thiol-ene reaction. Another possible reason may be due to the formation of disulphide bonds, due to the thiol groups of **2.3** undergoing oxidation from O_2 present in the atmosphere.

2.3.3 Formation of Titanium Complexes with Catechol

2.3.3.1 Formation of Complex with Methyl Catechol

In order to induce gelation in the saccharide system, the grafted catecholic moiety should bind with the group(IV) metal ions present in the crosslinking agent. In order to prove this, a simple catechol, 4-methyl catechol (MeCat) was reacted with a simple titanium complex, titanium(IV) tetraisopropoxide (TIPT), to give **2.6** as outlined in Scheme 2.4. Upon addition of the TIPT, the colour of the reaction mixture turned from colourless to blood red, indicating displacement of the isopropoxide groups, formation of four molecules of 2-propanol and the binding of the catechol molecule.[10]

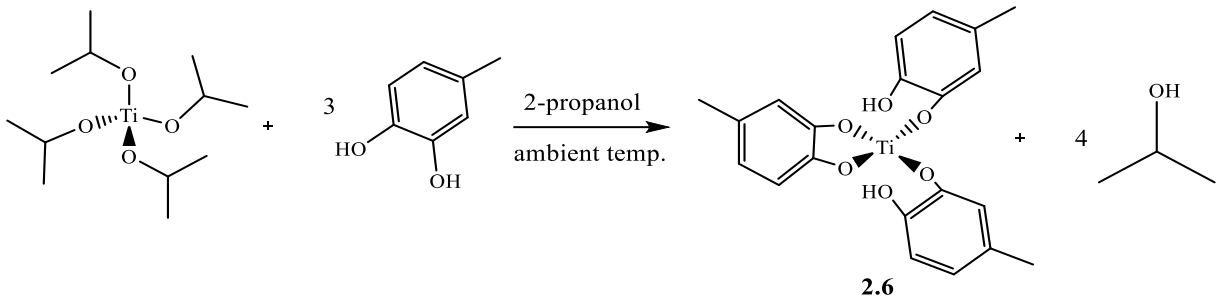

Scheme 2.4: Synthesis of titanium(IV) trismethylcatecholate 2.6

The ^{1}H NMR spectrum of **2.6** is shown in Figure 2.18.C. The doublet resonances at 6.71 and 6.56 ppm, and the singlet at 6.64 ppm correspond to the aromatic protons H_6, H_3 and H_7, respectively. The resonance at 2.21 ppm corresponds to the methyl protons, H_1. When compared with the ^{1}H NMR spectrum of TIPT (Figure 2.18.A), there are no resonances corresponding to this starting material present in the product, indicating the loss of all isopropoxide groups. When the ^{1}H NMR spectrum of **2.6** is compared to that of 4-methylcatechol (Figure 2.18.B), the resonances due to the protons of the hydroxyl groups have decreased, indicating binding to titanium *via* an alkoxide linkage. The ^{13}C NMR spectrum of **2.6**, Figure 2.19**,** only shows seven resonances corresponding to the aromatic ring (C_2-C_7) and methyl group (C_1) of the catechol moiety.

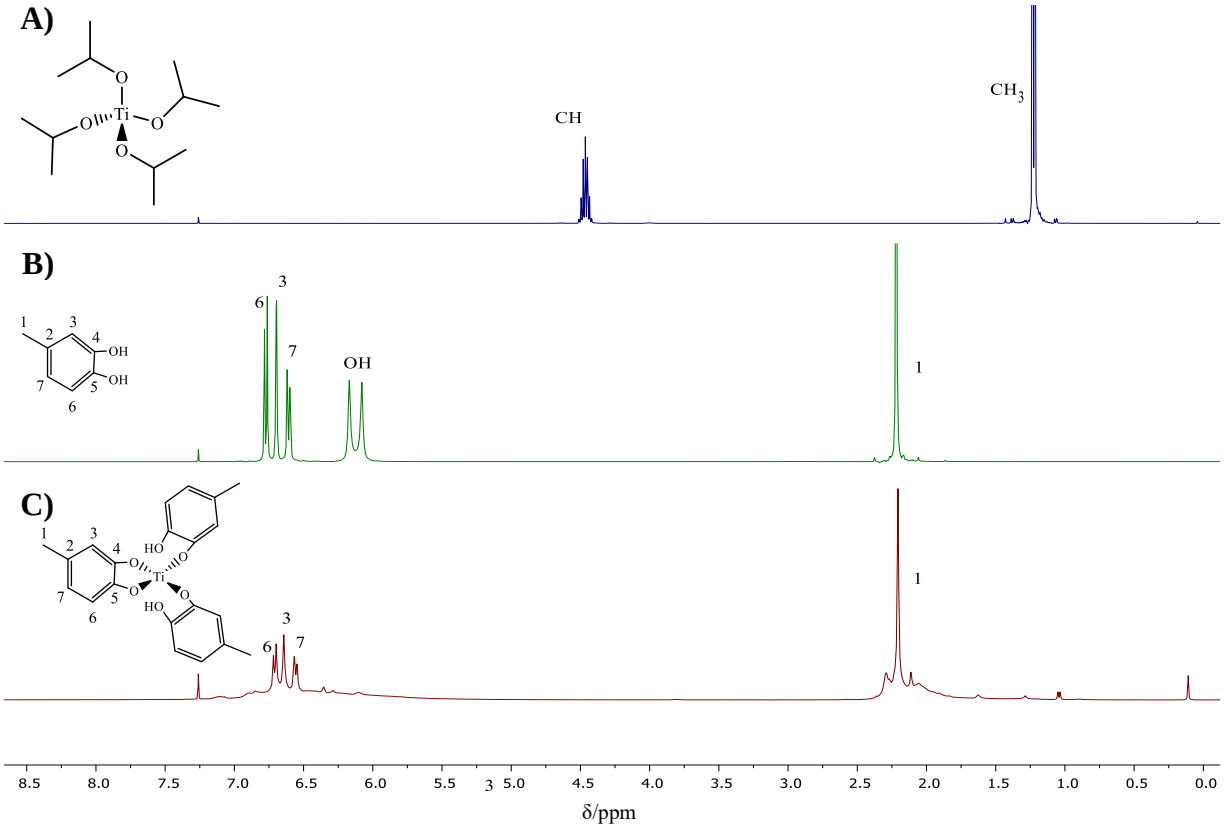

Figure 2.18: ^{1}H NMR spectra of A) TIPT, B) MeCat and C) titanium(IV) trismethylcatecholate 2.6, all in $CDCl_3$

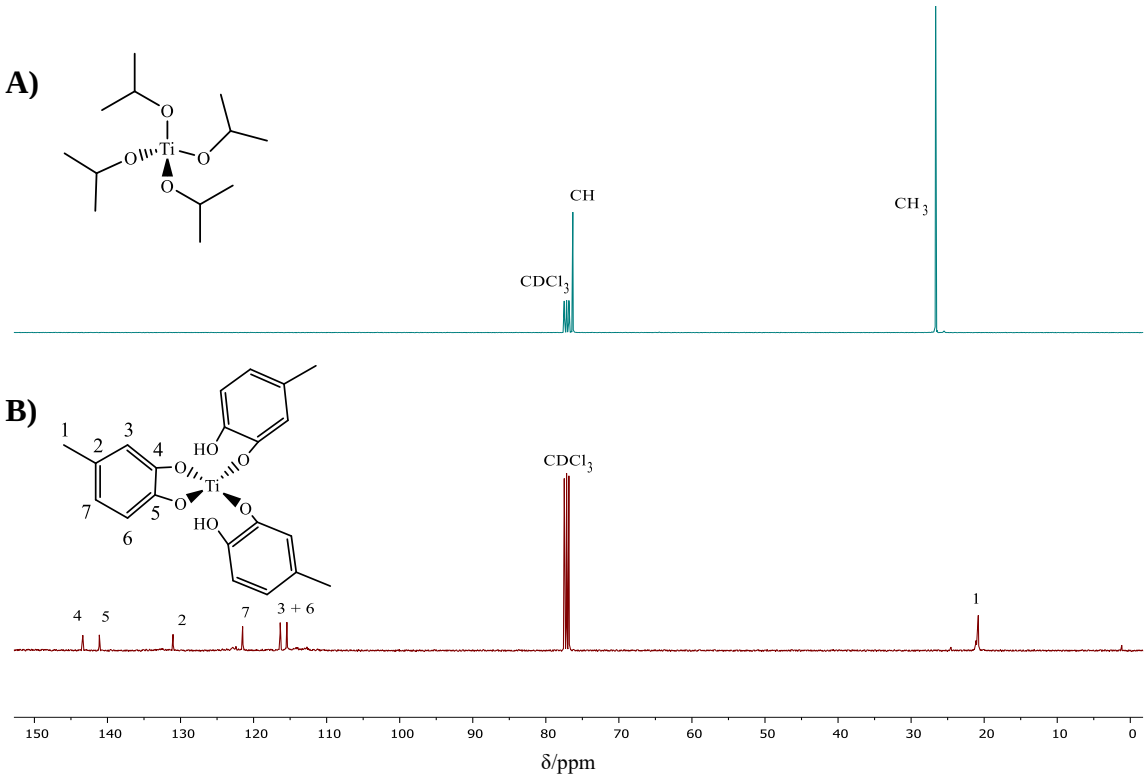

Figure 2.19: ^{13}C NMR spectrum of A) TIPT and B) titanium(IV) trismethylcatecholate 2.6 in $CDCl_3$

Electrospray ionisation (ESI) mass spectroscopy was used to prove that three equivalents of MeCat are bound to the titanium centre. The molecular ion was observed at 413.7 Da (100%, Figure 2.20), which corresponds to the empirical formula $C_{21}H_{20}O_6Ti^+$.

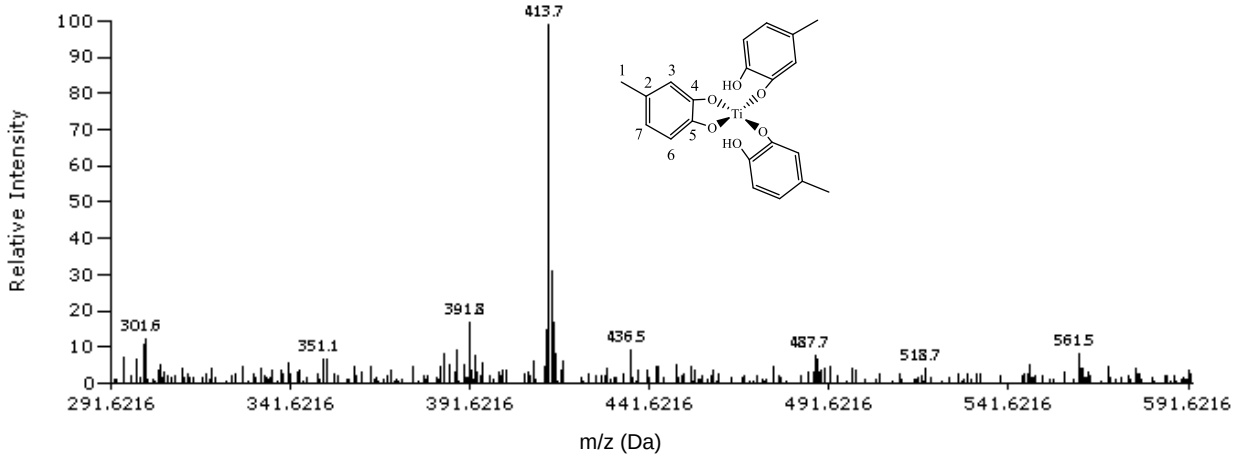

Figure 2.20: ESI-MS spectrum of 2.6

Additionally, CHN analysis was carried out with the results closely matching the predicted values; CHN expected %C = 60.58, %H = 4.85, %N = 0.00; measured %C = 60.86, %H = 5.09, %N = 0.00. This supports the rest of the data, indicating a successful reaction and the binding of three MeCat moieties.

2.3.3.2 Formation of Complex with Norbornene-Catechol 2.4

The norbornene-catechol compound, **2.4** was then reacted with titanium(IV) tetraisopropoxide, to give **2.7** as outlined in Scheme 2.5.

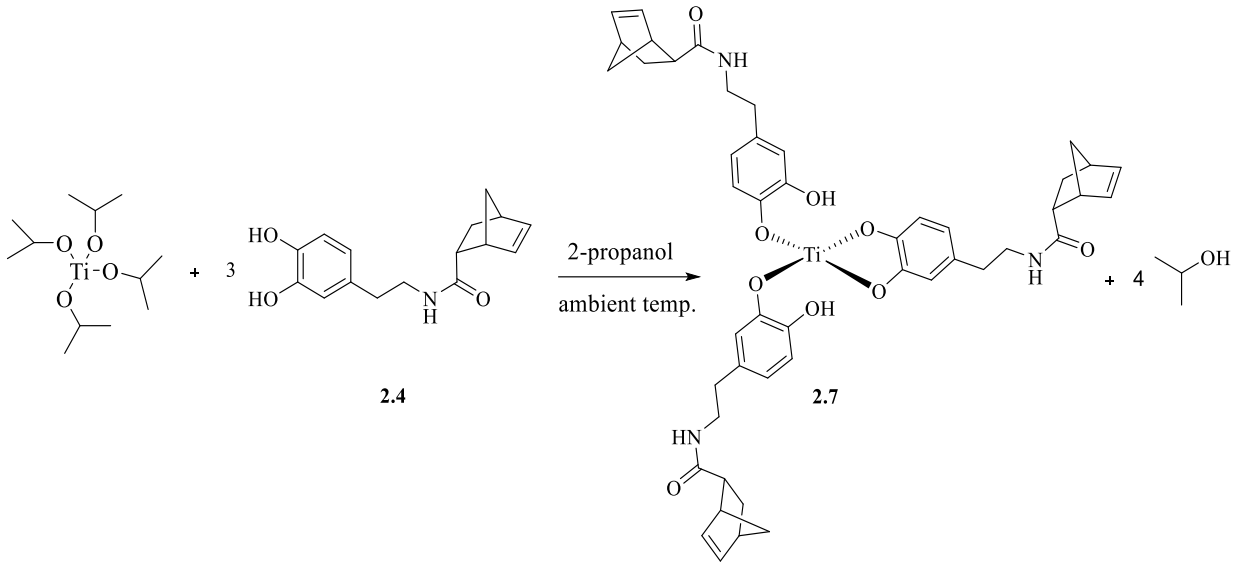

Scheme 2.5: Synthesis of titanium(IV) triscatechol norbornene 2.7

Upon addition of TIPT, the colour of the reaction mixture turned from colourless to blood red, indicating displacement of the isopropoxide groups and formation of 2-propanol. It was expected that three equivalents of **2.4** would bind to titanium, as observed with **2.6**. Comparison of the ^{1}H NMR spectrum of **2.7** (Figure 2.21) to that of **2.4** (Figure 2.14) shows the disappearance of the resonances attributed to the catecholic OH protons at 7.88 and 7.14 ppm, which is also indicative of Ti binding. However, Figure 2.21 suggests only partial displacement of the isopropoxide groups has occurred. The resonances at 4.04 and 1.20 ppm correspond to the CH and methyl protons of the isopropoxide group, respectively. The other resonances observed are broad and overlapped- assignments have been made based on the spectrum assignments of **2.4**, as they are expected to be similar.

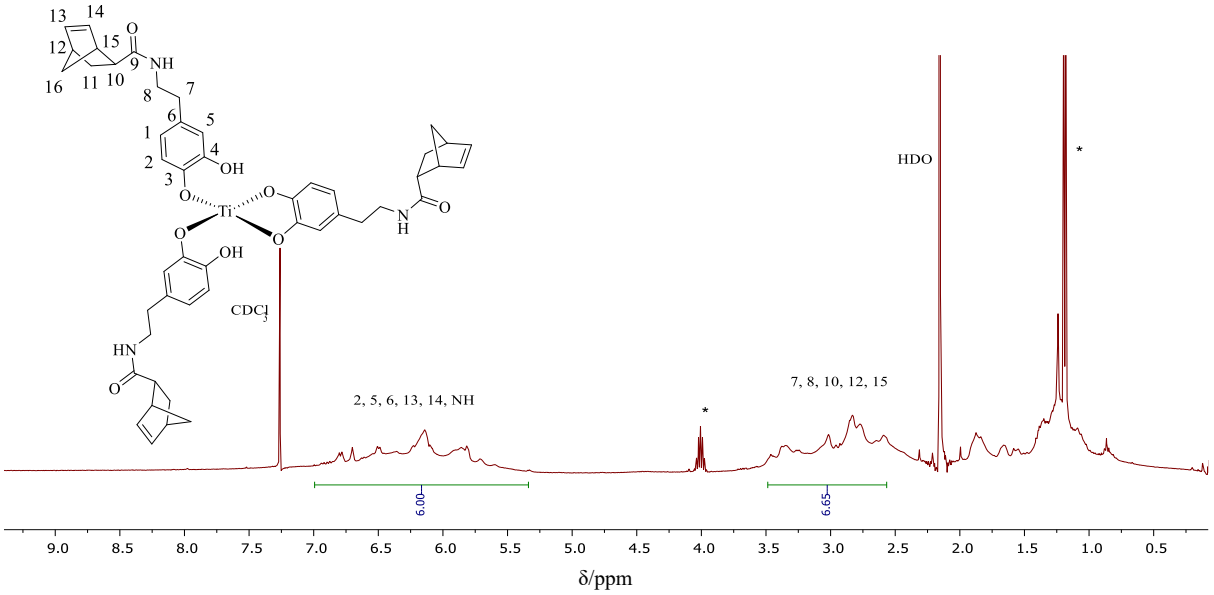

Figure 2.21: ^{1}H NMR spectrum of 2.7 in $CDCl_3$

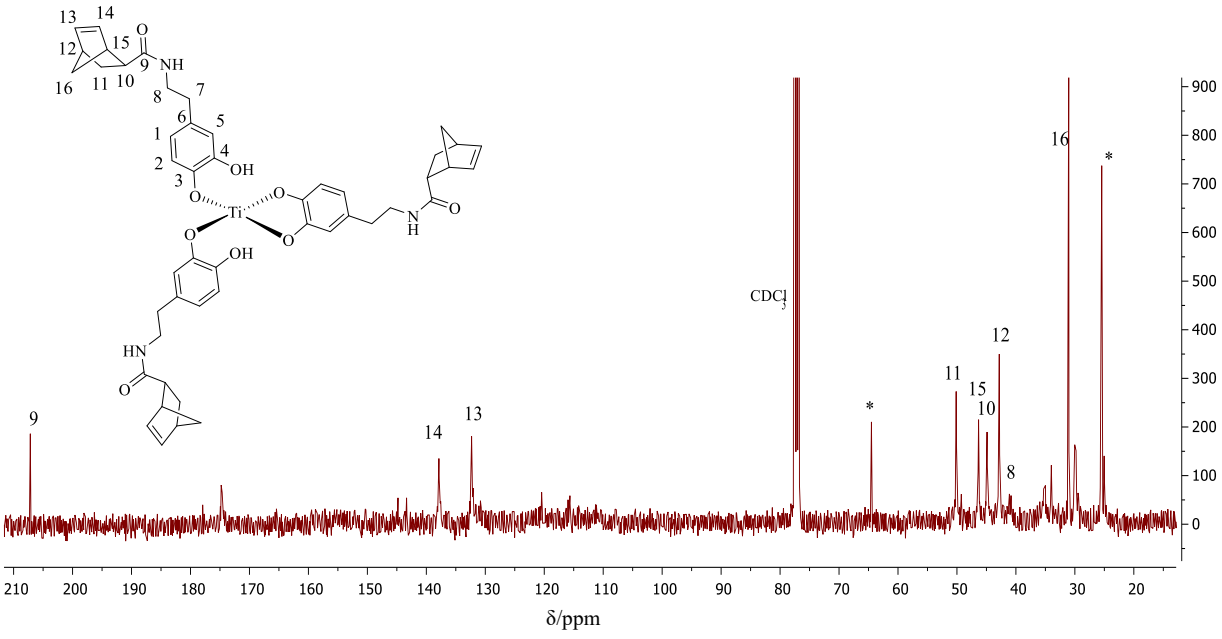

Figure 2.22: ^{13}C NMR spectrum of 2.7 in $CDCl_3$

The ^{13}C NMR spectrum of **2.7** (Figure 2.22) in comparison to that of **2.4** (Figure 2.15) shows that the amide carbonyl resonance (C_9) has shifted downfield from 175.9 to 207.2 ppm upon binding to titanium. The resonances at 137.9 and 132.3 ppm corresponding to the alkene carbon atoms C_{14} and C_{13} have not shifted, indicating the presence of the norbornene group. The large

resonances at 64.5 and 24.5 ppm are due to the CH and methyl carbon atoms of remaining isopropoxide groups.

ESI mass spectroscopy was performed in order to determine the number of catechol norbornene groups bound to the Ti centre. The molecular ion was observed at 884.7 Da, (10.14%, Figure 2.23.A), which is consistent with the empirical formula $[C_{48}H_{53}N_3O_9Ti + Na]^+$ due to the attachment of three groups. A secondary fragment was also observed at 591.2 Da (8.4%, Figure 2.23.B), the exact structure of which is not clear. It appears to be consistent with the empirical formula $C_{32}H_{34}N_2O_6Ti^+$, although it cannot be proved.

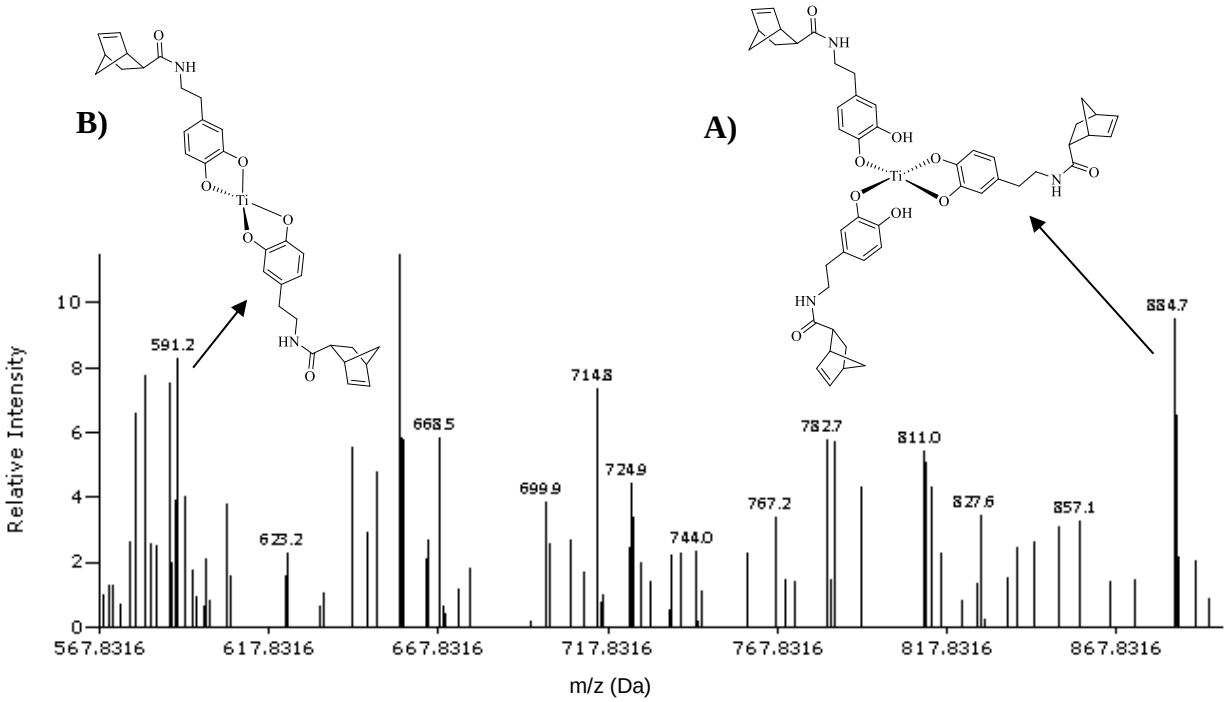

Figure 2.23: ESI-MS spectrum of 2.7

However, the presence of structure B in the product is not expected to cause any difficulties in the subsequent thiol-ene reactions, as it contains two norbornene species and is still capable of promoting cross-linking reactions.

2.4 Conclusions

Dithiolated trehalose **2.3** was synthesised *via* tosylation followed by acetylation, subsequent reaction with potassium thioacetate and then a final deacetylation step. Although the initial step in the synthesis of **2.1** afforded a low yield of 15% due to the multiple recrystallisation steps, the next steps in the reaction sequence afforded good yields, at 74% and 78% for **2.2** and **2.3**, respectively. UV mediated thiol-ene Click chemistry was utilised to induce a catecholic moiety with 46% conversion. It is thought the conversion was not higher due to the following reasons; some molecules of thiolated trehalose participated by only reacting *via* one of the two available thiol groups, or possible oxidation of **2.3** upon exposure to the atmosphere, leading to the formation of disulphide linkages.

^{1}H-^{13}C HSQC NMR, DEPT-135 NMR and FT-IR spectroscopies were found to be efficient characterisation tools. ^{1}H-^{13}C HSQC NMR indicated coupling between resonances in the ^{1}H and ^{13}C NMR spectra, allowing easier assignments. DEPT-135 NMR made it easier to follow the chemical shift of the inverted CH_2 resonances, illustrating the successful development of functionalisation throughout the reaction sequence. FT-IR indicated successful conversion of hydroxyl groups to acetyl groups, and also afforded easier visualisation of the subsequent deprotection step.

The catecholic moiety shows a good affinity for binding to titanium and shall be utilised in crosslinking larger polymer chains, such as HEC. NMR and ESI mass spectroscopies were found to be good characterisation tools for this purpose.

2.5 References

1. A. B. Richards, S. Krakowka, L. B. Dexter, H. Schmid, A. P. M. Wolterbeek, D. H. Waalkens-Berendsen, A. Shigoyuki, M. Kurimoto, *Food Chem. Toxicol.*, **2002**, *40*, 871.
2. K. Maruta, T. Nakada, M. Kubota, H. Chaen, T. Sugimoto, M. Kurimoto, Y. Tsujisaka, *Biosci. Biotechnol. Biochem.*, **1995**, *59*, 1829.
3. T. Higashiyama, A. B. Richards, in *Sweeteners and Sugar Alternatives in Food Technology*, Wiley-Blackwell, **2012**, 417-431.
4. J. M. Thevelein, *Microbiol. Rev.*, **1984**, *48*, 42.
5. J. Luyckx, C. Baudouin, *Clinical Ophthalmology*, **2011**, *5*, 577.
6. M. J. Paul, L. F. Primavesi, D. Jhurreea, Y. Zhang, *Annu. Rev. Plant Biol.*, **2008**, *59*, 417.
7. F. M. Menger, B. N. A. Mbadugha, *J. Amer. Chem. Soc.*, **2001**, *123*, 875.
8. B. Brady, R. Darcy, *Carbohydr. Res.*, **1998**, *309*, 237.
9. Q. Ye, X. Wang, S. Li, F. Zhou, *Macromolecules*, **2010**, *43*, 5554.
10. C. Creutz, M. H. Chou, *Inorg. Chem.*, **2008**, *47*, 3509.

Chapter 3

Modifications of HEC

3.1 Introduction

2-Hydroxyethyl cellulose (HEC) is a chemically modified cellulose derivative, which was developed to overcome the limitations of cellulose, improving its solubility, making it easier to process and leading to greater industrial application.[1] HEC is a highly water soluble polysaccharide that can act as a viscosifier of hydraulic fracturing fluids. However, as previously explained in Section 1.2.3.1, it is unable to participate directly in crosslinking reactions due to the C_2 and C_3 hydroxyl groups being in the *trans* configuration relative to each other.[2]

Therefore, further chemical modification of HEC is required to give rise to possible crosslinking sites. The abundance of hydroxyl groups, especially the highly reactive primary hydroxyls at the C_6 and C_9 positions, can undergo a range of conversions to different functional groups. Examples include nucleophilic substitution or deoxyhalogenation reactions, which can lead to the formation of ester and ether, or alkyl linkages, respectively.[3]

A small amount of literature on the silylation of HEC, and also some limited patents, exist on the chemical modification of HEC. Cellulose (either swollen or as a mixed slurry) is often preferred as the starting material. The reactions attempted were performed on cellulose in the literature, and have been modified so that HEC is used as the saccharide starting material.

This chapter investigates the modification of HEC by imparting small molecules containing carbonyl groups. The carbonyl bond is polarised, with the carbonyl carbon atom having a δ+ charge. The electrophilic nature of the carbonyl carbon atom makes it susceptible to nucleophilic attack from the primary OH groups on HEC. This leads to addition-elimination reactions where an alcohol or water molecule is often lost.[4] The attachment of molecules with diol (bis-MPA) or catecholic (3,4-DHPAA) 'hook' end-group functionalities is described. This modification is anticipated to allow HEC to undergo non-ionic crosslinking reactions by forming covalent bonds to group(IV) metal ions present in crosslinking agents. Surface esterification of HEC *via* the ring opening of succinic anhydride leading to the attachment of succinic acid is also reported. This reaction imparts carboxylic acid end-group functionality, which should allow HEC to undergo ionic crosslinking reactions through chelation to group(IV) metal ions.

3.2 Experimental

3.2.1 Materials

2-Hydroxyethyl cellulose (HEC) (M_w = ~2.5 x 10^5 g mol^{-1}, DS = 1, MS = 2), was purchased from Sigma-Aldrich and was dried in an oven for 24 h at 80 °C under reduced pressure. 2,2-bis(hydroxymethyl)propionic acid (bis-MPA), 2,2-dimethoxypropane, *p*-toluenesulfonic acid monohydrate (*p*-TSA), 3,4-dihydroxyphenylacetic acid (3,4-DHPAA), succinic anhydride, potassium methoxide, 4-(dimethylamino)pyridine (DMAP), acetic acid and DOWEX MR-3 mixed bed ion exchange resin were all purchased from Sigma-Aldrich and used without further purification. All dry solvents were obtained from Durham Chemistry Department Solvent Purification System (SPS). All other solvents were analytical grade purchased from Fisher Scientific and used without any purification. The NMR solvents deuterated chloroform ($CDCl_3$), deuterated dimethylsulfoxide (DMSO-d_6) and deuterium oxide (D_2O) were purchased from Apollo Scientific and used as supplied.

3.2.2 Instrumentation and Measurements

^1H and ^{13}C Nuclear magnetic resonance spectroscopy (NMR) and Fourier-transform infrared (FT-IR) spectroscopy were carried out as outlined in Chapter 2, Section 2.2.2. Inverse-gated ^{13}C NMR spectra were also recorded on a VNMRS 600 operating at 150 MHz.

3.2.3 Synthesis of Isopropylidene-2,2-bis(methoxy)propionic Acid (IBPA) 3.1

The synthesis was performed following the literature procedure.[5] To a 250 mL round bottom flask fitted with a water cooled condenser and magnetic stirrer bar, bis-MPA (20 g, 149 mmol, 1 eq.), 2,2-dimethoxypropane (32. mL, 261 mmol, 1.5 eq.) and pTSA (1.4 g, 7.5 mmol) were dissolved in acetone (100 mL) at ambient temperature for 2 h to afford a clear reaction mixture. The reaction was quenched with NH_3:EtOH (1 mL, 1:1 v/v) solution. The solvent was removed under reduced pressure to leave a white solid, which was dissolved in DCM (250 mL) and washed with deionised water (2 × 30 mL). The organic phase was dried over $MgSO_4$, filtered and the solvent removed under reduced pressure at 40 °C to give **3.1** as a white crystalline solid, yield 82% (21.36 g, 122.6 mmol).

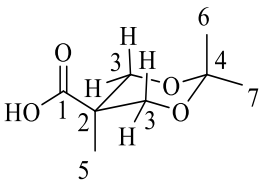

3.1

Figure 3.1: Structure of IBPA with numerical assignments for NMR

^{1}H NMR (600 MHz; DMSO-d_6): δ = 12.50 (s, 1H, OH), 4.00 (d, *J* = 17.5 Hz, 2H, $H_{3\,eq.}$), 3.55 (d, *J* = 17.5 Hz, 2H, $H_{3\,ax.}$), 1.33 (s, 3H, H_7), 1.26 (s, 3H, H_6), 1.07 (s, 3H, H_5). ^{13}C NMR (150 MHz; DMSO-d_6): δ = 175.6 (C_1), 97.3 (C_4), 65.3 (C_3), 40.8 (C_2), 24.6 (C_7), 22.8 (C_6), 18.4 (C_5). FT-IR: ν_{max} = 2997 cm^{-1} (C-H), 1716 cm^{-1} (C=O), 1458, 1380, 1255 (C-O).

3.2.4 Synthesis of IBPA Functionalised HEC 3.2

In a dry, round bottom flask equipped with magnetic stirrer, HEC (1 g, 0.004 mmol, ~4 mmol 1^{o} OH, 1 eq.) and IBPA **3.1** (1.05 g, 6 mmol, 1.5 eq.) were dissolved in dry DMF (40 mL) at 60 °C for 1 h under N_2 atmosphere. *p*-TSA (0.05 g, i.e 5 wt.%) was added and the flask was modified to perform distillation. The reaction mixture was stirred at 120 °C for 8 h. The reaction mixture became pale brown and a small amount of water was observed in the receiving flask. The polymer was precipitated into cold acetone (300 mL), recovered by filtration, dissolved in DMF and precipitated into acetone. The polymer was then dried in an oven for 24 h at 60 °C under reduced pressure to give **3.2** as an off-white solid, yield 89% (1.12 g).

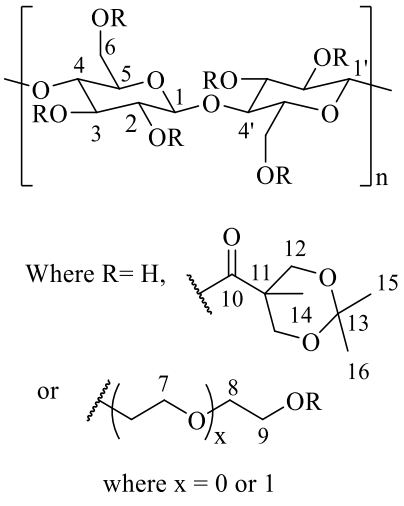

3.2

Figure 3.2: Structure of IBPA functionalised HEC with numerical assignments for NMR

^{13}C NMR (150 MHz; DMSO-d_6): δ = 176.7 (C_{10}), 96.9 (C_{13}), 74.2 (C_1), 72.4 (C_8), 69.8 ($C_{6,}$ $C_{6'}$ (R#H), C_7), 66.3 (C_{12}), 60.3 ($C_{6,}$ $C_{6'}$ (R=H), C_9), 40.8 (C_{11}), 25.9 (C_{16}), 21.8 (C_{15}), 19.6 (C_{14}).

3.2.5 Synthesis of Bis-MPA Functionalised HEC 3.3

The synthesis was performed following the method in the literature.[6] In a vial, IBPA functionalised HEC **3.2** (0.20 g) was dissolved in deionised water (10 mL) at ambient temperature. Acetic acid was added to adjust the pH to 5, and then the mixture stirred for 24 h. The mixture was precipitated into acetone to give an off-white solid, which was washed with acetone and further dried in an oven overnight at 60 °C under reduced pressure. Mass recovered = 0.16 g. The reaction was unsuccessful and **3.3** was not obtained- inverse-gated ^{13}C NMR spectroscopy only showed the presence of unmodified HEC starting material.

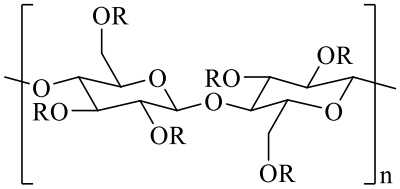

Where R= H,

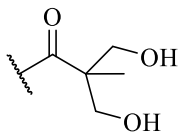

or

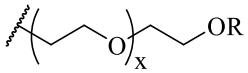

where x = 0 or 1

3.3

Figure 3.3: Structure of bis-MPA functionalised HEC

3.2.6 3,4-Dihydroxyphenylacetic Acid Functionalised HEC 3.4

HEC (1 g, 0.004 mmol, ~4 mmol 1^{o} OH, 1 eq.) and 3,4-DHPAA (0.34-2.02 g, 2-12 mmol, 0.5-3 eq.) were dissolved in dry DMF (20-40 mL) in a dry two-necked round bottom flask equipped with magnetic stirrer and condenser, and kept under N_2 atmosphere. *p*-TSA (5-10 wt.%) was added and the mixture was stirred at 80 °C for 24 h, or at 120 °C if it was necessary to perform distillation to remove the water by-product. The polymer product was precipitated into cold acetone, washed with acetone and dried in an oven at 60 °C for 24 h under reduced pressure to give a pale brown solid product. All reactions were unsuccessful and **3.4** was not obtained- inverse-gated ^{13}C NMR spectroscopy only showed the presence of unmodified HEC starting material.

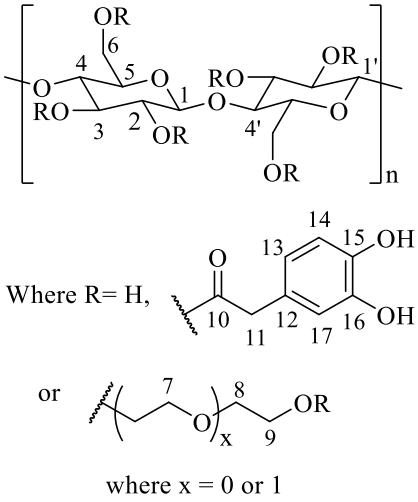

3.4

Figure 3.4: Structure of 3,4-dihydroxyphenylethanoate functionalised HEC, with numerical assignments for NMR

3.2.7 Succinylated HEC 3.5

Synthesis was performed following a known literature procedure used for cellulose which was modified and applied to HEC.[7] In a dry, round bottom flask equipped with magnetic stirrer, HEC (2 g, 0.008 mmol, ~8 mmol 1º OH, 1 eq.) was dissolved in DMSO (35 mL) at 60 °C for 1 h. Succinic anhydride (0.8 g, 8 mmol, 1 eq.) and DMAP (0.1 g, 0.8 mmol) were added. The mixture was stirred at 100 °C for 48 h, upon which the reaction mixture turned dark brown. The reaction mixture was quenched with methanol (5 mL). The polymer was precipitated into cold acetone (300 mL), washed with acetone and dried in an oven at 60 °C for 24 h under reduced pressure to give a pale brown solid **3.5**, yield 2.44 g (43% conversion, determined by inverse-gated ^{13}C NMR spectroscopy).

Further reactions were carried out under the same conditions, but with different reaction times: 30 h, yield 2.24 g (40% conversion); 20 h, yield 1.67 g (33% conversion); 15 h, yield 1.53 g (32% conversion); 10 h, yield 1.42 g (29% conversion).

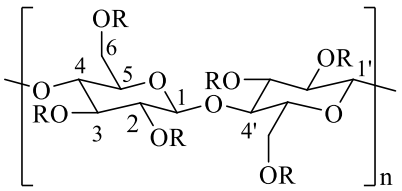

Where R= H,

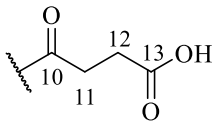

or

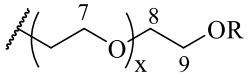

where x = 0 or 1

3.5

Figure 3.5: Structure of succinylated HEC, with numerical assignments for NMR

^{13}C NMR (150 MHz; D_2O): δ = 177.7 (C_{13}), 175.0 (C_{10}), 71.7 (C_8), 69.6 (C_6, $C_{6'}$ (R#H), C_7), 68.5 (C_6, C_9 modified), 64.0 (C_6, C_9 modified), 60.4 (C_6, $C_{6'}$ (R=H), C_9), 29.3 (C_{11}, C_{12}). FT-IR: ν_{max} = 3470 cm^{-1} (OH), 1722 (C=O).

3.3 Results and Discussion

The attachment of the bis-MPA moiety to HEC was performed in a three-step synthesis, outlined in Scheme 3.1. The synthesis involved the protection of the hydroxyl groups of bis-MPA with 2,2-dimethoxypropane to give the small molecule isopropylidene-2,2'-bis(methoxy) propionic acid (IBPA) **3.1**. This was followed by the attachment of **3.1** to HEC using *p*-TSA as a catalyst and removing H_2O as it is formed by distillation in order to obtain **3.2**. Subsequently, the acidic deprotection of the acetal group was performed to give diol end group functionality **3.3**.

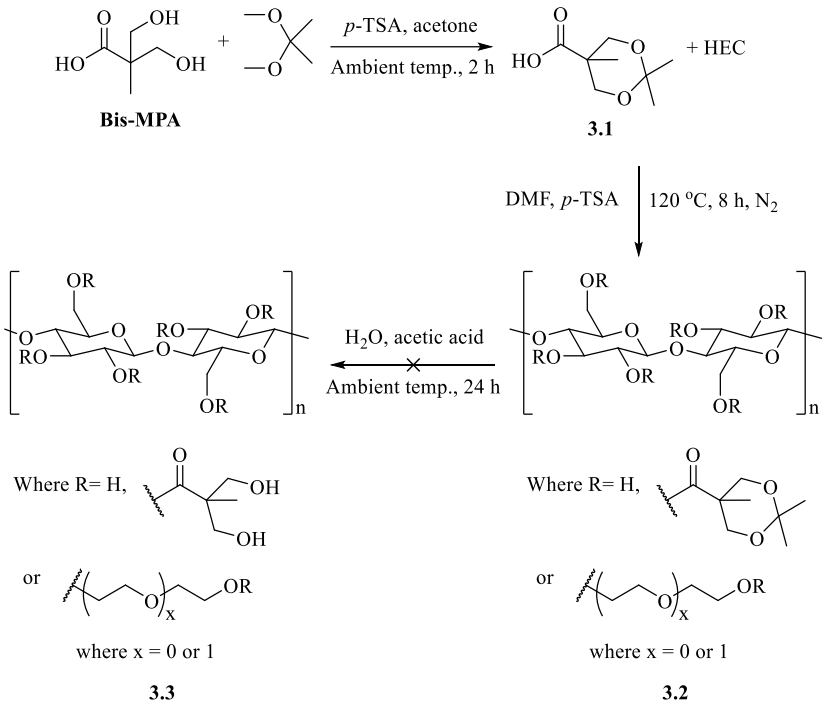

Scheme 3.1: Synthesis of bis-MPA functionalised HEC, 3.3

3.3.1 Isopropylidene-2,2-bis(methoxy)propionic Acid (IBPA) 3.1

The primary alcohol groups of bis-MPA were protected with an acetal group to afford an acetonide group, **3.1**, Scheme 3.1. This was done to prevent self-condensation from occurring in the next reaction step.

The NMR data obtained are consistent with those in the literature.[5] The ^{1}H NMR spectrum of **3.1**, Figure 3.6, shows only one broad hydroxyl resonance due to the carboxylic acid OH at 12.50 ppm. Also, the appearance of singlet resonances at 1.33 and 1.26 ppm are attributed to the methyl protons H_7 and H_6 of the acetal group, indicating the presence of the acetonide and hence a successful protection reaction of the bis-MPA moiety.

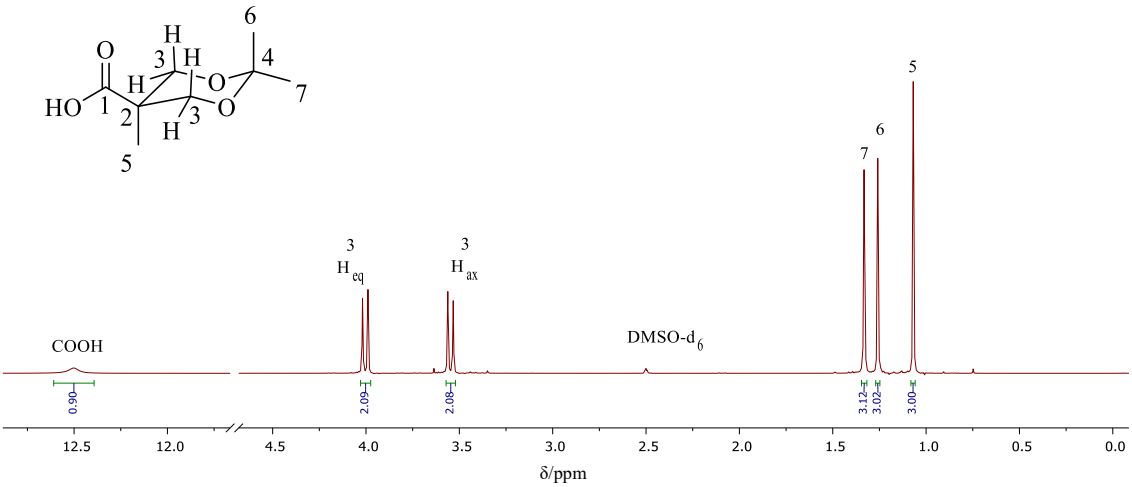

Figure 3.6: ^{1}H NMR spectrum of 3.1 in DMSO-d$_6$

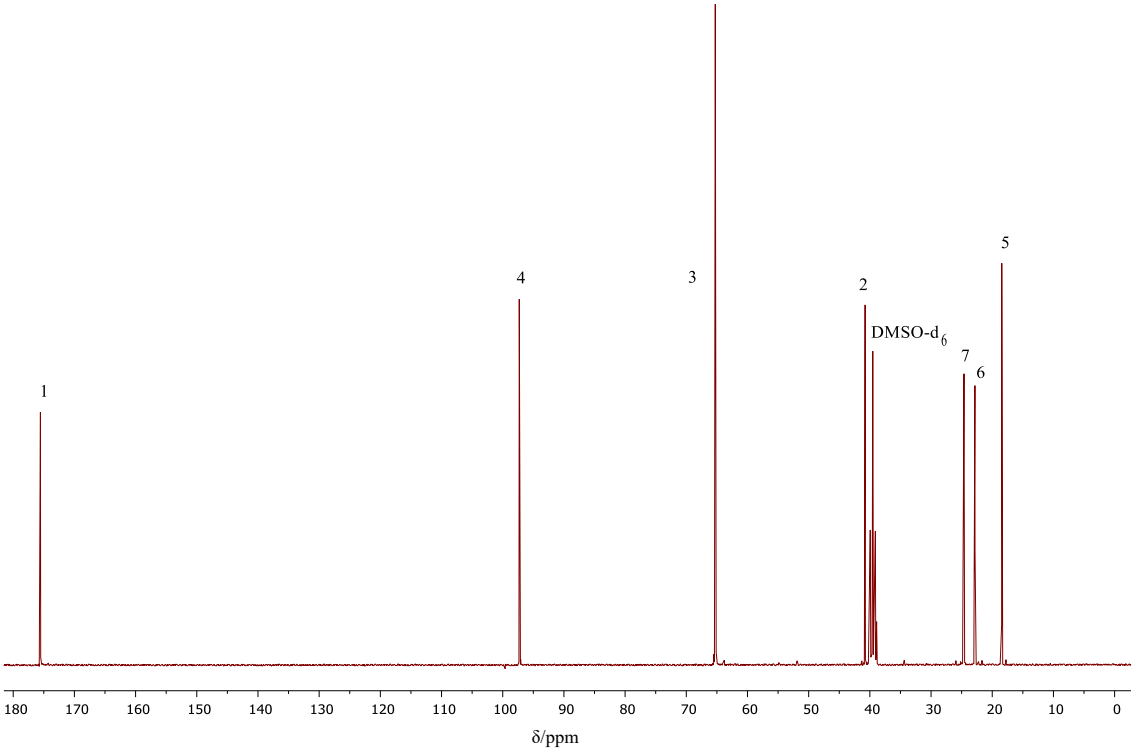

Figure 3.7: ^{13}C NMR spectrum of 3.1 in DMSO-d$_6$

Furthermore, the ^{13}C NMR spectrum of **3.1**, Figure 3.7, shows the resonances 22.8, 24.6 and 98.0 ppm, corresponding to the methyl carbon atoms C_6 and C_7, and the quaternary carbon atom C_4 of the acetal group, respectively. This also confirms complete protection of the primary alcohol groups on the bis-MPA moiety.

3.3.2 IBPA Functionalised HEC 3.2

IBPA functionalised HEC **3.2** was synthesised by the condensation reaction between the primary OH groups on HEC and carboxylic acid group of IBPA **3.1**, Scheme 3.1, using *p*-TSA as a catalyst.

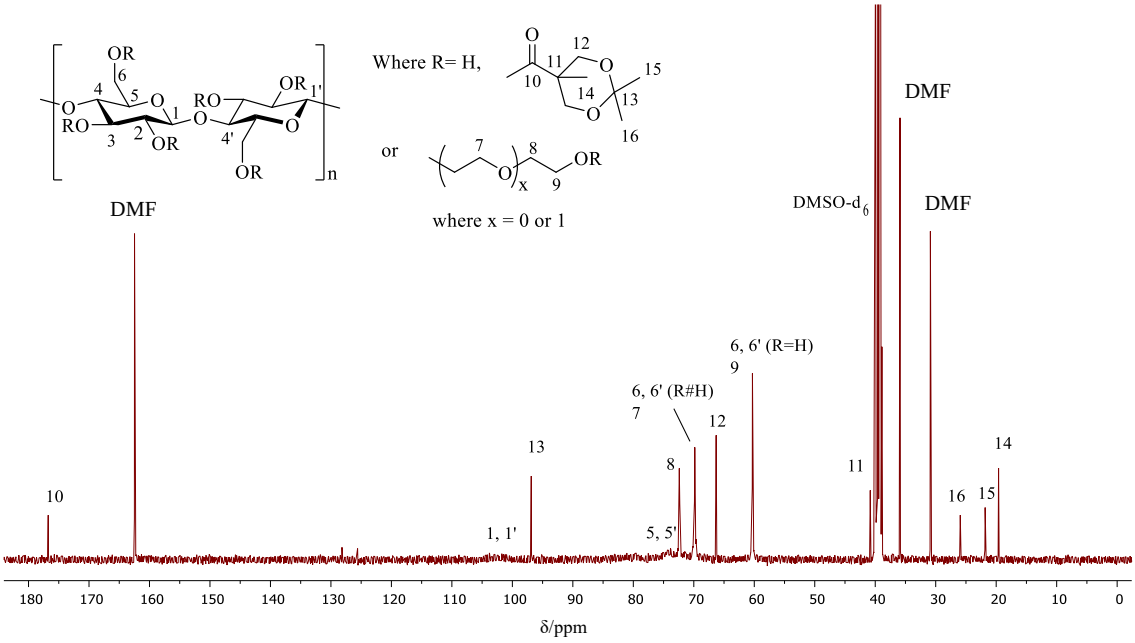

Figure 3.8: ^{13}C NMR spectrum of IBPA functionalised HEC 3.2 in DMSO-d_6

The ^{13}C NMR spectrum of the product **3.2**, Figure 3.8, is shown after two precipitations in acetone in order to remove any unreacted IBPA **3.1**, as a molar excess was used in the reaction. Resonances corresponding to the HEC backbone carbon atoms C_8, C_6 and C_7 (where R#H) and C_6 and C_9 (where R=H) are observed at 72.4, 69.8 and 60.3 ppm, respectively. The resonance at 176.7 ppm is due to the carbonyl carbon atom C_{10} of the IBPA moiety and those at 96.9, 66.3 and 40.8 ppm correspond to C_{13}, C_{12} and C_{11}, respectively, of the acetonide group. The resonances at 25.9, 21.8 and 19.6 ppm are attributable to the carbon atoms of the methyl groups C_{16}, C_{15} and C_{14}, respectively. Residual DMF is trapped within the polymer, based on the resonances observed at 162.5, 35.9 and 30.9 ppm, which was found to be difficult to remove, even after multiple precipitations and drying under reduced pressure.

3.3.3 Bis-MPA Functionalised HEC 3.3

The deprotection of the acetal group in **3.2** to give diol end-group functionality **3.3** was attempted under acidic conditions, Scheme 3.1, based on the literature procedure.[6] This would provide two free primary hydroxyl sites within close range of each other on HEC that could effectively act as a 'hook' and chelate to the metal centre of a group (IV) based crosslinker. This reaction was unsuccessful, as hydrolysis of the ester linkage occurs instead, leading to the removal of the entire IBPA moiety and reformation of HEC starting material. The ^{13}C NMR spectrum of the deprotected product, Figure 3.9, only shows resonances corresponding to the HEC backbone carbon atoms C_8, C_6 and C_7 (R#H), C_6 and C_9 (R=H) at 72.4, 69.8 and 60.3 ppm, respectively.

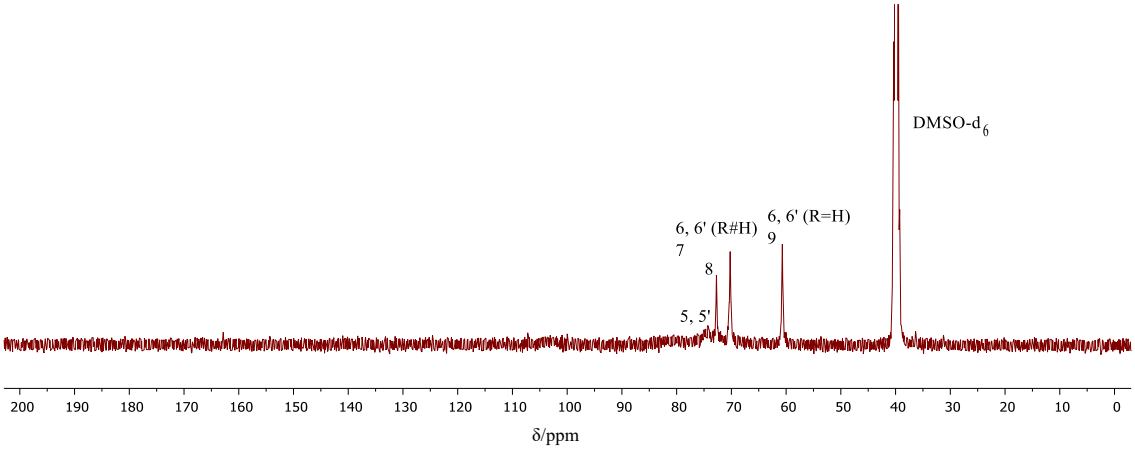

Figure 3.9: ^{13}C NMR spectrum of product after deprotection of polymer 3.2

An alternative method of deprotection of stirring **3.2** with DOWEX mixed bed ion exchange resin was also attempted,[5] but unfortunately yielded the same result as above.

3.3.4 3,4-Dihydroxyphenylacetic Acid Functionalised HEC 3.4

The incorporation of the small molecule 3,4-dihydroxyphenylacetic acid (3,4-DHPAA) was deemed to be a good way to modify HEC in order to allow the polymer to participate in crosslinking reactions. The catechol moiety shows a high affinity for binding to transition metals,[8] particularly titanium and zirconium.[9, 10] This was attempted *via* a condensation reaction (Scheme 3.2), using *p*-TSA as a catalyst to promote the reaction. Distillation techniques were also employed in order to drive the reaction forward by removing water as it was formed.

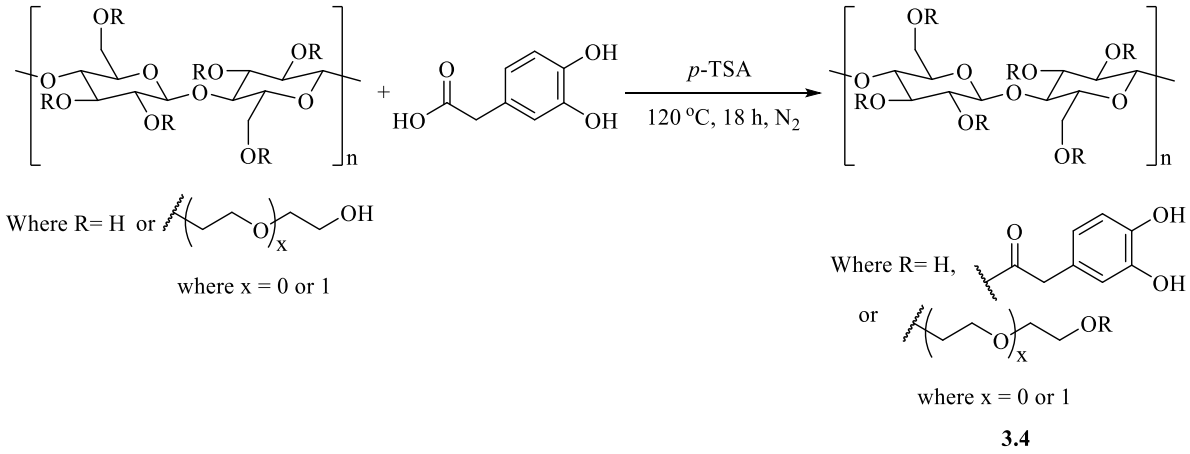

3.4

Scheme 3.2: Synthesis of 3,4-DHPAA functionalised HEC 3.4

However, all attempts at this reaction were unsuccessful, with the ^{13}C NMR spectra of the products only showing resonances corresponding to HEC in all cases, indicative of no attachment of the 3,4-DHPAA molecule. Subsequently, attaching a catechol moiety *via* this method was abandoned. This reaction is likely to have failed due to the presence of some water trapped within the HEC, which is difficult to completely remove due to strong hydrogen bonding. The water molecules may then also act as nucleophiles and attack the electrophilic carbon atom of the charge-polarised carbonyl bond of 3,4-DHPAA. This leads to competing side reactions, reducing the chances of the desired condensation reactions of HEC with 3,4-DHPAA occurring.

3.3.5 Succinylated HEC 3.5

HEC was utilised as an initiator in the ring opening of succinic anhydride. Successful ring opening would lead to the attachment of a succinic acid moiety *via* an ester linkage to give **3.5**. Carboxylic end-group functionalities are known to participate in reactions with group (IV) metal ions *via* chelation, and could afford another potential route to allow HEC to participate in crosslinking reactions.

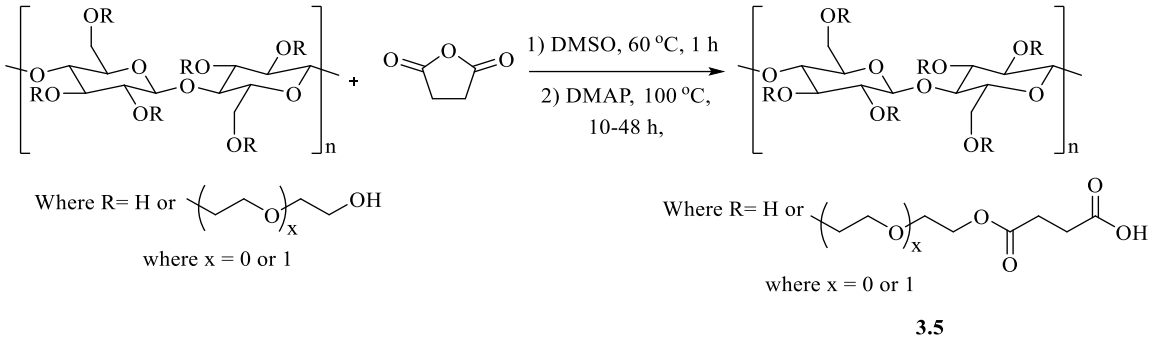

3.5

Scheme 3.3: Synthesis of succinylated HEC 3.5

Initial attempts were tried using either *p*-TSA or KOMe as catalysts, which were found to be unsuccessful. In all cases, no resonances due to succinic acid were observed in the ^{13}C NMR spectra, but resonances due to the unreacted succinic anhydride ring were present in the ^{13}C NMR spectra of the solvent washings.

Huang *et al.* successfully carried out surface esterification of cellulose fibres with succinic anhydride by using a small amount of DMSO as the solvent, DMAP as the catalyst and subjecting the reactants to ball milling to promote the reaction.[7] The combination of using DMSO and DMAP reagents was applied to this series of reactions, Scheme 3.3.

Inverse-gated ^{13}C NMR spectroscopy was utilised in order to allow the integration of the resonance at 60.4 ppm corresponding the unmodified C_6, $C_{6'}$ and C_9 carbon atoms against the resonances at 64.0 and 68.5 ppm corresponding to modified C_6, $C_{6'}$ and C_9 carbon atoms. Multiple reactions in the synthesis of **3.5** were carried out over a range of reaction times, to investigate the degree of succinylation at the HEC C_6 and C_9 primary hydroxyl groups. The inverse-gated ^{13}C NMR spectrum of **3.5** after 30 h reaction time is shown in Figure 3.10.

The appearance of two new resonances at 64.0 and 68.5 ppm corresponds to the modified CH_2 carbon atoms C_6, $C_{6'}$ and C_9, indicating attachment of succinic acid. The DEPT-135 ^{13}C NMR spectrum of **3.5** also confirms that these resonances are CH_2 groups, as they are in the same

phase as the other methylene carbon atoms. However, there is still a resonance observed at 60.4 ppm which corresponds to the unmodified CH_2 in HEC, indicating that complete functionalisation of the HEC primary OH groups has not occurred.

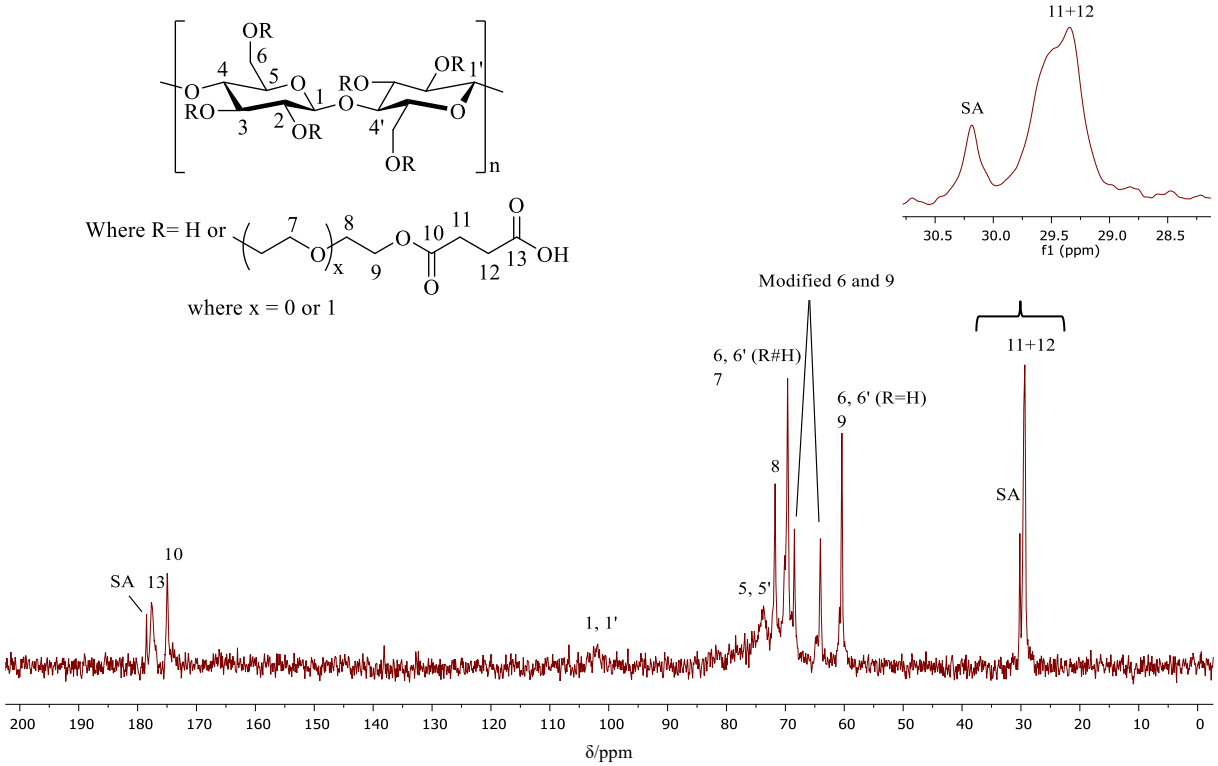

Figure 3.10: Inverse-gated ^{13}C NMR spectrum of succinylated HEC 3.5 after 30 h reaction time in D_2O

Resonances at 177.7 and 175.0 ppm are due to the new carbonyl groups formed by successful ring-opening of succinic anhydride; they correspond to the carboxylic acid (C_{13}) and ester functionalities (C_{10}), respectively, of succinic acid. The slightly broader resonance at 29.3 ppm is actually two overlapping resonances upon magnification, corresponding to the CH_2 groups C_{11} and C_{12}. Resonances at 178.5 and 30.2 ppm correspond to the carbonyl and CH_2 groups, respectively, of unreacted succinic anhydride starting material. This is residual reactant that is trapped within the polymer, remaining after multiple washes.

The effect of reaction time on the esterification reaction of HEC with succinic anhydride catalysed by DMAP and the formation of the desired product was investigated. The reaction was carried out for 48 h leading to successful succinylation of HEC. However, the abundance of newly attached carboxylic acid end groups increased the hydrophobic characteristics of the polymer. Therefore, heating was required in order for the polymer to fully dissolve in water. This will be undesirable as the polymer must be readily soluble in water at ambient temperature in order to be utilised in fracturing fluid applications. Therefore, a series of experiments were

performed at lower reaction times in order to reduce the functionalisation conversion, and hence the number of carboxylic acid groups on HEC. This was anticipated to improve the solubility of the polymer product in water.

Inverse-gated ^{13}C NMR spectroscopy allowed the integration values of the unmodified C_6 resonance at 60.4 ppm, and the modified C_6 resonance at 64.0 ppm to be determined. These values were then utilised to calculate approximate % conversion using Equation 3.1. The integral values and calculated % conversions are presented in Table 3.1. The change in % conversion with respect to reaction time is represented in Figure 3.11.

$$\%\ Conversion = \frac{C_6}{C_6 + C_{6\ modified}}\ x\ 100 \qquad \text{Equation 3.1}$$

As the reaction time increases, the calculated % conversion of the unmodified C_6 carbon atoms to modified C_6 carbon atoms also increases. The functionalised polymers with higher conversions (≥40%) exhibited low solubility in water, whilst the functionalised polymers with lower conversions (≤33%) exhibited very good solubility in water. Moreover, all succinylated polymers were no longer fully soluble in DMF in comparison to the HEC starting material.

Table 3.1: Integrals of unmodified and modified C_6 resonances from inverse-gated ^{13}C NMR spectroscopy, calculated % conversions and observed water solubility for succinylated HEC 3.5 at different reaction times

Reaction Time (h)	C_6-OH integral	Succinylated C_6 integral	% Conversion	Water solubility
48	1.00	0.76	43	Very low
30	1.00	0.66	40	Low
20	1.00	0.49	33	Very good
15	1.00	0.46	32	Very good
10	1.00	0.40	29	Very good

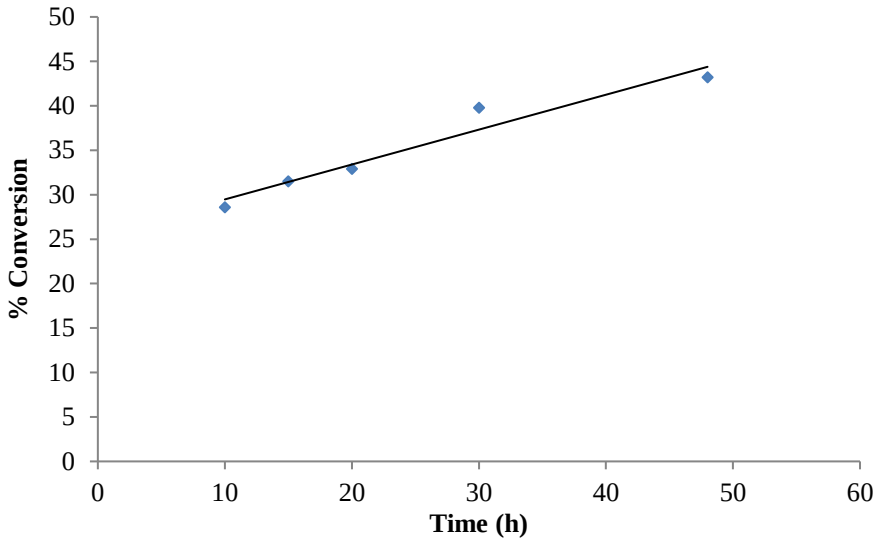

Figure 3.11: Effect of reaction time on C_6 % conversion in succinylated HEC 3.5

The addition of one equivalent of NaOH to the functionalised polymers showing a greater % conversion was intended to help improve their water solubility by converting the carboxylic acid functionalities to their sodium salts, as outlined in Scheme 3.4. The polymers became very soluble, but it was found in actuality the NaOH was facilitating the base-catalysed cleavage of the ester bonds, reforming unmodified HEC and producing free succinic acid.

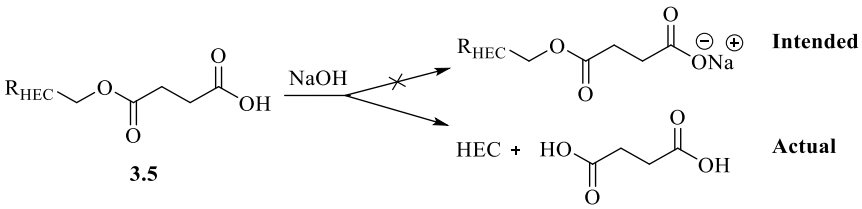

Scheme 3.4: Intended and actual reaction products of 3.5 with NaOH

The ^{13}C NMR spectrum of the product formed by treating **3.5** with NaOH is shown in Figure 3.12. In comparison to Figure 3.10, the resonances corresponding to the modified HEC C_6 carbon atoms at 64.0 and 68.5 ppm have disappeared, with only resonances due to the unmodified HEC backbone remaining. The appearance of the sharp resonances at 182.4 and 34.2 ppm correspond to the carbonyl (C_a) and CH_2 (C_b) groups, respectively, of free succinic acid,[11] indicating cleavage of the ester linkages.

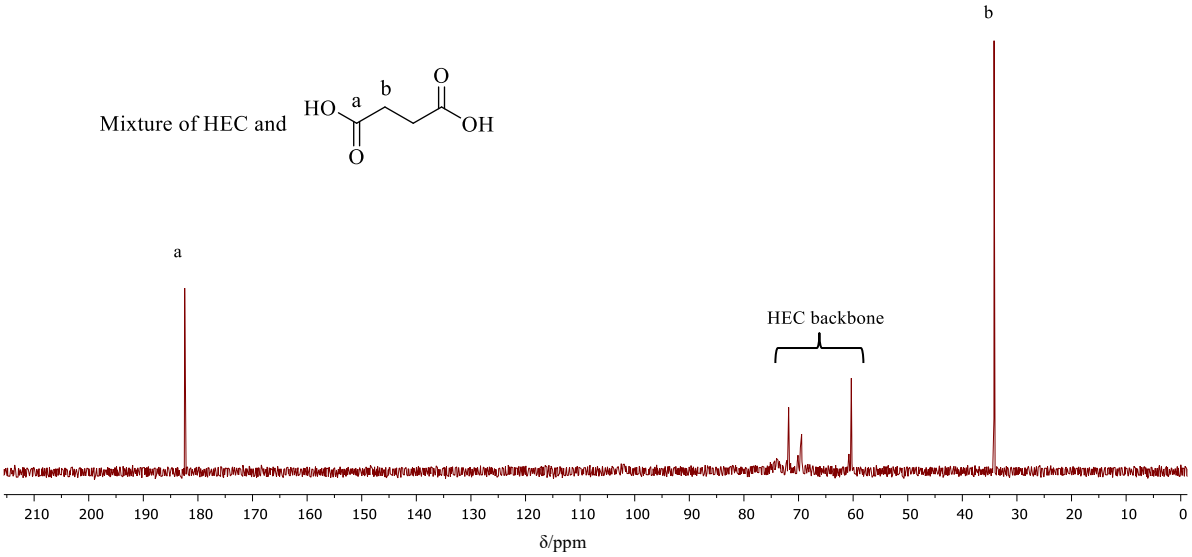

Figure 3.12: ^{13}C NMR spectrum of the products of NaOH treated succinylated HEC, in D_2O

3.4 Conclusions

Condensation reactions carried out on HEC in the work reported here were mostly unsuccessful, despite the use of a range of acid and base catalysts. This is believed to be due to the difficulties in completely drying HEC, as some water molecules remain due to strong hydrogen bonding within the backbone. The successful attachment of IBPA **3.1** *via* condensation reactions between the carboxylic acid group and the primary hydroxyl groups of HEC afforded IBPA functionalised HEC **3.2**. This reaction required high temperatures and the utilisation of distillation techniques in order to remove water and drive the reaction forward. Attempted deprotection of the acetal group of IBPA functionalised HEC **3.2** in order to produce bis-MPA functionalised HEC **3.3** using either acetic acid or H^+/OH^- mixed bed ion exchange resin was unsuccessful. The deprotection reaction induced the hydrolysis of the ester linkages, fully removing the IBPA moiety and reforming the HEC starting material.

Attempts were made to functionalise HEC with 3,4-dihydroxyphenylacetic acid to produce HEC with catecholic end-group functionality **3.4** *via* condensation reactions of the primary hydroxyl groups of HEC and the carboxylic acid 3,4-DHPAA. The catechol moiety is well known to bind to group (IV) transition metal ions in crosslinking reactions. Reactions using *p*-TSA as a catalyst were all unsuccessful, as only signals due to unmodified HEC were observed in the inverse gated ^{13}C NMR spectra of crude products.

Successful surface esterification of the primary hydroxyl groups of HEC *via* the ring opening of succinic anhydride using DMAP as a catalyst led to the attachment of succinic acid moieties and the formation of succinylated HEC **3.5**. Inverse-gated ^{13}C NMR spectroscopy was deemed to be the most useful method of characterisation, due to the broad resonances afforded by the large number of protons on the HEC backbone dominating the ^1H NMR spectra of succinylated HEC **3.5**. This method allowed the integration values of the unmodified C_6 resonance at 60.4 ppm, and the modified C_6 resonance at 64.0 ppm to be determined. These values were then utilised to calculate the approximate % conversion. As the reaction time increases, the calculated % conversion of the unmodified C_6 carbon atoms to modified C_6 carbon atoms also increases, up to 43% conversion after 48 h. The acid functionalised polymers with higher conversions (≥40%) exhibited low solubility in water, whilst the acid functionalised polymers with lower conversions (≤33%) exhibited very good solubility in water.

Addition of one equivalent of NaOH was added to the acid functionalised polymer solutions with 40% and 43% conversion of modified C_6 atoms. This was to improve their water solubility

by converting the carboxylic acid functionalities to their sodium salts. Unfortunately, this facilitated the base-catalysed cleavage of the ester bonds, reforming unmodified HEC and producing free succinic acid.

3.5 References

1. A. Sannino, C. Demitri, M. Madaghiele, *Materials,* **2009**, *2*, 353.
2. C. Montgomery, in *Effective and Sustainable Hydraulic Fracturing* (Eds.: A. P. Bunger, J. McLennan, R. Jeffrey), InTech, **2013**, 25-45.
3. S. Kamel, N. Ali, K. Jahangir, S. M. Shah, A. A. El-Gendy, *Exp. Polym. Lett.*, **2008**, *2*, 758.
4. J. Clayden, N. Greeves, S. Warren, P. Wothers, *Organic Chemistry*, Oxford University Press, New York, **2001**, 135-150.
5. H. Ihre, A. Hult, J. M. J. Fréchet, I. Gitsov, *Macromolecules,* **1998**, *31*, 4061.
6. K. A. V. Zubris, Y. L. Colson, M. W. Grinstaff, *Mol. Pharm.,* **2011**, *9*, 196.
7. P. Huang, Y. Zhao, S. Kuga, M. Wu, Y. Huang, *Nanoscale,* **2016**, *8*, 3753.
8. W. Tang, G. M. Policastro, G. Hua, K. Guo, J. Zhou, C. Wesdemiotis, G. L. Doll, M. L. Becker, *J. Am. Chem. Soc.,* **2014**, *136*, 16357.
9. P. A. Connor, K. D. Dobson, A. J. McQuillan, *Langmuir,* **1995**, *11*, 4193.
10. H. G. Upritchard, J. Yang, P. J. Bremer, I. L. Lamont, A. J. McQuillan, *Langmuir,* **2011**, *27*, 10587.
11. S. Dutta, L. Wu, M. Mascal, *Green Chem.*, **2015**, *17*, 2335.

Chapter 4

Thiolation and Click Reactions of HEC

4.1 Introduction

In hydraulic fracturing, guar and its derivatives are often employed as the main gelling agent in fracturing fluid, as these are known to undergo crosslinking reactions with group(IV) metal based crosslinkers.[1] 2-Hydroxyethyl cellulose (HEC) is a water soluble polymer currently utilised as a means to increase the viscosity of the fracturing fluid. However, due to the hydroxyl groups being in the *trans* position, HEC cannot participate in crosslinking and can therefore only be used as a secondary, linear gel.[2] Chemical modification to the hydroxyl groups must be carried out in order to provide crosslinking sites, enabling crosslinking reactions to take place.

Due to the successful modification of trehalose with thiol functionality in Chapter 2, the same functionalisations were to be applied to HEC. This would then allow the thiolated HEC to undergo thiol-ene Click reactions with a norbornene-catechol moiety. Catechol has been proven to show a good affinity for binding to titanium,[3] thus allowing the HEC to participate in crosslinking reactions.

A previous method of thiolation of HEC in the literature is outlined in Scheme 4.1. This involves the ring-opening of the glucose unit *via* periodate oxidation of the hydroxyl groups at the C_2 and C_3 positions to aldehyde groups, using sodium periodate as the oxidising agent.[4, 5] Cysteamine, which is the degradation product of the amino acid cysteine, is then attached in a reductive amination reaction using sodium borohydride as the reducing agent.

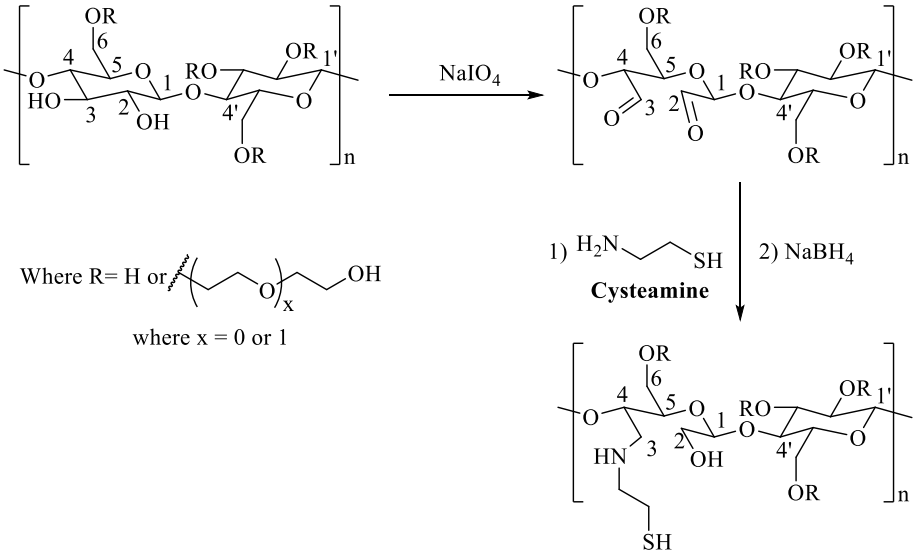

Scheme 4.1: Thiolation of HEC with cysteamine *via* periodate oxidation and reductive amination

However, this method of thiolation *via* cysteamine grafting breaks the sugar ring between the C_2 and C_3 carbon atoms, which may make the polymer chain weaker and affect its ability to build viscosity when undergoing crosslinking reactions. The addition of extra NH groups also increases the polymers ability to participate in hydrogen bonding, which in turn may decrease its solubility in water.

This chapter describes the attempts to synthesise thiol functionalised HEC, applying the knowledge and experience gained from previous work on the model compound trehalose. An alternative one-pot reaction is also utilised.

The chemical modification strategy carried out in this chapter should help to increase the diversity of polysaccharide backbone structural functionalisations.

4.2 Experimental

4.2.1 Materials

2-Hydroxyethyl cellulose (HEC) (M_w = ~2.5 x 10^5 g mol^{-1}, DS = 1, MS = 2), potassium thioacetate, triphenylphosphine (PPh_3), carbon tetrabromide (CBr_4), thiobenzoic acid, *p*-toluenesulfonyl chloride (TsCl), acetic anhydride, trimethylamine, hydrochloric acid (HCl), sodium hydroxide (NaOH), potassium carbonate and DOWEX H^+ resin were all purchased from Sigma-Aldrich and used without further purification, except HEC which was dried in an oven at 80 °C for 24 h under reduced pressure prior to use.

All dry solvents were obtained from Durham Chemistry Department Solvent Purification System (SPS). All other solvents were analytical grade purchased from Fisher Scientific and used without any purification. The NMR solvents deuterated dimethylsulfoxide (DMSO-d_6) and deuterium oxide (D_2O) were purchased from Apollo Scientific and used as supplied.

4.2.2 Instrumentation and Measurements

^1H and ^{13}C Nuclear magnetic resonance spectroscopy (NMR) and Fourier-transform Infrared (FT-IR) spectroscopy were carried out as outlined in Chapter 2, Section 2.2.2. Inverse-gated ^{13}C NMR spectra were also recorded on a VNMRS 600 operating at 150 MHz.

pH measurements were determined using a Jenway model 3020 pH meter.

4.2.3 Synthesis of Tosylated and Acetylated HEC 4.1

In a dry, two-necked round bottom flask equipped with magnetic stirrer and septum, HEC (2 g, 0.008 mmol, ~8 mmol 1º OH, 1 eq.) was dissolved in dry DMF (40 mL) at 60 °C for 1 h under N_2 atmosphere, followed by the addition of triethylamine (10 mL, 80 mmol). *p*-Toluenesulfonyl chloride (1.48 g, 8 mmol, 1 eq.) in dry DMF (15 mL) was then added to the reaction mixture dropwise *via* cannula at ambient temperature, upon which a colour change to bright orange was observed. Acetic anhydride (8.2 mL, 80 mmol, 10 eq.) was added and the mixture was stirred for 18 h at ambient temperature. The polymer was precipitated into ice water (600 mL), washed with water and dried in an oven at 70 °C for 24 h under reduced pressure to give **4.1** as a white solid (2.34 g, complete conversion of 1º OH).

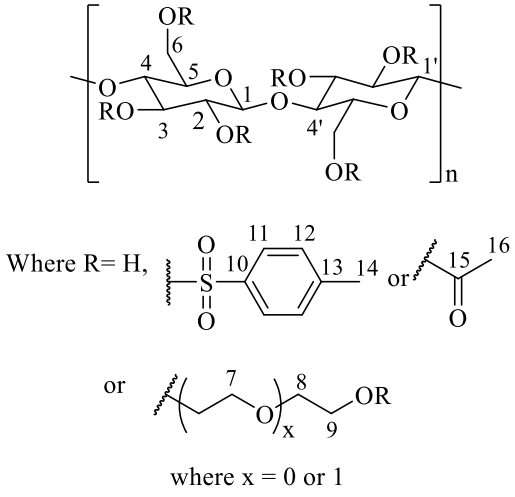

4.1

Figure 4.1: Structure of tosylated and acetylated HEC with numerical assignments for NMR

Key resonances in ^{13}C NMR (150 MHz; DMSO-d_6): δ = 170.3 (C_{15}), 128.1 (C_{11}), 125.5 (C_{12}), 63.2 (C_6, C_9 modified), 20.7 (C_{16}).

FT-IR: ν_{max} = 2980 cm^{-1} (aromatic CH), 1730 cm^{-1} (C=O).

4.2.4 Attempted Functionalisation of Tosylated and Acetylated HEC with Potassium Thioacetate 4.2

Tosylated and acetylated HEC **4.1** (0.5 g, ~2 mmol Ts groups) and potassium thioacetate (0.57 g, 5 mmol, 2.5 eq.) were dissolved in dry DMF (15 mL) in a dry two-necked round bottom flask equipped with magnetic stirrer, condenser, and kept under N_2 atmosphere. The reaction mixture was stirred at 70 °C for 36 h and a colour change to pale brown was observed. The polymer

was precipitated into ice water (200 mL), washed with water and dried in an oven at 70 °C for 24 h under reduced pressure to give a white solid **4.2**.

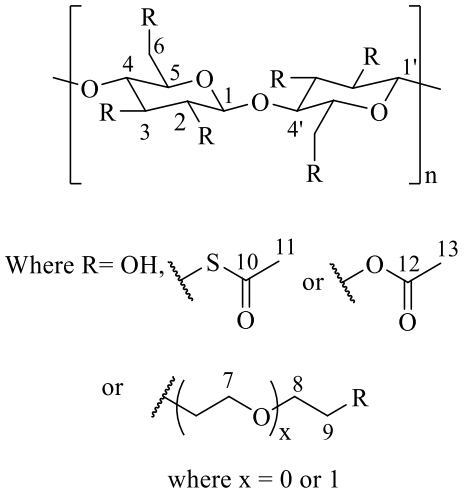

4.2

Figure 4.2: Structure of primary thioacetylated functionalised acetylated HEC with numerical assignments for NMR

However, the ^{13}C NMR spectrum only showed resonances corresponding to the starting material **4.1**.

4.2.5 Synthesis of Sodium Thiobenzoate 4.3

Sodium thiobenzoate was synthesised using the following procedure.[6]

To an ice-cold solution of thiobenzoic acid (10 g, 72 mmol) dissolved in deionised water, NaOH solution (10 M) was added until the solution just turned alkaline. The reaction mixture was then neutralised with the addition of aqueous thiobenzoic acid. The ice-cold mixture was then filtered, and evaporated to dryness under reduced pressure. The remaining solid was then dried in an oven for 24 h at 60 °C under reduced pressure to give **4.3** as a bright yellow solid, mp 209-212 °C, yield 92.4% (12.54 g, 78 mmol).

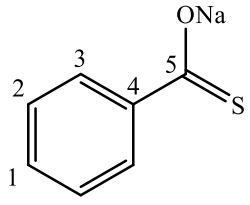

4.3

Figure 4.3: Structure of sodium thiobenzoate with numerical assignments for NMR

^{1}H NMR (600 MHz; D_2O): δ = 8.01 (d, *J* = 12 Hz, 2H, H_3), 7.53 (t, *J* = 12 Hz, 1H, H_1), 7.44 (t, *J* = 12 Hz, 2H, H_2). ^{13}C NMR (150 MHz; D_2O): δ = 215.7 (C_5), 143.7 (C_4), 131.5 (C_1), 128.1 (C_3), 127.7 (C_2).

CHN: Expected %C = 52.49, %H = 3.15, %N = 0.00; Measured %C = 51.62, %H = 3.32, %N = 0.00. The discrepancy in expected and obtained values may be due to the presence of a small amount of water in the sample.

4.2.6 Attempted Functionalisation of Tosylated and Acetylated HEC with Sodium Thiobenzoate 4.4

Tosylated and acetylated HEC **4.1** (0.5 g, ~2 mmol Ts groups) and sodium thiobenzoate (0.16 g, 1 mmol, 0.5 eq.) were dissolved in dry DMF (15 mL) in a dry two-necked round bottom flask equipped with magnetic stirrer, condenser, and kept under N_2 atmosphere. The reaction mixture was stirred at 70 °C for 36 h and a colour change to dark orange was observed. The polymer was precipitated into ice water (200 mL), washed with water and dried in an oven at 70 °C for 24 h under reduced pressure to give a pale brown solid.

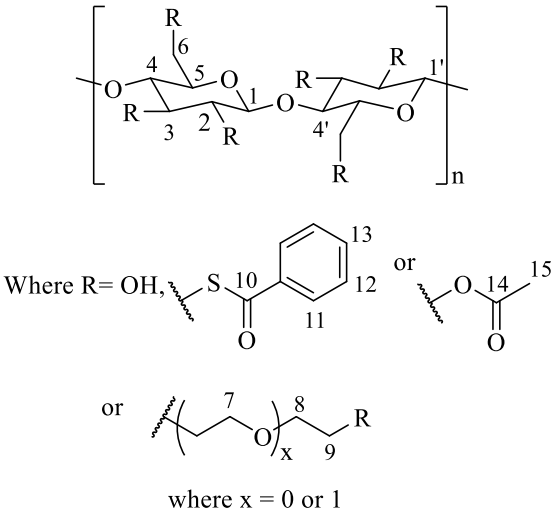

4.4

Figure 4.4: Structure of primary thiobenzoate functionalised acetylated HEC with numerical assignments for NMR

However, the ^{13}C NMR spectrum showed no resonances corresponding to attached thiobenzoate.

4.2.7 Synthesis of Trehalose Thiobenzoate 4.5

In a dry, three-necked round bottom flask equipped with magnetic stirrer and septum, trehalose dihydrate (1 g, 2.7 mmol, 1 eq.) and sodium thiobenzoate **4.3** (1.7 g, 10.8 mmol, 4 eq.) were dissolved in dry DMF (30 mL). The reaction mixture was heated to at 60 °C under N_2 atmosphere for 1 h, upon which a colour change to bright yellow was observed. The reaction mixture was then cooled in an ice water bath and triphenylphosphine (1.4 g, 5.3 mmol, 2 eq.) was added, upon which a colour change to orange was observed. Carbon tetrabromide (1.7 g, 5.3 mmol, 2 eq.) dissolved in dry DMF (5 mL) was then added dropwise *via* cannula, and the reaction mixture became brown. The reaction was stirred for 48 h at ambient temperature. Methanol (10 mL) was added to quench the reaction. The polymer was then precipitated into ethanol (300 mL), washed with ethanol and dried in an oven at 70 °C for 24 h under reduced pressure to give an off-white solid **4.5**, yield 82.1% (1.29 g, 2.2 mmol).

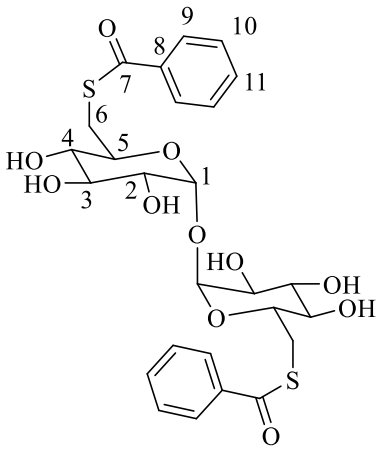

4.5

Figure 4.5: Structure of trehalose thiobenzoate with numerical assignments for NMR

^{1}H NMR (600 MHz; DMSO-d_6): δ = 7.88 (d, *J* = 12 Hz, 2H, H_9), 7.65-7.53 (m, 1H, H_{11}), 7.30 (dd, J_1 = 18 Hz, J_2 = 12 Hz, 2H, H_{10}), 4.89 (d, *J* = 3.6 Hz, 1H, H_1), 3.69-3.65 (m, 1H, H_5), 3.60 (t, *J* = 6 Hz, 1H, H_3), 3.55 (dd, J_1 = 12 Hz, J_2 = 1.8 Hz, 1H, H_6), 3.50 (dd, J_1 = 12 Hz, J_2 = 6 Hz, 1H, $H_{6'}$), 3.26 (dd, J_1 = 6 Hz, J_2 = 3.6 Hz, 1H, H_2), 3.17 (t, *J* = 6 Hz, 1H, H_4). ^{13}C NMR (150 MHz; DMSO-d_6): δ = 170.5 (C_7), 139.5 (C_8), 131.7 (C_{11}), 129.1 (C_9), 127.2 (C_{10}), 93.2 (C_1), 72.8 (C_5), 72.5 (C_3), 71.6 (C_2), 70.1 (C_4), 60.8 (C_6).

FT-IR: ν_{max} = 3520 cm^{-1} (OH), 3000 cm^{-1} (aromatic CH), 1720 cm^{-1} (C=O).

4.2.8 Synthesis of HEC Thiobenzoate 4.6

The product **4.6** was prepared using a modified literature procedure.[7]

In a dry, three-necked round bottom flask equipped with magnetic stirrer and septum, HEC (2 g, 0.008 mmol, ~8 mmol 1° OH, 1 eq.) and sodium thiobenzoate (5.4 g, 32 mmol, 4 eq.) were dissolved in dry DMF (50 mL). The reaction mixture was heated to 100 °C under N_2 atmosphere for 1 h, upon which a colour change to bright yellow was observed. The reaction mixture was then cooled in an ice water bath and triphenylphosphine (4.2 g, 16 mmol, 2 eq.) was added, upon which a colour change to orange was observed. Carbon tetrabromide (5.4 g, 16 mmol, 2 eq.) dissolved in dry DMF (10 mL) was then added dropwise *via* cannula, and the reaction mixture became brown. The reaction was stirred for 48 h at ambient temperature. Methanol (40 mL) was added to quench the reaction. The polymer was then precipitated into ethanol (500 mL), filtered and washed with ethanol until the washings ran clear to give a light green solid. This was further dried in an oven at 60 °C for 24 h under reduced pressure to give **4.6** as an off-white solid, yield 97% (1.28 g, ~0.0042 mmol).

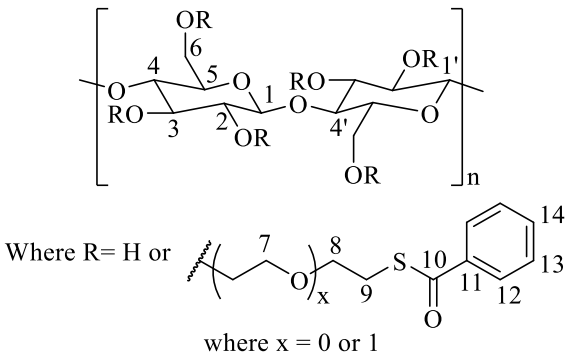

4.6

Figure 4.6: Structure of HEC thiobenzoate with numerical assignments for NMR

Key resonances in ^{13}C NMR (150 MHz; DMSO-d_6): δ = 165.7 (C_{10}), 133.3 (C_{14}), 129.7 (C_{11}), 129.1 (C_{12}), 128.7 (C_{13}), 68.3 (C_6, C_9 modified), 64.0 (C_6, C_9 modified).
FT-IR: ν_{max} = 3490 cm^{-1} (OH), 3020 cm^{-1} (aromatic CH), 1712 cm^{-1} (C=O) 1380 cm^{-1} (C=C), 1260 cm^{-1} (C=C).

4.2.9 Debenzoylation of HEC Thiobenzoate 4.6 to Thiolated HEC 4.7

The product **4.7** was prepared using a modified literature procedure.[8]

In a vial, HEC thiobenzoate **4.6** (0.3 g) was stirred in an aqueous NaOH solution (3 M, 15 mL) for 6 h at ambient temperature. The reaction mixture became yellow and the pH found to be

12.3. The mixture was acidified to pH 6 with the addition of HCl (2 M) solution, and then precipitated into cold acetone (150 mL) to give a swollen gel-like polymer. This was dried in an oven for 24 h at 60 °C under reduced pressure to give **4.7** as a light brown solid, yield ~73% (0.22 g, ~0.06 mmol SH).

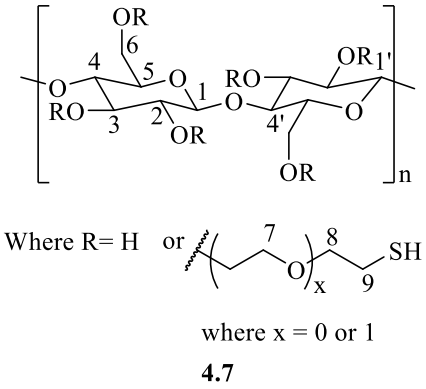

4.7

Figure 4.7: Structure of thiolated HEC with numerical assignments for NMR

Key resonances in ^{13}C NMR (150 MHz; DMSO-d_6): δ = 60.7 (*C*H_2-SH).

FT-IR: ν_{max} = 3417 cm^{-1} (OH), 2580 cm^{-1} (SH).

4.2.10 Thiol-ene Click of Thiolated HEC with Norbornene-catechol 4.8

In a vial, thiolated HEC **4.7** (0.1 g, ~0.06 mmol SH) and norbornene-catechol compound **2.4** (0.017 g, 0.06 mmol) were dissolved in DMF (5 mL) and heated for 1 h at 60 °C. The colour of the reaction mixture was pale yellow. The vial was irradiated with UV light for 48 h, upon which a colour change to dark yellow/brown was observed. The polymer was precipitated into cold acetone (50 mL), washed three times with acetone to give an off-white solid. This was further dried in an oven at 60 °C for 24 h under reduced pressure to give **4.8** as an off-white solid (0.092 g). The reaction was unsuccessful, as no decreases in the intensities of the alkene resonances attributed to **2.4** were observed in the ^{1}H NMR spectrum.

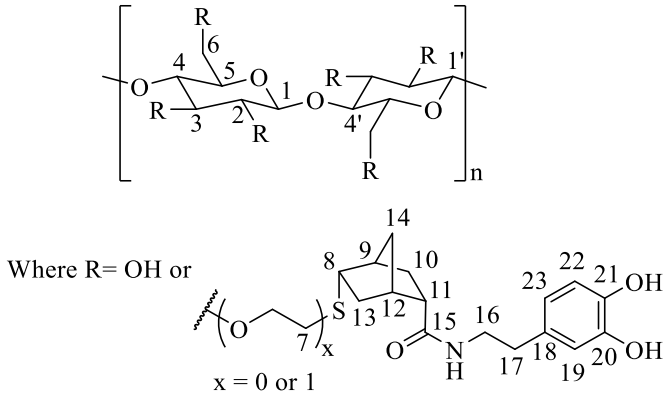

4.8

Figure 4.8: Structure of thiolated HEC clicked with norbornene-catechol, with numerical assignments for NMR

4.2.11 Synthesis of HEC Thioacetate 4.9

In a dry, three-necked round bottom flask equipped with magnetic stirrer and septum, HEC (1g, 0.004 mmol, ~4 mmol 1º OH, 1 eq.) and potassium thioacetate (5.4 g, 48 mmol, 12 eq.) were dissolved in dry DMF (50 mL). The reaction mixture was heated at 100 °C under N_2 atmosphere for 1 h, upon which a colour change to turquoise was observed. The reaction mixture was then cooled in an ice water bath and triphenylphosphine (2.1 g, 8 mmol, 2 eq.) added, upon which a colour change to orange was observed. Carbon tetrabromide (2.7 g, 8 mmol, 2 eq.) dissolved in dry DMF (10 mL) was then added dropwise *via* cannula, and the reaction mixture became brown. The reaction was stirred for 48 h at ambient temperature. Methanol (10 mL) was added to quench the reaction. The polymer was then precipitated into ethanol (500 mL), washed three times with ethanol and dried in an oven at 60 °C for 24 h under reduced pressure to give **4.9** as an off-white solid, yield 67% (1.63 g, approx. 0.006 mmol).

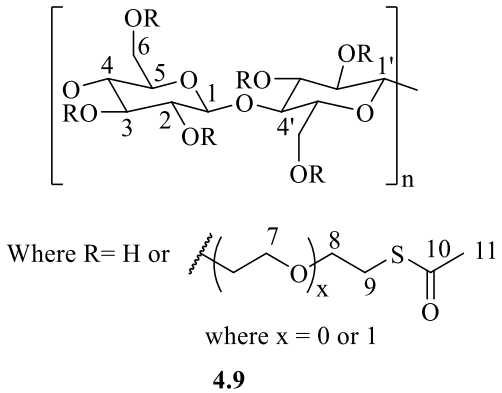

4.9

Figure 4.9: Structure of thioacetate functionalised HEC with numerical assignments for NMR

Key resonances in ^{13}C NMR (150 MHz; DMSO-d_6): δ = 172.1 (C_{10}), 170.5 ($C_{10'}$), 68.3 (C_6, C_9 modified), 63.2 (C_6, C_9 modified), 21.2 (C_{11}) 20.8 ($C_{11'}$).
FT-IR: ν_{max} = 3448 cm^{-1} (OH), 1695 cm^{-1} (C=O).

4.2.12 Attempted Deprotection of 4.9 with Acetic Acid

In a vial, thioacetate functionalised HEC **4.9** (0.4 g, 0.002 mmol) was dissolved in deionised water (10 mL) at ambient temperature. Acetic acid (1 ml, 17 mmol) was added and stirred for 18 h. The solvent was removed under reduced pressure to give an off-white solid, which was further dried in an oven overnight at 60 °C under reduced pressure. Mass recovered = 0.3 g. The reaction was unsuccessful, as signals corresponding to the acetyl groups were still present in the ^{13}C NMR spectrum.

Key resonances in ^{13}C NMR (150 MHz; DMSO-d_6): δ = 172.9 (C=O), 171.5 (C=O), 21.4 (CO-CH_3).

4.2.13 Attempted Deprotection of 4.9 with Sodium Hydroxide

In a vial, thioacetate functionalised HEC **4.9** (0.4 g, 0.002 mmol) was dissolved in deionised water (10 mL) at ambient temperature. NaOH (0.1 g, 25 mmol) was added and the mixture was stirred at 40 °C for 18 h. The mixture was allowed to cool to ambient temperature and neutralised with the addition of DOWEX H^+ resin. The mixture was then filtered and the solvent removed under reduced pressure to give an off-white solid, which was further dried in an oven overnight at 60 °C under reduced pressure. Mass recovered = 0.2 g.

Key resonances in ^{13}C NMR (150 MHz; DMSO-d_6): δ = 174.7 (C=O), 23.1 (CO-CH_3).

4.3 Results and Discussion

4.3.1 Thiol Functionalisation of HEC *via* Tosylated and Acetylated Intermediate

The attempted thiolation of HEC **4.7** is based on the steps as outlined in Scheme 4.2. The synthesis of **4.1** and **4.2** follows the same reactions as carried out in Chapter 2 on trehalose model compound.

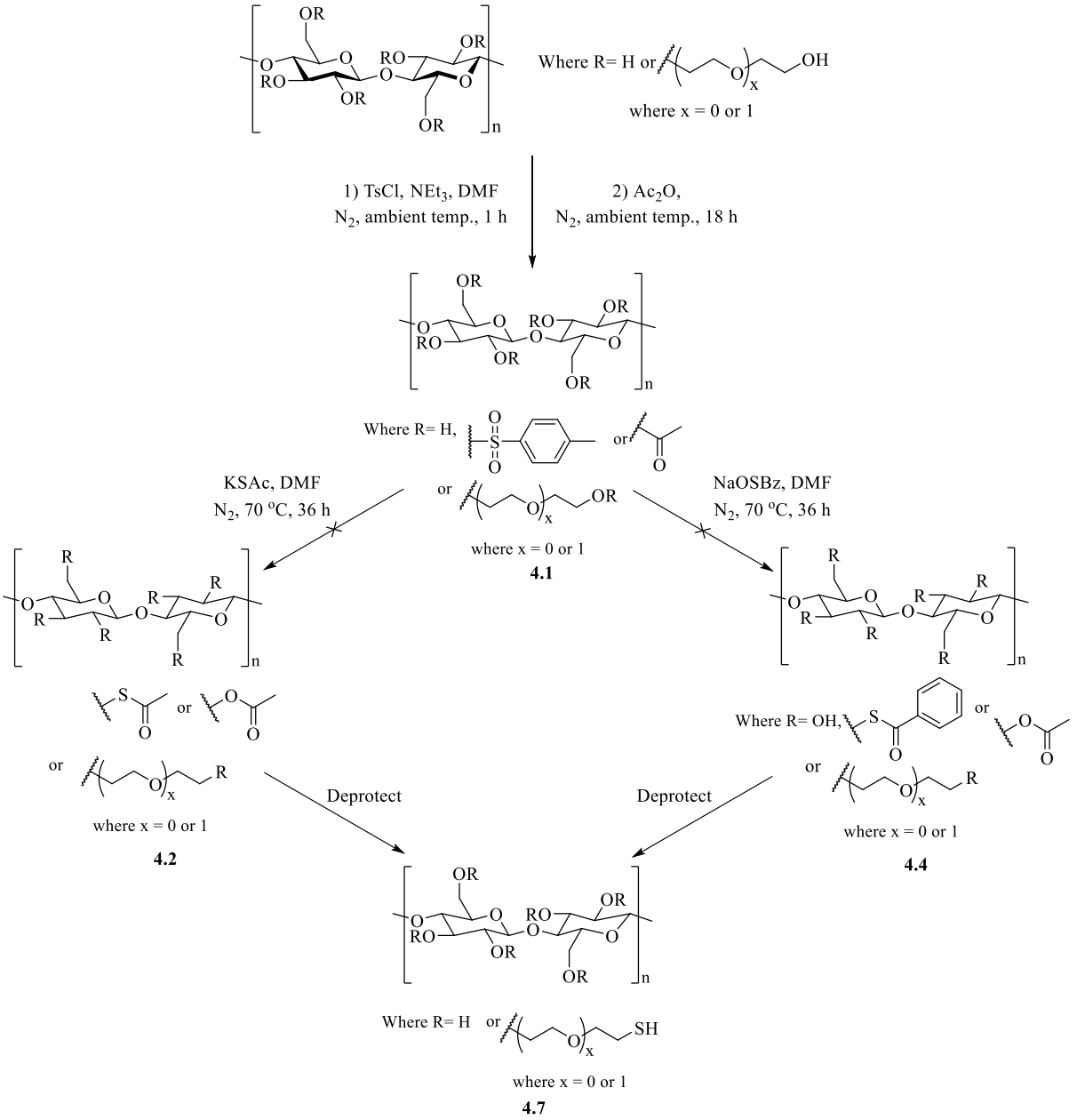

Scheme 4.2: Proposed reaction pathways to synthesise thiolated HEC 4.7

The intermediate **4.1** was prepared *via* the selective tosylation of the two primary hydroxyl groups, followed by the protection of the remaining secondary hydroxyl groups with acetic anhydride. The acetylation of the secondary hydroxyl groups induced hydrophobicity on HEC, allowing easier isolation of the product and is indicative of a successful reaction. The ^{13}C NMR spectra of the HEC ($M_w = 2.5 \times 10^5$ g mol^{-1}) was fully assigned (Figure 4.10).[9] The ^{13}C NMR spectra of compound **4.1** (Figure 4.11) shows resonances corresponding to C_{11}, C_{12} and C_{14} of the tosyl group at 128.1, 125.5 and 20.7 ppm, respectively. Resonances corresponding to the aromatic C_{10} and C_{13} are too weak to be observed. Resonances corresponding to the acetyl group carbonyl (C_{15}) and methyl carbon (C_{16}) are observed at 170 and 20.7 ppm, respectively. The resonances due to the methyl carbon atoms overlap each other, producing a slightly broader signal.

In the comparison of both ^{13}C NMR spectra, the resonance due to C_6 and C_9 carbon atoms at 60.2 ppm in the spectrum of the HEC starting material (Figure 4.10) has completely shifted to 63.3 ppm in the spectrum of **4.1** (Figure 4.11). This indicates complete conversion of the primary hydroxyl groups in HEC to tosyl groups.

Furthermore, the FT-IR spectra shows the presence of strong peaks at 1735 cm^{-1} and 2980 cm^{-1} for the carbonyl groups and aromatics of the tosyl group in **4.1**, respectively (Figure 4.12.B). The FT-IR spectra also shows the loss of the broad peak at 3365 cm^{-1} attributing to the hydroxyl groups on HEC (Figure 4.12.A), indicating the reaction of all hydroxyl groups.

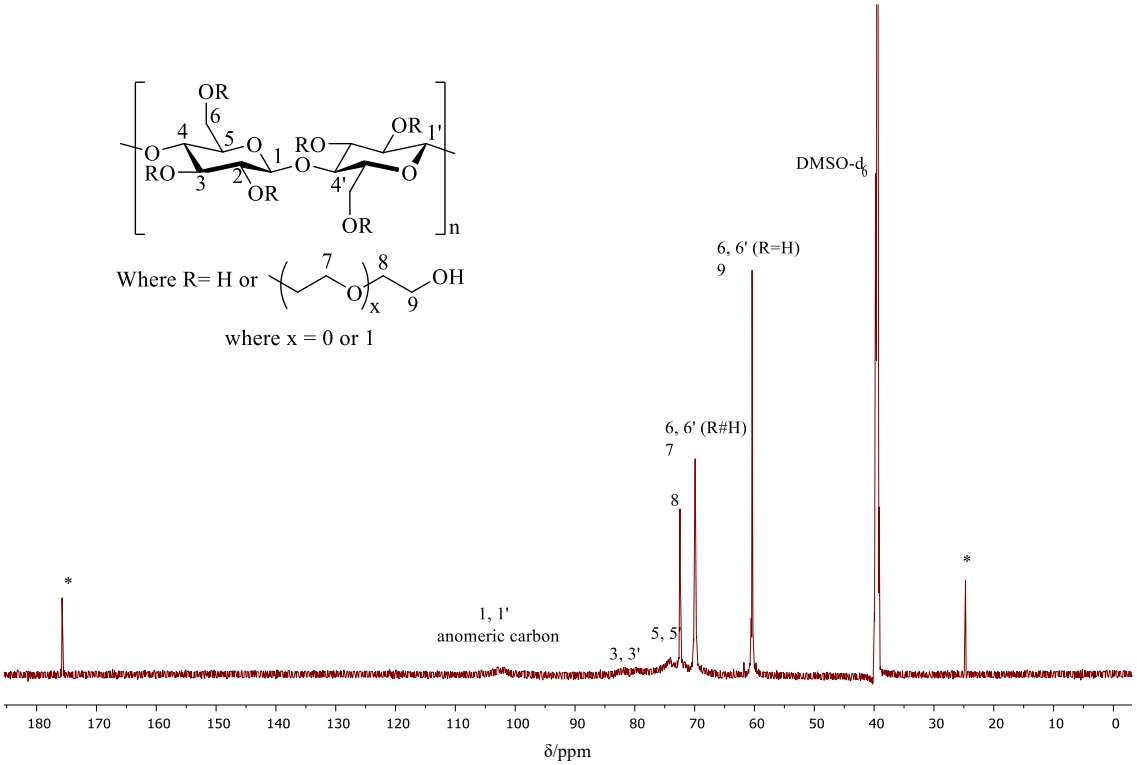

Figure 4.10: ^{13}C NMR spectrum of HEC in DMSO-d$_6$

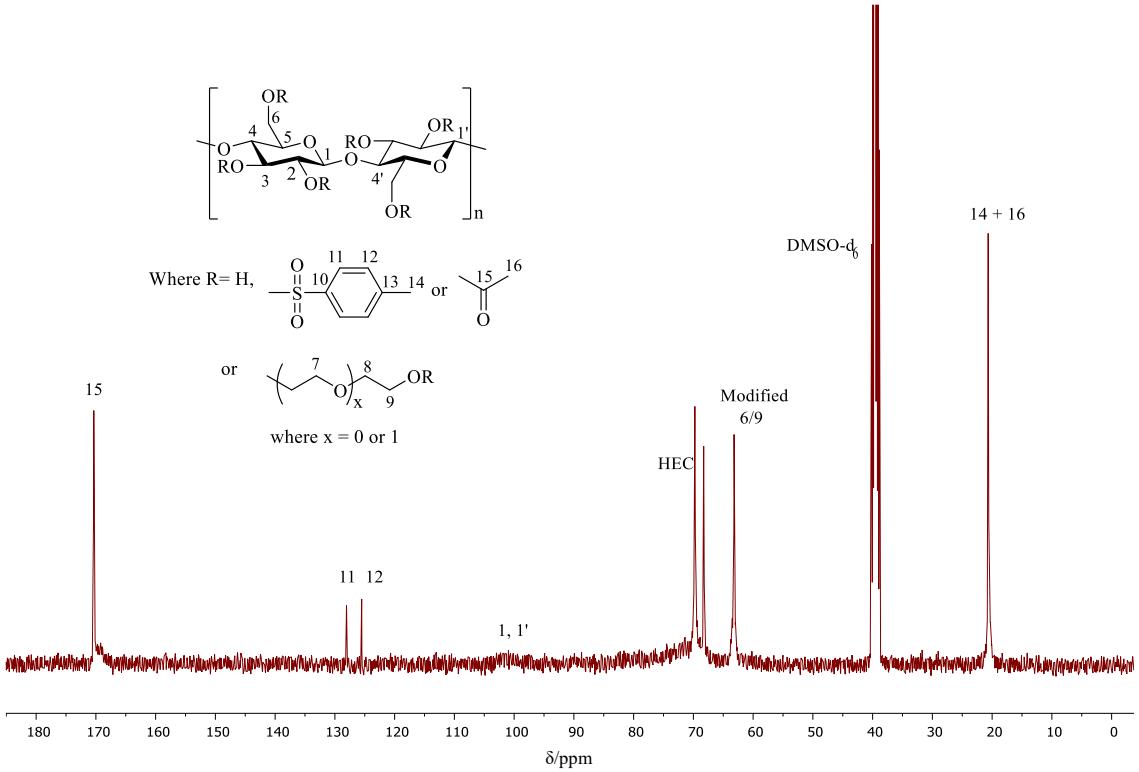

Figure 4.11: ^{13}C NMR spectrum of tosylated and acetylated HEC 4.1 in DMSO-d$_6$

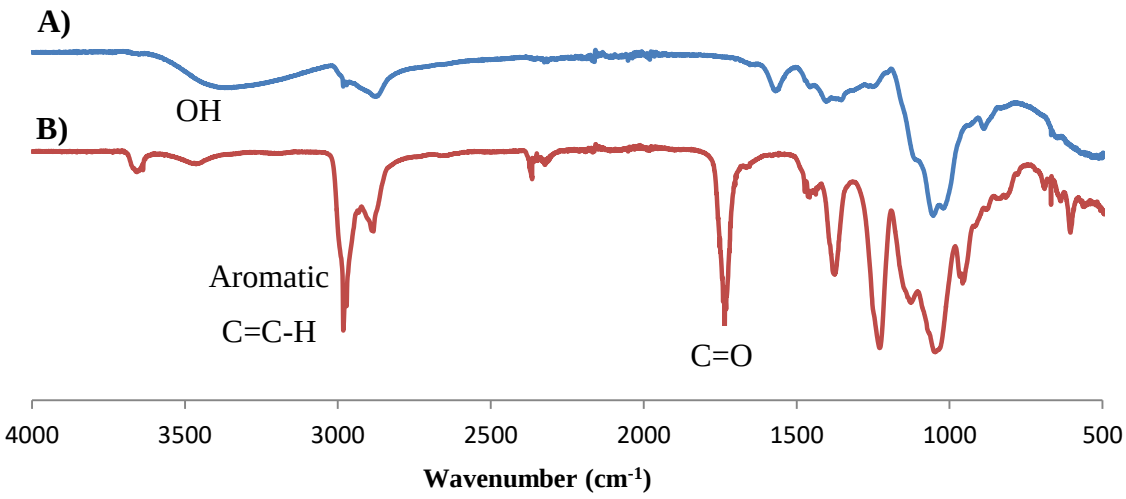

Figure 4.12: FT-IR spectra of A) HEC and B) tosylated and acetylated HEC 4.1

The reaction of **4.1** with potassium thioacetate was carried out in an attempt to synthesise the modified polymer **4.2**. This could then undergo deprotection to give thiol end-group functionality, as observed with the model compound trehalose. However, the synthesis of **4.2** was attempted under a range of experimental conditions; using 1 eq. and 2.5 eq. of KSAc, both carried out at 50 °C and 70 °C and all afforded no grafting of the thioacetate moiety- the ^{13}C NMR spectra were identical to that of **4.1**. This route was subsequently abandoned.

Another source of adding thiol functionality was sought, and it was decided that sodium thiobenzoate **4.3** would be a good nucleophile. Benzoyl is a common protecting group used in organic synthesis; therefore an abundance of literature exists on its use and deprotection.[10, 11] The synthesis of **4.3** is outlined in Scheme 4.3, the characterisation was in very good agreement with that reported in the literature.[6]

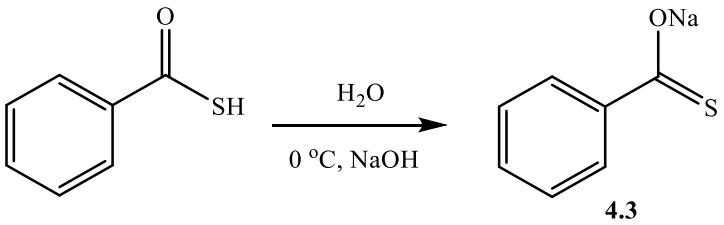

Scheme 4.3: Synthesis of sodium thiobenzoate 4.3

The ^{1}H NMR of **4.3** (Figure 4.13) shows three resonances corresponding to the aromatic protons H_3, H_1 and H_2 at 8.01, 7.53 and 7.44 ppm, respectively.

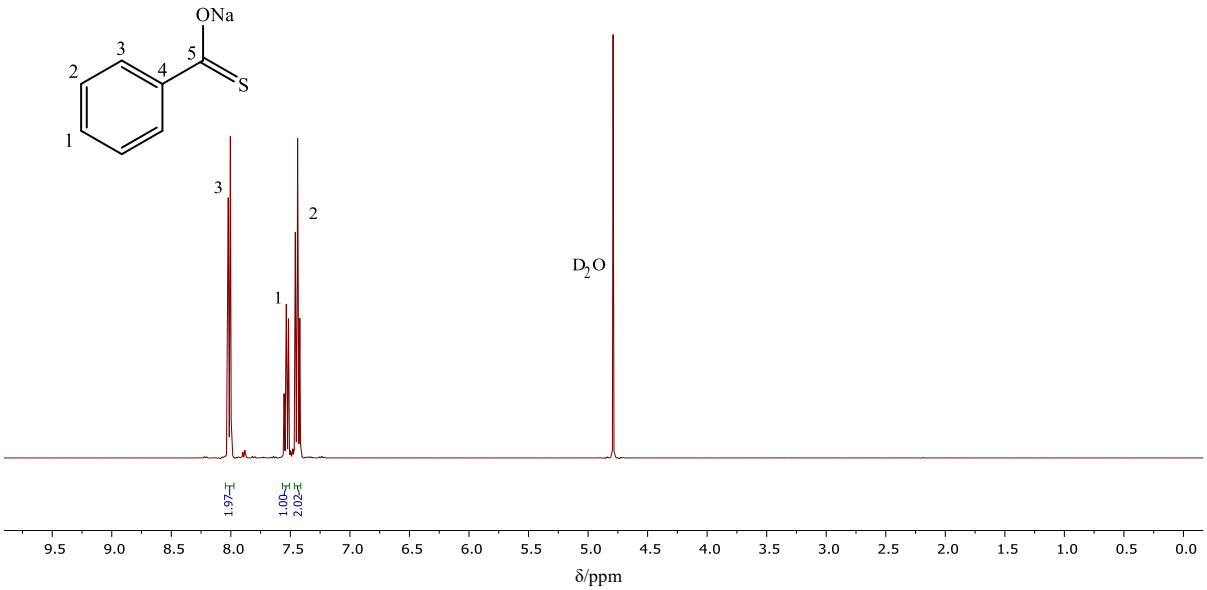

Figure 4.13: ^{1}H NMR spectrum of sodium thiobenzoate 4.3 in D_2O

The ^{13}C NMR spectrum of **4.3** (Figure 4.14) shows five resonances. Resonances corresponding to aromatic carbon atoms C_4, C_1, C_2 and C_3 are observed at 143.6, 131.5, 128.0 and 127.7 ppm, respectively, and a resonance corresponding to the thiocarbonyl carbon C_5 at 215.7 ppm.

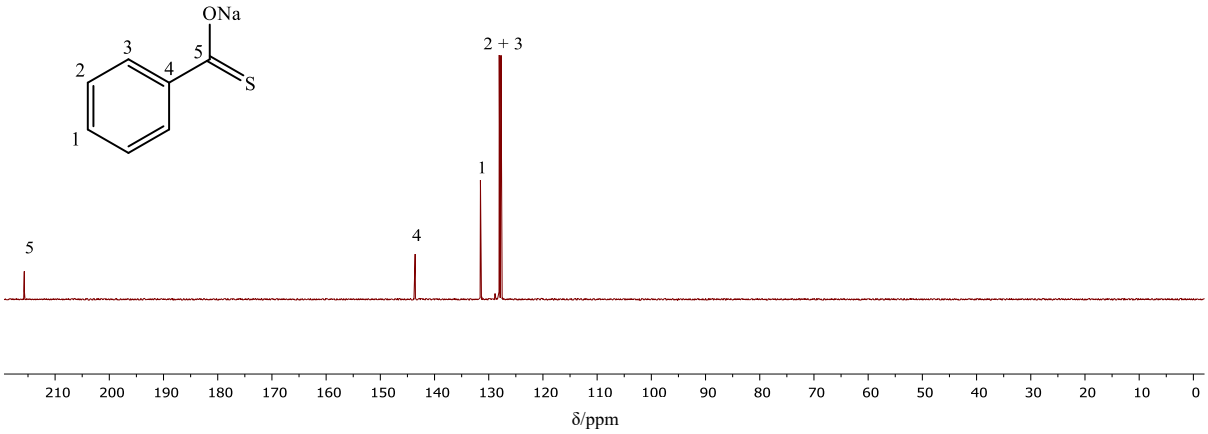

Figure 4.14: ^{13}C NMR spectrum of sodium thiobenzoate 4.3 in D_2O

Sodium thiobenzoate **4.3** was then reacted with tosylated and acetylated HEC **4.1**, in an attempt to synthesise polymer **4.4**, as outlined in Scheme 4.2. The ^{13}C NMR spectrum of the resulting product is shown in Figure 4.15.

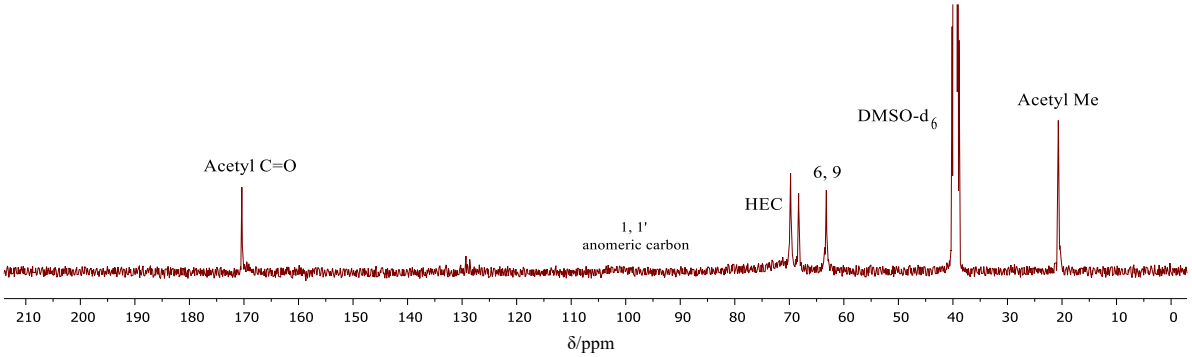

Figure 4.15: ^{13}C NMR spectrum of the product from the attempted synthesis of 4.4, in DMSO-d_6

The ^{13}C NMR spectrum provides evidence that the grafting of thiobenzoate was not successful. We would expect to observe multiple resonances between 130-150 ppm corresponding to the aromatic carbon atoms in the benzoyl group, and another resonance at approximately 200 ppm due to the carbonyl group. However, none of these resonances are observed. The fact that no signals are observed at all within the aromatic region also indicates detachment of the tosyl group from HEC. The FT-IR spectrum also showed a reduction in the aromatic peak at 2890 cm^{-1}.

Although the tosylation and acetylation of trehalose (compound **2.1**) allowed further functionalisation reactions to be easily performed, the same reactions when attempted on tosylated and acetylated HEC, **4.1**, were unsuccessful. This intermediate shows poor reactivity with nucleophiles in the substitution of tosyl groups, which may be due to the difference in molecular weights in comparison to trehalose.

4.3.2 One-Pot Thiol Functionalisation of HEC with Sodium Thiobenzoate

A method of selective C_6 functionalisation of high molecular weight polysaccharides was devised by Cimecioglu *et al.*[12] and further developed by Shey *et al.*[13] The method was applied to the azidation of amylose and starch, respectively. The method was recently applied to HEC by Eissa *et al*,[7] which was modified for use in the work reported here. The modification involves the use of sulfur containing sodium or potassium salts instead of sodium azide as a nucleophile.

4.3.2.1 One-Pot Thiobenzoate Graft with Trehalose Model Compound

In order to remain consistent, the one-pot grafting of thiobenzoate was first performed on the model compound of trehalose before being attempted on HEC. The selective thiobenzoylation of the primary hydroxyl groups of trehalose, **4.5**, was successfully carried out as shown in Scheme 4.4, with an 82% yield.

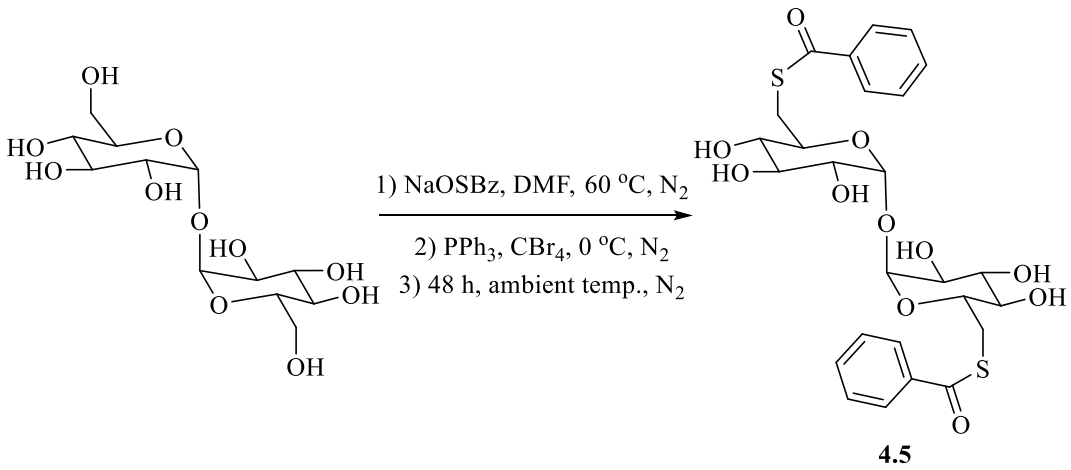

Scheme 4.4: Synthesis of thiobenzoated trehalose 4.5

It is believed that the one-pot reaction with a sulfur containing salt proceeds *via* a mechanism similar to that of the well-established Appel reaction,[14] due to the formation of a phosphonium salt intermediate. The general postulated mechanism for this reaction with a general saccharide is shown in Scheme 4.5.

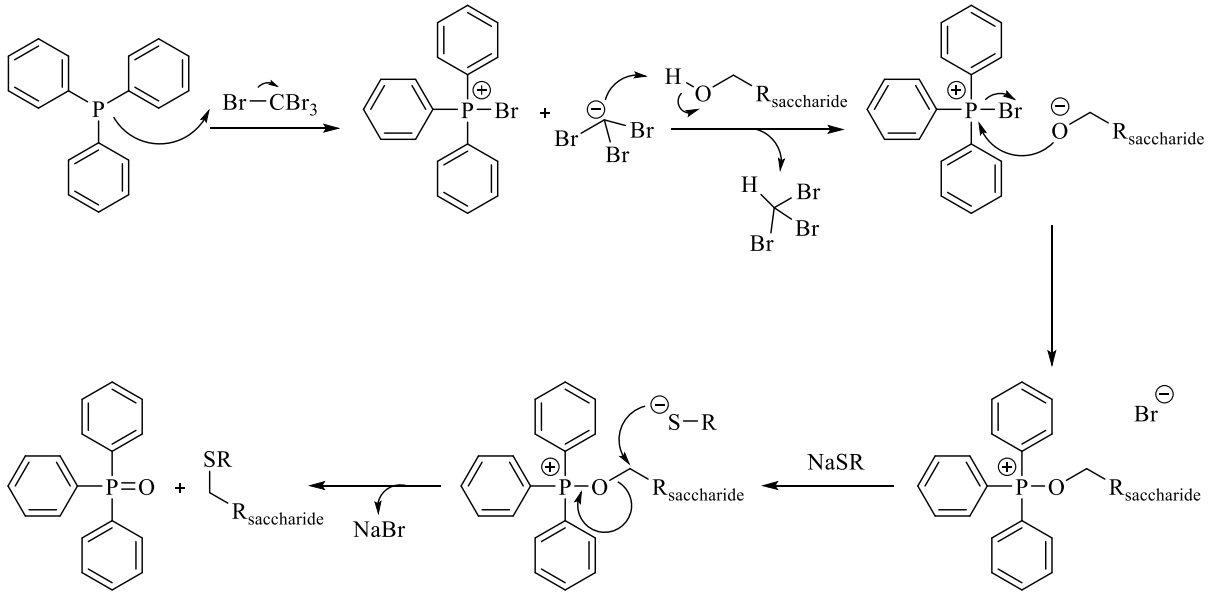

Scheme 4.5: Postulated mechanism for one-pot thiolation reaction

The halogenation of PPh_3 is followed by the formation of the saccharide alkoxide *via* the deprotonation of the hydroxyl group. Tribromomethane is produced as a by-product. The alkoxide subsequently attacks the phosphorus, displacing the halide leaving group. The sulfur nucleophile then attacks the carbon atom in an S_N2 nucleophilic substitution reaction, resulting in the final functionalised saccharide product. If the methylene carbon atom of the saccharide is a stereocentre, the S_N2 reaction step would lead to a product with inverted stereochemistry.[15] Triphenylphosphine oxide is also a by-product, of which the formation of the strong P=O bond is the driving force of the reaction.[16] Because of this, the Appel reaction shares similarities with the Mitsunobu reaction, which affords a wider range of functionalisations.[17]

The ^1H NMR spectrum of **4.5** (Figure 4.16) shows resonances at 7.88, 7.59 and 7.30 ppm corresponding to the aromatic protons H_9, H_{11} and H_{10}, respectively. The trehalose protons H_1, H_5, H_3, H_6, $H_{6'}$, H_2 and H_4 show resonances at 4.89, 3.67, 3.60, 3.55, 3.50, 3.26 and 3.17 ppm, respectively. The resonances due to the methylene C_6 protons are split, due to each proton being in a slightly different chemical environment. This causes the H_5 resonance to appear as a multiplet, as it couples to both H_6 and H_4 protons. Resonances at 7.94, 2.88 and 2.72 ppm are due to residual DMF.

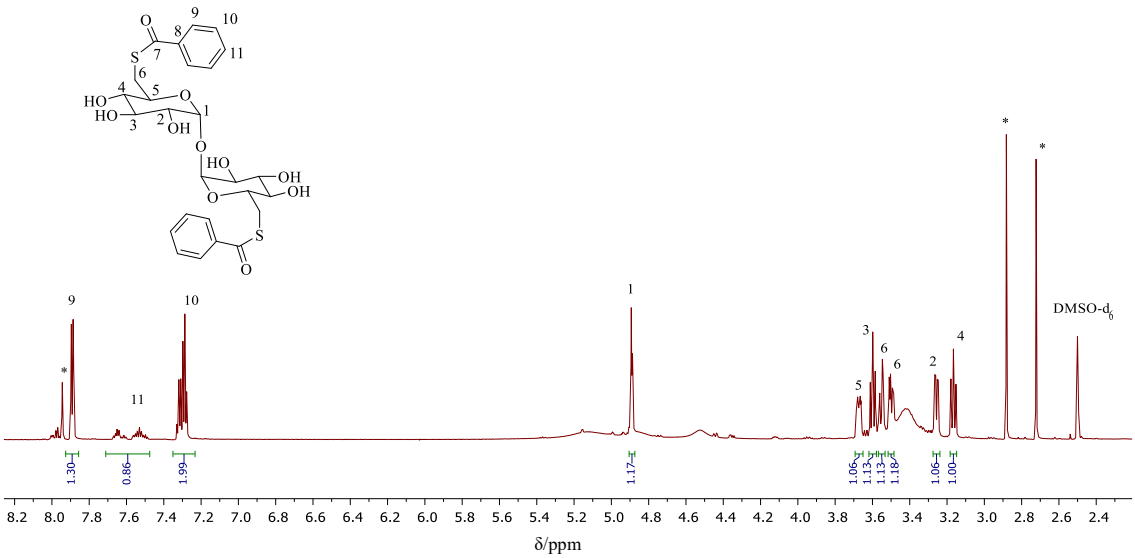

Figure 4.16: ^{1}H NMR spectrum of thiobenzoated trehalose 4.5 in DMSO-d$_6$

The ^{13}C NMR spectrum of **4.5** (Figure 4.17) shows resonances at 139.5, 131.7, 129.1 and 127.2 ppm due to the aromatic carbon atoms C_8, C_{11}, C_9 and C_{10}, respectively. The resonances due to trehalose C_1, C_5, C_3, C_2, C_4 and C_6 are observed 93.2, 72.8, 72.5, 71.6, 70.1 and 60.8 ppm, respectively. Again, residual DMF resonances are present at 162.4, 35.9 and 30.8 ppm.

In comparison to the ^{13}C NMR spectrum of the sodium thiobenzoate salt **4.3** (Figure 4.14), the C_7 carbon resonance has shifted from 215.7 ppm to a lower δ-value of 170.5 ppm, indicating a change from a thiocarbonyl to carbonyl, and is a further evidence for the thiobenzoate being chemically bonded to the trehalose *via* the sulfur atom.

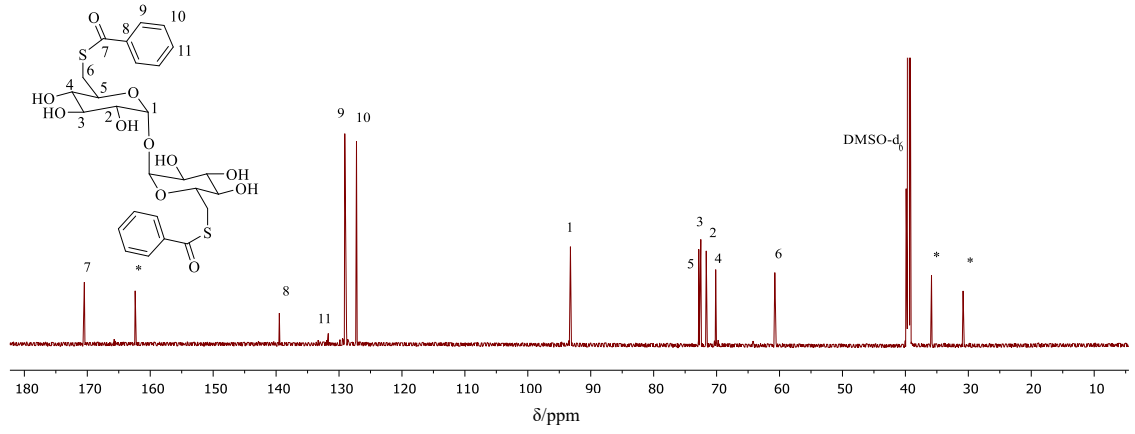

Figure 4.17: ^{13}C NMR spectrum of thiobenzoated trehalose 4.5 in DMSO-d$_6$

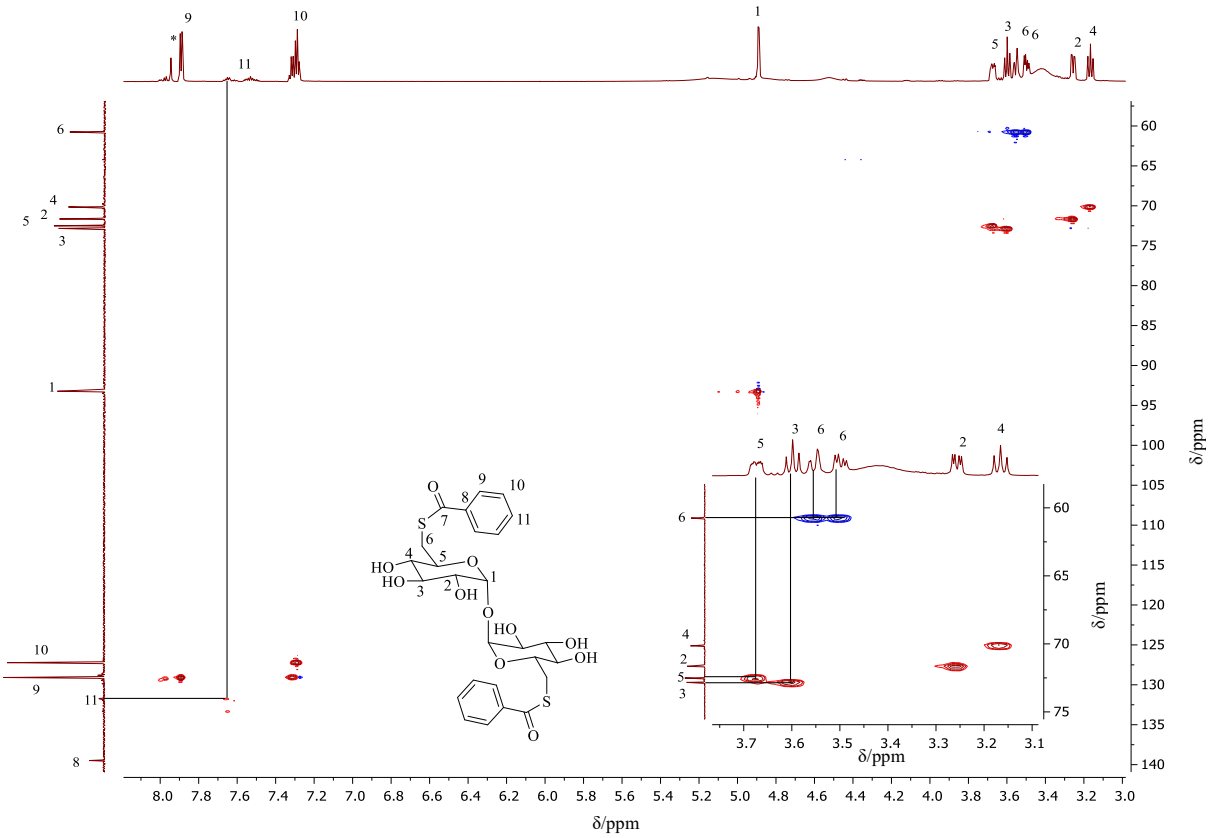

Figure 4.18: ^{1}H-^{13}C HSQC NMR spectrum of 4.5 in DMSO-d_6

^{1}H-^{13}C HSQC NMR spectroscopy (Figure 4.18) was used to confirm the resonances at 3.55 and 3.50 ppm both corresponded to H_6, as both H_6 resonances correlated to the same C_6 resonance at 60.8 ppm.

4.3.2.2 One-Pot Thiobenzoate Graft with HEC

The one-pot grafting reaction of thiobenzoate was then performed on HEC as outlined in Scheme 4.6. The selective thiobenzoylation of the primary hydroxyl groups of HEC was successful. A higher temperature was initially required in comparison to when the reaction was performed on trehalose; 100 °C compared to 60 °C, in order to facilitate the dissolution of HEC. The colour of the reaction mixture was bright yellow due to the sodium thiobenzoate salt. Upon cooling to ambient temperature both components remained in solution; the reaction mixture remained clear and no precipitate was observed. After treatment with PPh_3, the slow, dropwise addition of CBr_4 was carried out with the flask cooled in an ice water bath, as a slight exotherm was produced. This caused a colour change in the reaction mixture to pale brown. The precipitated and dried product **4.6** exhibited a change in its solubility properties, and was now water insoluble in comparison to HEC starting material.

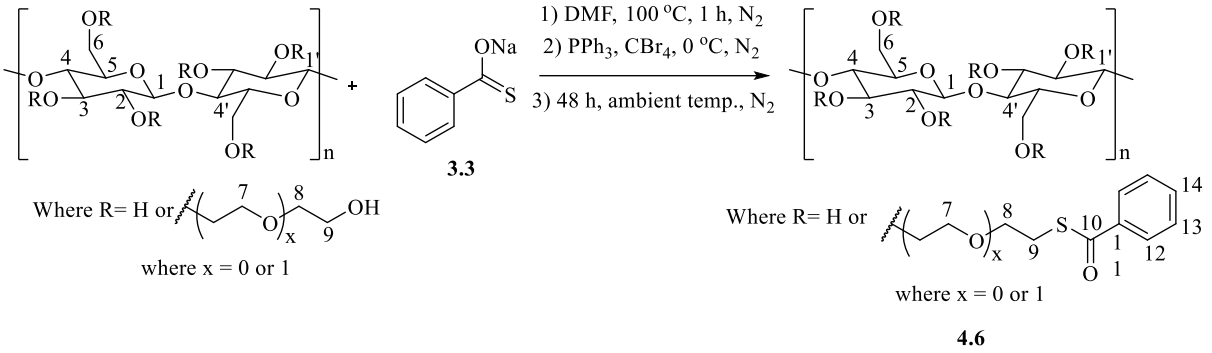

Scheme 4.6: Synthesis of HEC thiobenzoate 4.6

^{1}H NMR spectroscopy was carried out on the product **4.6**, however, due to the large amount of saccharide backbone and hydroxyl protons, the resonances observed were extremely broad, difficult to integrate accurately and no useful information could be obtained from this method of analysis. Inverse-gated ^{13}C NMR spectroscopy was utilised, with spectra being recorded over long acquisition times (average time approximately 22 h). The inverse-gated ^{13}C NMR spectrum of **4.6** after 30 h reaction time is shown in Figure 4.19.

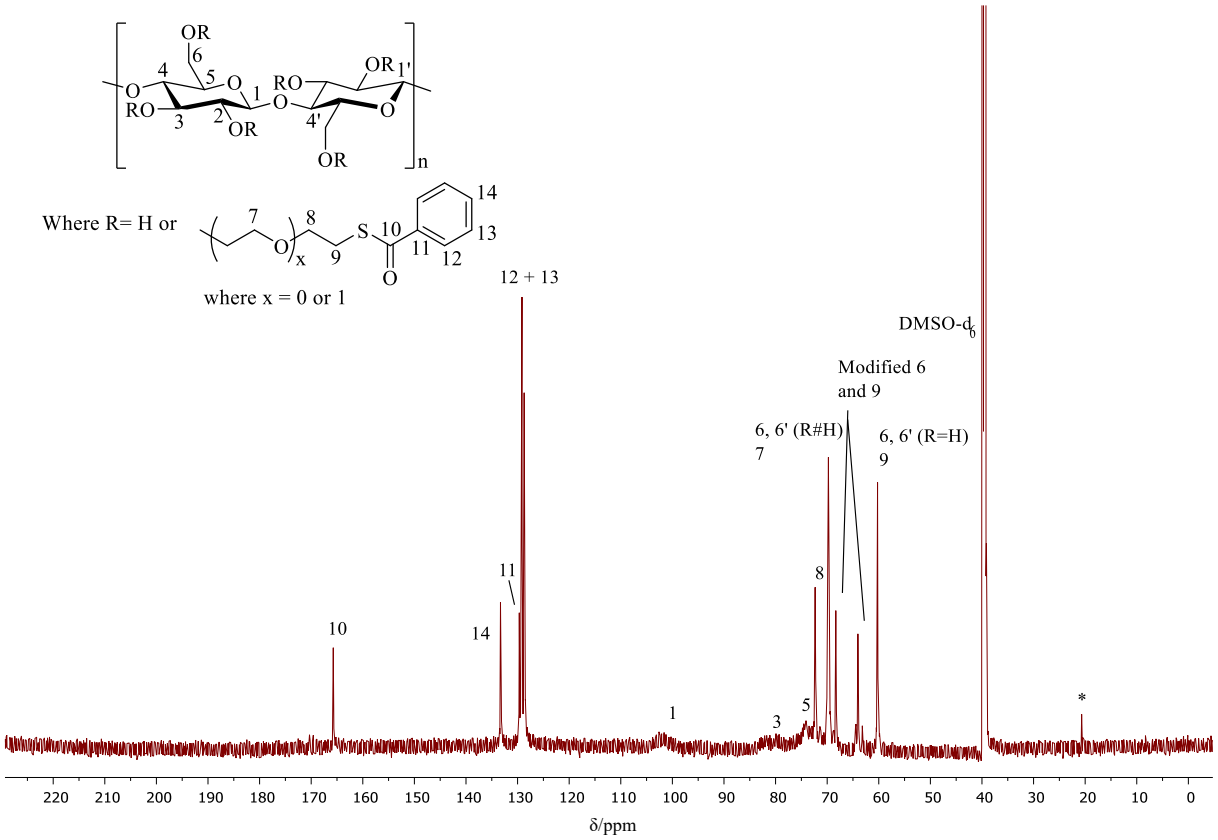

Figure 4.19: Inverse-gated ^{13}C NMR spectrum of HEC thiobenzoate 4.6 after 30 h reaction time, in DMSO-d$_6$

The comparison of the ^{13}C NMR spectrum of HEC thiobenzoate **4.6** to that of HEC (Figure 4.10) shows the appearance of two new resonances at 64.0 and 68.3 ppm which correspond to the modified CH_2 carbon atoms C_6 and C_9, indicating attachment of the thiobenzoate group. However, there is still a resonance observed at 60.2 ppm which corresponds to the unmodified CH_2 in HEC, indicating that complete functionalisation has not occurred. Other key resonances observed in the ^{13}C NMR spectrum of **4.6** include that at 165.7 ppm corresponding to the carbonyl group C_{10}; also those at 133.3, 129.7, 129.1 and 128.7 ppm due to the aromatic carbon atoms C_{14}, C_{11}, C_{12} and C_{13}, respectively.

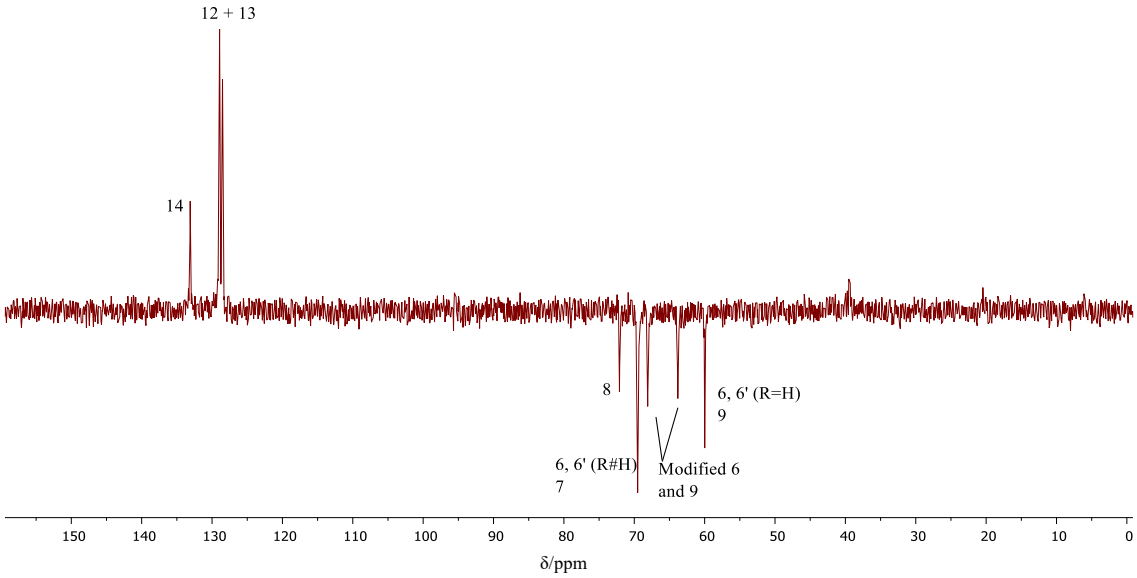

Figure 4.20: DEPT-135 ^{13}C NMR spectrum of HEC thiobenzoate 4.6, in DMSO-d_6

The DEPT-135 ^{13}C NMR spectrum of **4.6** (Figure 4.20) shows that the resonances at 64.0 and 68.3 ppm due to the modified CH_2 carbon atoms are in the same phase as the other methylene carbon atoms C_8, C_7 and unmodified C_6 and C_9. This confirms that these are also methylene carbon atoms on which functionalisation has occurred. The resonance due to the quaternary carbon atom (C_{11}) at 129.7 ppm is not observed in DEPT-135 NMR spectroscopy.

A method was utilised to in order to quantify the degree of functionalisation by calculating the ratios of integration of the unreacted C_6 and C_9 resonance to the newly observed modified methylene resonances. Although integration of ^{13}C NMR spectra is uncommon, it is possible to compare resonances for carbon atoms if they correspond to the same carbon with the same number of hydrogen atoms. As previously mentioned, inverse-gated ^{13}C NMR spectra were recorded in order to allow the integration of carbon resonances to give "semi-quantitative" results. This increases the relaxation delay time between pulses in order to minimise nuclear

Overhauser effects (NOEs), therefore improving the sensitivity of the probe.[18] However, the number of repetitions must be increased in order to obtain a sufficient signal-to-noise ratio that allows integration, which in turn increases the length of time required to complete each ^{13}C NMR experiment. Table 4.1 shows the % conversion calculated from the "semi-quantitative" inverse-gated ^{13}C NMR spectra for the synthesis of **4.6** carried out at different reaction times.

Table 4.1: Effect of reaction time on % conversion of methylene carbon atoms C_6 and C_9 in HEC thiobenzoate 4.6

Reaction Time (h)	% Conversion of C_6/C_9
4	45
20	54
30	55
48	55

The highest conversion reached after 48 h is 55%. However, the reaction almost reaches this limit after 4 h, so it could be argued that a longer reaction time is unnecessary, as little improvement to the conversion will be observed. Unfortunately, further investigations into increasing the conversion by altering the molar ratios of the reactants were not made due to time constraints. For this work, a conversion of approximately 50% of the C_6 and C_9 methylene carbon atoms should be sufficient to induce gelation in the material when crosslinking is invoked.

4.3.2.3 Deprotection of 4.6 to Thiolated HEC

Deprotection of the benzoate group of **4.6** with NaOH to give thiolated HEC **4.7** is outlined in Scheme 4.7.[10] Although the intermediate **4.6** is water insoluble, addition of NaOH assisted the dissolution and formed a homogenous solution. Initially deprotection was attempted with potassium carbonate as in the literature,[11] however, this base was too weak with the carbonate anion having a pK_a of 10, and no deprotection was observed. The literature procedure is carried on a small molecule; this base may be sterically hindered by the much larger HEC polymer chain. NaOH is a slightly stronger base, (H_2O has a pK_a of 15.7), and is also smaller so less sterically hindered.

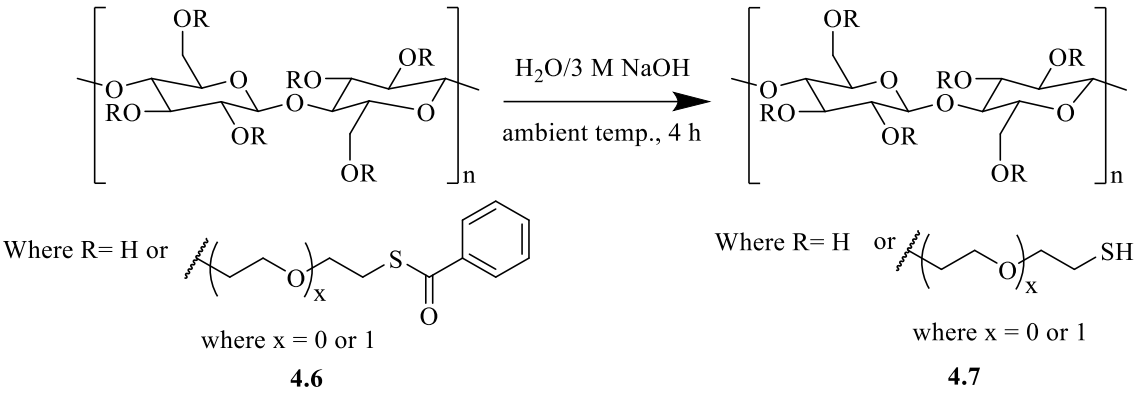

Scheme 4.7: Deprotection of 4.6 to thiolated HEC 4.7

The ^{1}H NMR spectrum of **4.7** is shown in Figure 4.21. In comparison to the ^{1}H NMR spectrum of **4.6** (Figure 4.19) there are no resonances observed at 165.7, 133.3, 129.7, 129.1 and 128.7 ppm corresponding to the benzoyl group carbon atoms C_{10}, C_{14}, C_{11}, C_{12} and C_{13}, respectively. This indicates removal of the benzoyl group and that successful deprotection has occurred.

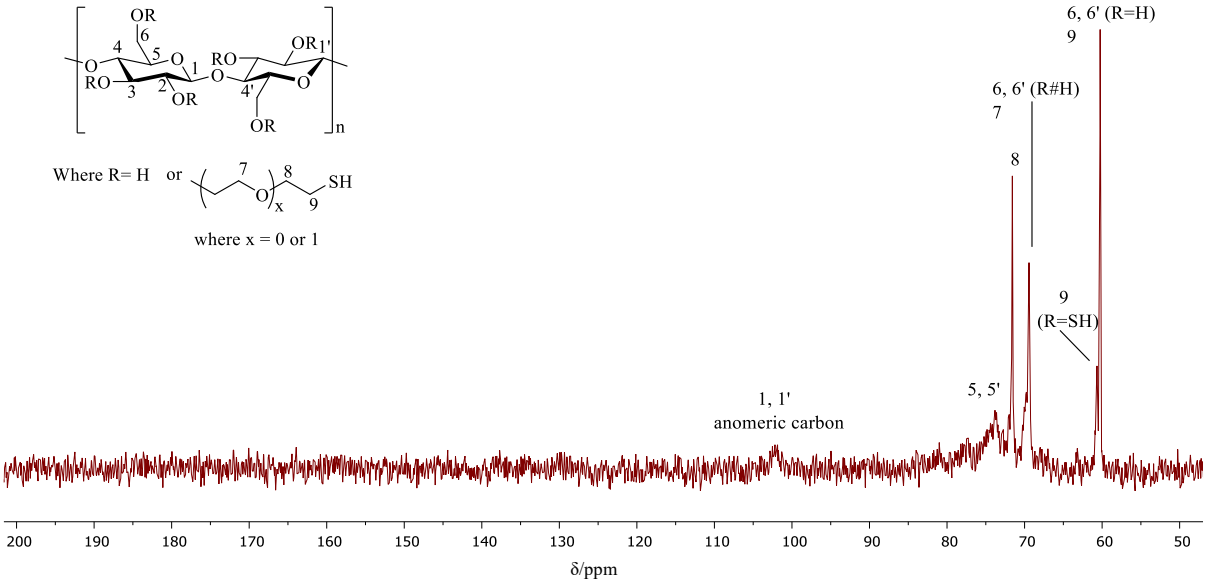

Figure 4.21: ^{13}C NMR spectrum of thiolated HEC 4.7 in DMSO-d_6

The appearance of a new resonance at 60.7 ppm corresponds to the C_9 carbon successfully modified with a thiol group. The magnified regions of the backbone resonances in the ^{13}C NMR spectra are shown in Figure 4.22. In the comparison of HEC (Figure 4.22.A) with HEC thiobenzoate **4.6** (Figure 4.22.B), the appearance of two new resonances at 64.0 and 68.3 ppm corresponding to thiobenzoate modified CH_2 are observed. There is also a visible decrease in the intensity of the resonance at 60.3 ppm attributed to the unmodified CH_2 carbon atoms C_6 and C_9.

When the magnified region of **4.6** is then compared with thiolated HEC **4.7** (Figure 4.22.C), the resonances attributed to the thiobenzoate modified CH_2 carbon atoms have disappeared indicating successful deprotection; the presence of a new resonance at 60.7 ppm is observed corresponding to the thiol modified CH_2 carbon atoms.

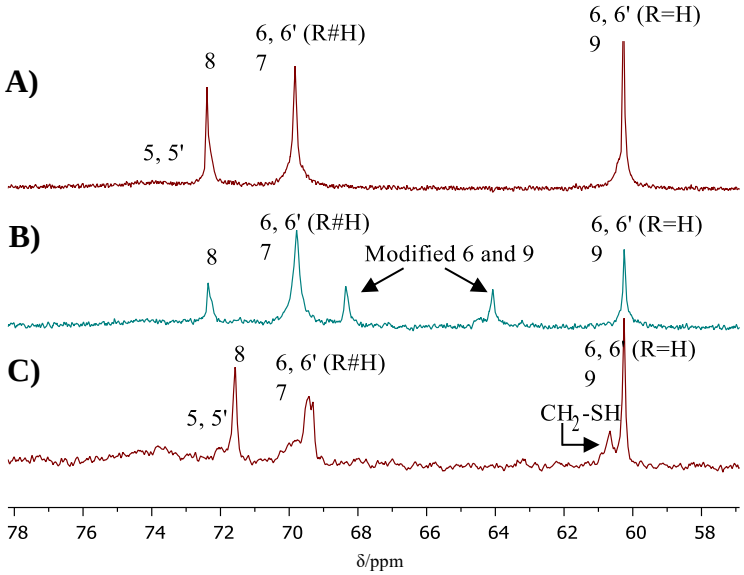

Figure 4.22: Magnification of backbone resonances in the ^{13}C NMR spectra of A) HEC, B) HEC thiobenzoate 4.6 and C) thiolated HEC 4.7, all in DMSO-d_6

Although the signal of the CH_2-SH carbon atom overlaps slightly with the unmodified CH_2-OH resonance, an attempt was made to quantify the amount of thiol conversion. The amount of thiol functionalisation was approximately calculated to be 15% by integration.

Furthermore, comparison of the FT-IR spectrum of **4.7 (**Figure 4.23.C) to the FT-IR spectrum of **4.6** (Figure 4.23.B) shows the appearance of a small resonance at 2580 cm^{-1} characteristic of thiol, as well as the reappearance of a broad resonance at 3417 cm^{-1} corresponding to hydroxyl groups. Also there is a loss of resonances at 3020 cm^{-1} and 1712 cm^{-1} which correspond to the aromatic and carbonyl groups, respectively.

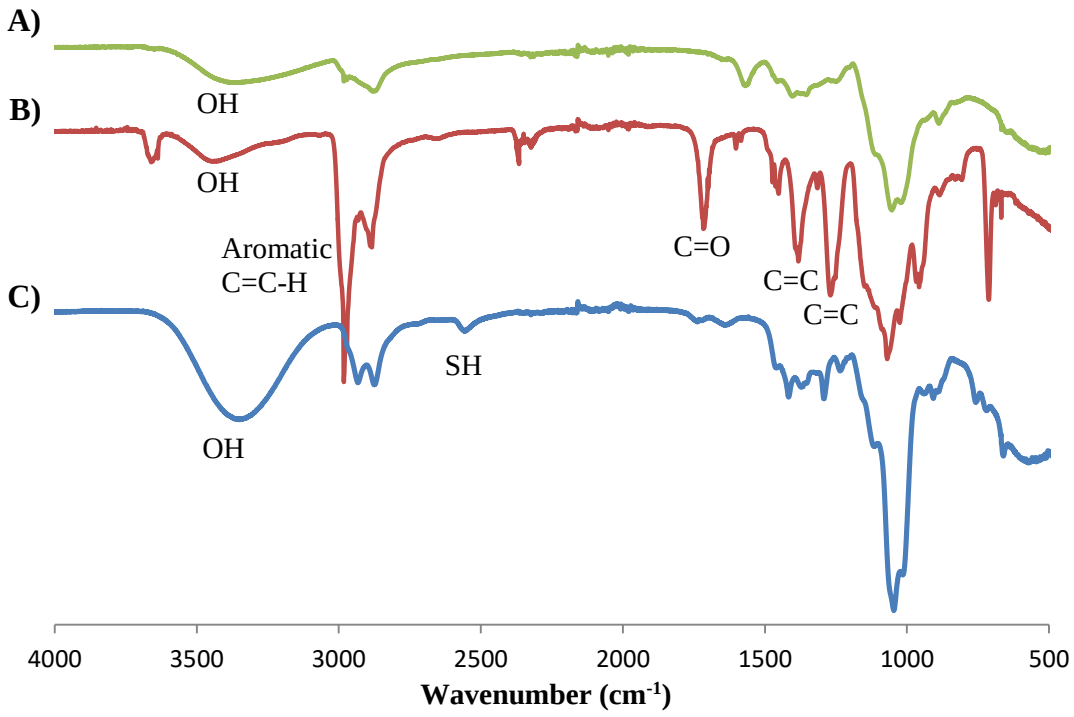

Figure 4.23: FT-IR spectra of A) HEC, B) HEC thiobenzoate 4.6 and C) thiolated HEC 4.7

4.3.3 Functionalisation of HEC *via* Thiol-ene Click

The synthesis of **4.8** was attempted via the thiol-ene Click of the thiol substrate **4.7** and the alkene substrate **2.4** (Scheme 4.8). UV irradiation was utilised for 48 h in order to induce the reaction. An off-white solid product was precipitated.

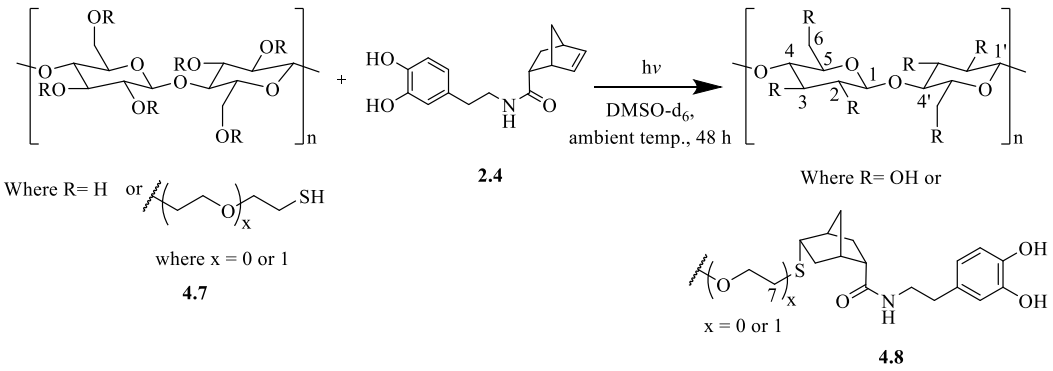

Scheme 4.8: Synthesis of thiol-ene Click product 4.8

^{1}H NMR spectroscopy was utilised in an effort to characterise the product. The ^{1}H NMR spectrum of the thiol-ene product **4.8** is shown in Figure 4.24, magnified at the area of interest pertaining to the alkene protons.

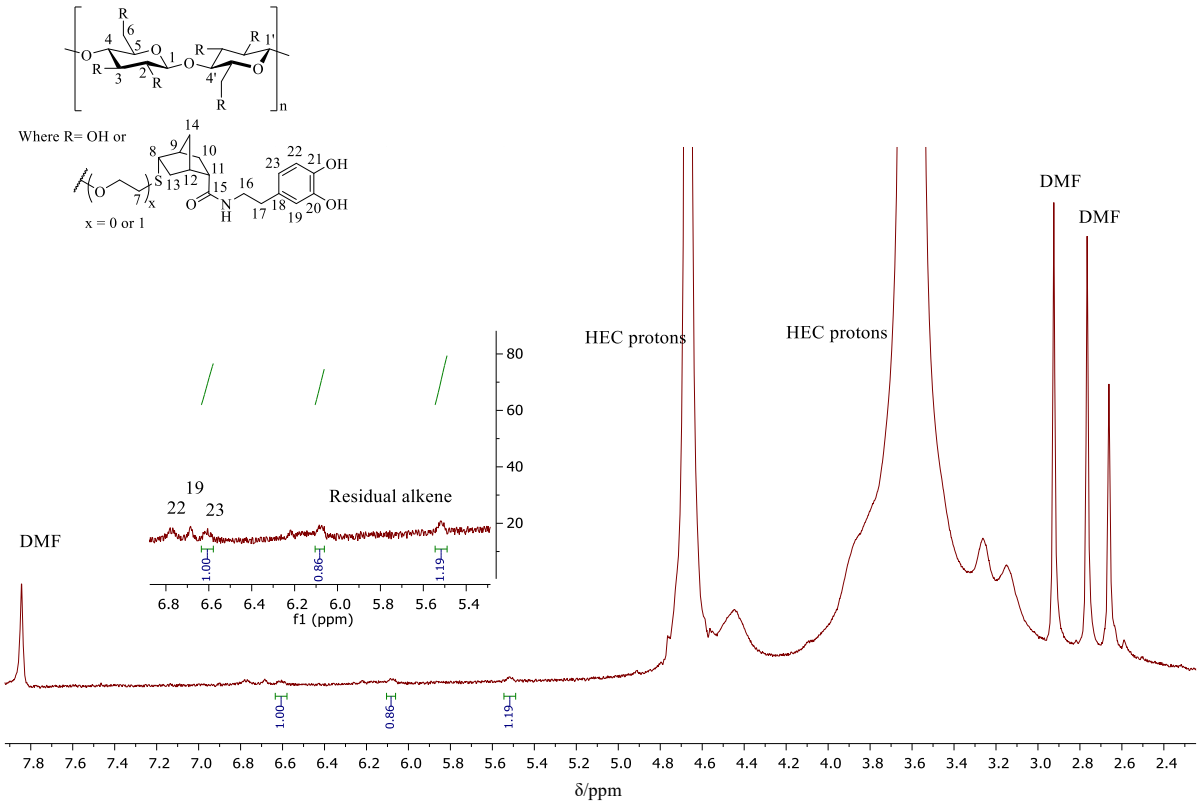

Figure 4.24: ^{1}H NMR spectrum of attempted thiol-ene 'Click' reaction product 4.8 in DMSO-d$_6$

The spectrum exhibits extremely broad resonances due to the large amount of protons present on HEC. The spectrum must be vastly scaled in intensity in order to see any resonances due to the less intense norbornene-catecholic moiety. This causes the norbornene-catechol resonances to be broad and noisy within the baseline, therefore will be inaccurate when integrated. However, the spectrum was integrated similar to that for trehalose Click product **2.5**, in an attempt to quantify the reaction product. Attempting to integrate the resonances at 6.08 and 5.51 ppm due to the vinylic protons of the norbornene moiety against the resonance at 6.60 ppm due to the catecholic proton (H_{23}) affords a ratio of 2:1 (norbornene:catechol). This is indicative of an unsuccessful Click reaction, as we would expect to observe a decrease in intensity of the residual alkene resonances with respect to the H_{23} resonance.

The ^{13}C NMR spectrum of **4.8** afforded no information in determining the success of the reaction; any resonances due to the grafted norbornene-catechol moiety were too weak to be observed.

However, the FT-IR spectrum of the thiol-ene Click product **4.8** (Figure 4.25.B) shows the disappearance of the resonance at 2580 cm^{-1} attributed to SH in comparison to the FT-IR spectrum of thiolated HEC **4.7** (Figure 4.25.A), which could be an indication of the thiol groups undergoing a reaction.

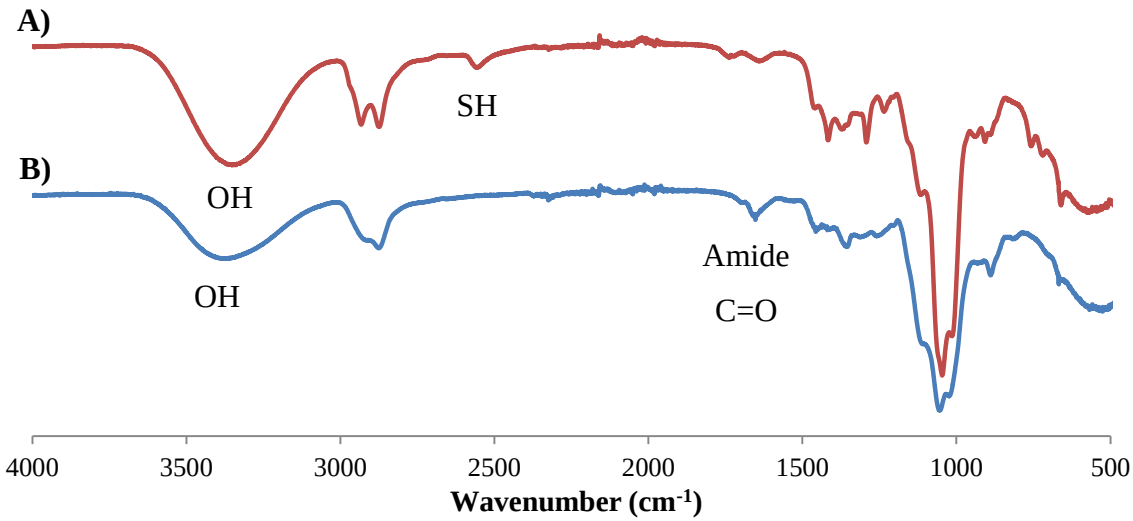

Figure 4.25: FT-IR spectra of A) thiolated HEC 4.7 and B) attempted thiol-ene Click reaction product 4.8

4.3.4 One-Pot Thiol Functionalisation of HEC with Potassium Thioacetate

The one-pot synthesis of **4.9** was applied using potassium thioacetate as the thiol nucleophile, with the aim of increasing the overall conversion to thiol functionality. This nucleophile afforded a good yield during the deprotection step (78%) when carried out on trehalose. The grafting of potassium thioacetate to HEC is outlined in Scheme 4.9. A higher temperature of 100 °C was required in order to facilitate the dissolution of HEC, upon which the reaction mixture turned turquoise due to the potassium thioacetate salt. The reaction mixture remained homogeneous throughout.

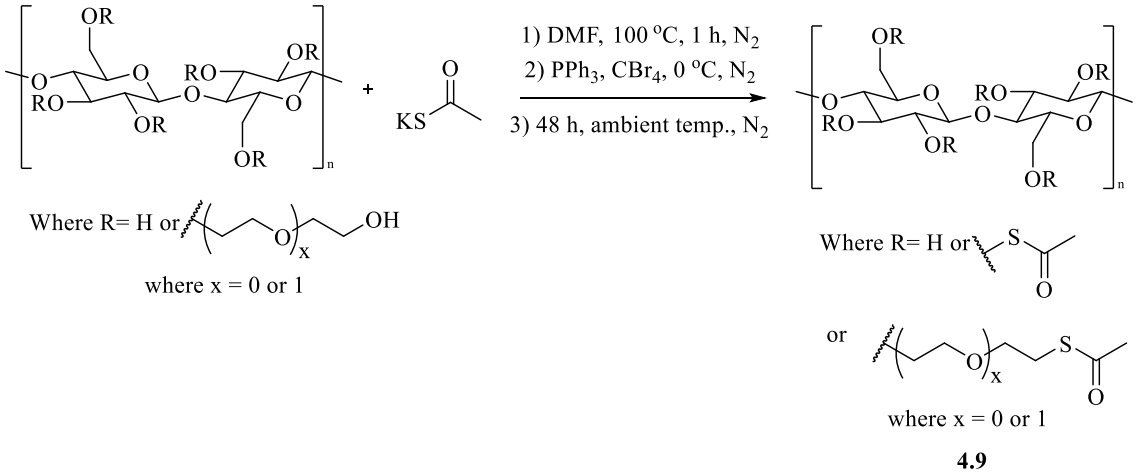

Scheme 4.9: Synthesis of HEC thioacetate 4.9

The reaction mechanism in the synthesis of HEC thioacetate **4.9** is also expected to proceed in a similar way to the Appel reaction as outlined in Scheme 4.5. The off-white solid product was no longer as readily soluble in water compared to the HEC starting material.

The common problems associated with the analysis of HEC based compounds occurred- ^{1}H NMR spectra were comprised of extremely broad resonances and could not be integrated. Again, inverse-gated ^{13}C NMR spectroscopy was utilised in order to quantify the degree of thioacetation. An example inverse-gated ^{13}C NMR spectrum of HEC thioacetate **4.9**, obtained after a 48 h reaction time with 12 eq. of potassium thioacetate is shown in Figure 4.26.

In comparison to the ^{13}C NMR spectrum of HEC (Figure 4.10), there is the appearance of two new resonances at 63.2 and 68.3 ppm corresponding to the thioacetate modified CH_2 carbon atoms. There is also the appearance of two carbonyl resonances (C_{10}, $C_{10'}$) at 172.1 and 170.4 ppm, and two methyl resonances (C_{11}, $C_{11'}$) at 21.2 and 20.8 ppm corresponding to the thioacetate groups. These signals are still present after further precipitation and washing of the

product and are good evidence of chemical attachment. Furthermore, the carbonyl resonance of any trapped unreacted potassium thioacetate salt starting material would be observed at a much higher δ-value of 210 ppm.

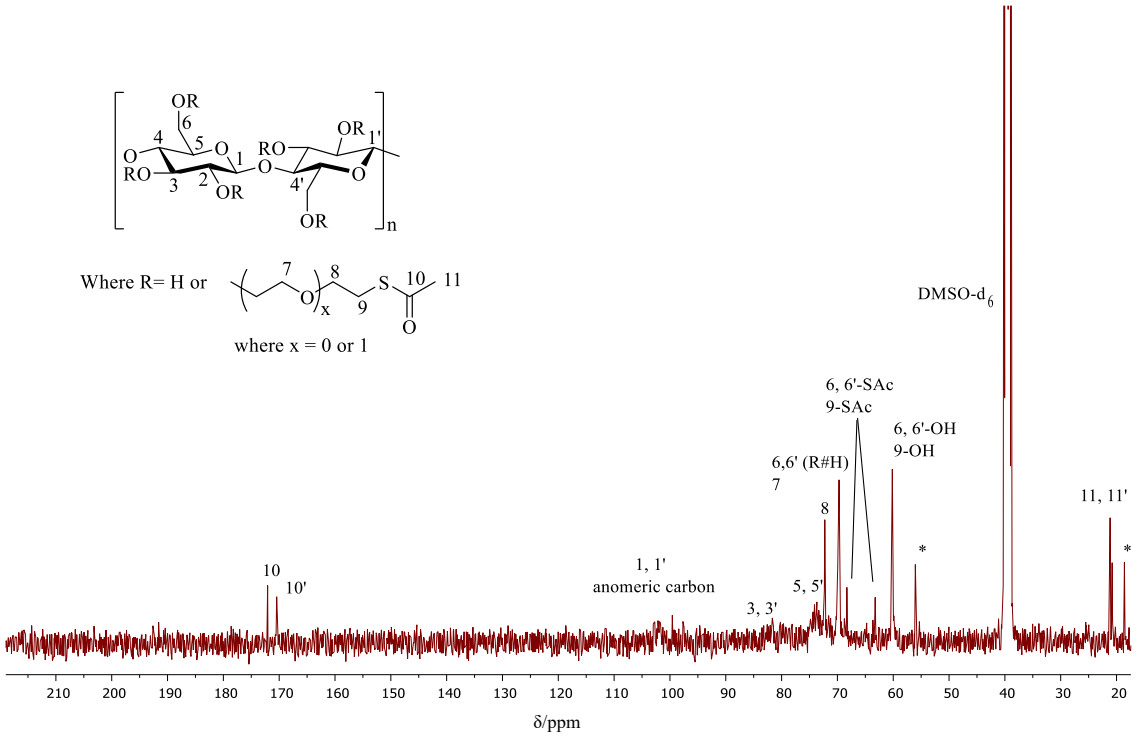

Figure 4.26: Inverse-gated ^{13}C NMR spectrum of HEC thioacetate 4.9 after 48 h reaction time, in DMSO-d_6

The appearance of a second carbonyl resonance may be due to possible thioacetylation reaction of some of the secondary hydroxyl groups. When compared to the ^{13}C NMR spectrum of dithioacetylated trehalose **2.2**, only one resonance is observed due to the thioacetate carbonyl carbon at 194.8 ppm. However, this is due the symmetrical trehalose undergoing complete conversion. As HEC has a much higher molecular weight, not all of the primary hydroxyl groups will react equally, leading to the molecule becoming unsymmetrical and creating different chemical environments.

The resonances at 18.6 and 56.0 ppm are due to trapped residual EtOH solvent.

The reaction was performed with different molar quantities of potassium thioacetate. The equivalents of triphenylphosphine and carbon tetrabromide used were kept the same. Aliquots were withdrawn from the reaction mixture at different times and analysed by inverse-gate ^{13}C NMR spectroscopy. Table 4.2 shows the % conversion of the methylene carbon atoms C_6 and C_9, with respect to both the number of equivalents of KSAc added and the reaction time.

Table 4.2: Effect of reaction time on % conversion of methylene carbon atoms C_6 and C_9 in HEC thioacetate 4.9

Time (h)	% Conversion of C_6 and C_9 (when R=H)	
	4 eq. KSAc	12 eq. KSAc
4	3	19
20	7	24
30	8	23
48	13	23

Again, in both reactions, 100% conversion is not achieved. Generally, the conversion is higher in all cases when a larger quantity of KSAc is used. As the length of the reaction time increases, when four equivalents of KSAc are used, a greater increase in the % conversion is observed. When 12 equivalents are used, the conversion plateaus at approximately 23% after 20 h, so further reaction time is unnecessary.

4.3.4.1 Deprotection of 4.9 to Thiolated HEC 4.7

Deprotection of the acetyl groups on **4.9** was then attempted in order to give thiol functionality to HEC (**4.7**). Attempted deprotection with weak acetic acid did not work, due to the carboxylate anion having a low pK_a of 4.76; there was no change observed in the ^{13}C NMR spectrum. The stronger base of sodium hydroxide (pK_a H_2O = 15.7) was used, as outlined in Scheme 4.10. Addition of NaOH helped solubilise the polymer in water.

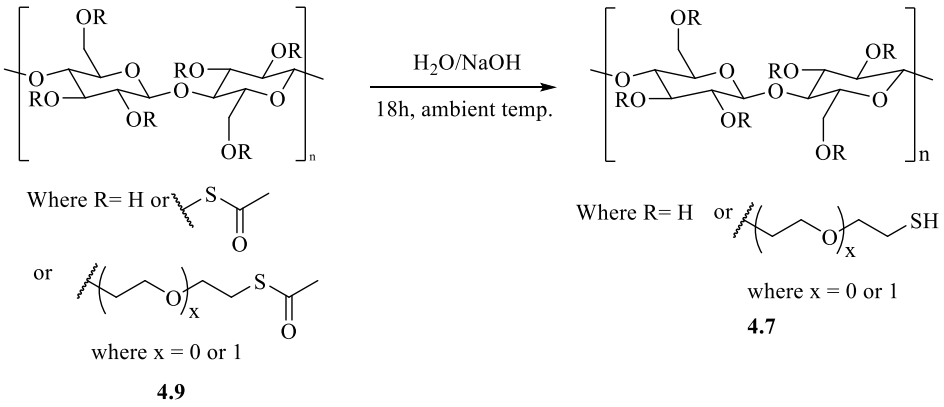

Scheme 4.10: Deprotection of HEC thioacetate 4.9 to thiolated HEC 4.7

The ^{13}C NMR spectrum of the deprotection product is shown in Figure 4.27.B. The resonances are broad and the sample became viscous upon dissolution, this may be to the presence of more hydrogen bonding interactions occurring between polymer chains due to successful

deprotection. When compared to the ^{13}C NMR spectrum of HEC thioacetate **4.9** (Figure 4.27.A), there is a decrease in intensity at 63.2 and 68.3 ppm corresponding to the thioacetate modified CH_2 carbon atoms. There is also a decrease in the methyl resonances at 21.2 and 20.8 ppm corresponding to the acetyl group carbon atoms C_{11} and $C_{11'}$. The loss of one carbonyl resonance at 170.4 ppm is also observed.

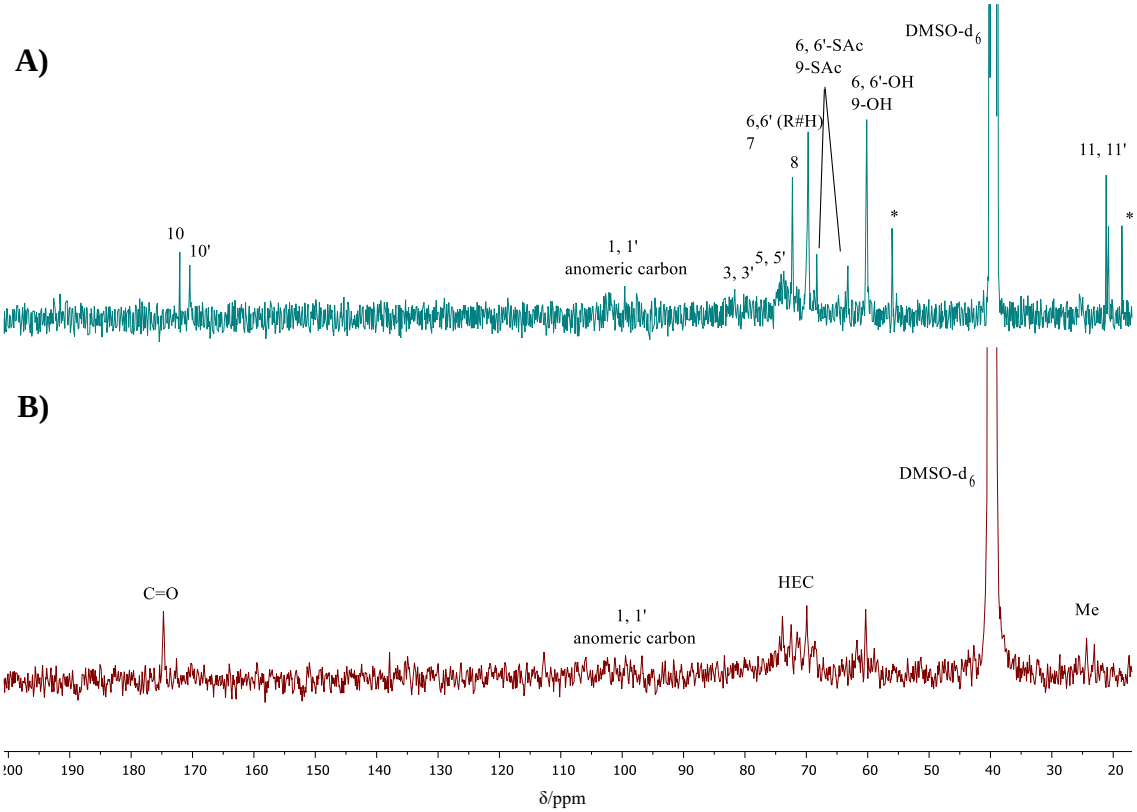

Figure 4.27: ^{13}C NMR spectra of A) HEC thioacetate 4.9 and B) deprotection product, both in DMSO-d_6

The loss of only one carbonyl resonance indicates that compound **4.9** has undergone selective deprotection. It is not possible to tell which carbon atoms are still protected from just the ^{13}C NMR spectrum. Further investigations into the exact nature of thiol conversion and whether this deprotected material could undergo thiol-ene Click reactions would have liked to have been carried out, but unfortunately time constraints did not allow.

4.4 Conclusions

A range of methods were utilised in an order to impart thiol functionality to HEC, preferably at the primary hydroxyl groups (C_6 and C_9 carbon atoms). Tosylation followed by the acetylation of HEC led to the successful synthesis of **4.1**. The analysis indicates complete conversion of primary hydroxyl groups to tosyl groups. Reaction of **4.1** with potassium thioacetate to afford thioacetylated HEC **4.2** was unsuccessful, unlike the trehalose counterpart **2.3**, as described in Chapter 2. An alternate nucleophilic thiol source, sodium thiobenzoate **4.3**, was prepared and then reacted with **4.1** in order to afford thiobenzoated HEC **4.4**. The analysis showed that this was also unsuccessful as no displacement of the tosyl groups to thiobenzoate was observed.

Compound **4.5** was successfully synthesised using an alternate synthetic route. This involved triphenylphosphine being halogenated by carbon tetrabromide. The bromine is then displaced by the saccharide to form a phosphonium salt intermediate. Finally, the phosphine group is displaced by the sulfur nucleophile in an S_N2 reaction. Trehalose model compound was reacted with **4.3** in a one-pot synthesis to afford trehalose thiobenzoate **4.5**. This reaction was successful and afforded a good yield of 82%.

The same methodology was applied to HEC with **4.3** to produce HEC thiobenzoate **4.6** in a one-pot synthesis. A maximum conversion of 55% of the primary C_6 and C_9 HEC hydroxyl groups was achieved after 20 h. Successful deprotection of the benzoyl groups in **4.6** afforded thiol containing HEC **4.7**, with approximately 15% of the primary hydroxyl groups converted to SH. Accurate quantification of thiol groups was difficult due to the overlapping resonances corresponding to the HEC backbone in the ^{13}C NMR spectrum. The compound **4.7** was then reacted with the norbornene-catechol **2.4** in a thiol-ene Click reaction to produce norbornene-catechol functionalised HEC **4.8**. This reaction was also deemed unsuccessful as there was no decrease in the intensity of the resonances due to vinyllic protons of the norbornene moiety in the ^1H NMR spectrum.

The one-pot synthesis was carried out with potassium thioacetate in order to afford HEC thioacetate **4.9**. The analysis showed that functionalisation of both the primary and secondary hydroxyl groups in HEC had occurred, as two C=O resonances were observed in the ^{13}C NMR spectrum. The maximum conversion of primary hydroxyl groups in this case was much lower, 23%, obtained after 20 h. Furthermore, this polymer was found to undergo selective deacetylation during the process of reaction with sodium hydroxide, as the loss of only one

C=O resonance was observed. Unfortunately, time constraints did not allow investigation into whether this polymer would participate in thiol-ene Click reactions.

Generally, HEC based compounds are very viscous in solutions of water, DMF and DMSO, and this resulted in inaccurate analysis data. Furthermore, ^{1}H NMR spectroscopy was found to be a poor analytical technique, due to the presence of broad resonances caused by the large number of protons present in HEC. Inverse-gated ^{13}C NMR spectroscopy was found to be a good method of analysis. This allowed the integration of the resonances due to C_6 and C_9 of the HEC backbone against the resonances corresponding to the functionalised C_6 and C_9 in thiobenzoated **4.6**, thiolated **4.7** and thioacetylated **4.9** HEC. However, this method is only "semi-quantitative" and unfortunately the values are still not completely accurate. This method is also not very time effective as the data required for this type of ^{13}C NMR experiment is obtained over a much longer period of time.

FT-IR spectroscopy was also found to be a quick and easy analytical method used to examine the presence of any functional groups, particularly in the carbonyl and aromatic regions of the products **4.1**, **4.5** and **4.6**.

4.5 References

1. C. Lei, P. E. Clark, *J. Soc. Petrol. Eng.*, **2007**, 316.
2. C. Montgomery, in *Effective and Sustainable Hydraulic Fracturing* (Eds.: A. P. Bunger, J. McLennan, R. Jeffrey), InTech, **2013**, 25-45.
3. C. Creutz, M. H. Chou, *Inorg. Chem.*, **2008**, *47*, 3509.
4. G. Leonaviciute, S. Bonengel, A. Mahmood, M. Ahmad Idrees, A. Bernkop-Schnürch, *Carbohydr. Polym.*, **2016**, *144*, 514.
5. D. Rahmat, D. Sakloetsakun, G. Shahnaz, G. Perera, R. Kaindl, A. Bernkop-Schnürch, *Int. J. Pharm.*, **2011**, *411*, 10.
6. J. Engels, M. Herrlein, R. Konrad, M. Mag, US 5 659 025 A1, **1997.**
7. A. M. Eissa, E. Khosravi, A. L. Cimecioglu, *Carbohydr. Polym.*, **2012**, *90*, 859.
8. S. P. Perrine, US 2008/75692 A1, **2008.**
9. E. Abderahmane, S. Elbarkany, A. Hassan, M. Abdel-Karim, *J. Appl. Polym. Sci.*, **2013**, *127*, 3633.
10. K.-i. Yamada, M. Nakano, M. Maekawa, T. Akindele, K. Tomioka, *Org. Lett.*, **2008**, *10*, 3805.
11. J. D. Winkler, M. B. Rouse, M. F. Greaney, S. J. Harrison, Y. T. Jeon, *J. Am. Chem. Soc.*, **2002**, *124*, 9726.
12. A. L. Cimecioglu, D. H. Ball, S. H. Huang, D. L. Kaplan, *Macromolecules*, **1997**, *30*, 155.
13. J. Shey, K. M. Holtman, R. Y. Wong, K. S. Gregorski, A. P. Klamczynski, W. J. Orts, G. M. Glenn, S. H. Imam, *Carbohydr. Polym.*, **2006**, *65*, 529.
14. R. Appel, *Angew. Chem. Int. Ed. Engl.*, **1975**, *14*, 801.
15. R. M. Denton, J. An, B. Adeniran, A. J. Blake, W. Lewis, A. M. Poulton, *J. Org. Chem.*, **2011**, *76*, 6749.
16. R. A. Stockland, in *Practical Functional Group Synthesis*, John Wiley & Sons, Inc, **2016**, 557-677.
17. M. B. Smith, J. March, *March's Advanced Organic Chemistry: Reactions, Mechanisms, and Structure*, Wiley, **2007**, 464-468.
18. D. A. L. Otte, D. E. Borchmann, C. Lin, M. Weck, K. A. Woerpel, *Org. Lett.*, **2014**, *16*, 1566.

Chapter 5

Application of HEC as a Macroinitiator

5.1 Introduction

This chapter investigates using HEC as a macroinitiator in the ROP of glycidol, with the aim of inducing numerous hydroxyl sites that could chelate to group(IV) metal crosslinkers, thus allowing HEC to participate in crosslinking reactions. Literature information on the grafting of glycerol to HEC is limited to a vague patent where organic solvents such as acetone and alcohols are used as the diluent, in which HEC is not fully soluble.[1]

Glycidol is a highly reactive hydroxy epoxide that is commercially available at a low cost and is an example of a latent AB_2 type monomer. The anionic ring-opening polymerisation (ROP) of glycidol produces a hyperbranched polyglycerol structure which contains an abundance of primary and secondary hydroxyl end group functionalities within close proximity to each other on a flexible aliphatic polyether backbone, Scheme 5.1. This is anticipated to increase the likelihood of participation of HEC in the non-ionic mechanism of crosslinking with group(IV) metal crosslinkers

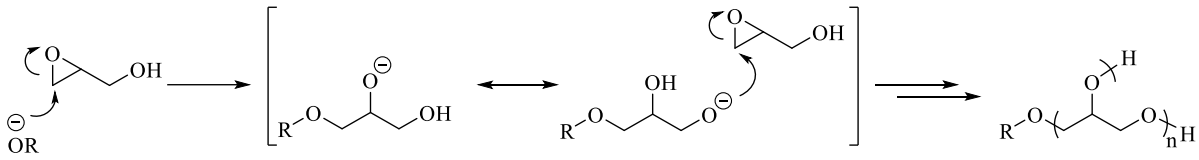

Scheme 5.1: Mechanism of the anionic ROP of glycidol to produce polyglycerol

Poly(ε-caprolactone) (PCL) is a hydrophobic aliphatic polyester which is biocompatible and approved by the Food and Drug Administration (FDA); it is used in drug delivery systems, absorbable sutures and dental packing.[2] When grafted to an HEC backbone, it may give rise to amphiphilic materials of varying architectures with potential biodegradability. This chapter will also investigate the ROP of ε-caprolactone using HEC-*g*-polyglycerol as a macroinitiator, which has not been carried out previously. The aim will be to vary the lengths of the grafted PCL chains to give rise to new polysaccharide based materials. The longer PCL chains mean that the end groups are further away from the HEC backbone. This should make the hydroxyl end groups more readily accessible and less sterically hindered, increasing the likelihood of participating in reactions with group(IV) metal based crosslinking agents.

5.2 Experimental

5.2.1 Materials

2-Hydroxyethyl cellulose (HEC), glycidol, ε-caprolactone (ε-CL), tin(II) 2-ethylhexanoate ($Sn(Oct)_2$) and sodium hydroxide (NaOH) were purchased from Sigma-Aldrich and used as received unless stated otherwise. HEC was dried in an oven at 80 °C for 24 h under reduced pressure prior to use. Glycidol was purified by vacuum distillation and stored at 4 °C under N_2 atmosphere. ε-CL was distilled over CaH_2 under reduced pressure prior to use.

All dry solvents were obtained from Durham Chemistry Department Solvent Purification System (SPS). All other solvents were analytical grade purchased from Fisher Scientific and used without any purification, except *N,N′*-dimethylpropylene urea (DMPU) which was purchased form Sigma-Aldrich. The NMR solvents deuterated dimethylsulfoxide (DMSO-d_6) and deuterated *N,N'*-dimethylformamide (DMF-d_7) were purchased from Apollo Scientific and used as supplied.

5.2.2 Instrumentation and Measurements

^1H and ^{13}C Nuclear magnetic resonance spectroscopy (NMR) and Fourier-transform Infrared (FT-IR) spectroscopy were carried out as outlined in Chapter 2, Section 2.2.2. NMR spectra in DMF-d_7 are referenced to its solvent trace (^1H = 8.03 ppm, ^{13}C = 163.2 ppm).

Dropwise additions were carried out using a KDS-100-CE syringe pump.

Thermogravimetric analysis (TGA) data was obtained by a Perkin Elmer Pyris 1 thermogravimetric analyser, heated from 23-500 °C at a rate of 10 °C min^{-1} under N_2 atmosphere.

Differential Scanning Calorimetry (DSC) was carried out on a TA Instruments DSC Q1000 over a temperature range of -80 °C to 150 °C at a rate of 10 °C min^{-1}. The enthalpy of melting (ΔH_m) was calculated from the heating scans and the enthalpy of crystallisation (ΔH_c) from the cooling scans. Two repeat scans were taken for each sample.

Size exclusion chromatography (SEC) analysis was carried out by Malvern Instruments Ltd. on a Malvern OMNISEC fitted with 2 × LT7000L columns with triple detection (refractive index (RI), intrinsic viscosity (IV) and right angle light scattering (RALS)), using DMF as the eluent with a flow rate of 1.0 mL min^{-1} at 35 °C.

5.2.3 Synthesis of HEC-*g*-polyglycerol 5.1 a-e

This series of reactions was performed using the literature procedure, modified to use HEC as the starting material.[3]

HEC (1 g, 4.0×10^{-3} mmol, ~4 mmol 1° OH) was dissolved in water (10 mL) in a three-necked round bottom flask equipped with mechanical stirrer, septum and water cooled condenser. The flask was heated to 95 °C under N_2 atmosphere until a homogenous mixture was observed and then aqueous sodium hydroxide (0.02 mL, 2.5% mol., 5 M, 0.1 mmol) was added. Glycidol (1.06 mL, 400% mol, 16 mmol) was added dropwise at a rate of 0.53 mL h^{-1} and stirred for 24 h. The reaction mixture was then cooled to ambient temperature and neutralised with HCl (5 M). The polymer was precipitated into cold acetone (250 mL) and washed with methanol. The resulting white solid was dialysed against water (dialysis tubing cut-off M_w = 12,000 g mol^{-1}) for 48 h, then again precipitated from water into acetone. The purified white solid was dried in an oven at 60 °C for 24 h under reduced pressure to give **5.1a**.

Graft copolymers HEC-*g*-polyglycerol **5.1 b-e** were prepared using different amounts of reactants. **5.1b**, water (10 mL), NaOH (0.04 mL, 5% mol., 5 M, 0.2 mmol), glycidol (1.06 mL, 400% mol., 16 mmol); **5.1c**, water (10 mL), NaOH (0.08 mL, 10% mol., 5 M, 0.4 mmol), glycidol (1.06 mL, 400% mol., 16 mmol); **5.1d**, water (10 mL), NaOH (0.08 mL, 10% mol., 5 M, 0.4 mmol), glycidol (0.53 mL, 200% mol., 8 mmol); **5.1e**, water (5 mL), NaOH (0.04 mL, 5% mol., 5 M, 0.2 mmol), glycidol (1.06 mL, 400% mol., 16 mmol).

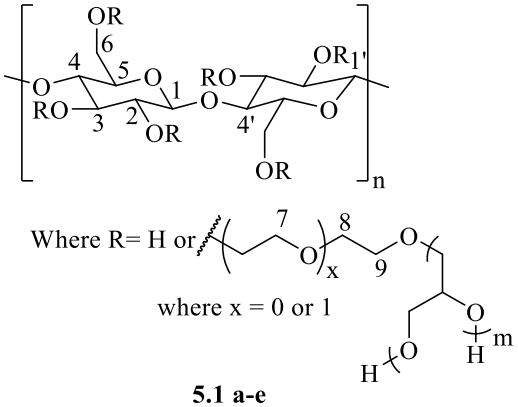

5.1 a-e

Figure 5.1: Structure of HEC-*g*-polyglycerol with assignments for NMR

Key resonances in ^{13}C NMR (150 MHz; DMSO-d_6): δ = 74.29 ($C_{5,\,5'}$), 73.3 (T *C*H_2-OH) 72.9 (D *C*H), 72.8 (C_8), 72.7 ($L_{1,4}$ °CH_2CH), 71.0 (T *C*H), 70.5 (D °CH_2CH), 70.2 ($C_{6,\,6'(R\#H),}$ C_7), 69.0 ($L_{1,4}$ *C*H), 63.5 (T °CH_2CH), 61.4 ($L_{1,3}$ *C*H_2OH), 60.7 ($C_{6,\,6'(R=H),}$ C_9).

FT-IR: ν_{max} = 3340 cm^{-1} (strong, broad, OH). SEC (DMF): M_w = 3.96-4.63 × 10^5 g mol^{-1}, Đ = 3.27-3.89.

5.2.4 Synthesis of HEC-*g*-polyglycerol-*g*-PCL_{10} 5.2

To a flame dried Schlenk tube, HEC-*g*-polyglycerol **5.1d** (75 mg, 2.5 × 10^{-4} mmol) and a magnetic stirrer bar were added. The system was sealed with a rubber septum and placed under vacuum for 1 h. The tube was then kept under an N_2 atmosphere, ε-caprolactone (0.097 mL, 0.88 mmol) and tin(II) 2-ethylhexanoate (0.1 mL of a 0.044 M stock solution in toluene, 1.8 mg, 4.5 × 10^{-3} mmol) were added and the system was stirred at 120 °C for 18 h. The polymer discoloured from white to yellow. The polymer was dissolved in DMF and precipitated into cold methanol twice to give a white solid, which was dried in an oven at 80 °C for 24 h under reduced pressure to give the product **5.2**, yield 92.4% (0.16 g, 2.7 × 10^{-4} mmol).

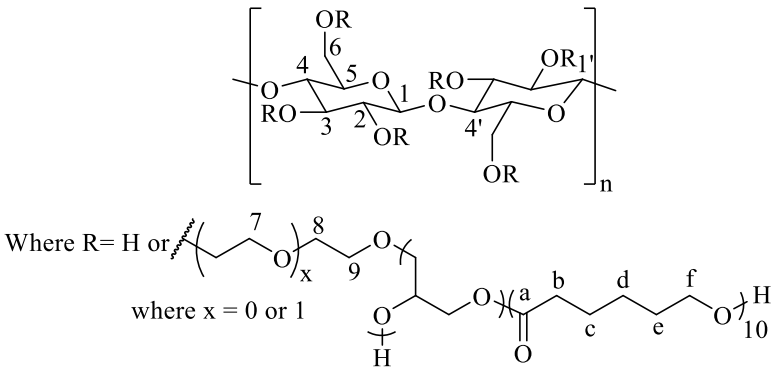

5.2

Figure 5.2: Structure of HEC-*g*-polyglycerol-*g*-PCL_{10} with assignments for NMR

^{1}H NMR (600 MHz; DMF-d_7): δ = 4.95-4.42 (m, b, HEC), 4.22 (H_f), 4.03-3.32 (m, b, HEC), 2.36 (H_b), 1.62 (H_c, H_e), 1.39 (H_d). ^{13}C NMR (150 MHz; DMF-d_7): δ = 73.7 (C_8), 71.2 ($C_{6,\ 6',\ R\#H,}$ C_7), 61.9 ($C_{6,\ 6',\ R=H,}$ C_9).

FT-IR: ν_{max} = 3380 cm^{-1} (broad, OH), 1730 cm^{-1} (C=O). SEC (DMF): M_w = 0.59 × 10^6 g mol^{-1}, Đ = 8.99.

5.2.5 Synthesis of HEC-*g*-polyglycerol-*g*-PCL_{50} 5.3

To a flame dried Schlenk tube, HEC-*g*-polyglycerol **5.1d** (25 mg, 8.3 × 10^{-5} mmol) and a magnetic stirrer bar were added. The system was sealed with a rubber septum and placed under vacuum for 1 h. The tube was then kept under an N_2 atmosphere, ε-caprolactone (0.17 mL, 1.5 mmol) and tin(II) 2-ethylhexanoate (33 μL of a 0.044 M stock solution in toluene, 0.61 mg, 1.5 × 10^{-3} mmol) were added and the system was stirred at 120 °C for 18 h. The polymer

discoloured from white to yellow. The polymer was dissolved in DMF and precipitated into cold methanol twice to give a white solid, which was dried in an oven at 80 °C for 24 h under reduced pressure to give the product **5.3**, yield 86.3% (0.16 g, 9.6×10^{-5} mmol).

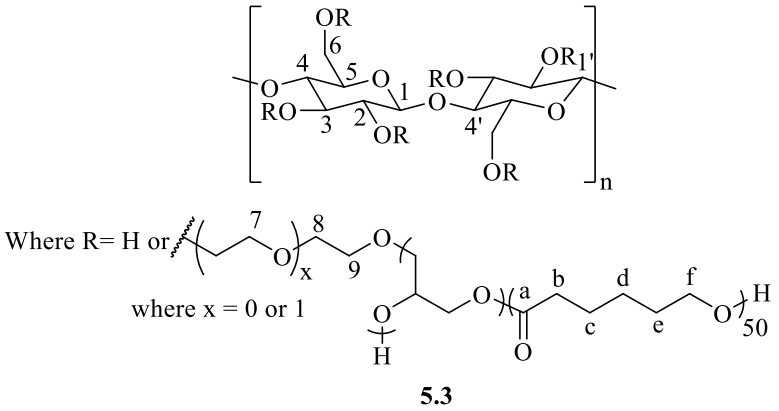

5.3

Figure 5.3: Structure of HEC-*g*-polyglycerol-*g*-PCL$_{50}$ with assignments for NMR

^{1}H NMR (600 MHz; DMF-d_7): δ = 4.10 (t, b, H_f), 3.82-3.55 (m, HEC), 2.35 (t, H_b), 1.71-1.56 (m, $H_{c,\ e}$), 1.45-1.34 (m, H_d). ^{13}C NMR (150 MHz; DMF-d_7): δ = 174.0 (C_a), 71.3 (C_8), 69.9 ($C_{6,\ 6'\ R\#H,}$ C_7), 64.8 (C_f), 62.2 ($C_{6,\ 6'\ R=H,}$ C_9), 34.6 (C_b), 29.3 (C_e), 26.3 (C_d), 25.5 (C_c).
FT-IR: ν_{max} = 3440 cm^{-1} (OH), 2945 cm^{-1} (C-H), 1730 cm^{-1} (C=O), 1200 cm^{-1} (O-C-O). SEC (DMF): M_w = 1.66×10^6 g mol^{-1}, Đ = 7.59.

5.2.6 Synthesis of HEC-*g*-polyglycerol-*g*-PCL$_{100}$ 5.4

To a flame dried Schlenk tube, HEC-*g*-polyglycerol **5.1d** (25 mg, 8.3×10^{-5} mmol) and a magnetic stirrer bar were added. The system was sealed with a rubber septum and placed under vacuum for 1 h. The tube was then kept under an N_2 atmosphere, ε-caprolactone (0.33 mL, 3 mmol) and tin(II) 2-ethylhexanoate (33 µL of a 0.044 M stock solution in toluene, 0.61 mg, 1.5×10^{-3} mmol) were added and the system was stirred at 120 °C for 18 h. The colour of the reaction mixture changed from clear to yellow and became viscous. The polymer was dissolved in DMF and precipitated into cold methanol twice to give a white solid, which was dried in an oven at 80 °C for 24 h under reduced pressure to give the product **5.4**, yield 70.4% **(**0.27 g, 1.2×10^{-4} mmol).

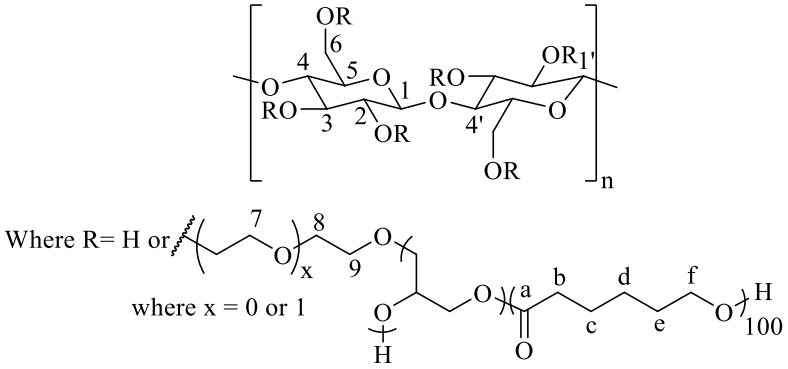

5.4

Figure 5.4: Structure of HEC-*g*-polyglycerol-*g*-PCL$_{100}$ with assignments for NMR

^{1}H NMR (600 MHz; DMF-d$_7$): δ = 4.07 (t, b, H$_f$), 2.35 (t, *J* = 6.6 Hz, H$_b$), 1.70-1.57 (m, H$_c$, $_e$), 1.45-1.34 (m, H$_d$). ^{13}C NMR (150 MHz; DMF-d$_7$): δ = 174.0 (C$_a$), 64.7 (C$_f$), 62.2 (C$_{6,\,6',\,R=H,}$ C$_9$), 34.6 (C$_b$), 29.3 (C$_e$), 26.3 (C$_d$), 25.5 (C$_c$).

FT-IR: ν_{max} = 3440 cm^{-1} (weak, OH), 2945 cm^{-1} (C-H), 1730 cm^{-1} (strong, C=O), 1200 cm^{-1} (O-C-O). SEC (DMF): M_w = 2.28 × 10^6 g mol^{-1}, Đ = 3.27.

5.2.7 Synthesis of HEC-*g*-polyglycerol-*g*-poly(caprolactone)$_{250}$ 5.5

To a flame dried Schlenk tube, HEC-*g*-polyglycerol **5.1d** (25 mg, 8.3 × 10^{-5} mmol) and a magnetic stirrer bar were added. The system was sealed with a rubber septum and placed under vacuum for 1 h. The tube was then kept under an N_2 atmosphere, ε-caprolactone (0.83 mL, 7.5 mmol) and tin(II) 2-ethylhexanoate (33 μL of a 0.044 M stock solution in toluene, 0.61 mg, 1.5 × 10^{-3} mmol) were added and the system was stirred at 120 °C for 18 h. The colour of the reaction mixture changed from clear to yellow and became viscous. The polymer was dissolved in DMF and precipitated into cold methanol twice to give a white solid, which was dried in an oven at 80 °C for 24 h under reduced pressure to give the product **5.5**, yield 73.4% (0.74 g, 1.1 × 10^{-4} mmol).

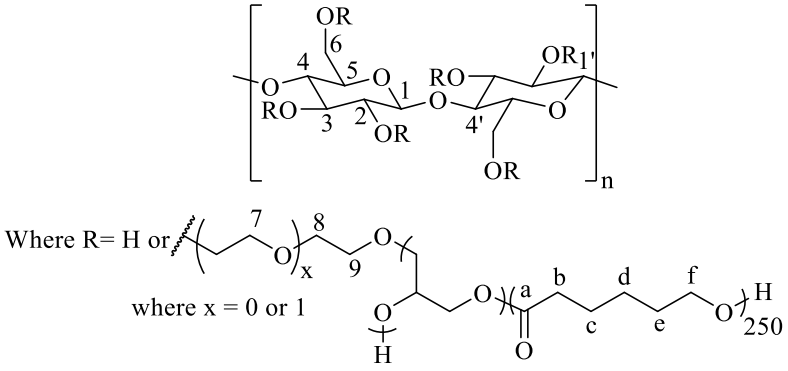

5.5

Figure 5.5: Structure of HEC-*g*-polyglycerol-*g*-PCL$_{250}$ with assignments for NMR

^{1}H NMR (600 MHz; DMF-d$_7$): δ = 4.07 (t, *J* = 6.6 Hz, H$_f$), 2.35 (t, *J* = 6.6 Hz, H$_b$), 1.69-1.59 (m, H$_{c,\ e}$), 1.44-1.36 (m, H$_d$). ^{13}C NMR (150 MHz; DMF-d$_7$): δ = 174.1 (C$_a$), 64.8 (C$_f$), 62.3 (C$_{6,\ 6'\ R=H,\ 9}$), 34.7 (C$_b$), 29.4 (C$_e$), 26.4 (C$_d$), 25.6 (C$_c$).

FT-IR: ν_{max} = 2945 cm^{-1} (C-H), 1730 cm^{-1} (strong, C=O), 1200 cm^{-1} (O-C-O). SEC (DMF): M_w = 6.52 × 10^6 g mol^{-1}, Đ = 3.76.

5.3 Results and Discussion

5.3.1 HEC-*g*-polyglycerol

HEC-*g*-polyglycerol was synthesised using HEC as a macroinitiator for the ring-opening polymerisation (ROP) of glycidol as outlined in Scheme 5.2. The NaOH base is added first as it is most likely to deprotonate the HEC at the primary hydroxyl groups, forming highly reactive alkoxide nucleophiles. Glycidol is then added slowly, to produce HEC-*g*-polyglycerol **5.1**.

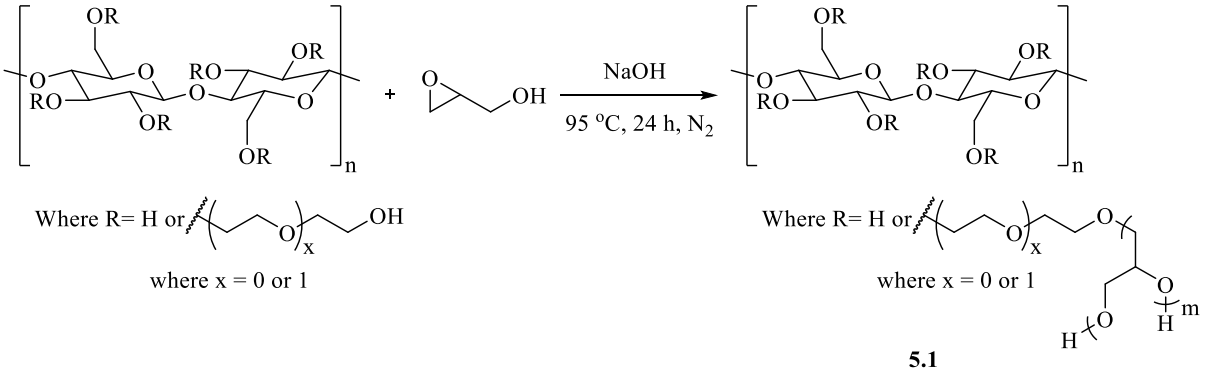

5.1

Scheme 5.2: Synthesis of HEC-*g*-polyglycerol

A number of experiments were carried out, following the reaction conditions outlined in Table 5.1 to produce HEC-*g*-polyglycerol **5.1 a-e**. The minimum of HEC in water of 10 wt.% was determined to be sufficient. In the synthesis of graft copolymer **5.1e**, the concentration was increased to 20 wt.% which resulted in a very viscous reaction mixture that was difficult to stir even by mechanical means. The ratio of NaOH was adjusted in order to vary the number of reactive alkoxide sites on HEC, therefore creating more initiating sites for the ROP of glycidol. In the synthesis of **5.1a** where the smallest investigated amount of NaOH is used, no grafting had occurred as there were no resonances corresponding to polyglycerol present in the ^{13}C NMR spectrum of the product.

Table 5.1: Reaction conditions for synthesis of HEC-*g*-polyglycerol 5.1 a-e

Code	Wt.% of HEC in H_2O	Mol. Eq. % NaOH	Mol. Eq. % Glycidol	Notes
a	10	2.5	400	Polyglycerol signals not visible in NMR
b	10	5	400	
c	10	10	400	
d	10	10	200	
e	20	5	400	Product very viscous

In all cases, the rate of dissolution of the polymers in water increased, due to the presence of grafted polyglycerol. The polymers were purified by being dialysed against water for 48 h, using dialysis tubing with a cut-off of M_w = 1.2 × 10^4 g mol^{-1}. This will remove any unreacted glycidol or low M_w glycerol homopolymer, whilst ensuring that any glycerol grafted to the higher M_w HEC remained.

Initial trial experiments were carried out in organic solvents DMF and DMPU, but were abandoned due to their limited ability to solubilise NaOH and lack of observed polyglycerol grafting. Water was chosen as the reaction solvent, based on previous work carried out within the group by Dr. P. A. King investigating grafting of polyglycerol to poly(vinyl alcohol).[3]

It was thought that carrying out the reaction in water would result in poor grafting, due to molecules of water also acting as competing nucleophiles alongside the hydroxyl groups of HEC. This was found not to be the case, but it is important that the minimum amount of water is used to solubilise the HEC to reduce the probability of this side reaction. The slow, dropwise addition of the glycidol monomer *via* syringe pump was found to be essential. The use of syringe pump has also been demonstrated to synthesise hyperbranched polyols in a controlled manner, reducing the dispersity (Đ) of the resulting polymer.[4]

There are four different structural units that can be observed within hyperbranched polyglycerol (Figure 5.6), depending on the reacted number of hydroxyl groups: terminal (T) (Figure 5.6.B), dendritic (D) (Figure 5.6.C), linear 1, 3 ($L_{1,3}$) (Figure 5.6.A) and linear 1, 4 ($L_{1,4}$) (Figure 5.6.D).

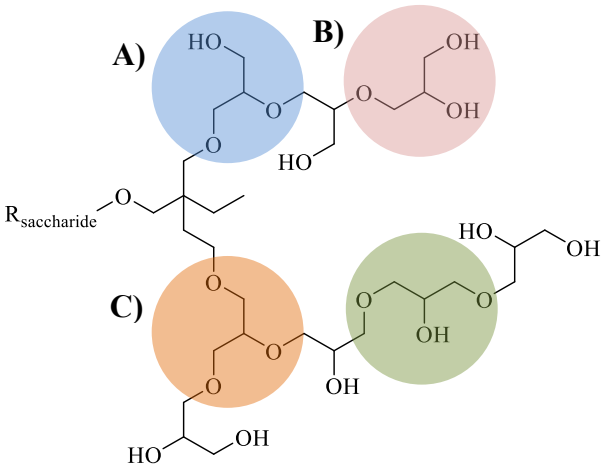

Figure 5.6: Structure of branched polyglycerol A) $L_{1,3}$ unit B) T unit C) D unit and D) $L_{1,4}$ unit

^{1}H NMR spectroscopy was not an effective method of analysis, as the resonances due polyglycerol were overlapped by those corresponding to HEC. Inverse-gated ^{13}C NMR spectroscopy was therefore utilised instead.

Polyglycerol had previously been synthesised[3] by Dr. King and the ^{13}C NMR resonances were assigned based on those presented by Spears *et al*.[5] The individual structural units can be distinguished by ^{13}C NMR spectroscopy as each unit has characteristic resonances. The ^{13}C NMR spectra of polyglycerol is shown in Figure 5.7.A, and was used as the reference for the HEC grafted polyglycerol ^{13}C NMR assignments in this work, an example of which (compound **5.1c**) is shown in Figure 5.7.B. The results were in good agreement, indicative of the successful synthesis of polyglycerol grafts.

Not all of the polyglycerol resonances are observed in the ^{13}C NMR spectrum of HEC-*g*-polyglycerol, due to the spectrum being dominated by the HEC resonances at 72.8, 70.2 and 60.7 ppm corresponding to $C_{8,}$ C_6 and C_7 (R#H), and C_6 and C_9 (R = H), respectively, as it is present in a much higher relative concentration. The resonances corresponding to the $L_{1,3}$ unit at 80.0 and 69.8 ppm and one of the D unit resonances at 78.5 ppm are not clearly observed in Figure 5.7.B, whilst the resonances corresponding to the $L_{1,4}$ unit at 72.7 ppm and one of the D unit resonances at 70.5 ppm are overlapped by HEC resonances. Resonances due to the three T units are clearly observed at 63.5, 71.0 and 73.3 ppm.

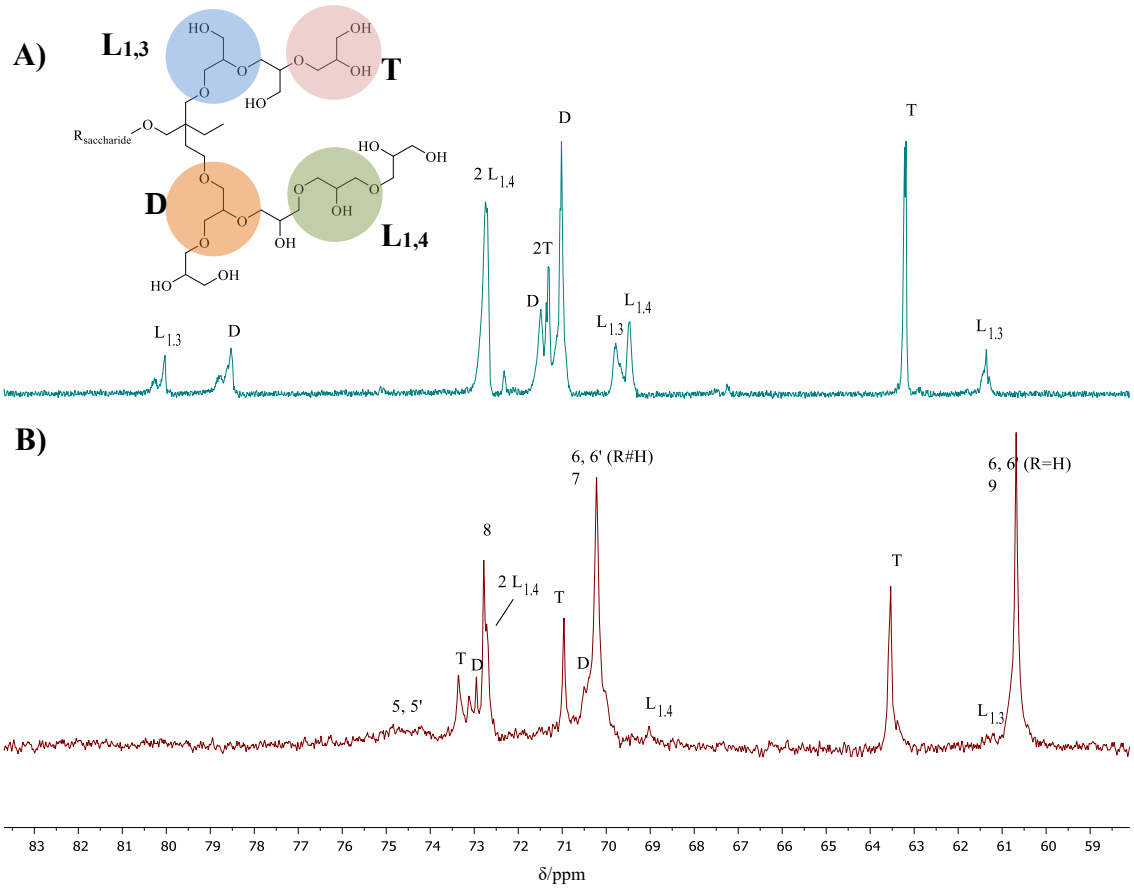

Figure 5.7: A) ^{13}C NMR spectrum of polyglycerol in D_2O, B) Inverse-gated ^{13}C NMR spectrum of HEC-*g*-polyglycerol 5.1c in DMSO-d_6

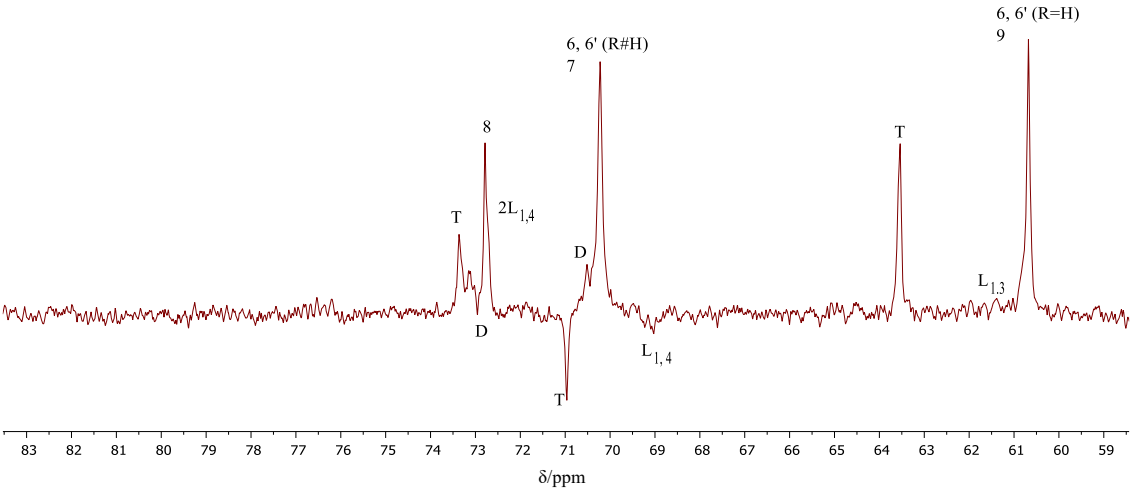

Figure 5.8: DEPT-135 ^{13}C NMR spectrum of HEC-*g*-polyglycerol 5.1c in DMSO-d_6

The DEPT-135 ^{13}C NMR spectrum of **5.1c** (Figure 5.8) shows the inversion of the CH resonances corresponding to the D, T and $L_{1,4}$ units at 72.9, 71.0 and 69.0 ppm, respectively. The positions of the resonances agree with those presented in the literature for polyglycerol.[4]

The inverse-gated ^{13}C NMR spectra of **5.1d** are shown comparing the initial (Figure 5.9.A) against the dialysed (Figure 5.9.B) product. A decrease in intensity of the resonances

corresponding to the D and T units at 72.6 and 63.5 ppm, respectively, is observed. However, the fact that polyglycerol resonances remain after dialysis is a good indication of chemical grafting to the HEC backbone.

The dialysate that the sample was submerged in was changed and analysed by ^{1}H NMR spectroscopy after 8 h and 48 h, Figure 5.10. After 8 h (Figure 5.10.A), multiplet resonances over the range 3.43-3.25 ppm were observed due to the presence of polyether.[6] These corresponded to homopolymer oligomers of polyglycerol, formed *via* ROP side reactions of glycidol initiated by water, which were removed by dialysis. Furthermore, the presence of a broad resonance at 3.66 ppm corresponding to HEC backbone protons was also observed. This was due to some low molecular weight HEC oligomers passing through the membrane which were also subsequently removed by dialysis. After 48 h (Figure 5.10.B), the samples were fully dialysed; this was indicated by the absence of resonances corresponding to homopolymer of polyglycerol and low molecular weight HEC in the ^{1}H NMR spectrum of the dialysate solution.

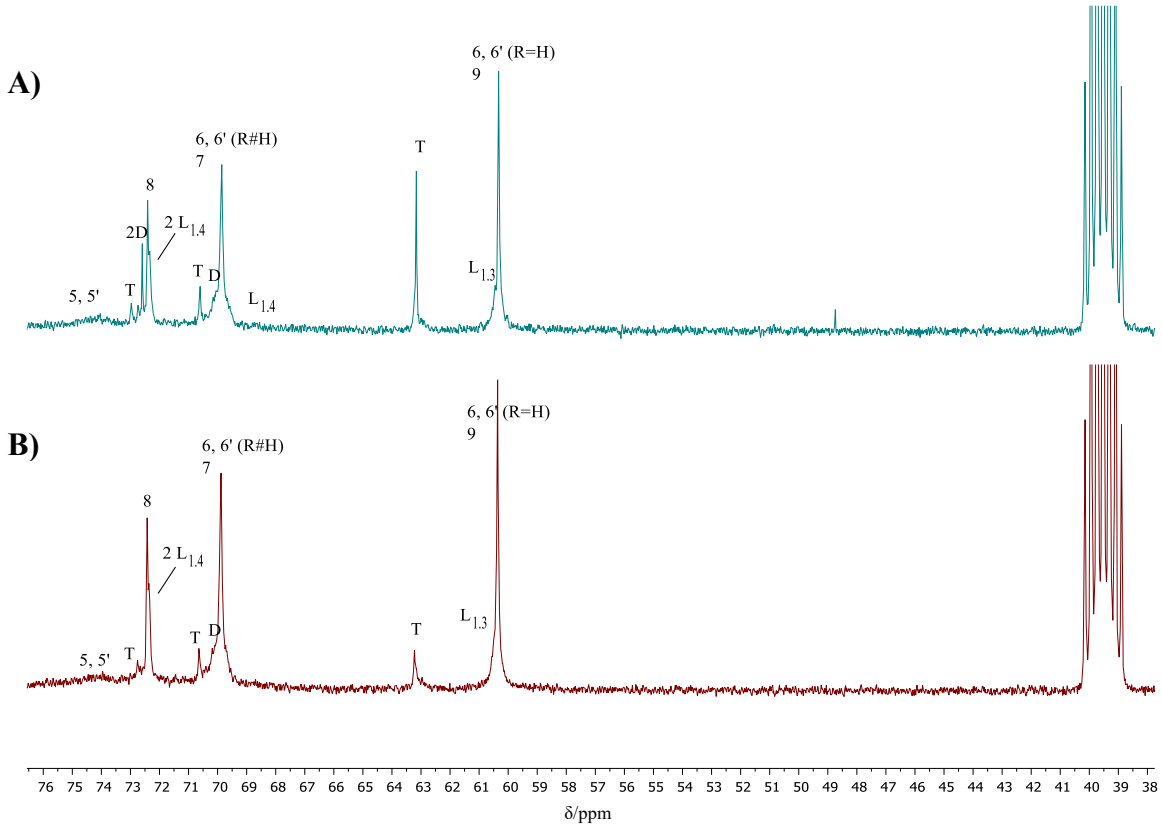

Figure 5.9: ^{13}C NMR spectra of HEC-*g*-polyglycerol 5.1d A) initial product and B) dialysed product, both in DMSO-d_6

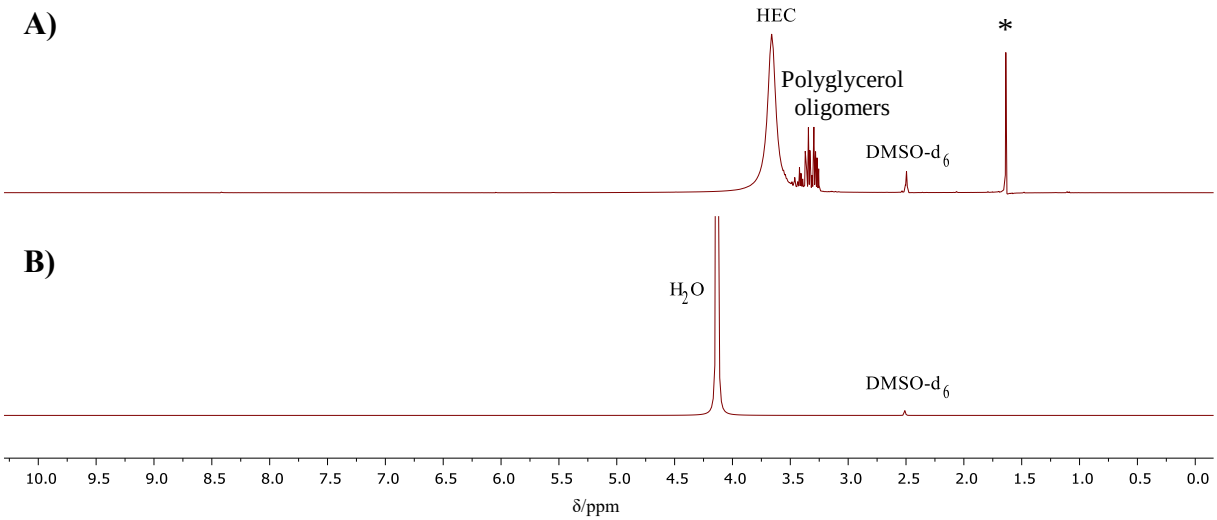

Figure 5.10: ^{1}H NMR spectra of the dialysate solution after A) 8 h and B) 48 h, both in DMSO-d_6

Table 5.2 presents the inverse-gated ^{13}C NMR spectroscopy and TGA data, as well as M_w, M_n and dispersity (Đ) data as calculated by SEC (triple detection of refraction index (RI), intrinsic viscosity (IV) and right angle light scattering (RALS)) for HEC-*g*-polyglycerol **5.1 a-e**.

Table 5.2: Inverse-gated ^{13}C NMR, TGA and SEC data for HEC and HEC-*g*-polyglycerol 5.1 a-e

Code	^{13}C NMR ratio of C_6, C_9:T	TGA onset (°C)	M_w (× 10^5 g mol^{-1})	M_n (× 10^5 g mol^{-1})	Đ
HEC	-	263	3.54	0.65	5.40
a	-	310	-	-	-
b	1:0.15	282	4.48	1.23	3.65
c	1:0.58	294	4.63	1.41	3.27
d	1:0.25	299	3.96	0.54	3.89
e	1:0.10	292	-	-	-

The ^{13}C NMR data give the ratio of the resonance attributed to HEC C_6 and C_9 (60.7 ppm) to the isolated resonance of the T unit (63.5 ppm). This was calculated in order to quantify the number of terminal units present in each graft copolymer and give an estimate of the amount of grafting. No ratio could be calculated for graft copolymer **a** as the reaction was unsuccessful and therefore no polyglycerol resonances were observed in the ^{13}C NMR spectrum.

The SEC chromatograms of the graft copolymers **5.1 b, c** and **d** are given in Figure 5.11. The M_w of the HEC starting material was determined to be greater than reported by Sigma-Aldrich (expected ~2.50 × 10^5 g mol^{-1}, determined 3.54 × 10^5 g mol^{-1}) and with a high dispersity of

5.40. All of the analysed modified polymers **b**, **c** and **d** exhibited lower values of Đ of 3.65, 3.27 and 3.89, respectively.

For the synthesis of graft copolymers **b** to **c**, 5% and 10% molar equivalents of NaOH were used, respectively. Graft copolymer **c** afforded a higher ratio of terminal units and also higher M_w and M_n values. This is due to the deprotonation of more hydroxyl groups in HEC, creating more potential initiation sites for participation in ROP reactions. Graft copolymer **d** affords a lower ratio of terminal units when compared to **c** (approximately half), which was expected as half the amount of glycidol was added. Graft copolymer **c** also affords the lowest dispersity out of all of the polymers.

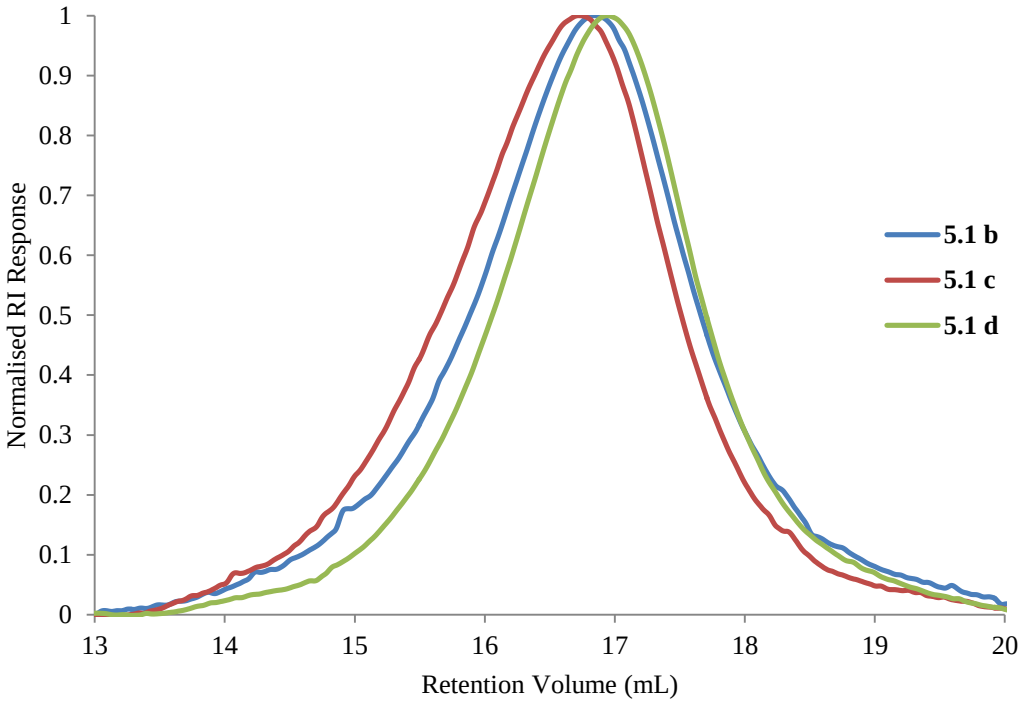

Figure 5.11: Plot of normalised RI vs retention volume of HEC-*g*-polyglycerol graft copolymers 5.1b, 5.1c and 5.1d

A representative TGA thermogram of graft copolymer d is shown in

Figure 5.12. All of the graft copolymers afforded a higher TGA onset temperature, from 263 °C to an average of 300 °C, which is the initial temperature where mass loss due to degradation is observed. This indicates that the grafting of polyglycerol improves the thermal stability of the graft copolymer overall.

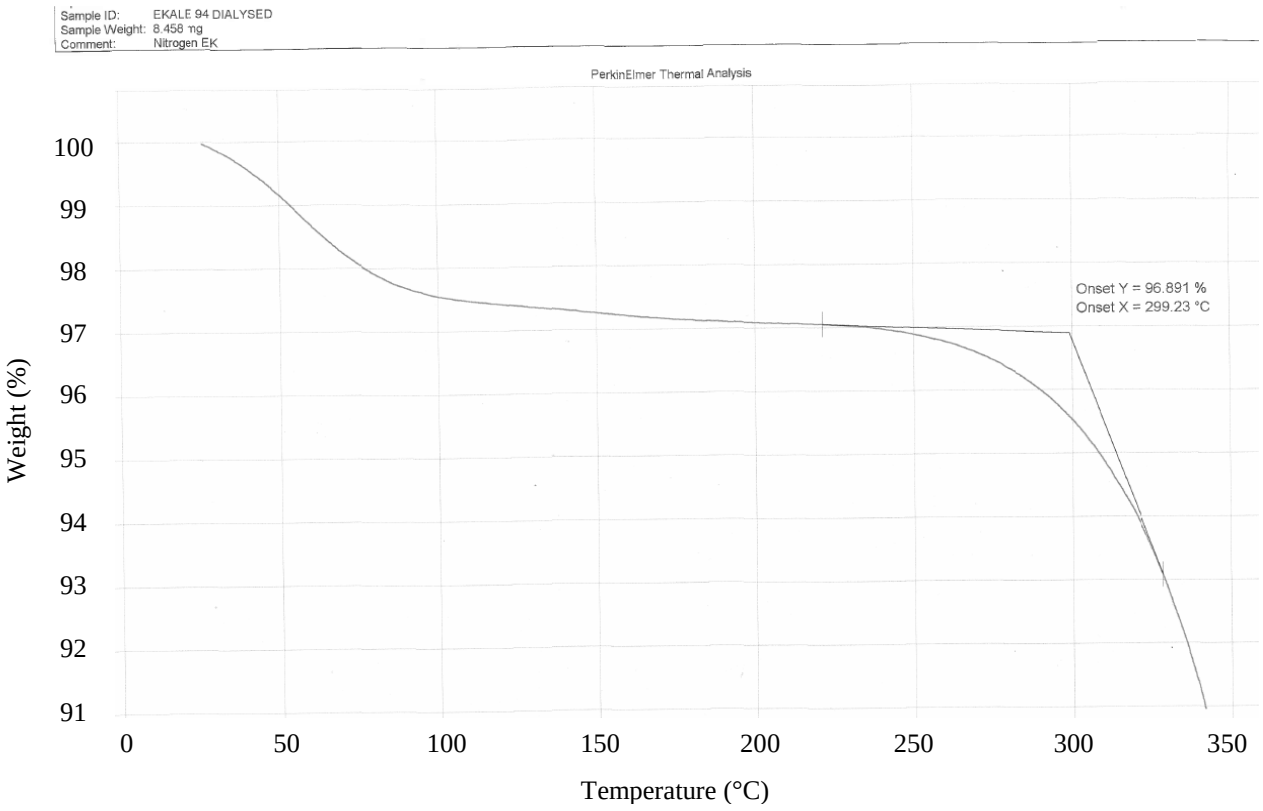

Figure 5.12: TGA thermogram of HEC-*g*-polyglycerol 5.1d

5.3.2 HEC-*g*-polyglycerol as a Macroinitiator

HEC-*g*-polyglycerol **5.1d** was used as a macroinitiator and $Sn(Oct)_2$ as a catalyst for the ring-opening polymerisation of ε-CL (Scheme 5.3). The molar ratio of ε-CL to initiator was varied to achieve PCL grafts with $\overline{DP}_{Th}$ of 10, 50, 100 and 250 per arm in HEC-*g*-polyglycerol-*g*-PCL **5.2**, **5.3**, **5.4** and **5.5**, respectively. It is thought that the hydroxyl end groups will be further away from the backbone and grafted by flexible arms. This should reduce steric hindrance, thus increasing the likelihood of interacting with group(IV) metal ions of crosslinking agents.

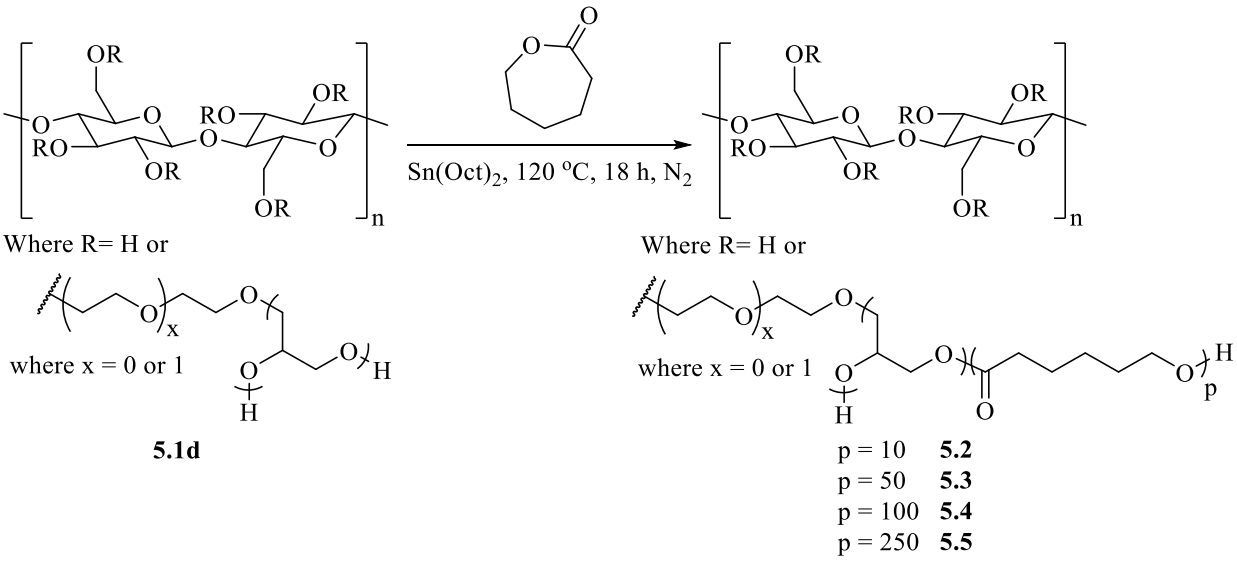

Scheme 5.3: ROP of ε-CL using HEC-*g*-polyglycerol as a macroinitiator to give 5.2-5.5

The ^{1}H NMR spectra for the HEC-*g*-polyglycerol-*g*-PCL are shown for **5.2** (Figure 5.13.A), **5.3** (Figure 5.13.B), **5.4** (Figure 5.13.C) and **5.5** (Figure 5.13.D), where $\overline{DP}_{Th}$ of the PCL chains is 10, 50, 100 and 250 units, respectively. Broad resonances due to the protons of HEC are observed at 3.35-4.00 ppm when smaller PCL lengths are grafted. As the lengths increase, the PCL resonances become more prominent, with H_f, H_b, H_{c+e} and H_d being observed at 4.07, 2.35, 1.64 and 1.40 ppm, respectively. The starred resonance present in all spectra in Figure 5.13 at 3.54 ppm is due to residual MeOH.

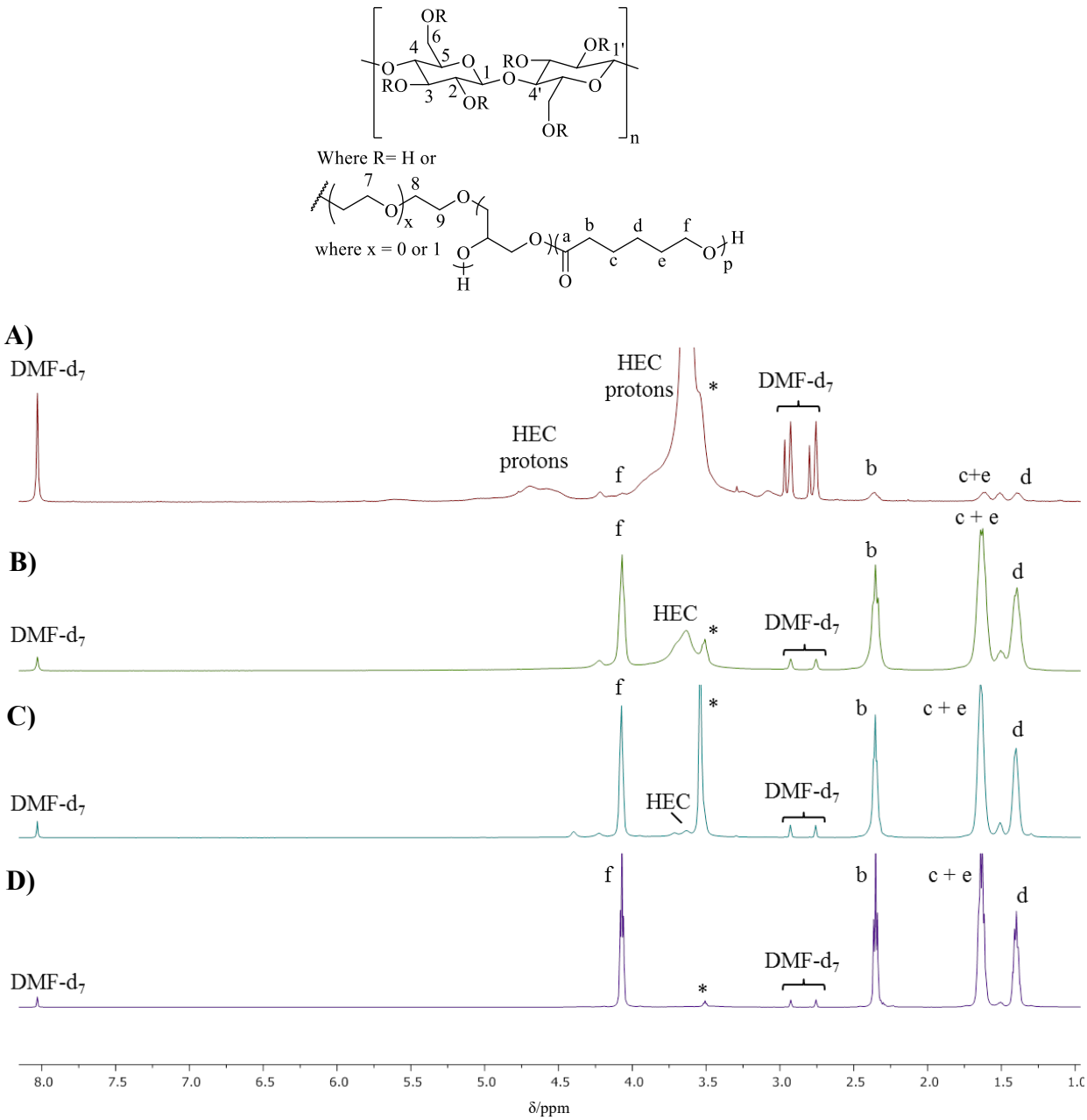

Figure 5.13: ^{1}H NMR spectra of HEC-*g*-polyglycerol-*g*-PCL with $\overline{DP}_{Th}$ of PCL A) 10, B) 50, C) 100 and D) 250, all in DMF-d_7

The ^{13}C NMR spectra of HEC-*g*-polyglycerol-*g*-PCL **5.2-5.5** are shown in Figure 5.14.A-D. The PCL carbonyl resonance C_a is observed at 174.0 ppm. The characteristic methylene resonances in PCL corresponding to C_f, C_b, C_e, C_d and C_c are observed at 64.8, 34.7, 29.4, 26.4 and 25.6 ppm, respectively.

^{1}H-^{13}C HSQC NMR spectroscopy of the polymers was used to confirm that the proton resonance at 1.64 ppm corresponded to both carbon resonances C_e and C_c at 29.4 and 25.6 ppm. The pertinent region in the ^{1}H-^{13}C HSQC spectrum of **5.5** is shown in Figure 5.15.

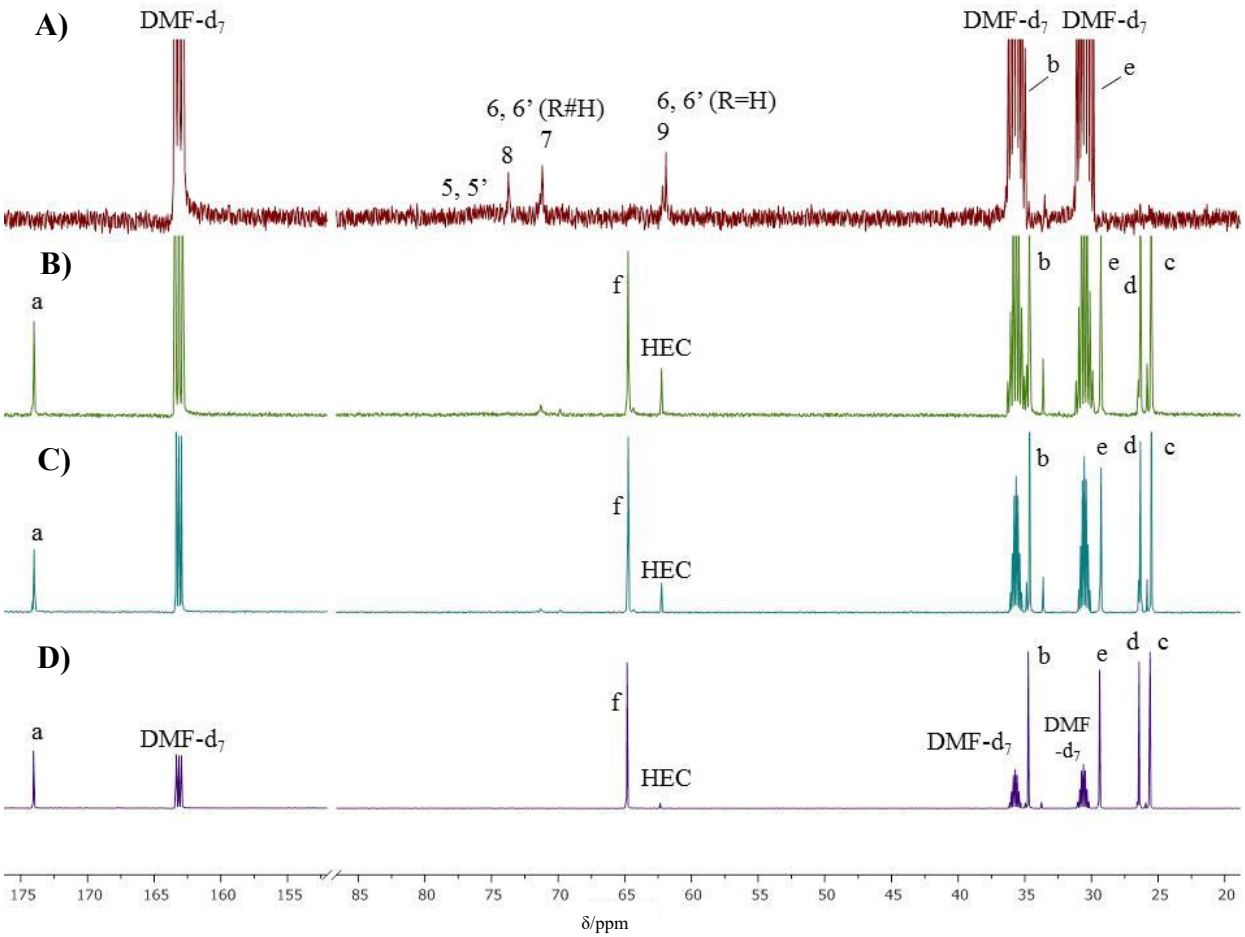

Figure 5.14: ^{13}C NMR spectra of HEC-*g*-polyglycerol-*g*-PCL with $\overline{DP}_{Th}$ of PCL A) 10, B) 50, C) 100 and D) 250, all in DMF-d$_7$

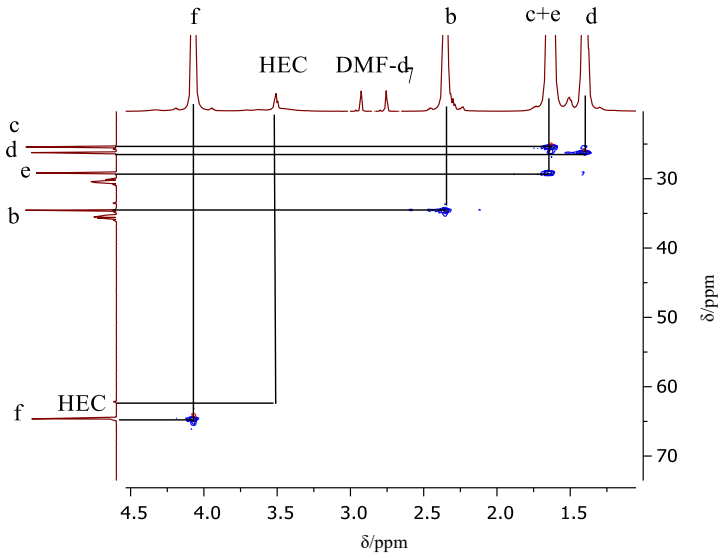

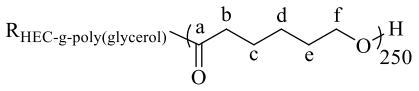

Figure 5.15: Magnified portion of the ^{1}H-^{13}C HSQC NMR spectrum of 5.5 in DMF-d$_7$

Graft copolymers **5.2** and **5.3** with short PCL chains are both water soluble, as these polymers are comprised of a larger ratio of HEC. As the $\overline{DP}_{Th}$ increases, the solubility properties of the polymers are altered, becoming insoluble in water and newly soluble in chloroform as they become more PCL-like. When **5.5** ($\overline{DP}_{Th}$ = 250) was washed with water, ^{1}H NMR analysis of these washings revealed the presence of small resonances corresponding to both HEC and residual PCL. These were attributed to a small amount of HEC grafted with PCL oligomers of a low enough molecular weight so that HEC retained its water solubility property.

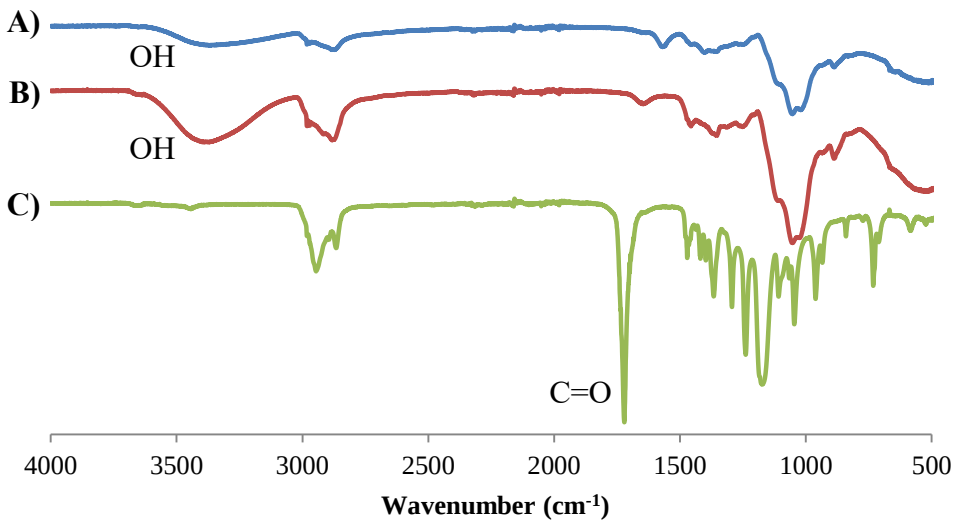

Figure 5.16: FT-IR spectra of A) HEC, B) HEC-*g*-polyglycerol 5.1d and C) HEC-*g*-polyglycerol-*g*-PCL$_{250}$ 5.5

FT-IR spectroscopy presented another useful tool for the characterisation of the products. The comparison of spectra of HEC (Figure 5.16.A) with **5.1d** (Figure 5.16.B) showed an increase in intensity of the hydroxyl resonance at 3440 cm^{-1}, as the glycidol undergoes ring-opening resulting in an abundance of OH groups. The FT-IR spectrum of graft copolymer **5.5** shows a strong absorption at 1730 cm^{-1} attributed to the carbonyl groups of the PCL chains, Figure 5.16.C. There is also a reduction in the strong resonance corresponding to OH, as the hydroxyl groups act as initiating sites for the ROP of ε-CL, indicative of successful grafting and leading to the hydrophobic character of the product.

The comparison of M_w^{Th}, M_w^{SEC}, M_n^{SEC} and Đ for the PCL containing polymers **5.2-5.5** are shown in Table 5.3.

Table 5.3: Molecular weight and dispersities for HEC-*g*-polyglycerol-*g*-PCL 5.2-5.5

Code	$\overline{DP}_{Th}$	[a]M_w^{Th} ($\times 10^6$ g mol^{-1})	[b]M_w^{SEC} ($\times 10^6$ g mol^{-1})	[b]M_n^{SEC} ($\times 10^6$ g mol^{-1})	Đ
5.2	10	0.59	0.59	0.067	8.99
5.3	50	1.90	1.66	0.22	7.59
5.4	100	3.60	2.28	0.71	3.27
5.5	250	8.80	6.52	1.73	3.76

[a]Determined by feed ratio; [b]Determined by SEC analyses

The SEC chromatograms of the graft copolymers (Figure 5.17) show that as the $\overline{DP}_{Th}$ increases, the M_w observed by SEC increases, as expected. Lower molecular weight graft copolymers **5.2** and **5.3** with M_w^{Th} values of 0.59 × 10^6 g mol^{-1} and 1.90 × 10^6 g mol^{-1} are in good agreement with the M_w^{SEC} values of 0.59 × 10^6 g mol^{-1} and 1.66 × 10^6 g mol^{-1}, respectively. These values were calculated using a dn/dc value of 0.044 mL g^{-1}, corresponding to cellulose tributyrate in DMF.[7]

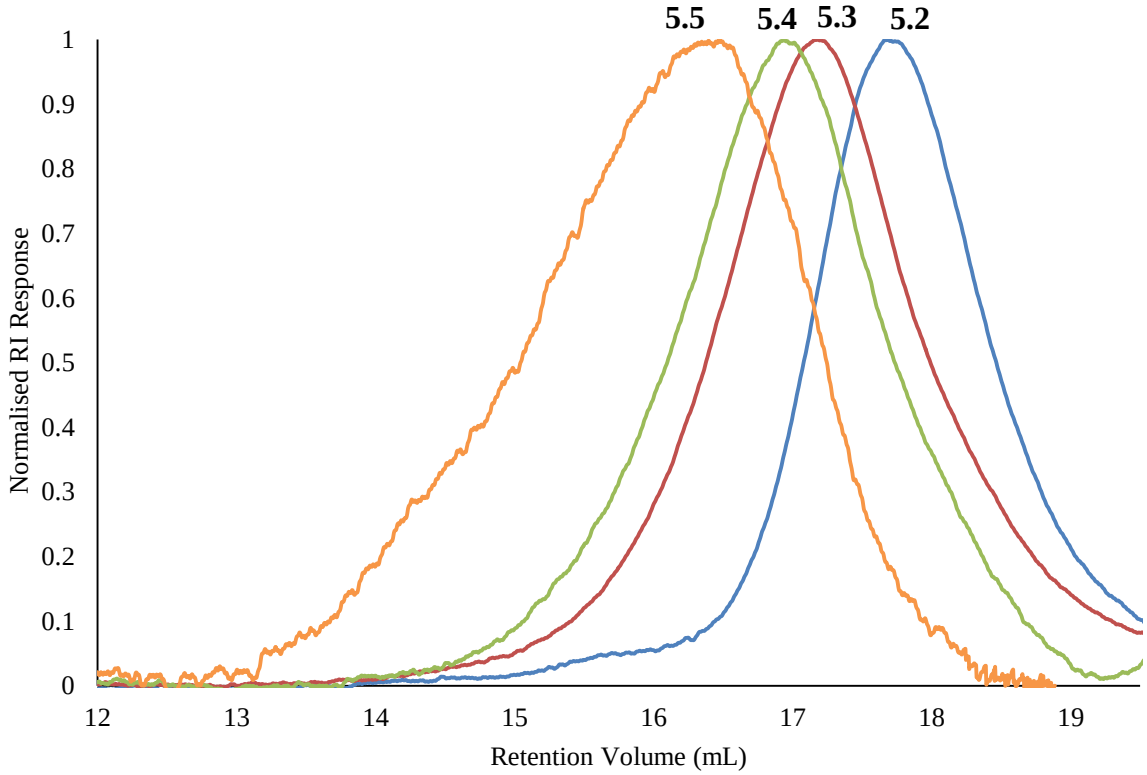

Figure 5.17: Plot of normalised RI vs retention volume demonstrating increase to higher molecular weight as the length of grafted PCL increases. Blue line = 5.2; red line = 5.3; green line = 5.4 and orange line = 5.5

However, higher molecular weight graft copolymers **5.4** and **5.5** with M_w^{Th} values of 3.60×10^6 g mol^{-1} and 8.80×10^6 g mol^{-1} show poor agreement with M_w^{SEC} values of 2.28×10^6 g mol^{-1} and 6.52×10^6 g mol^{-1}, respectively. These values were calculated using a dn/dc value of 0.013 mL g^{-1}, obtained from the accurate concentration calculation of the samples of copolymers **5.4** and **5.5**. The dn/dc literature value of 0.044 mL g^{-1} was not applicable here as this corresponds to a cellulose based polymer- as the M_w increases in **5.4** and **5.5**, the ratio of PCL to HEC increases, thus the polymers will exhibit a different hydrodynamic volume.

The greater discrepancy in the M_w values for the larger PCL-containing graft copolymers is due to the method in which SEC data is collected. The longer graft copolymer chains are more likely to undergo intramolecular hydrogen-bonding, resulting in more coiled, denser structures, with a lower hydrodynamic volume than anticipated.

All of the graft copolymers also exhibit high Đ values, indicating that generally, there was a lack of control over the polymerisation and that the $\overline{DP}$ of each PCL arm is unlikely to be equal. This suggests that the rate of initiation of the ROP is slower than the rate of propagation, possibly due to initiation sites being trapped within the coiled PCL chains.[8, 9]

The thermal analyses of the graft copolymers **5.1-5.5** including TGA onset, melting temperature (T_m), crystallisation temperature (T_c), enthalpy of melting (ΔH_m), enthalpy of crystallisation (ΔH_c) and calculated % degree of crystallinity (χ_c) are shown in Table 5.4.

Table 5.4: Thermal analyses of HEC and graft copolymers 5.1-5.5 determined by TGA and DSC analysis

Code	PCL $\overline{DP}_{Th}$	TGA onset (°C)	T_m (°C)	T_c (°C)	ΔH_m (J g^{-1})	ΔH_c (J g^{-1})	Weight fraction of 5.1d	Weight fraction of PCL, *w*	χ_c (%)
HEC	-	263	-	-	-	-	-	-	-
5.1d	-	299	-	-	-	-	-	-	-
5.2	10	-	48	-	2	-	0.429	0.571	2.74
5.3	50	295	47	27	8	7	0.128	0.872	5.83
5.4	100	319	53	26	25	20	0.068	0.932	19.34
5.5	250	305	62	35	36	28	0.028	0.972	26.34

The TGA onset value is the temperature at which thermal degradation begins. The grafting of polyglycerol to HEC increases the TGA onset value from 263 °C to 299 °C, increasing the thermal stability. When PCL chains are grafted, the TGA onset temperature slightly increases to 305 °C. The thermograms obtained by TGA analysis of the HEC starting material and graft copolymers **5.1d**, **5.3**, **5.4** and **5.5** are shown in Figure 5.18.

The mass loss of up to 4 wt.% observed over the temperature range 80-100 °C in HEC and graft copolymer **5.1d** is due to the loss of water, as both of these materials are hygroscopic due to the abundance of hydroxyl groups present.

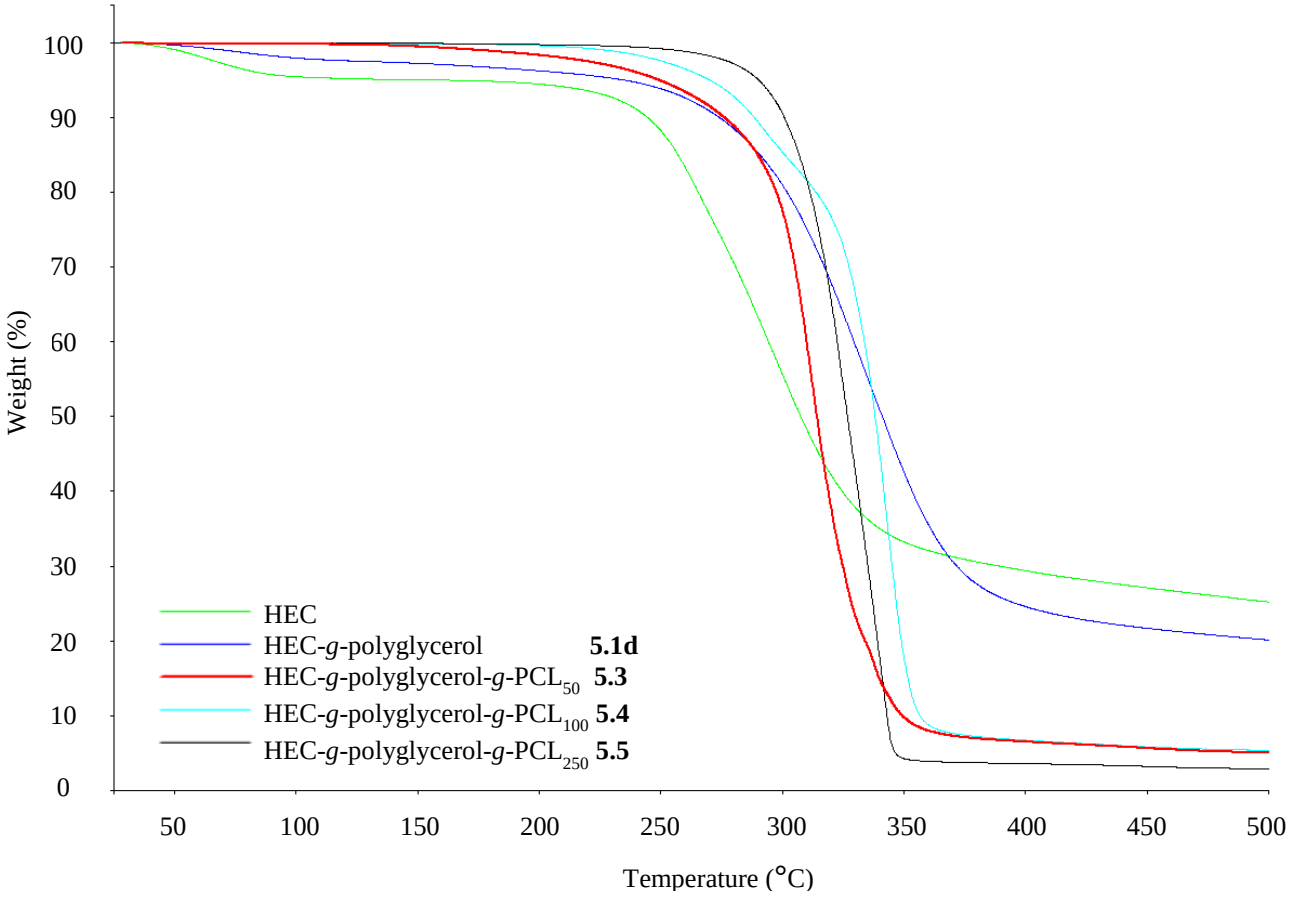

Figure 5.18: TGA thermograms of HEC and graft copolymers 5.1d, 5.3, 5.4 and 5.5

The thermal properties were determined by DSC analyses for the HEC graft copolymers **5.2-5.5**, Table 5.4. A representative DSC thermogram of graft copolymer **5.4** is shown in Figure 5.19, where a heating cycle up to 150 °C affords an endothermic peak from which the values of ΔH_m and T_m are determined, and a cooling cycle affords an exothermic peak from which the values of ΔH_c and T_c are determined.

As the $\overline{DP}$ of the PCL chains increases, the T_m values showed an increase from 48 °C to 62 °C, whilst the T_c values showed little change from 27 °C to 35 °C. Moreover, the observed values of both ΔH_m and ΔH_c showed an increase from 2 to 36 J g^{-1} and from 7 to 28 J g^{-1}, respectively, with increasing $\overline{DP}$ of PCL.

The degree of crystallinity (%X_c) was calculated using Equation 5.1.[10] The value of ΔH_m^o refers to the standard enthalpy of melting of 100% crystalline PCL, and was taken as 139.5 J g^{-1}.[11]

$$\%X_C = \frac{\Delta H_m}{\Delta H_m^o \, x \, w} \, x \, 100 \qquad \text{Equation 5.1}$$

It is important to note that HEC does not undergo crystallisation as it does not exhibit a melting temperature. At temperatures above 150 ˚C, HEC begins to show signs of degradation, dependent upon the molecular weight.[12] Therefore Equation 5.1 was modified to discount the weight fraction of HEC, and thus is representative of only the crystallisation of the PCL component of the polymer. As the $\overline{DP}$ of the PCL chains increases, the value of X_c also increases, up to 26.3% crystallinity for the highest molecular weight polymer, as this is comprised of the biggest weight fraction of PCL. The $\%X_c$ values are also based on the assumption of complete incorporation of PCL; actual $\overline{DP}$ values could not be calculated as accurate proton or inverse-gated carbon integration could not be determined from the NMR spectra.

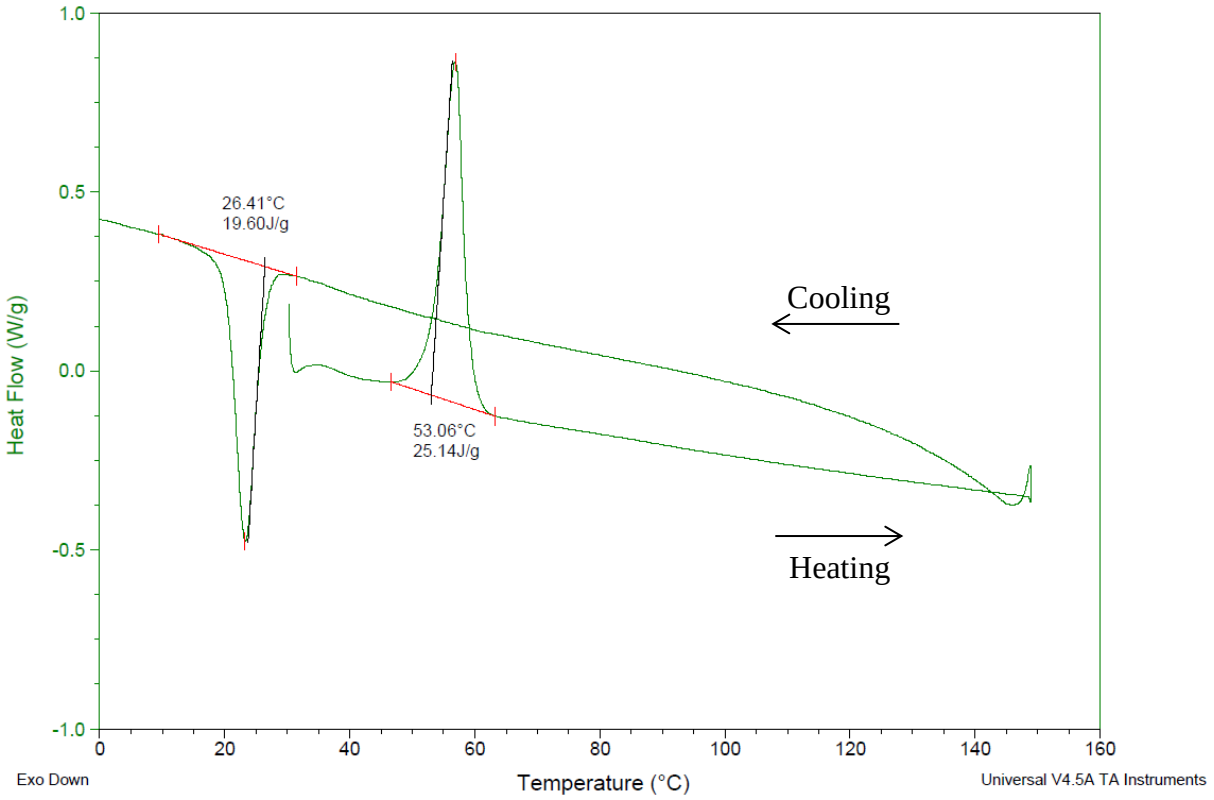

Figure 5.19: DSC thermogram of HEC-*g*-polyglycerol-*g*-PCL$_{100}$ 5.4

Atomic force microscopy (AFM) was utilised to investigate the architecture of the HEC-*g*-polyglycerol and HEC-*g*-polyglycerol-*g*-PCL graft copolymers. Tapping-mode micrographs were obtained in an attempt to visualise surface features of individual polymer chains. Samples were prepared for imaging by spin coating clean silicon wafers with a very dilute polymer solution (~1 mg/10 mL) in either water or THF. This ensures sufficient dispersal of the polymer chains. Analysis of tapping mode AFM images indicated that HEC-*g*-polyglycerol **5.1d** formed worm-like chains with length of ~500 nm as shown in Figure 5.20.A, with a height of ~1 nm and apparent width of ~40 nm, Figure 5.20.B. The length of ~500 nm is consistent with the fully extended conformation of the chain, assuming 5 Å per repeat unit and the existence of 1000 average repeat units. This structure is very different to that of the HEC starting material, which was observed to exhibit hemi-ellipsoidal (rugby-ball) features with an average height of ~10 nm and width of ~50 nm.[13]

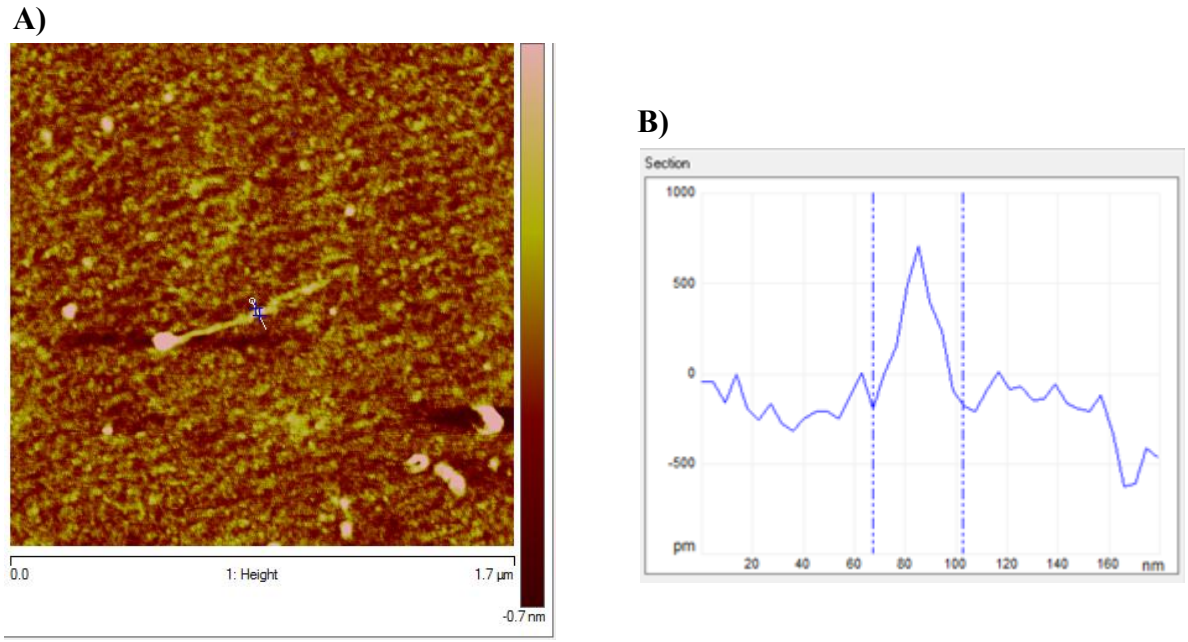

Figure 5.20: A) Tapping mode AFM image of HEC-*g*-polyglycerol 5.1d at 1.7 µm scale, B) cross-sectional analysis

AFM analysis of HEC-*g*-polyglycerol-*g*-PCL_{10} **5.2** afforded a uniform, fine capillary-like network, Figure 5.21.A, with an average height of ~2.5 nm and apparent width of ~50 nm, Figure 5.21.B. This formation of thin worms is characteristic of polymer brushes,[14] and is exhibited due to the HEC backbone being in an extended conformation with the side chains stretched and flattened on the surface, presumably due to steric repulsion of the short PCL side chains.

AFM analysis of polymers with a bigger PCL component, HEC-*g*-polyglycerol-*g*-PCL_{250} **5.5** afforded larger globules, Figure 5.22.A, with an average height of ~3.7 nm and apparent width of ~80 nm, Figure 5.22.B. For graft copolymer **5.5**, if it is assumed the M_w^{Th} of 9.0×10^6 g mol^{-1} is the polymer mass and density is ~1 g cm^{-3}, this suggests a volume per single macromolecule of approximately 15,000 nm^3. If these are individual molecules, the area would be ~15,000 nm^3/3.7 nm = 4,100 nm^2, or ~70 nm in diameter. This is in agreement with what the AFM data presented in Figure 5.22 shows. This suggests that the longer PCL chains coil in on themselves, resulting in a larger hydrodynamic volume.

All of the width measurements are likely to be overestimated because they also include the effective width of the AFM probe, which is ~15 nm.

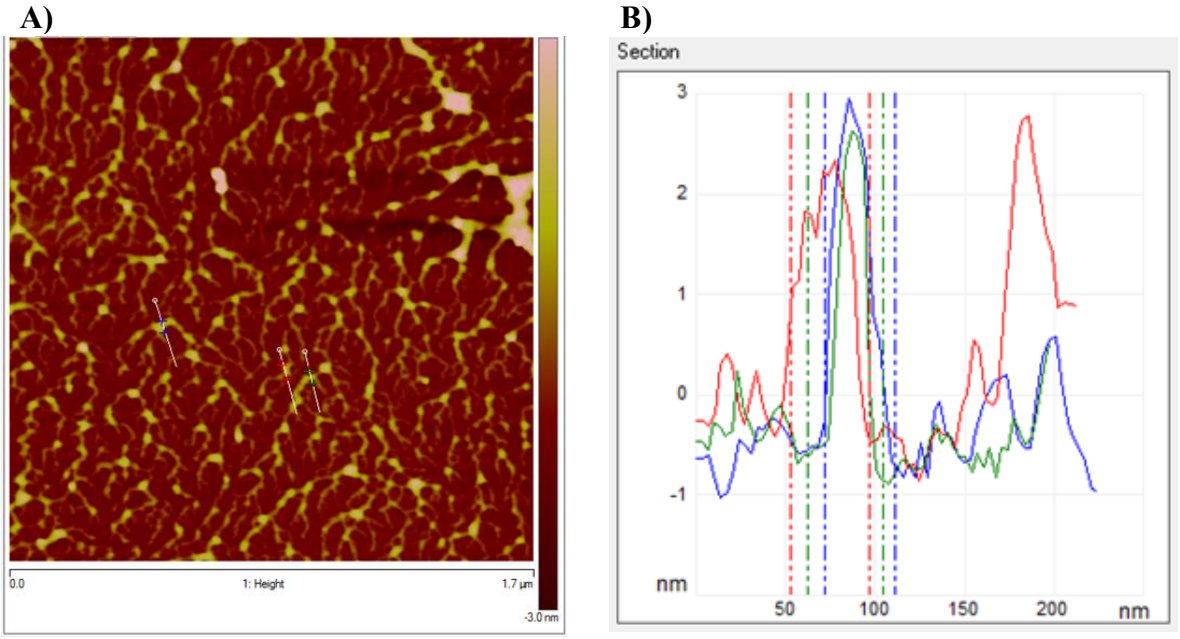

Figure 5.21: A) Tapping mode AFM image of HEC-*g*-polyglycerol-*g*-PCL$_{10}$ 5.2 at 1.7 µm scale, B) cross-sectional analysis

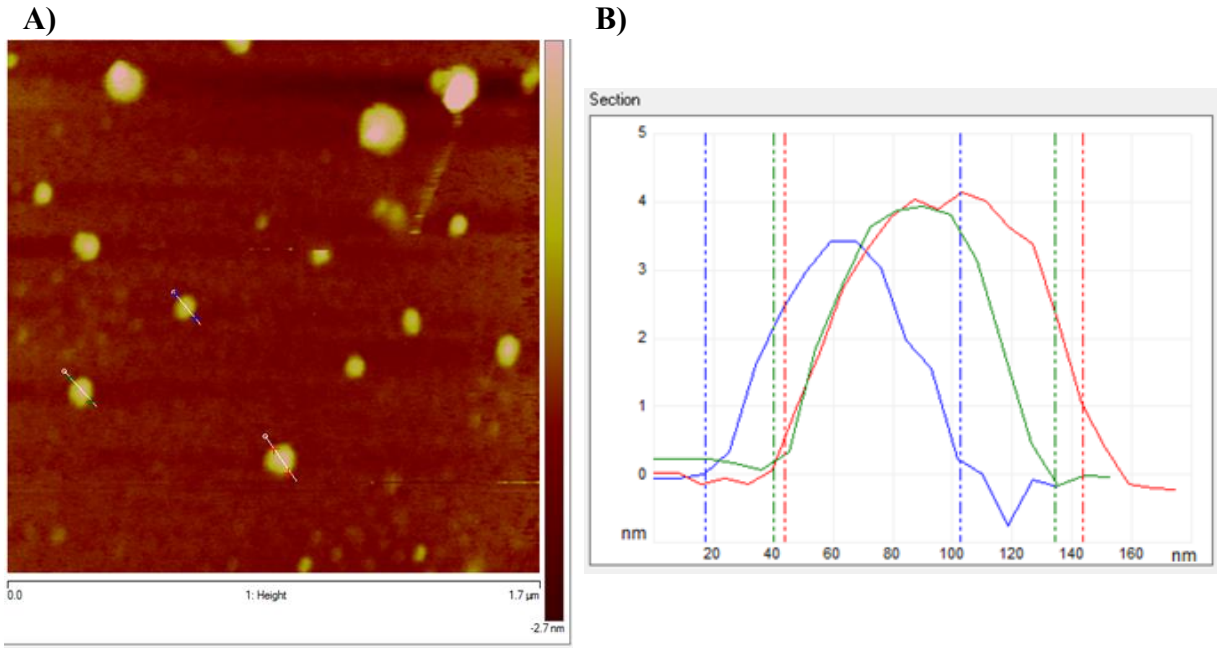

Figure 5.22: A) Tapping mode AFM image of HEC-*g*-polyglycerol-*g*-PCL$_{250}$ 5.5 at 1.7 µm scale, B) cross-sectional analysis

5.4 Conclusions

HEC-*g*-polyglycerol materials were prepared through the ROP of glycidol using HEC as a macroinitiator and NaOH as a base. The graft copolymers were purified by dialysis and then analysed by inverse-gated ^{13}C NMR spectroscopy and SEC. Resonances corresponding to grafted polyglycerol remained in the ^{13}C NMR spectra after dialysis for the graft copolymers **b-e**, but it was difficult to accurately quantify the extent of the reactions due to the broad overlapping resonances corresponding to the HEC backbone. However, no polyglycerol resonances were observed in the ^{13}C NMR spectrum of graft copolymer **5.1a** as the reaction was unsuccessful because the lowest molar equivalence (2.5%) of base was used. The amount of base added to deprotonate the primary hydroxyl groups on HEC was found to be at least a 5% molar equivalence, as observed for the synthesis of graft copolymers **b-e**.

Synthesis of graft copolymer **5.1b**, with 5% molar equivalence of base successfully underwent ROP with 400% molar equivalents of glycidol to afford a material with M_w of 4.48×10^5 g mol^{-1}, as indicated by SEC analysis. The synthesis of graft copolymer **5.1c**, with the greatest molar equivalents of both base and glycidol monomer (10% and 400%, respectively) afforded the highest M_w graft copolymer material of 4.63×10^5 g mol^{-1}, as expected. This is due to the formation of more deprotonated hydroxyl sites that can initiate ROP, as well as the availability of more glycidol monomer that can be incorporated. Graft copolymer **5.1c** also exhibited a Đ value of 3.27 in comparison to the HEC starting material, with a Đ value of 5.40.

The synthesis of graft copolymer **5.1d,** with 10% and 200% molar equivalents of base and glycidol, respectively, afforded a material with M_w of 3.96×10^5 g mol^{-1}. This graft copolymer exhibited a Đ value of 3.89. It also exhibited the greatest increase in TGA value, in comparison to HEC, from 263 to 299 $^{\circ}$C, implying good thermal stability. It can be inferred that only 5% and 200% molar equivalents of base and glycidol, respectively, are required, as when greater amounts of either reactant are used the observed molecular weights of the graft copolymers are the same, when taking SEC error into consideration. However, the extent of reaction as calculated by the integral of the T unit of polyglycerol in the inverse-gated ^{13}C NMR spectra is different, at 0.15, 0.58 and 0.25 for **5.1b**, **5.1c** and **5.1d**, respectively. The difference in the extent of reaction but similarity in observed M_w values is most likely due to the products having similar hydrodynamic volumes.

The synthesis of graft copolymer **5.1e** was undertaken using a 20 wt.% solution of HEC, which is double the amount used in all of the aforementioned HEC-*g*-polyglycerol graft copolymers.

This afforded a viscous solution which was analysed by inverse-gated ^{13}C NMR spectroscopy. Resonances corresponding to terminal units (CH_2-OH) in polyglycerol were observed in the ^{13}C NMR spectrum, however, the extent of the reaction could not be quantified due to the poor quality of the ^{13}C NMR spectrum.

HEC-*g*-polyglycerol **5.1d** was then successfully used as a macroinitiator in the ring-opening of ε-CL. The attachment of long PCL chains means that the hydroxyl end groups are further away from the HEC backbone, therefore are less sterically hindered and readily available to participate in reactions with group(IV) metal based crosslinking agents. A series of four graft copolymers containing PCL, **5.2**, **5.3**, **5.4** and **5.5** were synthesised with a $\overline{DP}_{Th}$ of 10, 50, 100 and 250 ε-CL units per arm, respectively. Longer PCL chain grafts (≥ 100 units) conferred hydrophobicity to the HEC backbone, whilst the grafting of smaller lengths (≤ 50) allowed the copolymers to retain partial water solubility.

For graft copolymers **5.2** and **5.3** with smaller $\overline{DP}_{Th}$ of 10 and 50, respectively, the calculated theoretical M_w values agreed with the M_w values calculated by SEC. As the value of $\overline{DP}$ increases, the M_w values calculated by SEC began to show poor agreement. This discrepancy may arise due to the longer PCL chains of **5.4** and **5.5** ($\overline{DP}_{Th}$ of 100 and 250, respectively) exhibiting greater crystallinity resulting in denser structures, leading most likely to different hydrodynamic volumes.

Changes in thermal properties of the graft copolymers were monitored by TGA and DSC analyses. In comparison to HEC, grafting of PCL increased the observed TGA onset temperature in all graft copolymers, from 263 °C to approximately 300 °C. As the $\overline{DP}$ of the PCL chains increases, the T_m values showed a small increase from 48 °C to 62 °C, whilst the T_c values showed little change, from 27 to 35 °C. Furthermore, the observed values of both ΔH_m and ΔH_c showed an increase from 2 to 36 J g^{-1} and from 7 to 28 J g^{-1}, respectively, with increasing $\overline{DP}$ of PCL.

DSC analysis of the copolymers also showed that as $\overline{DP}$ of the PCL graft increased, the crystallinity, $\%X_c$, also increased from 2.74% in **5.2** to 26.34% in **5.5**. This was expected, as longer PCL chains show greater crystallinity. However, it is important to note that these values only consider the crystallinity of the PCL component of the graft copolymer, as HEC does not show a melting temperature (therefore does not undergo crystallisation when cooled), and only

degrades at elevated temperatures, dependant on the M_w (determined by Sigma-Aldrich to be 288-290 °C (dec.) for HEC $M_w = 2.5 \times 10^5$ g mol^{-1}).

AFM imaging allowed investigation into the architecture of the graft copolymers. It showed that when HEC was grafted with polyglycerol, HEC-*g*-polyglycerol **5.1d**, it changed from hemi-ellipsoidal particles to worm-like structures. The length of the worm is consistent with the fully extended conformation of the chain, assuming 5 Å per repeat unit and the existence of 1000 average repeat units in the HEC backbone. Upon grafting of PCL, the structural architecture of the copolymers changed to a capillary-like fibrous network in **5.2**, then to larger globules in **5.5** as the PCL arm length increased. The AFM data of graft copolymer **5.5** suggests that each observed globule is an individual macromolecule.

5.5 References

1. G. L. Brode, J. P. Stanley, E. M. Partain, US 0 176 940 B1, **1991.**
2. B. Azimi, P. Nourpanah, M. Rabiee, S. Arbab, *J. Eng. Fiber. Fabr.*, **2014**, *9*, 74.
3. P. A. King, PhD Thesis, Durham University, **2015**.
4. A. Sunder, R. Hanselmann, H. Frey, R. Mülhaupt, *Macromolecules*, **1999**, *32*, 4240.
5. B. R. Spears, J. Waksal, C. McQuade, L. Lanier, E. Harth, *Chem. Comm.*, **2013**, *49*, 2394.
6. G. Wang, L. Li, J. Lan, L. Chen, J. You, *J. Mater. Chem.*, **2008**, *18*, 2789.
7. A. Theisen, C. Johann, M. P. Deacon, S. E. Harding, *Refractive Increment Data-book*, Nottingham University Press, **2000**.
8. D. P. Cole, E. Khosravi, O. M. Musa, *J. Polym. Sci. A Polym. Chem.*, **2016**, *54*, 335.
9. N. M. L. Hansen, M. Gerstenberg, D. M. Haddleton, S. Hvilsted, *J. Polym. Sci. A Polym. Chem.*, **2008**, *46*, 8097.
10. E. G. Bajsić, V. O. Bulatović, V. Rek, *Polym. Eng. & Sci.*, **2015**, *55*, 1920.
11. B. Gupta, Geeta, A. R. Ray, *J. Appl. Polym. Sci.*, **2012**, *123*, 1944.
12. T. T. Kararli, J. B. Hurlbut, T. E. Needham, *J. Pharm. Sci.*, **1990**, *79*, 845.
13. A. M. Eissa, E. Khosravi, A. L. Cimecioglu, *Carbohydr. Polym.*, **2012**, *90*, 859.
14. Y. Xia, J. A. Kornfield, R. H. Grubbs, *Macromolecules*, **2009**, *42*, 3761.

Chapter 6

Crosslinking Reactions for Hydraulic Fracturing Applications

6.1 Introduction

Group(IV) metal complexes, primarily those that are titanium or zirconium based, have been shown to be useful for crosslinking applications with hydraulic fracturing fluids due to their stability over wide temperature and pH ranges. This allows the crosslinking performance to be tuned to meet the specific needs of individual wells, which often require different conditions.[1] Ideally, the metal centre of the crosslinker should be complexed with Lewis basic ligands, such as OH, alkoxides, α-hydroxycarboxylic acids or alkanolamines.[2, 3]

Upon the addition of the crosslinker, the final fluid component of the hydraulic fracturing formulation, it is beneficial to have a delay in the gelation of the fluid. This allows a less viscous fluid to initially travel down the well, reducing pumping costs and minimising the shear effects that a more viscous fluid would experience.[1] Crosslinking would then °Ccur at the required position in the well leading to more efficient proppant delivery.[4] Delay time can often be controlled either by addition time or temperature.

Alkanolamine ligands are stabilising chelating agents which are present in a number of commercially available crosslinkers.[4] They have been utilised in an attempt to control the gelation time delay, as they effectively enclose the metal centres, reducing ligand exchange and also slowing the rate of hydrolysis of the crosslinker in solution. Diethanolamine based complexes were initially used, but zirconium complexes with this ligand showed poor gelation and delay control.[5]

A triethanolamine based zirconium crosslinker developed by Williams showed good fluid stability at high temperatures and pH.[6] A modification to the preparation of the crosslinker by Vaughn *et al.* 25 years later found that the addition of a small amount of water induced a gelation delay effect.[7] The triethanolamine ligand containing complex was found to show greater efficacy and stability when used to crosslink high pH fluids.

This chapter describes the investigation into tuning the gelation delay time of a guar based solution with a triethanolamine based zirconium crosslinker, by altering the number of molar equivalents of water added during crosslinker synthesis.

This chapter also describes six-coordinate alkanolamine complexes of titanium and zirconium that were also synthesised and evaluated for their crosslinking abilities. These proved fruitless due to the metal ions being fully chelated and therefore tightly bound. Displacement of these

ligands from the stable complex by polysaccharide chains would be unfavourable, as the metal ions are in a highly stable constitution.

Finally, this chapter also describes the crosslinking efficacy of the functionalised HEC materials successfully synthesised within this work using the aforementioned zirconium triethanolamine crosslinker, and an aqueous α-hydroxycarboxylic acid zirconate based crosslinker.

6.2 Experimental

6.2.1 Materials

Triethanolamine (TEA), titanium(IV) tetraisopropoxide (TIPT), *N*,*N*,*N*',*N*'-tetrakis(2-hydroxyethyl)ethylenediamine (THEED) and potassium hydroxide (KOH) were all purchased from Sigma-Aldrich and used without further purification. *N*,*N*,*N'*,*N*'-Tetrakis(2-hydroxypropyl)ethylenediamine (THPED) was purchased from Fisher Scientific and used without further purification. Zirconium(IV) *n*-propoxide (NPZ) solution (75% *w/w* in ^{n}PrOH) and a proprietary aqueous α-hydroxycarboxylic acid-based zirconate crosslinker were provided by Catalytic Technologies Ltd. A sample of guar gum powder was obtained from Rama Industries.

All solvents were analytical grade purchased from Fisher Scientific and used without any purification. The NMR solvent deuterated chloroform ($CDCl_3$) was purchased from Apollo Scientific and used as supplied.

6.2.2 Instrumentation and Measurements

^{1}H and ^{13}C Nuclear magnetic resonance spectroscopy (NMR) were carried out as outlined in Chapter 2, Section 2.2.2.

Viscosity measurements were recorded using a Fann 35 6-speed viscometer, comprising of a R1-B1 rotor/bob combination.

pH measurements were determined using a Jenway model 3020 pH meter with universal electrode probe.

Electrospray ionisation mass spectra (ESI-MS) were recorded by a TQD mass spectrometer setup for flow injection analysis with an operating mass range of 100-2000 u.

Crystallography data was collected on an Agilent Gemini S-Ultra diffractometer equipped with Cryostream open-flow nitrogen cryostat using graphite monochromated λMoKα radiation (λ=0.71073 Å, ω-scan, 1.0°/frame) at 120 K. The structures were solved by direct method and refined by full-matrix least squares on F^2 for all data using SHELXTL[8] and OLEX2[9] software. All non-disordered non-hydrogen atoms were refined with anisotropic displacement parameters; disordered atoms of methylene groups were refined isotropically with fixed SOF

0.8 and 0.2. All H-atoms were located on the difference map and refined isotropically except those on the disordered carbon atoms which were refined in "riding mode".

6.2.3 General Synthesis of Triethanolamine Zirconate Crosslinker 6.1 a-i

The products **6.1 a-i** were prepared using a modified procedure outlined by Vaughan *et al*.[7] In a dry beaker containing triethanolamine (8.41 g, 56.38 mmol, 6.2 eq.) in *n*-propanol (2.74 mL), zirconium(IV) *n*-propoxide solution (2.99 g, 9.11 mmol, 1 eq.) was added slowly with stirring at ambient temperature, and then allowed to stir for a further 15 min. to afford crosslinker **6.1a** as a transparent pale yellow liquid. The crosslinker was used in gelation tests without any further purification. For characterisation purposes, the solvent was removed under reduced pressure to afford a viscous yellow oil, yield 89.4% based on Zr, (9.16 g).

Crosslinkers **6.1 b-i** were prepared by addition of a certain molar equivalent of distilled water and the reaction mixture was stirred until homogenous. Amount of distilled water added: **6.1b** (0.14 mL, 7.47 mmol, 0.82 eq.), **6.1c** (0.33 mL, 18.22 mmol, 2 eq.), **6.1d** (0.49 mL, 27.33 mmol, 3 eq.), **6.1e** (0.82 mL, 45.55 mmol, 5 eq.), **6.1f** (1.23 mL, 68.32 mmol, 7.5 eq.), **6.1g** (1.65 mL, 91.10 mmol, 10 eq.), **6.1h** (2.46 mL, 136.7 mmol, 15 eq.), **6.1i** (3.28 mL, 182.20 mmol, 20 eq.). All crosslinkers were transparent pale yellow liquids and were used in gelation tests without any further purification.

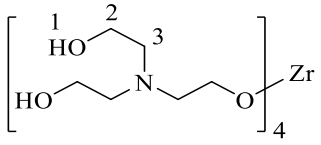

6.1

Figure 6.1: Simplified structure of triethanolamine zirconate with numerical assignments for NMR

^{1}H NMR (400 MHz; $CDCl_3$): δ = 5.19 (s, 8H, OH), 3.58 (t, *J* = 4.0 Hz, 24 H, H_2), 2.53 (t, *J* = 4.0 Hz, 24 H, H_3). ^{13}C NMR (400 MHz; $CDCl_3$): δ = 59.5 (C_2), 57.1 (C_3).

6.2.4 Synthesis of *N,N,N',N'*-Tetrakis(2-hydroxyethyl)ethylenediamine Titanate 6.2

In a dry beaker containing *N,N,N',N'*-tetrakis(2-hydroxyethyl)ethylenediamine (3.33 g, 14.1 mmol, 1 eq.), titanium(IV) tetraisopropoxide (4.0 g, 14.1 mmol, 1 eq.) was slowly added with fast, constant stirring at ambient temperature, and then allowed to stir for a further 20 min. The solvent was removed under reduced pressure to give a white solid, which was then recrystallised

from hot isopropanol. The crystals were dried in an oven overnight at 60 °C under reduced pressure to give **6.2** as a white solid, yield 51.48% (3.88 g, 7.2 mmol).

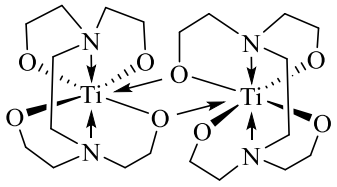

6.2

Figure 6.2: Structure of *N,N,N',N'*-tetrakis(2-hydroxyethyl)ethylenediamine titanate

Single crystal X-ray diffraction was used to determine the crystal structure.

$C_{20}H_{40}N_4O_8Ti_2$; MS: *m/z* ES^+, $[M+Na]^+$ = 583.5 Da.

6.2.5 Synthesis of *N,N,N',N'*-Tetrakis(2-hydroxyethyl)ethylenediamine Zirconate 6.3

In a dry beaker containing *N,N,N',N'*-tetrakis(2-hydroxyethyl)ethylenediamine (3.77 g, 15.9 mmol, 1 eq.), zirconium(IV) *n*-propoxide solution (5.23 g, 15.9 mmol, 1 eq.) was slowly added with fast, constant stirring at ambient temperature, and then allowed to stir for a further 20 min. The solvent was removed under reduced pressure to give a white solid, which was then recrystallised from hot methanol/water (9:1 *v/v*). The crystals were dried in an oven overnight at 60 °C under reduced pressure to give **6.3** as a white solid, yield 47% (2.98 g, 4.8 mmol).

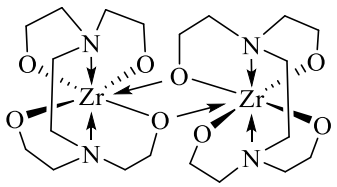

6.3

Figure 6.3: Structure of *N,N,N',N'*-tetrakis(2-hydroxyethyl)ethylenediamine zirconate

Single crystal X-ray diffraction was used to determine the crystal structure.

$C_{20}H_{40}N_4O_8Zr_2$; MS: *m/z* ES^+, M^+ = 644.4 Da.

6.2.6 Synthesis of *N,N,N',N'*-Tetrakis(2-hydroxypropyl)ethylenediamine Zirconate 6.4

In an oven dried 250 ml round bottom flask, *N,N,N',N'*-tetrakis(2-hydroxypropyl)ethylenediamine (4.67 g, 15.9 mmol, 1 eq.) was dissolved in dichloromethane (40 mL). Tetra *n*-propyl zirconate solution (5.23 g, 15.9 mmol, 1 eq.) was added slowly, and the mixture heated to reflux at 60 °C for 24 h. The solvent was removed under reduced pressure to give the product **6.4** as a viscous pale yellow liquid, yield 49% (5.29 g).

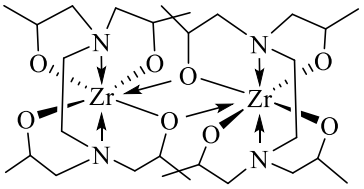

6.4

Figure 6.4: Structure of *N,N,N',N'*-tetrakis(2-hydroxypropyl)ethylenediamine zirconate

$C_{28}H_{56}N_4O_8Zr_2$; MS: *m/z* ES^+, M^+ = 758.60 Da.

6.2.7 General Procedure of Gelation Delay Measurements

In a 250 mL beaker, guar gum powder (0.35 g) was slowly sprinkled into distilled H_2O (100 mL) with constant stirring in order to prevent clumping. The solution was allowed to hydrate for 2 h with rapid stirring until the guar had fully dissolved and a homogeneous solution was observed. The pH of the solution was adjusted to 10.25 by addition of potassium hydroxide solution (2 M), upon which a colour change was observed from pale brown to pale yellow. To this gel solution, a 3.5 cm stirrer bar was added and stirring set to the maximum rate possible to create a vortex in the centre of the beaker. Zirconium triethanolamine crosslinker solution **6.1**, *x* (0.098–0.120 g) was injected into the centre of the vortex and a stopwatch started. The time taken was recorded when the vortex was fully closed and the surface of the gel became smooth.

6.2.8 General Procedure of Determining Viscosity with Fann 35 Viscometer

In a 250 mL stainless steel Fann 35 cup, guar gum powder (0.63 g) was slowly sprinkled into distilled H_2O (180 mL) with constant stirring in order to prevent clumping. The solution was allowed to hydrate for 2 h with rapid stirring until the guar had fully dissolved and a homogeneous solution was observed. The pH of the solution was adjusted to 10.25 by addition

of potassium hydroxide solution (2 M), upon which a colour change was observed from pale brown to pale yellow. The cup was placed on the Fann 35 viscometer stage and adjusted so that the bob was submerged in the gel solution up to the scribed line on the jacket. The viscometer was set to rotate at 100 rpm and the initial viscosity was recorded. Zirconium triethanolamine crosslinker solution **6.1** (0.09–0.46 g) was injected into the guar solution and the stopwatch started. The heating element and thermocouple were also turned on at this point if recording data with respect to heating. The viscosity value (and temperature, if applicable) were recorded at one minute intervals over 30 min.

6.3 Results and Discussion

6.3.1 Delay of Gel Formation of Guar Solutions

6.3.1.1 Zirconium TEA Crosslinker

Zirconium triethanolamine ($Zr(TEA)_4$) **6.1** was synthesised by reacting triethanolamine (TEA) with zirconium(IV) *n*-propoxide (NPZ) (Scheme 6.1). The *n*-propoxide groups are displaced by four molecules of TEA, which are also attached *via* an oxygen atom.

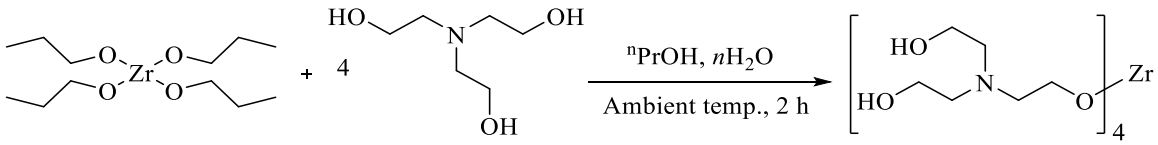

6.1

Scheme 6.1: Synthesis of zirconium triethanolamine crosslinker 6.1

The reaction was performed in *n*-propanol instead of in bulk, in order to improve the tractability of the crosslinker. Each crosslinker was a homogenous, transparent, pale yellow solution, but when the solvent was removed under reduced pressure, a viscous dark yellow oil was formed. The product cannot easily be evaporated to dryness to produce a solid, due to the strong hydrogen bonding interactions present between the TEA groups.

The ^{1}H NMR spectrum of the zirconium TEA crosslinker **6.1** is shown in Figure 6.5. The two triplet resonances at 3.58 and 2.53 ppm correspond to the H_2 and H_3 protons of the ethyl linkage, respectively, whilst the broad resonance at 5.19 ppm is due to the free hydroxyl groups, H_1. The small, broad resonances at 4.15 and 2.90 ppm are likely due to the protons of dative OH ligands coordinating to the zirconium centre. As zirconium can be eight coordinate, it is likely that the structure is more complex than that shown in Scheme 6.1, as it will be fluxional at room temperature in solution. The ^{13}C NMR spectrum of **6.1** (Figure 6.6) shows two resonances corresponding to the CH_2 groups C_2 and C_3 at 59.5 and 57.1 ppm, respectively.

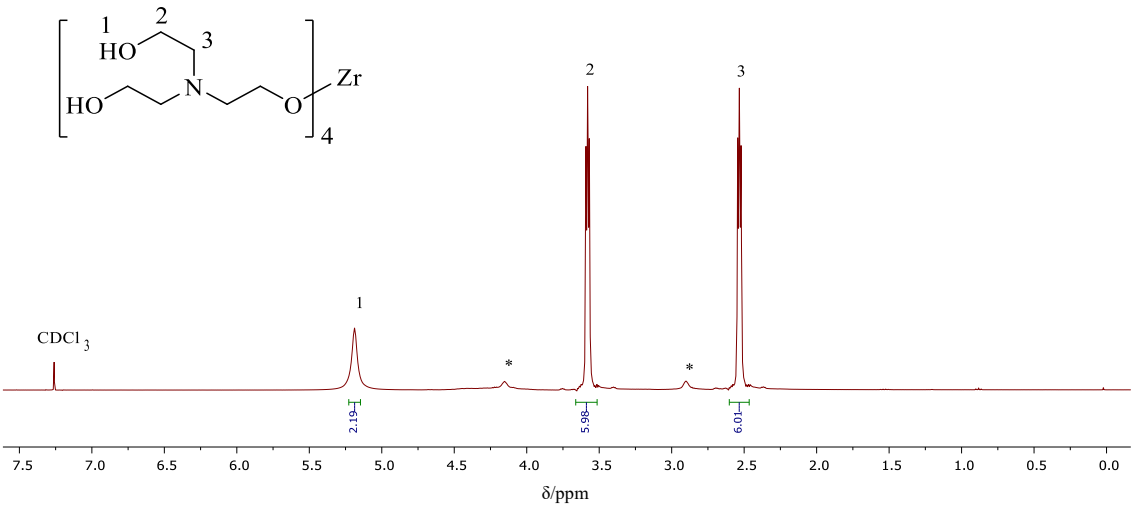

Figure 6.5: ^{1}H NMR spectrum of 6.1 in $CDCl_3$

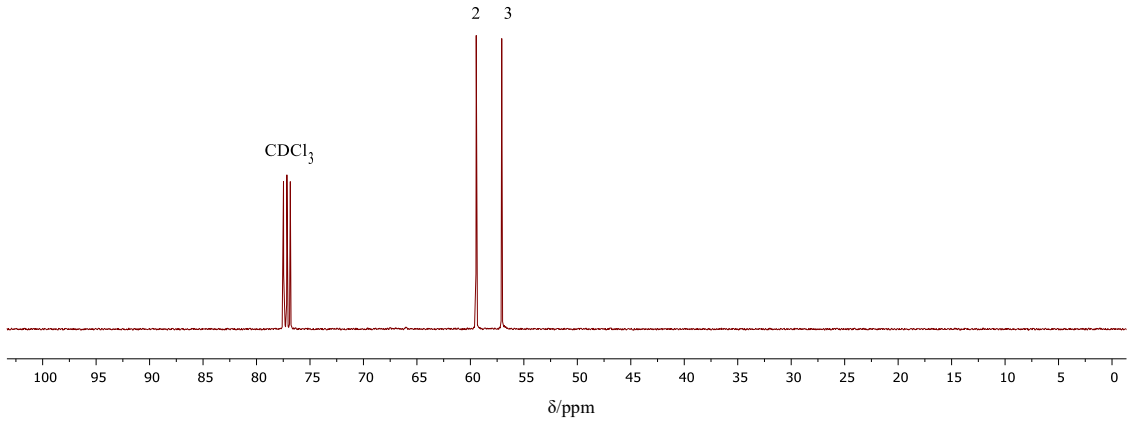

Figure 6.6: ^{13}C NMR spectrum of 6.1 in $CDCl_3$

6.3.1.2 Delay Testing with $Zr(TEA)_4$

The patent by Vaughn *et al.*[7] describes the addition of a small amount of water to the formulation in order to induce a short delay in the gelation of the guar solution. An investigation was carried out into how the addition of different molar amounts of water would affect the observed crosslinking time. The amounts of added water ranged from 0 to 20 molar equivalents. The addition of 0.82 equivalents of water was carried out in the patent, so crosslinker **6.1b** shall be referred to as the 'standard'.

Table 6.1 outlines the amount of water present in each $Zr(TEA)_4$ crosslinker **6.1 a-i**, and the calculated ZrO_2 content by weight. The zirconium content was calculated in terms of ZrO_2 concentration, based on Catalytic Technology Ltd.'s standard practice.

Table 6.1: Amount and molar equivalent of water present in crosslinkers 6.1 a-i, along with their calculated ZrO_2 wt.% content

	H_2O			
Code	**mL**	**mmol**	**Molar Eq.**	**ZrO_2 wt.%**
a	0	0	0	5.94
b Standard	0.14	7.47	0.82	5.87
c	0.33	18.22	2	5.80
d	0.49	27.33	3	5.74
e	0.82	45.55	5	5.62
f	1.23	68.32	7.5	5.47
g	1.65	91.10	10	5.32
h	2.46	136.65	15	5.06
i	3.28	182.20	20	4.82

Delay testing was carried out using "fracturing fluid" gel samples comprised of 100 ml of water containing 0.35 wt.% concentration of dissolved guar gum. The amount of guar gum utilised in industrial fracturing applications can vary within the limits from 0.35-2.0 wt.% of the total fracturing fluid.[10] The lower limit was chosen in order to allow a greater number of experiments to be performed with the limited amount of guar sample acquired, and was sufficient to observe when gelation occurred. Gelation times were recorded using the 'vortex closure' method.

Specifications given by Catalytic Technologies Ltd. requested that the total zirconium content, in the form of ZrO_2 in the crosslinker, added to the system should remain constant and equal to 5.80 wt.%. The weight of crosslinker added (x g) would have to be adjusted for each set of experiments in order to maintain effective concentration of 5.80 wt.% ZrO_2. The weight of each crosslinker, x, to be added was calculated using Equation 6.1, where 4.707×10^{-5} is the number

of moles of ZrO_2 in 0.1 g of crosslinker **6.1c**, which was calculated to contain 5.80% ZrO_2 by weight, 123.2 is the molecular weight of ZrO_2 (in g mol^{-1}) and the value of ZrO_2 wt.% is taken from Table 6.1.

$$x = \frac{\left(4.707\ x\ 10^{-5}\right)\ x\ 123.2}{ZrO_2\ wt.\%}\ x\ 100 \qquad \text{Equation 6.1}$$

Table 6.2 shows the values of *x* calculated for each crosslinker, and the recorded gelation times. Each crosslinker was tested at zero, one and seven months, in order to investigate how the effects of ageing may alter the gelation delay time. Each crosslinker was tested in triplicate in order to confirm reproducibility and provide an average time for each data point, except for the experiments carried out at seven months which were only performed once, due to the lack of a sufficient amount of remaining guar gum sample. The data are represented in Figure 6.7. Error bars, where calculated, are equal to one standard deviation.

Table 6.2: Mass of crosslinker, *x*, added per experiment, with recorded gelation times at 0, 1 and 7 months

			0 Month				1 Month				7 Months
Code	**H_2O Eq.**	***x* (g)**	**Time (s)**			**Average Time (s)**	**Time (s)**			**Average Time (s)**	**Time (s)**
a	0	0.097	33	31	29	**31**	35	39	34	**36**	**65**
b standard	0.82	0.099	38	44	41	**41**	58	50	52	**53**	**66**
c	2	0.100	59	61	55	**58**	64	68	65	**66**	**60**
d	3	0.101	63	62	64	**63**	61	55	59	**58**	**57**
e	5	0.103	64	68	63	**65**	53	48	54	**52**	**70**
f	7.5	0.106	63	65	66	**65**	57	58	54	**56**	**66**
g	10	0.109	67	56	59	**61**	43	48	52	**48**	**73**
h	15	0.115	64	62	64	**63**	58	55	55	**56**	**61**
i	20	0.120	78	68	72	**73**	60	55	54	**56**	**76**

From the initial delay data obtained using freshly prepared crosslinkers at 0 month, the general trend is that as the added molar equivalence of water increases, the delay time of gelation also increases. The trend is more prominent for crosslinkers **a-e** where smaller volumes of water are added, up to five equivalents, where a 20 s delay is observed in comparison to the standard. After this the data can be considered to effectively plateau, due to the larger error bars associated with the crosslinkers **g** and **i** containing 10 and 20 molar equivalents of water, respectively. However, these crosslinkers still produce delay times longer than the standard.

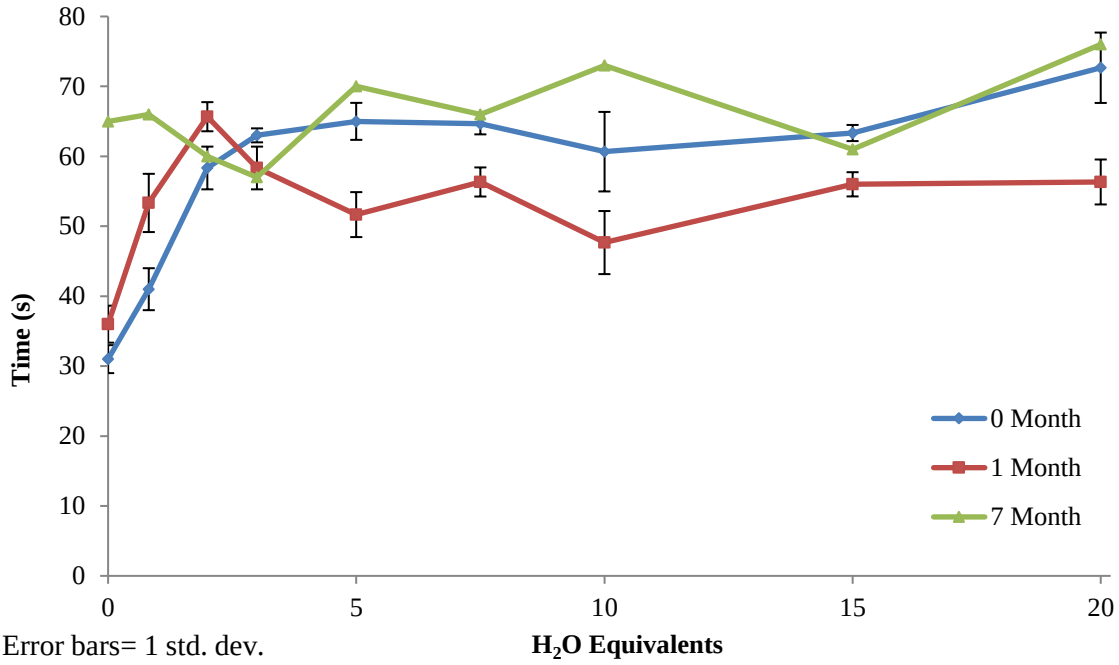

Figure 6.7: The effect of molar equivalence of H_2O present in $Zr(TEA)_4$ crosslinker on the gelation time of fracturing fluid, when the crosslinker has aged 0, 1 and 7 months

The increase in delay time can be attributed to the fact that as a larger amount of water is present, more hydrolysis reactions can occur between Zr species and so a larger number of Zr-O-Zr linkages are formed.[11] This leads to the formation of aggregates, which are more stable than the structure formed when only TEA is attached to the Zr metal centre. The Zr centre is only partially hydrolysed, however, with some arms of the TEA molecule remaining coordinated. It is probable this makes the Zr centres less available for crosslinking with the guar, and more energy is required to overcome the energy barrier to break aggregation, thus increasing the time it takes to afford crosslinking between the polymer chains.[7]

The data may show signs of beginning to plateau due to there being a limit to the number of bonds being able to be formed to the zirconium (maximum coordination of eight), regardless of the amount of water added.[12] Another possible explanation is due to steric hindrance. As the steric bulk increases around the metal centre due to new Zr-O-Zr linkages being created, and if not all of the TEA molecules are displaced, there will eventually come a point where the water molecules can no longer attack the metal centre to propagate further hydrolysis reactions.[13] A further possible explanation is one proposed by Bradley, in that the species will preferentially form the smallest possible oligomer unit consistent with all of the metal atoms attaining a higher coordination number, as to confer maximum stability to each unit.[14] Once the most stable

conformation is achieved, the remaining water will be present in excess and show no interaction with the metal centres.

Gelation delay times were retested after the crosslinkers had aged one and seven months. It was hypothesised that there would be a noticeable change due to degradation of the Zr/TEA species over time, which may have occurred due to more hydrolysis reactions occurring due to exposure to the atmosphere or after the prolonged exposure to the added water.

After one month, the general trend of crosslinkers containing up to three equivalents of water (**a**-**d**) is the same as that for the initial tests, but show longer delay times, with an increase up to 12 s for the standard. For crosslinkers containing three molar equivalents or greater, the delay times are lower than those recorded initially, but again crosslinkers **f-i** containing 7.5-20 equivalents show a similar trend of reaching a plateau when the associated errors are taken into account. After seven months, the crosslinkers **a** and **b** exhibit much longer delay times than previously observed, whilst the rest of the crosslinkers gave times that appear to fluctuate wildly, but all generally showed higher values than previously observed at 0 and 1 months.

6.3.2 Viscosity Building of Guar Solutions

6.3.2.1 Ambient Temperature

Investigation into the viscosity build of the guar gum solution upon crosslinker addition over time was also carried out. This was in an attempt to replicate the methods of analysis produced with a more sophisticated Fann 50 viscometer to measure viscosity change as found in the literature, but using a smaller benchtop Fann 35 model, due to equipment costs.[4, 7, 15] The viscosity of a crosslinked gel is reported to be higher than that of a linear gel (HEC or xanthan gum for example), due to the larger 3D network afforded by crosslinked polymer chains.[16]

Different loading amounts of the standard zirconium triethanolamine crosslinker **6.1b** were added to samples of 0.35 wt.% guar gum solution gel solution, and the viscosity change over 30 min was recorded. The data obtained for experiments carried out at ambient temperature with four different crosslinker loadings, 0.09, 0.18, 0.36 and 0.46 g, is represented in Figure 6.8.

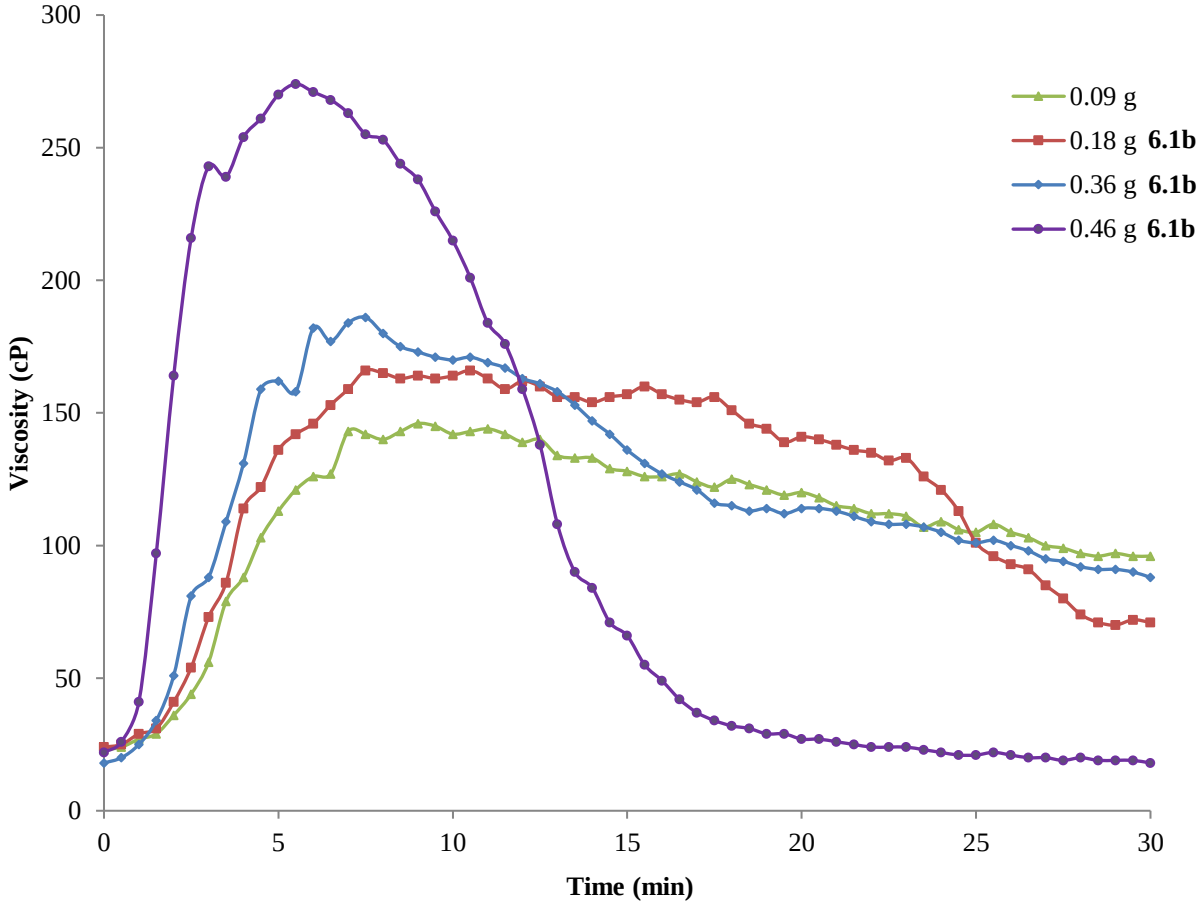

Figure 6.8: Observed viscosity profiles obtained over 30 min of 0.35 wt% guar gel solution with addition of increasing loadings of standard crosslinker, 6.1b, at ambient temperature

As expected, the data presented in Figure 6.8 show that as the amount of crosslinker loading increases, the maximum observed viscosity also increases. This is due to the presence of a greater amount of active Zr species, so more crosslinking reactions can occur between the high molecular weight polymer chains, forming a much larger 3D polymer network and thus affording a viscosity build. There is a slight delay of 7 min in each sample as the viscosity builds until maximum viscosity is achieved of 146 cP, 165 cP and 186 cP for the crosslinker loadings of 0.09 g, 0.18 g, 0.36 g, respectively. These three loadings then begin to show a slow but steady decrease in viscosity, decreasing by approximately 1 cP every minute, with a much faster rate of decrease occurring after 18 min for the 0.18 g loading.

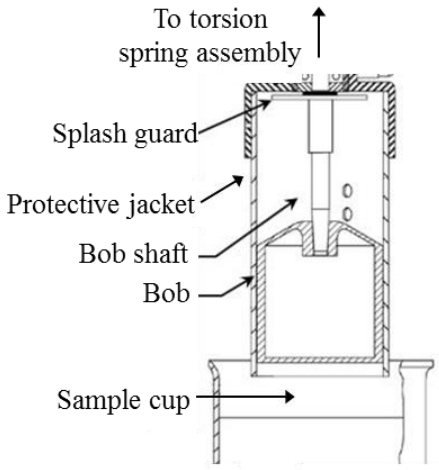

Figure 6.9: Cutaway diagram of Fann 35 viscometer rotor and bob mechanism, showing how viscosity is measured

However, for the 0.46 g loading, a greater maximum viscosity of 274 cP is achieved more quickly, after 5 min. Once this has occurred, a rapid decrease is then observed indicating what is believed to be shearing of the polymer, resulting in a measured viscosity of 18 cP- this value is lower than the initial viscosity of the gel before crosslinker addition. However, in actuality, the low viscosity is observed due to the crosslinked gel not being in contact with the bob, so accurate viscosity measurements are no longer being acquired. Figure 6.9 shows how the viscosity is measured by the Fann 35 viscometer, involving a bob shaft attached to a torsion spring. The fluid enters the shear gap between the bob and protective jacket, which then rotates. Any force exerted on the bob is then relayed back to the torsion spring. The standard B1 bob affords a gap of 0.117 cm, which was used to obtain these results. Furthermore, the literature shears the fluid at 100 s^{-1}, but the closest shear rate afforded by the current Fann 35 viscometer setup is 170 s^{-1} when the rate of rotation is set at 100 rpm.[17] The combination of small shear gap and higher shear rate makes it difficult for the fluid to remain inside the jacket and in contact with the bob as it becomes more viscous, so the rotation of the bob forces the fluid out and it is

unable to re-enter. Therefore the viscosity of the fluid appears to suddenly decrease, but in actuality the fluid is no longer being accurately measured. Further investigations with different combinations of rotation speeds and bobs in order to generate more suitable shear rates would be desired, but the expense of purchasing new bobs, as well as difficulty in obtaining further guar samples did not make this a feasible option.

6.3.2.2 Elevated Temperature

Viscosity profiles were also obtained for loadings of standard crosslinker **6.1b** at 0.18 g and 0.36 g with heating up to 90 °C, the results of which are presented in Figure 6.10 and Figure 6.11, respectively. This was to simulate real fractured well conditions, where temperature increases at the bottom hole are often observed.[15] We chose a maximum temperature of 90 °C, in order to get as hot as possible without beginning to boil the aqueous gel solution.

The addition of heat appears to accelerate the crosslinking reactions, with the maximum viscosity in both cases being achieved in approximately 4 min, in comparison to 7 min at ambient temperature. Again, there is a large rate of decrease in recorded viscosity once the maximum peak has been reached, most likely due to the reason described previously, with the polymer being forced out of the shear gap and no longer being in contact with the bob. This may also be the reason to why the greater crosslinker loading gives the smaller observed peak viscosity (84 cP for 0.36 g, compared to 154 cP for 0.18 g); the combination of heating and increased crosslinker loading causes the rate of crosslinking to increase, thus the viscous gel is also forced out from the shear gap at a greater rate. The final viscosity values are approximately 8 cP in both cases- lower than the initial gel viscosities of 23 cP and 13 cP before the crosslinker additions of 0.18 g and 0.36 g loading, respectively.

The general shapes and trends within Figure 6.10 and Figure 6.11 look similar to those presented in the patent literature,[7] however, the average recorded viscosities reported are much higher, at approximately 1200 cP. There are a number of variables that will affect viscosity measurements, including, but not limited to: viscometer type, bob type, rotation speed, M_w of guar used, wt.% of gel solution and crosslinker loading. Moreover, the fluid is also subjected to a higher shear rate for a small amount of time at periodic intervals during data collection. This was in an attempt to observe how high mechanical stresses may breakdown the crosslinked network, affect the rate of viscosity decrease and overall robustness of the fluid.

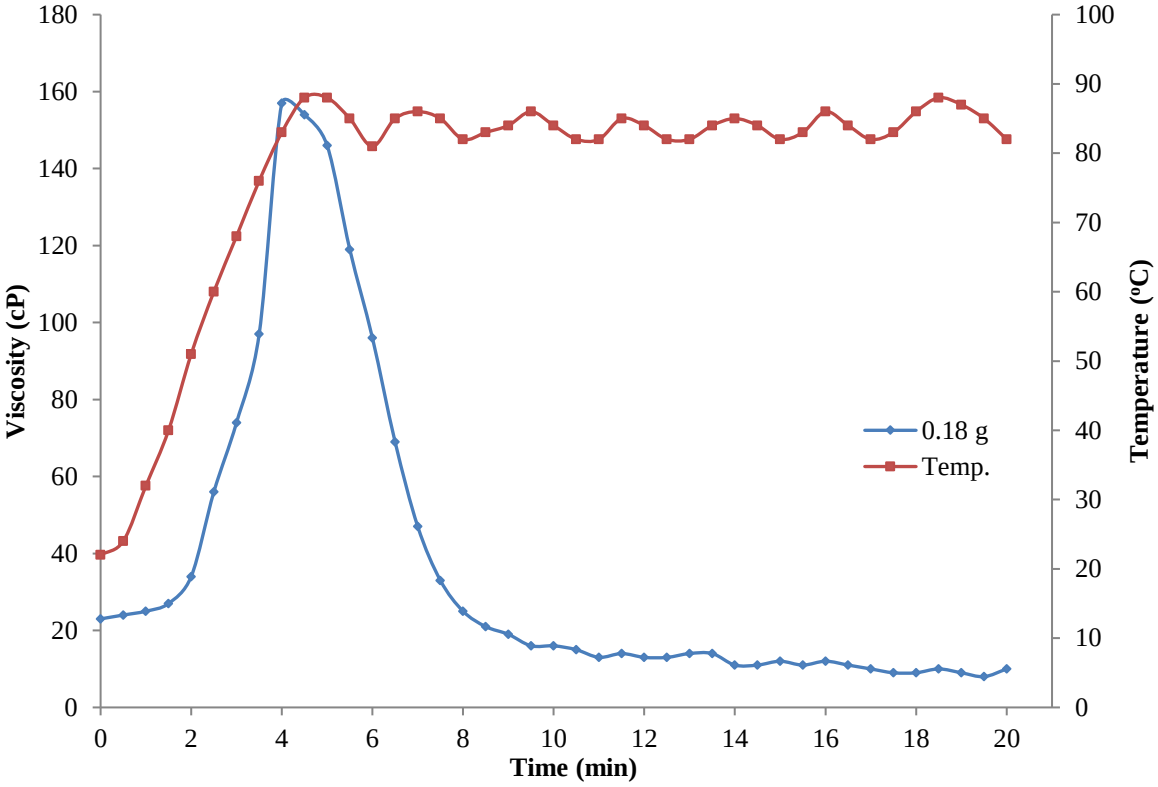

Figure 6.10: Observed viscosity profile of 0.35 wt% guar gel solution with addition of 0.18 g loading of standard crosslinker, 6.1b, up to 90 °C

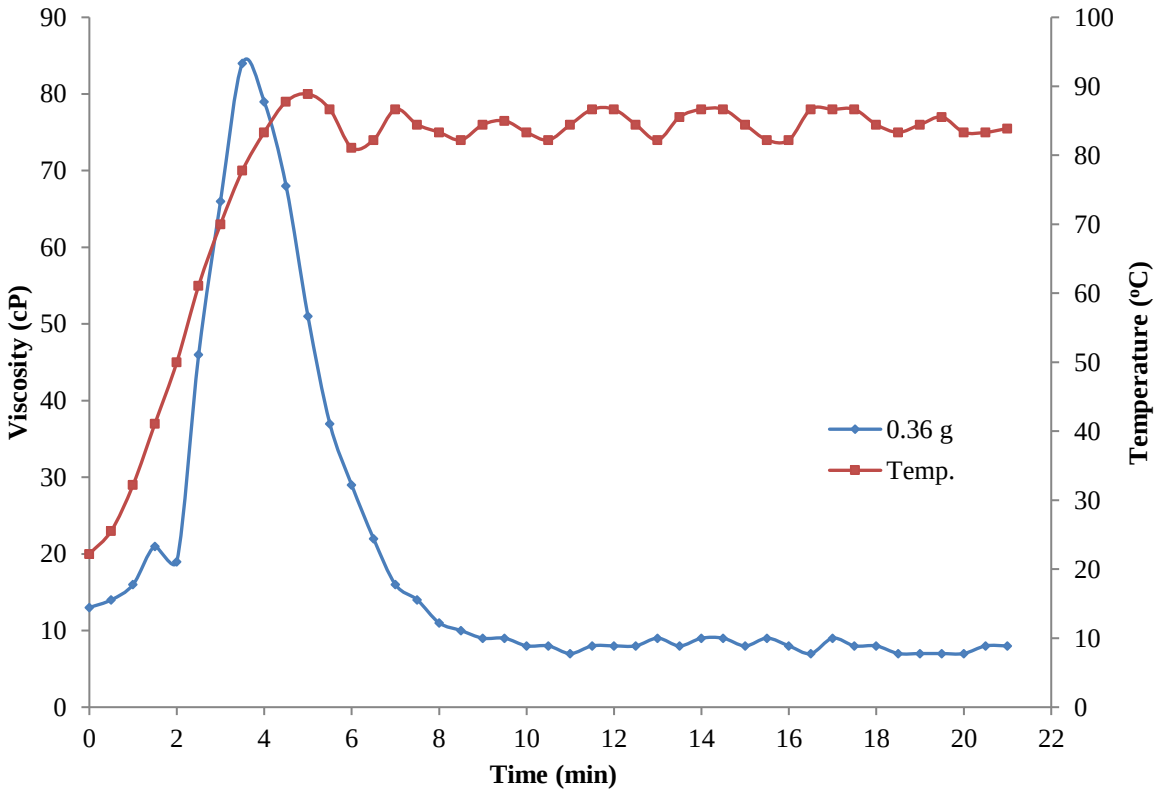

Figure 6.11: Observed viscosity profile of 0.35 wt% guar gel solution with addition of 0.36 g loading of standard crosslinker, 6.1b, up to 90 °C

6.3.3 Titanium and Zirconium THEED Complexes

Alkanolamine derivative based complexes, containing a greater number of metal chelation sites, were investigated in order to determine the effect on the delay of crosslinking. The six-coordinate ligands *N,N,N',N'*-tetrakis(2-hydroxyethyl)ethylenediamine (THEED) and *N,N,N',N'*-tetrakis(2-hydroxypropyl)ethylenediamine (THPED) were used. Evans *et al.* showed that THPED acted as a good chelation agent in the synthesis of $[Ti(THPED)_2]$,[18] although their use as crosslinkers with respect to hydraulic fracturing has not been investigated.

Both titanium and zirconium complexes of THEED were synthesised from TIPT or NPZ, to afford $[Ti(THEED)]_2$ **6.2** and $[Zr(THEED)]_2$ **6.3** as shown in Scheme 6.2 and Scheme 6.3, respectively.

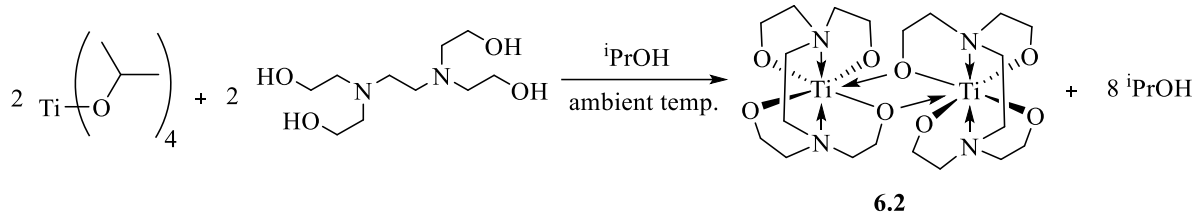

6.2

Scheme 6.2: Synthesis of $[Ti(THEED)]_2$ 6.2

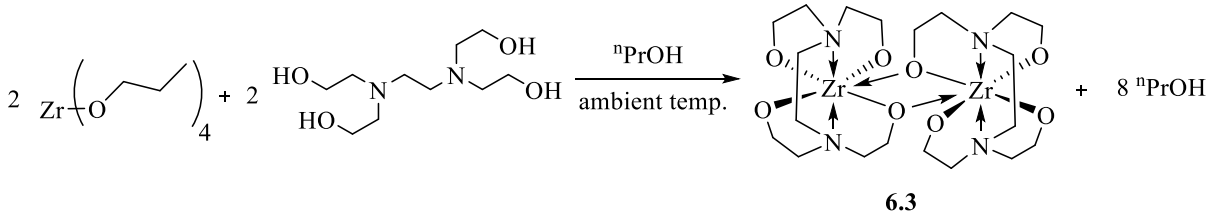

6.3

Scheme 6.3: Synthesis of $[Zr(THEED)]_2$ 6.3

Attempts to characterise the complexes **6.2** and **6.3** in solution by NMR spectroscopy were carried out, but afforded little help in the structure determination of the complexes. They did confirm the presence of numerous isomers of ambient temperature fluxionality afforded by the alkanolamine products **6.2** and **6.3**; the ^1H NMR spectra of the complexes showed that racemisation was slow on the NMR time-scale. There is a degree of overlap due to the inability of NMR spectroscopy to distinguish between diastereomers, however, the system remains complex and thus individual signal assignments cannot be made. Electrospray ionisation mass spectroscopy (ESI-MS) was used to determine the mass of the complexes. The molecular ion of **6.2** was observed at 583.5 Da (100%, Figure 6.12), which is consistent with the empirical formula $[C_{20}H_{40}N_4O_8Ti_2 + Na]^+$. This molecular weight implies that the complex exists as a

dimer, similar to that observed in the literature for [Ti(THPED)$_2$],[18] where each titanium atom is chelated to an N_2O_5 donor set.

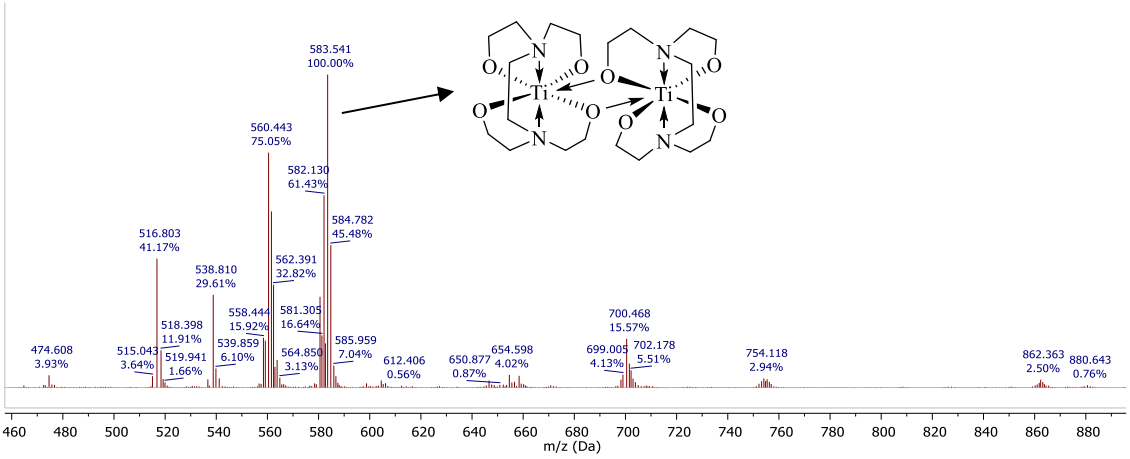

Figure 6.12: ESI-MS spectrum of 6.2

The molecular ion of **6.3** was observed at 644.4 Da (68.17%, Figure 6.13), which is consistent with the empirical formula $C_{20}H_{40}N_4O_8Zr_2^+$. The mass spectrum additionally shows major peaks corresponding to unreacted THEED starting material at 236.9 Da (81.04%) and a four coordinate monomeric complex at 325.3 Da (100%), which are consistent with the empirical formulae $C_{10}H_{24}N_2O_4^+$ and $C_{10}H_{22}N_2O_4Zr^+$, respectively.

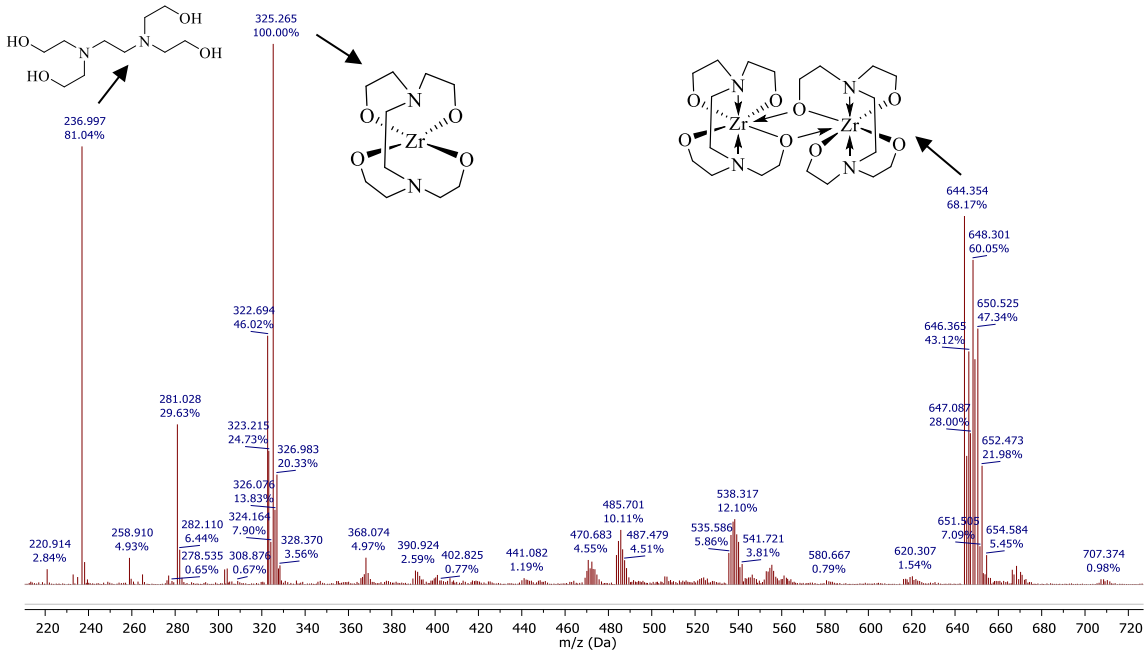

Figure 6.13: ESI-MS spectrum of 6.3

Furthermore, both compounds were successfully recrystallised and single crystal X-Ray diffraction crystallography was used to determine the definitive structures of the products. The

crystal data and structure refinement for both compounds are presented in Table 6.3. The crystal structures of **6.2** and **6.3** are shown in Figure 6.14 and Figure 6.15, respectively.

Table 6.3: Summary of crystallographic data for compounds 6.2 and 6.3

	6.2 (M=Ti)	**6.3** (M=Zr)
Empirical formula	$C_{20}H_{40}N_4O_8Ti_2$	$C_{20}H_{40}N_4O_8Zr_2 \times 4\ H_2O$
M_w **(g mol^{-1})**	560.36	719.06
Crystal system	orthorhombic	monoclinic
Space group	$P2_12_12_1$	$C2/c$
***a* (Å)**	11.1231(3)	14.7427(3)
***b* (Å)**	12.8856(7)	9.6163(2)
***c* (Å)**	16.3847(3)	19.3344(4)
***α* (º)**	90.00	90.00
***β* (º)**	90.00	101.5737(2)
***γ* (º)**	90.00	90.00
Volume (Å^3)	2348.40(6)	2685.33(9)
Z	4	4
ρ_{calc} (mg mm^{-3})	1.585	1.779
μ (mm^{-1})	0.735	0.844
wR_2	$wR_2 = 0.0735$	$wR_2 = 0.0485$
R_1	0.0308	0.0219

The X-ray crystal structures show both molecules to be dimeric, with each metal atom being seven-coordinate, binding to all six of the potential donor atoms of the ligand. One oxygen atom in each ligand ([O1] and [O8] in **6.2** and [O1] and [O1'] in **6.3**) is binucleating, forming an oxo-bridge between adjacent metal species, as observed in $[Ti(THPED)]_2$.[18]

Complex **6.2** (Figure 6.14) is a chiral species. The central Ti_2O_2 ring is not planar, with all four bond lengths and bonding angles different from one another, where Ti1-O1 = 2.104 Å, Ti1-O8 = 2.053 Å, Ti2-O1 = 2.059 Å, and Ti2-O8 = 2.084 Å; Ti1-O1-Ti2 = 112.03º, Ti1-O8-Ti2 = 113.10º, O1-Ti1-O8 = 66.88º and O1-Ti2-O8 = 67.15º. The methylene groups at [C17], [C18] and [C19] showed slight disorder, indicating that more than one configuration for the complexed THEED ligand can exist in the solid state. It is possible the chirality of the structure arose due to enantioselective discrimination occurring during crystallisation, but this cannot be confirmed on the basis of the X-ray data alone. Circular dichroism testing could be used to determine the difference in the enantiomeric ratio of the compound before and after recrystallisation.

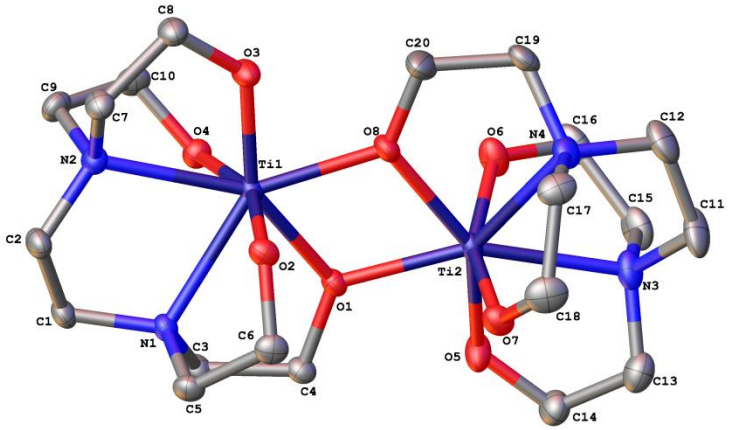

Figure 6.14: X-ray crystal structure of [Ti(THEED)]$_2$ 6.2

In comparison, structure **6.3** (Figure 6.15) is centrosymmetric with a crystallographic centre of symmetry at the centre of the planar Zr_2O_2 four-membered ring. The transannular Zr1···Zr1' distance is 3.647(8) Å and the O-Zr-O and Zr-O-Zr angles are 67.54° and 112.46°, respectively. The Zr1-O1 and Zr1'-O1' bonds are slightly longer at 2.238 Å, in comparison to the Zr1-O1' and Zr1'-O1 bonds with a length of 2.149 Å in the ring, indicating these are most likely to be formed by dative covalent bonds.

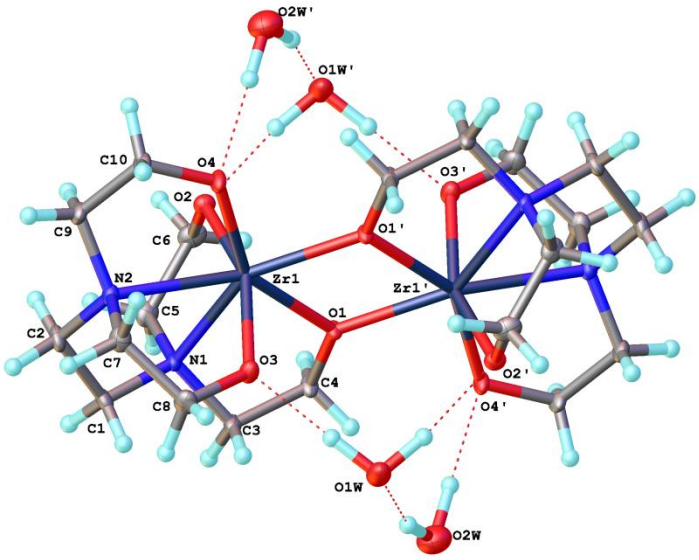

Figure 6.15: X-ray crystal structure of [Zr(THEED)]$_2$ 6.3

There are also four water molecules of crystallisation associated with the molecule *via* hydrogen bonding. As the dimeric species is centrosymmetric, the relative configurations about the two zirconium centres are enantiomeric.

The efficacy of these crosslinkers in causing gelation in an aqueous 0.35 wt.% guar gum solution is poor. Viscosity profiling with both crosslinkers [Ti(THEED)]$_2$ **6.2** and

$[Zr(THEED)]_2$ **6.3** using the Fann 35 viscometer afforded only a two cP change after 20 min. Because of this, vortex closure testing also afforded poor results, with the viscosity build of the fluid being insufficient enough to fully close the vortex. This is most likely due to the six-coordinate THEED ligand fully chelating and stabilising the metal centres. The titanium and zirconium metal ions are bound so tightly that crosslinking reactions with the guar polymer chains are suppressed.

It is also interesting to note that after three days of standing, both crosslinkers had formed heterogeneous mixtures in their respective vials. Complex **6.2** had formed solid residue on the sides and bottom of the vial. Complex **6.3** had formed a white solid zirconium-containing bottom layer with a distinct *n*-propanol layer above. This indicates that both species readily crystallise in a solution of their parent alcohols. To investigate this, additional batches of **6.2** were synthesised, with one being diluted by 25% *v/v* with ^{i}PrOH and another with the addition of one molar equivalent of water. Once again, the crosslinker in ^{i}PrOH precipitated out of solution after three days, but the batch containing the added water remained homogeneous. One possibility is that in solution, the metal species actually exist as monomeric structures and the addition of water end caps the metal at the seventh coordination site, stabilising the monomer further and preventing dimer formation. In the parent alcohol, the individual monomeric species are not as stable and therefore prefer to combine to form stable, insoluble dimers which precipitate out of solution.

6.3.4 Zirconium THPED Complex

The synthesis of zirconium complex of THPED was also carried out from NPZ, to afford the proposed dimer $[Zr(THPED)]_2$ **6.4**, as outlined in Scheme 6.4. THPED is an analogue of THEED, and differs by the addition of an extra methyl group on each of the hydroxyethyl arms.

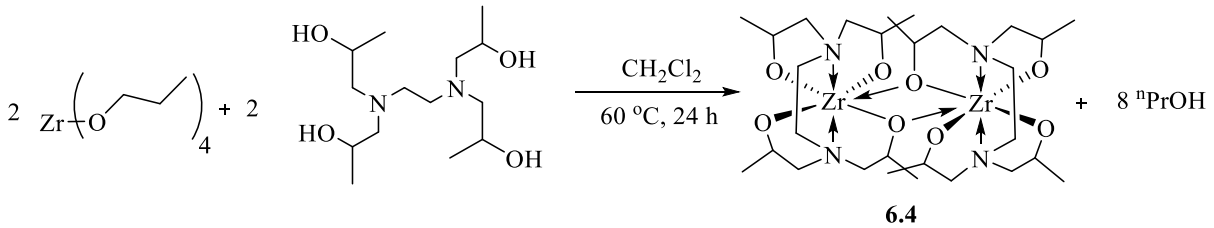

6.4

Scheme 6.4: Synthesis of $[Zr(THPED)]_2$ 6.4

Again, NMR spectroscopy confirmed the presence of numerous isomers, with the ^{1}H NMR spectrum consisting of many overlapping resonances which were difficult to assign and reliably integrate. Attempts at recrystallisation did not yield any suitable single crystals for X-ray diffraction analysis. However, ESI-MS data indicate that this complex also exists as a dimer in some capacity, similar to the titanium analogue,[18] with the molecular ion observed at m/z = 758.60 Da (100%, Figure 6.16), which is consistent with the empirical formula $C_{28}H_{56}N_4O_8Zr_2^+$.

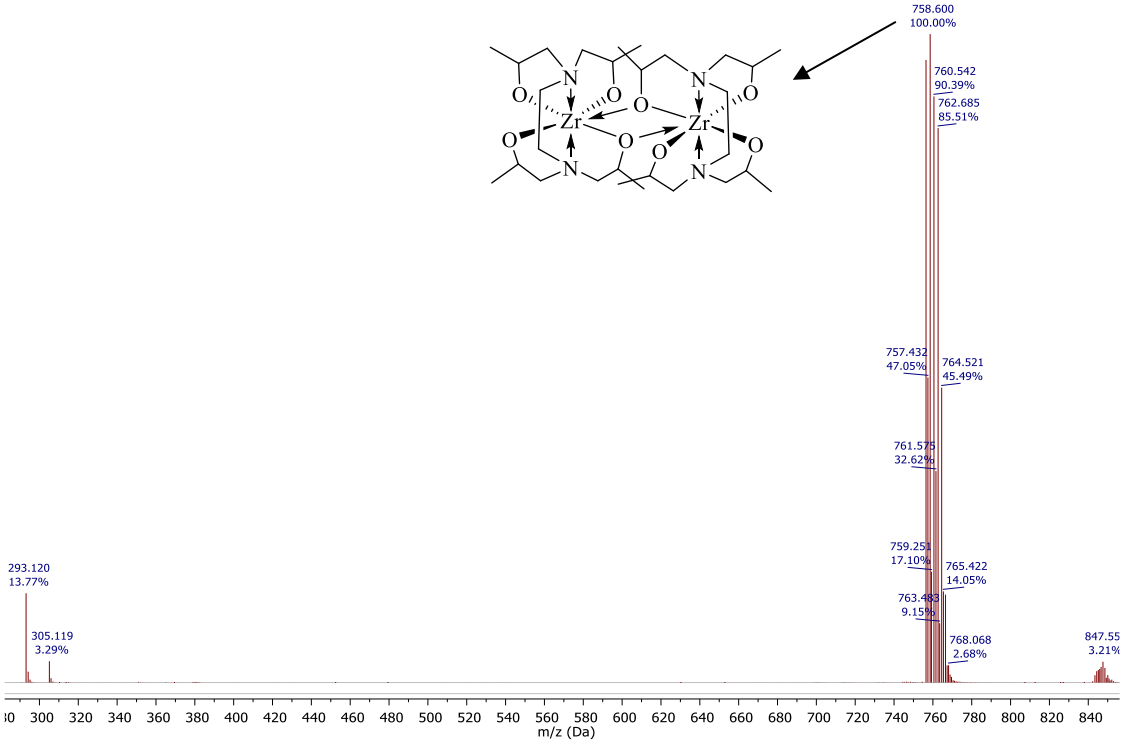

Figure 6.16: ESI-MS spectrum of 6.4

There are several possible reasons why the titanium THPED complex can crystallise in contrast to the zirconium THPED complex **6.4**: a) minor structural differences in the number of possible isomers of the complex, b) different methods of packing throughout the molecules, and c) the formation of other oligomers are preferred over the dimer.

6.3.5 Gelation Testing of Functionalised HEC

The graft copolymers HEC-*g*-polyglycerol **5.1 b-e** (Figure 6.17.A), HEC-*g*-polyglycerol-*g*-PCL_{10} **5.2**, HEC-*g*-polyglycerol-*g*-PCL_{50} **5.3** (Figure 6.17.B) and the functionalised polymer succinylated HEC **3.5** (Figure 6.17.C) were evaluated for their crosslinking abilities in order to afford viscous, gel-like materials.

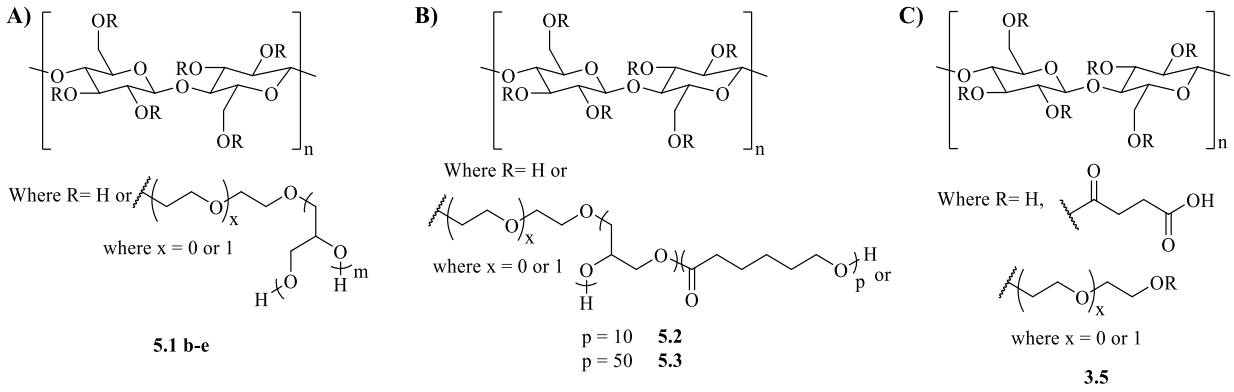

Figure 6.17: Chemical structures of A) HEC-*g*-polyglycerol 5.1 b-e, B) HEC-*g*-polyglycerol-*g*-PCL 5.2, 5.3 and C) succinylated HEC 3.5

The crosslinkers utilised were $Zr(TEA)_4$ **6.1b** and a α-hydroxycarboxylic acid zirconate-based crosslinker. The pH of the dissolved polymer solutions were adjusted to 10.25 or 5.3, respectively, depending on the crosslinker used, as these were previously determined by Catalytic Technologies Ltd. to be the optimum pH values for crosslinker efficacy.

Based on the patent literature, the most effective amount of polymer generally ranges between 0.35-2.0 wt.% of the fracturing fluid.[10] A standard wt.% ratio of 3.5:1.0 (polymer:crosslinker) was utilised in each gelation test.

6.3.5.1 HEC-*g*-polyglycerol 5.1 b-e

Crosslinking reactions with both **6.1b** and α-hydroxycarboxylic acid zirconate crosslinkers were attempted with the graft copolymers **5.1 b-e**, all at 0.35, 1.0 and 2.0 wt.% concentrations. It was thought the abundance of hydroxyl groups may participate in crosslinking reactions through the formation of multiple covalent bonds with group (IV) metal ions. However, no gelation or viscosity increase was observed in any case. An increase beyond the standard range to a higher concentration of 3.0 wt.% also afforded no gelation.

6.3.5.2 HEC-*g*-polyglycerol-*g*-PCL 5.2 and 5.3

Crosslinking reactions with both **6.1b** and α-hydroxycarboxylic acid zirconate crosslinkers with the graft copolymers HEC-*g*-polyglycerol-*g*-PCL_{10} **5.2** and HEC-*g*-polyglycerol-*g*-PCL_{50} **5.3** were also carried out at 0.35, 1.0 and 2.0 wt.% concentrations. It was thought the hydroxyl end group functionalities of the PCL chains would be likely to participate in crosslinking reactions with group(IV) metal ions, due to being further away from the HEC backbone and attached *via* flexible arms. Thus, the end groups are less sterically hindered and should be more freely available to undergo reactions with crosslinking agents.. However, no gelation or viscosity increase was observed in any case with the graft copolymers **5.2** and **5.3**. An increase beyond the standard range to a higher concentration of 3.0 wt.% also afforded no gelation. The PCL graft copolymers with $\overline{DP}_{Th}$ of 100 (**5.4**) and 250 (**5.5**) are insoluble in water and therefore could not be evaluated for their gelation properties.

6.3.5.3 Succinylated HEC 3.5

Crosslinking reactions with both **6.1b** and α-hydroxycarboxylic acid zirconate crosslinkers with succinylated HEC **3.5** (20 h reaction time) were also carried out at 0.35, 1.0 and 2.0 wt.% concentrations. In all of these cases, unfortunately, no gelation or viscosity increase of these solutions was observed.

However, when the concentration of functionalised polymer **3.5** was increased to 3.0 wt.%, addition of the α-hydroxycarboxylic acid zirconate crosslinker appears to have induced a successful crosslinking reaction. Figure 6.18.A shows the homogenous aqueous solution of polymer before crosslinking addition. No viscosity change was observed right away (within 1 h) after the addition of crosslinker. After 8 h, the polymer had crashed out of solution and settled in the bottom of the vial, as shown in Figure 6.18.B.

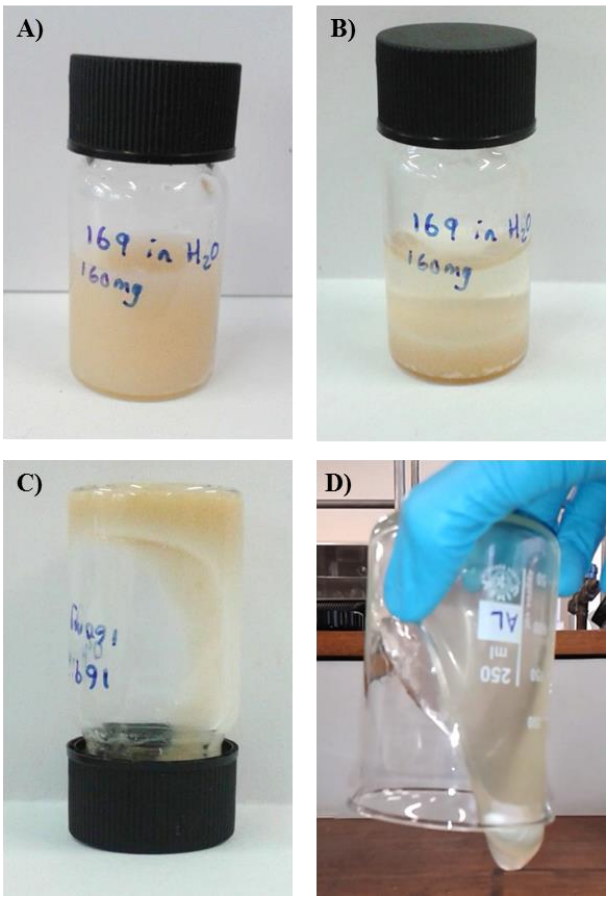

Figure 6.18: A 3.0 wt.% solution of succinylated HEC 3.5, A) homogenous solution to which an α-hydroxycarboxylic acid zirconate crosslinker is added, B) after 8 h, C) inversion of vial containing viscous gel, D) crosslinked guar solution with suspended stirrer bar

Upon investigation, the material was very viscous (gel-like). This leads to the loss of its flow characteristics; upon inversion of the vial the majority of the material remained in place, before slowly beginning to pour down the vial (Figure 6.18.C). This is comparable to the flow characteristics observed of the crosslinked guar solution (Figure 6.18.D), which also pours very slowly, and exhibits such a high viscosity that a stirrer bar can be suspended within the gel.

However, the drawback of this crosslinked system is that nine times the amount of polymer than the lower range limit of 0.35 wt.% is required before any gelation occurs. This will lead to increased costs as a much larger amount of polymer is required per fracturing job, therefore it may not be the most beneficial fracturing fluid solution for industrial application.

6.4 Conclusions

Gelation delay times of guar based "fracturing fluids" with triethanolamine based zirconium crosslinkers can be increased by the addition of a small amount of water to the crosslinker during its preparation, as evidenced in the synthesis and use of crosslinkers **6.1 a-i**. Additions of up to five molar equivalents of water show a steady rate of increasing delay time, whilst observed times of equivalents greater than five effectively form a plateau, but still afford longer delays than the standard crosslinker described in the literature. Crosslinking efficacy is dependent on the age of the crosslinker, with shorter delay times observed, on average, with one month old crosslinkers. However, crosslinkers aged seven months generally show a longer delay time in comparison to their initial and one month old counterparts.

As the loading amount of the standard crosslinker is increased, the maximum viscosity of the guar-based gel also increases, as determined by Fann 35 viscometer analysis. This was to be expected, as greater loadings contain a greater ZrO_2 content, leading to more crosslinking sites. However, accurate viscosity measurements with larger crosslinker loadings and experiments at high temperatures cannot be performed with the current Fann 35 set-up, as the gel is unable to stay within the shear gap between the bob and protective jacket.

The six-coordinate alkanolamine ligand analogues THEED and THPED were used in the synthesis of seven-coordinate titanium and zirconium dimeric structures. THEED was used to afford the titanium and zirconium complexes **6.2** and **6.3**, respectively. Both THEED-containing complexes are air stable and can crystallise. Single crystal X-ray crystallography determined that an oxygen atom from each ligand is binucleating, acting as a bridge to form a central M_2O_2 ring. In the case of zirconium **6.3**, this ring is planar and the bridging Zr-O bonds were found to be longer, indicative of being formed by dative covalent bonding. Its structure was found to be centrosymmetric. However, the titanium analogue **6.2** is a chiral species that shows signs of disorder, indicating that more than one configuration for the complexed ligand can exist in the solid state.

The efficacy of these THEED containing complexes as crosslinkers of aqueous 0.35 wt.% guar gum solutions is poor, most likely due to the six-coordinate THEED ligand tightly chelating to the metal centres and conferring stability, causing the crosslinking reactions with the guar polymer chains to be suppressed.

THPED is an analogue of THEED, differing by the addition of an extra methyl group on each of the hydroxyethyl arms. The zirconium complex of THPED **6.4** was synthesised. It is likely that this complex will also form the seven-coordinate dimeric structure $[Zr(THPED)]_2$, due to the previously synthesised titanium analogue existing in this conformation,[18] and ESI-MS evidence supports this. However, single crystals of **6.4** could not be isolated; therefore the structure could not be elucidated by X-ray crystallographic methods.

Aqueous solutions of the graft copolymers HEC-*g*-polyglycerol **5.1 b-e**, HEC-*g*-polyglycerol-*g*-PCL_{10} **5.2** and HEC-*g*-polyglycerol-*g*-PCL_{50} **5.3**, and functionalised polymer succinylated HEC **3.5** (reaction time = 20 h) were evaluated for their crosslinking abilities with the triethanolamine zirconate crosslinker **6.1b** and a α-hydroxycarboxylic acid based zirconium crosslinker. The graft copolymers **5.1 b-e**, **5.2** and **5.3** showed no signs of gelation or viscosity build with either of the crosslinkers mentioned above at 0.35, 1.0, 2.0 and 3.0 wt.% concentrations.

The functionalised polymer succinylated HEC **3.5** also showed no signs of gelation with crosslinker **6.1b** at 0.35, 1.0, 2.0 and 3.0 wt.% concentrations, or with α-hydroxycarboxylic acid zirconate crosslinker at 0.35, 1.0 and 2.0 wt.% concentrations. However, gelation of polymer **3.5** was induced by addition of the α-hydroxycarboxylic acid zirconate crosslinker at 3.0 wt.% concentration. The observed viscosity build was comparable to that of crosslinked guar. However, the polymer concentration required is nine times larger than the lower limit used in industrial fracturing applications. The requirement of a greater amount of polymer will lead to increased costs, and therefore is unlikely to be utilised for industrial applications.

6.5 References

1. C. Montgomery, in *Effective and Sustainable Hydraulic Fracturing* (Eds.: A. P. Bunger, J. McLennan, R. Jeffrey), InTech, **2013**, 25-45.
2. Dorf Ketal Tyzor, Tyzor Frac Fluid Crosslinkers for Oil and Gas Production, https://www.dorfketal.com/including/PDF%20Files/K17581_tyzor_oil_gas_final.pdf, (Accessed Sept. 2016).
3. L. R. Norman, J. R. Carlise, J. J. C. Corbea, J. William S. Rees, M. Weck, US 7 595 391 B2, **2009.**
4. D. E. Putzig, J. D. St.Clair, in *Hydraulic Fracturing Technology Conference, Vol. SPE 105066*, Houston, Texas, USA, **2007**.
5. D. J. Hanlon, S. W. Almond, US 4 460 751, **1984.**
6. D. A. Williams, US 4 534 870, **1985.**
7. D. E. Vaughn, R. H. Duncan, D. N. Harry, D. A. Williams, US2009/0288828 A1, **2009.**
8. G. M. Sheldrick, *Acta Cryst. Sect. A,* **2008**, *64*, 112.
9. O. V. Dolomanov, L. J. Bourhis, R. J. Gildea, J. A. K. Howard, H. Puschmann, *J. Appl. Cryst.*, **2009**, *42*, 339.
10. G. L. Brode, J. P. Stanley, E. M. Partain, US 0 176 940 B1, **1991.**
11. F. Rubio, J. Rubio, J. L. Oteo, *J. Mater. Sci. Lett.*, **1998**, *17*, 1839.
12. B. E. Yoldas, *J. Mater. Sci.*, **1986**, *21*, 1080.
13. N. Y. Turova, E. P. Turevskaya, V. G. Kessler, M. I. Yanovskaya, *The Chemistry of Metal Alkoxides*, Kluwer Academic Publishers, Norwell, MA, USA, **2002**.
14. D. C. Bradley, *Nature*, **1958**, *182*, 1211.
15. D. E. Vaughn, R. H. Duncan, D. N. Harry, D. A. Williams, US 7 879 771, **2011.**
16. C. Montgomery, in *International Conference for Effective and Sustainable Hydraulic Fracturing*, Brisbane, Australia, **2013**.
17. FannInstruments, *Model 35 Viscometer Instruction Manual, Revision P*, **2016**.
18. D. F. Evans, J. Parr, S. Rahman, A. M. Z. Slawin, D. J. Williams, C. Y. Wong, J. D. Woolins, *Polyhedron*, **1993**, *12*, 337.

Chapter 7

Conclusions and Future Perspectives

7.1 Conclusions

This thesis involved the chemical modification of HEC *via* a range of methods to impart various different end-group functionalities, ultimately to create materials to be utilised for industrial hydraulic fracturing applications. This was to make it possible for HEC to undergo crosslinking reactions with group(IV) metal-based crosslinkers in aqueous solution, leading to a viscosity increase and gelation of the solution. Inverse-gated ^{13}C NMR spectroscopy was deemed to be a very useful characterisation technique, due to the broad resonances afforded by the large number of protons on the HEC backbone dominating the ^{1}H NMR spectra of all modified HEC materials. The downside of this method is that long acquisition times are required (approximately 22 h) for each inverse-gated ^{13}C NMR experiment in order to obtain a signal-to-noise ratio that is sufficient to allow integration of the spectra.

Chapter 1 gave an introduction to hydraulic fracturing, including a discussion on the various components that comprise a fracturing fluid. Analysis of the literature pertaining to cellulose, hydrolysis of group(IV) metal alkoxides, the development of Click reactions and the ROP of ε-caprolactone was reported.

Chapter 2 used trehalose, a disaccharide molecule, as a model compound, and described the synthetic strategy employed in order to convert the primary hydroxyl groups to thiol groups. The primary hydroxyl groups underwent tosylation and the secondary hydroxyl groups acetylation, to afford 2,3,4,2',3',4'-hexa-O-acetyl-6,6'-ditosyl-6,6'-dideoxy-D-trehalose **2.1**. The tosyl leaving group was then readily displaced by thioacetate groups, giving 2,3,4,2',3',4'-hexa-O-acetyl-6,6'-di-S-acetyl-6,6'-dithio-D-trehalose **2.2**. The characterisation of these compounds agreed with the literature. Finally, the acetate groups were removed by basic deprotection to afford 6,6'-dithiolated trehalose **2.3**, which was fully characterised. Although the synthesis of **2.1** afforded a low yield of 15% due to the multiple recrystallisation steps carried out, the synthesis of **2.2** and **2.3** afforded good yields of 74.3% and 78.2%, respectively. The compound *N*-(3,4-dihydroxyphen-ethyl)bicyclo[2.2.1]hept-5-ene-2-carboxamide **2.4** was synthesised *via* an amidation reaction between dopamine hydrochloride and 5-norbornene-2-carboxylic acid. Some of the ^{13}C NMR peak assignments of this compound reported in the literature were incorrect. Therefore, 2D ^{1}H-^{13}C HSQC NMR spectroscopy was utilised to assign the resonances correctly. The alkene group of the norbornene in **2.4** was then reacted in a UV-mediated thiol-ene Click reaction with **2.3**, resulting in 46% conversion. The low conversion was thought to be due to participation of only one of the two available thiol groups. The catecholic moiety of

2.4 was found to show good affinity for binding to group(IV) metal ions, with of up to three molecules of **2.4** binding to one titanium centre.

Chapter 3 described the modification of HEC *via* the attachment of small carbonyl-containing molecules. Attachment of bis-MPA *via* a three-step approach involved the protection of the hydroxyl groups of bis-MPA with 2,2-dimethoxypropane to give IBPA **3.1**, followed by attachment to HEC, **3.2**, using distillation and a *p*-TSA catalyst. Removal of the protecting acetal group was unsuccessful as it led to hydrolysis of the ester linkages, fully removing the IBPA and reforming HEC. Successful surface esterification of HEC *via* the ring opening of succinic anhydride using DMAP as a catalyst led to the attachment of succinic acid moieties and the formation of succinylated HEC, **3.5**. As the reaction time was increased, the calculated % conversion of unmodified primary C_6 carbon atoms on HEC to succinylated C_6 carbon atoms also increased, up to approximately 43% conversion after 48 h reaction time. The acid-functionalised HEC materials with higher conversions (≥40%) exhibited low solubility in water, whilst those with lower conversions (≤33%) exhibited very good solubility in water.

Chapter 4 described the synthetic methods to impart thiol functionality to HEC, using the same reaction conditions performed in Chapter 2 on trehalose model compound. The tosylation and acetylation of HEC, **4.1**, were successful, with ^{13}C NMR spectroscopy showing complete tosylation of the primary hydroxyl groups. However, unlike the trehalose counterpart, the displacement of the tosyl groups to thioacetate groups was unsuccessful. The displacement of the tosyl groups with another nucleophilic thiol source, sodium thiobenzoate **4.3** was also unsuccessful. An alternate synthetic route was used involving triphenyl phosphine being halogenated by carbon tetrabromide, and then the bromine being displaced by a primary hydroxyl group on either trehalose or HEC to form a phosphonium salt intermediate. Finally, the phosphine oxide group was displaced by the sulfur nucleophile in an S_N2 reaction. When this one-pot synthesis was applied to trehalose model compound and sodium thiobenzoate **4.3**, trehalose thiobenzoate, **4.5**, 82% yield was obtained. However, the same methodology for HEC to produce HEC thiobenzoate **4.6** gave a maximum conversion of primary HEC hydroxyl groups to thiobenzoate groups of 55% after 20 h, as determined by inverse-gated ^{13}C NMR spectroscopy. Successful deprotection of the benzoate groups produced thiolated HEC, **4.7**, with approximately 15% of the primary hydroxyl groups converted to SH, as determined by inverse-gated ^{13}C NMR spectroscopy. Accurate quantification of thiol groups was difficult due to the overlapping resonances corresponding to the HEC backbone in the ^{13}C NMR spectrum. Thiolated HEC **4.7** was then reacted with the aforementioned norbornene-catechol compound

2.4 in a UV mediated thiol-ene Click reaction to produce catechol-functionalised HEC **4.8**. This reaction was deemed unsuccessful as no decrease in the intensity of the resonances corresponding to the vinyllic protons of the norbornene moiety was observed in the ^{1}H NMR spectrum. The one-pot methodology was again applied to HEC using potassium thioacetate as the sulfur nucleophile to afford HEC thioacetate **4.9**. Inverse-gated ^{13}C NMR spectroscopy showed that functionalisation of both the primary and secondary hydroxyl groups in HEC had occurred, as two acetate C=O resonances were observed in the ^{13}C NMR spectrum. The maximum conversion of primary hydroxyl groups after 20 h was observed to be lower, at 23%. Deprotection of **4.9**, as another route to afford thiolated HEC **4.7**, resulted in selective deacetylation with sodium hydroxide, as the loss of only one C=O resonance was observed. Unfortunately, time constraints did not allow investigation into whether this polymer would participate in thiol-ene Click reactions.

Chapter 5 described the use of HEC as a macroinitiator for the ROP of glycidol monomer in aqueous solution for the preparation of HEC-*g*-polyglycerol materials. It was anticipated that the abundance of hydroxyl groups of polyglycerol would readily participate in crosslinking reactions through the formation of multiple covalent bonds with titanium or zirconium ions. Dialysis was utilised as a good purification technique in order to remove any unreacted monomer and low molecular weight HEC oligomers, and the graft copolymers were analysed by inverse-gated ^{13}C NMR spectroscopy and SEC. It was difficult to accurately quantify the extent of these reactions due to the broad overlapping resonances corresponding to the HEC backbone. It was determined that the amount of sodium hydroxide required to deprotonate the primary hydroxyl groups on HEC in order to initiate ROP should be at least a 5% molar equivalence, as observed for the synthesis of graft copolymers **5.1 b-e**. Since, the synthesis of graft copolymer **5.1a**, utilising 2.5% molar equivalence of base was unsuccessful, as no resonances corresponding to polyglycerol were observed in its ^{13}C NMR spectrum. Graft copolymer **5.1b** synthesised using 5% and 400% molar equivalence of base and glycidol, respectively, afforded a material with M_w of 4.48 × 10^5 g mol^{-1}. When only the base was increased to a 10% molar equivalence, graft copolymer **5.1c** was obtained with M_w of 4.63 × 10^5 g mol^{-1}. The extent of reaction as calculated by the integral of the T units of polyglycerol in the inverse-gated ^{13}C NMR spectra were found to be 0.15 and 0.58 for **5.1b** and **5.1c**, respectively. These results were due to the formation of more deprotonated hydroxyl sites on HEC in the synthesis of **5.1c** from which ROP could be initiated. Graft copolymer **5.1d,** synthesised with 10% and 200% molar equivalents of base and glycidol, respectively, afforded

a material with M_w of 3.96×10^5 g mol^{-1} and an extent of reaction of 0.25. Furthermore, graft copolymer **5.1d** exhibited a Đ value of 3.89 as well as the greatest increase in TGA value in comparison to HEC, from 263 °C to 299 °C, implying good thermal stability. It can be concluded that only 5% and 200% molar equivalents of base and glycidol, respectively, are required, as when greater amounts of either reactant are used the observed molecular weights of the graft copolymers are the same, when taking SEC error into consideration. The difference in the extent of reaction, but similarity in observed M_w values, is most likely due to the products having similar hydrodynamic volumes. Graft copolymer **5.1e** was synthesised using an aqueous solution containing double the wt.% of HEC (20 wt.% instead of 10 wt.%). This afforded a highly viscous solution, and meant the reaction could not be quantified due to the poor quality of the ^{13}C NMR spectrum obtained.

The graft copolymer HEC-*g*-polyglycerol **5.1d** was then successfully used as a macroinitiator in the ring-opening of ε-CL using $Sn(Oct)_2$ as the catalyst. Four novel HEC-*g*-polyglycerol-*g*-PCL graft copolymers **5.2**, **5.3**, **5.4** and **5.5** were synthesised with a $\overline{DP}_{Th}$ of 10, 50, 100 and 250 ε-CL units per arm, respectively. The aim here was to move the hydroxyl end group functionalities of the PCL chains further away from the HEC backbone, where they are less sterically hindered and free to move *via* flexible arms, increasing the likelihood of participating in crosslinking reactions with titanium or zirconium metal ions. The M_w values of graft copolymers **5.2** ($\overline{DP}_{Th}$ = 10) and **5.3** ($\overline{DP}_{Th}$ = 50) were calculated by SEC to be 0.59×10^6 g mol^{-1} and 1.66×10^6 g mol^{-1}, respectively, and showed very good agreement with the theoretical M_w values. These polymers also retained their water solubility. The calculated M_w values of the graft copolymers **5.4** ($\overline{DP}_{Th}$ = 100) and **5.5** ($\overline{DP}_{Th}$ = 250) were 2.28×10^6 g mol^{-1} and 6.52×10^6 g mol^{-1}, respectively. These were much lower than their expected theoretical M_w values, most likely due to denser polymer structures leading to different hydrodynamic volumes. These longer PCL chain lengths also conferred hydrophobicity to the HEC backbone, and hence these systems were water insoluble. Thermal analyses of the HEC-*g*-polyglycerol-*g*-PCL graft copolymers were performed *via* TGA and DSC methods. In comparison to HEC, grafting of PCL increased the observed TGA onset temperature in all graft copolymers, from 263 °C to approximately 300 °C. As the $\overline{DP}$ of the PCL chains increases, the T_m, ΔH_m and ΔH_c values all increased, from 48 °C to 62 °C, 2 to 36 J g^{-1} and 7 to 28 J g^{-1}, respectively. Furthermore, as $\overline{DP}$ increases, the %crystallinity also increased from 2.7% in **5.2** to 26% in **5.5**. This was expected, as longer PCL chains show greater crystallinity. However, these values only take the PCL component of the graft copolymers into consideration, as HEC does not melt (therefore it does

not undergo crystallisation when cooled), and it only degrades at high temperatures. AFM analysis showed a change in architecture from hemi-ellipsoids in HEC to worm-like structures in HEC-*g*-polyglycerol **5.1d**, of which the length of the worm is consistent with a fully extended HEC backbone chain conformation. Upon grafting of PCL, a capillary-like fibrous network was observed for **5.2**, and larger globules were observed for **5.5** as the PCL arm length increased. The AFM data of graft copolymer **5.5** suggest that each observed globule is an individual macromolecule.

Chapter 6 described the crosslinking reactions performed with guar and functionalised HEC materials. Triethanolamine based zirconium crosslinkers containing different molar equivalents of water **6.1 a-i** were shown to afford a delay in the gelation time of aqueous guar solutions. Crosslinking efficacy was shown to be dependent upon the age of the crosslinker, with shorter gelation delay times on average observed with one month old crosslinkers. Much longer delay times were observed with older crosslinkers aged seven months. Accurate viscosity measurements using greater crosslinker loadings could not be accurately measured by the current Fann 35 viscometer setup, as the rapid viscosity build of the fluid meant it was unable to stay within the shear gap between the bob and protective jacket. Alkanolamine ligand analogues were used in the synthesis of seven-coordinate group(IV) metal dimeric structures. The six-coordinate ligand *N*,*N*,*N'*,*N'*-tetrakis(2-hydroxyethyl)ethylenediamine (THEED) was used to afford the titanium and zirconium complexes **6.2** and **6.3**, respectively. Structures of these compounds determined by single crystal X-ray crystallography showed that an oxygen atom from each ligand is binucleating, acting as a bridge to form a central M_2O_2 ring. The titanium complex **6.2** was found to be a chiral species showing signs of disorder indicating that more than one configuration for the complexed ligand can exist in the solid state. The zirconium analogue **6.3**, was found to have a planar central ring, with longer bridging Zr-O bonds, indicative of being formed by dative covalent bonding. Its structure was found to be centrosymmetric. The efficacy of both of these complexes as crosslinkers with guar solution was found to be very poor, as no viscosity increase was observed. This is most likely due to the six-coordinate THEED ligand fully chelating and stabilising the metal centres. The titanium and zirconium metal ions are bound so tightly that the crosslinking reactions with guar polymer chains are suppressed.

The THEED analogue *N*,*N*,*N'*,*N'*-tetrakis(2-hydroxypropyl)ethylenediamine (THPED) was used to synthesise the zirconium THPED complex **6.4**. It is likely that this will exist in a dimeric structure similar to aforementioned complexes **6.2** and **6.3**, and the $[Ti(THPED)]_2$ analogue

within the literature. Unfortunately, single crystals of **6.4** could not be isolated so X-ray crystallographic methods could not be utilised, but ESI-MS evidence strongly supports dimeric structure formation, with the molecular ion of 758.60 Da corresponding to dimeric $[Zr(THPED)]_2$.

The graft copolymers HEC-*g*-polyglycerol **5.1 b-e**, HEC-*g*-polyglycerol-*g*-PCL_{10} **5.2**, HEC-*g*-polyglycerol-*g*-PCL_{50} **5.3** and succinylated HEC **3.5** were evaluated for their crosslinking abilities with $Zr(TEA)_4$ **6.1b** and a α-hydroxycarboxylic acid zirconate-based crosslinker. The graft copolymers **5.1 b-e**, **5.2** and **5.3** showed no signs of gelation or viscosity build with either of the crosslinkers mentioned above at 0.35, 1.0, 2.0 and 3.0 wt.% concentrations. The succinylated HEC **3.5** also showed no signs of gelation with crosslinker **6.1b** at 0.35, 1.0, 2.0 and 3.0 wt.% concentrations, or with α-hydroxycarboxylic acid zirconate crosslinker at 0.35, 1.0 and 2.0 wt.% concentrations. However, gelation of a 3.0 wt.% aqueous solution of succinylated HEC **3.5** occurred upon the addition of an α-hydroxycarboxylic acid-based zirconium crosslinker. However the utilised polymer concentration of **3.5** was nine times higher than the lower limit used in industrial fracturing applications. The fact that a greater amount of polymer is required will mean increased costs, and therefore it is unlikely to be utilised for industrial applications.

7.2 Future Perspectives

The successful selective deacetylation of HEC thioacetate **4.9** to thiolated HEC **4.7** due to the loss of carbonyl resonances in the ^{13}C NMR spectrum indicates the presence of thiol end group functionality, but due to time restrictions this was not investigated further. Additional analysis is therefore required in order to determine if these are primary or secondary thiol groups. It would then be beneficial to investigate if this material is able to participate in thiol-ene Click reactions with the norbornene-catechol compound **2.4**.

Industrial hydraulic fracturing utilises a wide range of crosslinking agents such as those based upon titanium, zirconium and boron, suitable for a range of well conditions. During this project, it was only possible to have access to two crosslinking agents; triethanolamine zirconate **6.1** and an α-hydroxycarboxylic acid zirconate. It would be very interesting to investigate if any of the modified HEC materials synthesised during this work show crosslinking with other zirconium-containing crosslinkers featuring different attached ligands (such as polyols, or different alkoxides or α-hydroxycarboxylic acids), or group(IV) metal based crosslinkers containing either titanium or hafnium. It would also be advantageous to explore the crosslinking

affinity of boron-based crosslinkers (such as tetrahydroxyborate anions) with the functionalised HEC materials, in order to determine if the viscosity of the gel is reversible to mechanical shear, as observed with the guar/tetrahydroxyborate gel system. However, the exact preparation of the crosslinkers utilised within industry is often kept secret and not fully disclosed in the patent literature, making it difficult to fully explore this avenue.

It would also be interesting to carry out the attachment of simple sugar rings (such as glucose, galactose and mannose) acting as glycosyl donors to the C_6 hydroxyl groups of HEC, in order to afford materials that mimic the structure of guar. The hydroxyl groups of the sugar rings to be attached require protection (usually by acetal or benzyl groups), and the group at the anomeric carbon atom (C_1) could be displaced in order to form a new glycosidic bond.[1] An example is shown in Scheme 7.1, where BF_3 is used as a catalyst in the attachment of glucose pentaacetate to HEC.[2] Deprotection of the acetate groups to hydroxyl groups is then required.

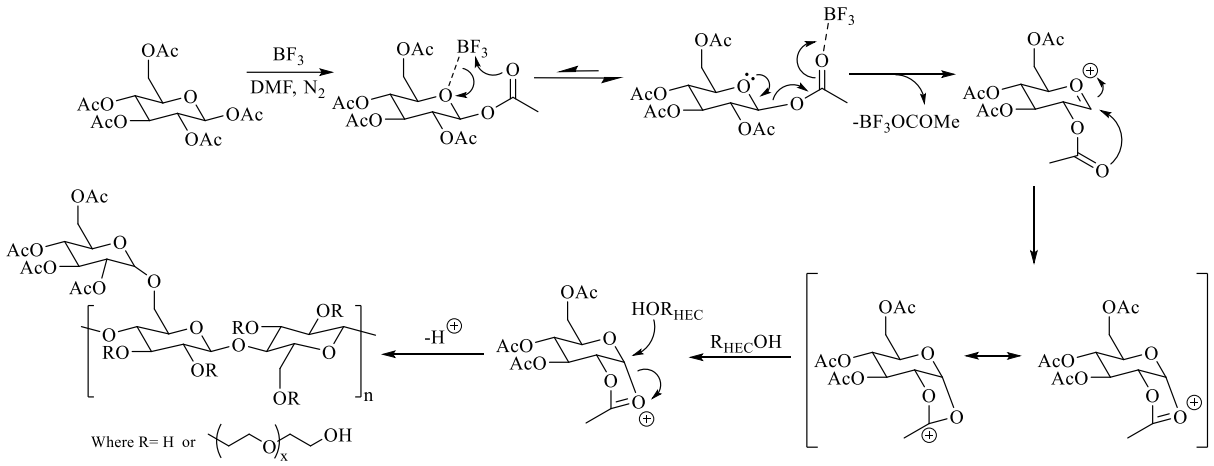

Scheme 7.1: Attachment of acetylated glucose to HEC

These monosaccharide functionalised HEC materials could then be evaluated for their ability to undergo crosslinking reactions with the range of aforementioned crosslinking agents, in order to determine if they can offer gelation comparable to the guar based system.

7.3 References

1. T. K. Lindhorst, *Essentials of Carbohydrate Chemistry and Biochemistry*, Wiley, Weinheim, **2007**.
2. Z. D. Wang, Y. Mo, C.-L. Chiou, M. A. Liu, *Molecules*, **2010**, *15*, 374.